DATA MINING AND TIME SERIES ANALYSIS OF BRAIN DYNAMICAL BEHAVIOR WITH APPLICATIONS IN EPILEPSY

By

MICHAEL ANDREW BEWERNITZ

A DISSERTATION PRESENTED TO THE GRADUATE SCHOOL
OF THE UNIVERSITY OF FLORIDA IN PARTIAL FULFILLMENT
OF THE REQUIREMENTS FOR THE DEGREE OF
DOCTOR OF PHILOSOPHY

UNIVERSITY OF FLORIDA

2008

To my family, my loving fiancée Teddi, and all those whom have helped me along the way of this challenging journey.

ACKNOWLEDGMENTS

I would first like to thank Panos Pardalos for his guidance, wisdom, and his persistent drive towards excellence which helped me and numerous students to think big, aim high, and repeatedly achieve great feats throughout the years. Most of all, I thank Dr. Pardalos for the effort he exerted to assist me during a difficult portion of my graduate schooling. I would also like to thank Dr. Basim Uthman for teaming up with me to share his brilliant ideas, time, energy, and financial support. The benefits of his impact on my graduate experience are beyond measure. I'm very grateful for opportunity to work with Dr. Georges Ghacibeh and for the large positive impact he has had on my career as a Ph.D. student. I would also like to thank Dr. Mingzhou Ding, Dr. Steven Roper, and Dr. Hans Van Oostrom for serving on my graduate committee and providing valuable feedback.

I thank Dr. J. Chris Sackellares for his guidance and support throughout the years, especially when we worked together at the Brain Dynamics Laboratory at the University of Florida. In addition, I commend Dr. Deng-Shan Shiau for his continual assistance in all areas of my graduate career for the last five years. I'm also grateful for the guidance of my BDL labmates, Dr. Wanpracha Chaovalitwongse, Linda Dance, Chang-Chia Liu, Dr. Sandeep Nair, and Wichai Suharitdamrong as well as Dr. Wendy Norman for their assistance with work and just keeping my bearings during this challenging chapter of my life.

I would also like to thank Dr. Paul Carney for his guidance throughout the years during meetings, conferences, seminars, or just in passing on campus. He has helped me in numerous ways and I extend sincere thanks. I am also grateful for Dr. Kevin Kelly for providing me the privilege of a fruitful and engaging experience working at his facility. I thoroughly enjoyed the summer of 2005 working in his Pittsburgh lab on our challenging task. I am grateful to have

made the acquaintance of Peter Jukkola, Dr. Elena Kharlamov, Kathy Schmitt, and all the Allegheny-Singer Research Institute staff that helped me along the way.

I'm very grateful for my most recent group of friends in the Center for Applied Optimization at the University of Florida. The broad spectrum of research experience available my CAO colleagues such as Ashwin Arulselvan, Dr. Vladimir Boginski, Nikita Boyko, Dr. Stanislav Busygin, Dr. Altannar Chinchuluun, Alla Kammerdiner, O. Erhun Kundakcioglu, Dr. Antonio Mucherino, Dr. Oleg Prokopyev, Steffen Rebennack, Dr. Onur Seref, Oleg Shylo, and Petros Xanthopoulos helped provide me with rapid answers to many research questions, numerous perspectives to attacking a problem, as well some tasty ethnic food, drink and insider information for world travel! Short of becoming a United Nations ambassador, I doubt I will ever work with such a unique and diverse group of friends ever again.

I also appreciate the efforts of Scott Bearden, David Juras, and all the staff at the Malcom Randall VA Medical Center of the North Florida/South Georgia Veterans Health System who have collaborated with our University of Florida research team and provided invaluable support for my Ph.D. studies.

I would also like to thank Professor Jens Timmer, Professor Andreas Schulze-Bonhage, Dr. Björn Schelter, Dr. Michael Jachan, Hinnerk Feldwisch, Armin Brandt, Jakob Nawrath, Raimar Sandner, Johannes Wohlmuth, Thomas Maiwald, Christiane Lehmann, Carolin Gierschner, Dr. Matthias Winterhalder, Dipl. Ing. Richard Aschenbrenner-Scheibe, Dr. Henning Voss of the Freiburg Center for Data Analysis and Modeling, University of Freiburg, Germany, for providing publicly available de-identified EEG signals for research purposes. Their generosity has greatly benefited my studies. In addition, General Clinical Research Center,

Grant # MO1-RR00082 has provided the means to conduct a portion of the research conducted in this dissertation.

I would like to acknowledge the efforts of April-Lane Derfinyak, Anide Pierre-Louis, Laura Studstill, Kristi Wagner, Kathryn Whitesides, as well as Tifiny Dyer, Michelle Griffin, Danielle Wise, and Cindy Hansen for helping keep me on schedule with graduate school deadlines and comply with all the university guidelines that were a challenge to keep track of.

Outside of my professional contacts, I would like to thank all my friends and my entire family, Howard, Noreen, Julie, and Mark Bewernitz for countless hours of encouragement in good and bad times. They have shared my ups and downs and maintained a steady supply of loving support throughout it all. I thank my loving fiancee, Teddi, for her continued support throughout the various phases of my graduate career. You mean everything to me Teddi.

Above all, I thank The Father, The Son, and The Holy Spirit for the grace and blessings to persevere throughout the greatest challenge of my life thus far.

TABLE OF CONTENTS

page

LIST OF TABLES

LIST OF FIGURES

Figure page

LIST OF ABBREVIATIONS

AED	Anti-epileptic drug
ApEnt	Approximate entropy
DNA	Deoxyribonucleic acid
DTW	Dynamic time warping
EEG	Electroencephalogram
FN	False negative
FP	False positive
GCRC	General Clinical Research Center
IID	Independent and identically distributed
IRB	Institutional Review Board
LR	Logistic regression
PLED	Periodic lateralized epileptiform discharge
STL_{max}	Short-term maximum Lyapunov exponent
SVM	Support vector machine
SWD	Spike-and-wave discharge
TN	True negative
TP	True positive
VNS	Vagus nerve stimulation
$\overline{\Omega}$	Mean angular frequency in phase space

Abstract of Dissertation Presented to the Graduate School
of the University of Florida in Partial Fulfillment of the
Requirements for the Degree of Doctor of Philosophy

DATA MINING AND TIME SERIES ANALYSIS OF BRAIN DYNAMICAL BEHAVIOR WITH APPLICATIONS IN EPILEPSY

By

Michael Andrew Bewernitz

May 2008

Chair: Panagote M. Pardalos
Major: Biomedical Engineering

Epilepsy is a neurological disorder characterized by recurrent seizures. Approximately 30% of patients with epilepsy have seizures that are resistant to anti-epileptic drug (AED) therapy. If these patients are unable to undergo epilepsy surgery, they may choose to utilize the Vagus Nerve Stimulator (VNS) implant. The VNS therapy® system has been approved by the FDA to electrically stimulate the left vagus nerve for epilepsy treatment. Patients with newly implanted VNS systems undergo an adjustment period of several months involving numerous medical check-ups to fine tune the electrical stimulation parameters based on clinical response. This sub-optimal adjustment method leaves the patient at risk of seizures and imposes financial burden. Identification of a marker of desired VNS operation would greatly expedite this adjustment process. The utility of non-invasive electroencephalogram (EEG), success of neural state classification research for diagnosis and treatment of neurological disorders, and the potential for real-time application due to advances of computer technology motivate this study. This dissertation outlines data mining approaches involving biclustering, logistic regression, and support vector machines as well as statistical comparisons of a range of relevant EEG dynamical measures for the characterization of electroencephalographic patterns associated with VNS therapy. The preliminary results are consistent with biological processes and clinical

observations. One explanation for the electroencephalographic behavior is that VNS mimics a theorized therapeutic seizure effect where a seizure "resets" the brain from an unfavorable preictal state to a more favorable interictal state. The preliminary results suggest a connection between the EEG patterns and the stimulation parameters which may require a range of linear and nonlinear measures for adequate characterization.

In addition, support vector machines are utilized to create a seizure detection and stratification algorithm in patients with generalized absence epilepsy. The algorithm utilizes dynamic time warping distance and Teager-Kaiser energy as the representative EEG features. The algorithm performed slightly better at seizure onset detection than for seizure offset. This is likely due to increased waveform consistency shortly after onset compared to offset. Such an algorithm may benefit clinicians and researchers by providing a means to rapidly annotate EEG signals as well as a means to provide a clinically interesting measure of therapeutic efficacy for drug evaluation studies (e.g. distribution of seizure durations may vary before and after drug therapy, and thus a measure of this distribution may find clinically relevant information which a raw seizure count would miss). A future direction of this project is to test additional EEG feature inputs and assess how the algorithm copes with the challenges presented in online EEG analysis.

CHAPTER 1
INTRODUCTION

Recent advances in mathematics provide new tactics for the analysis of complex datasets. These advances provide new options for analyzing and modeling seemingly complex system behavior such as that seen in biological systems. In addition, the rapid growth of computational capabilities in the modern computer provides the possibility for real-time computational analysis of biological datasets. Such scientific milestones have revolutionized the direction of scientific research in many disciplines, among them, the study of epilepsy. In recent decades, a growing body of evidence has surfaced in research reports suggesting the existence of a pre-ictal state has resulted in a great interest in quantitatively characterizing this theorized "seizure imminent" state. Due to the superior time resolution and large availability of the electroencephalographs, much research has been devoted to characterizing the preictal state in terms of electroencephalogram (EEG) datasets.

Advances in the understanding of non-linear system dynamics have lead to massive breakthroughs for the challenging task of characterizing the dynamics governing the behavior of complex systems. In many instances, these novel system modeling approaches can achieve better results than were previously attainable with standard linear approaches.

One major premise for the characterization of neural states is that the dynamics directing brain function are often best examined within a nonlinear deterministic framework (Savit et al., 2003). Such a framework can provide a useful means to analyze systems that that exhibit adaptive behavior and are non-autonomous (both of which are traits of biological systems). For the example of seizure prediction, this method bypasses the explicit underlying neurophysiological processes involved in seizure generation and instead focuses on predicting "undesirable" neural states (e.g. seizures) by measuring and modeling the temporal progression

of various observable features of brain behavior. Whether predicting seizure or other neural state changes, such features may currently include brain electrical or magnetic field fluctuations, blood flow, neurochemical concentration profiles. Of these measures, electrical activity as measured in EEG data sets is the most commonly used feature for describing neural state in epilepsy.

Computational Therapeutic Approaches: a New Frontier in Medical Treatment

The computational power and memory storage abilities of modern computational age have revolutionized the way that scientists and engineers approach problems. One of the most exciting achievements of the 20th century is the invention of the semiconductor transistor, which was followed by a cascade of computational advances throughout the last 50 years. Moore's Law is a famous model of the observed growth rate of computational abilities and has remained astonishingly accurate for several decades (Intel Corporation, 2005). The state of modern technology provides modern researchers the ability to not only solve problems that could be not practically be solved a few decades ago, but now we are in a unique position to solve many such problems in real-time applications.

While the benefits of such technology are manifesting at an almost alarming pace in every aspect of life, the fields of biology and medicine have capitalized in ways that may have seemed inconceivable only decades ago.

Necessity is the mother of invention, and such is the driving force for many of the numerous serendipitous medical discoveries. One prime example is a solution to the many problems plaguing the functionality of hospital bedside cardiac regulation devices. The original device utilized an external bedside machine which regulated the cardiac pacing. Among the many difficulties included impeded patient mobility due to the size and mass of the equipment, alternating current power requirement, as well as skin burns at electrode sites (Nelson, 1993).

The advent of implantable devices forever revolutionized the field of medical treatment when a Swedish group first implemented the previously unheard-of idea of utilizing an implantable device for cardiac pacing (Nelson, 1993). The success of cardiac pacemakers opened the eyes of physicians and engineers alike that were seeking new solutions to the challenge of improving the state of medical treatment.

The cardiac pacemaker was highly sophisticated solution to the treatment of damaged and diseased hearts and helped pave the way for a revolution in medicine; the use of computational devices (implantable or bedside) to help regulate the physiology of patients afflicted with some chronic condition. This new engineering direction added numerous challenges such a biocompatibility and safety issues, as well as new concepts (e.g. designing implantable devices with the expectation that the treatment device is likely to or guaranteed to fail in lifetime of the patient).

In recent years, microelectromechanical devices (MEMs) have been able to strongly capitalize on the advancements of computers. As computers became smaller, faster, and more efficient, savvy engineers were able to capitalize on the new options available to them. For example, the combination of MEM sound sensors, processors, and transcutaneous transmitters provides the possibility of mimicking the role of the cochlea in patients with a specific cause of hearing impairment (Chapin and Moxon, 2001). While the device is far from being as precise or accurate as the original brain tissue, such a device helped pioneer a new research direction for augmenting impaired brain function.

Additionally, retinal implants are being heavily researched to compensate for certain types of blindness (Schanze et al., 2007). The device is able to mimic some of the tasks of a

function retinal including photo detection and the directing preprocessing phase output to the optic nerve.

Despite the astonishing milestones of progress in these brain machine interfaces (BMI), these two implantation devices are still being heavily researched. Another intensely researched field of BMI aims to integrate the state of the art computational technology combined with the modern marvels of neuroscience in order to overcome certain types of paralysis (Nicolelis et al., 2001; Kim et al., 2007). Such an apparatus provides the ability of the brains muscle movement signals to execute actions in a prosthetic limb.

The above BMIs face numerous challenges which must be overcome before such devices can become a mainstay of treatment. For one, adequate input data acquisition is massive challenge in and of itself. All such devices assume that obtaining samples of the brain's electrical signals can serve as sufficient inputs (as the specific knowledge of neurotransmitter chemistry and exact neuronal connectivity cannot currently be obtained as successfully as the electrical signals can be recorded). Also, while our understanding of the roles of the secondary and primary motor cortices in the planning and execution of motor movements have sufficed to provide exciting preliminary results for such BMIs, the time and spatial resolution of such recordings required for optimal external limb control remains uncertain. In addition, one massive challenge of itself is to extract useful features from such signals in order to serve as the proper inputs to the underlying model governing the action of such a device. Furthermore, the proper choice of model is a field of heavy research in and of itself. As is expected, the available models of brain function have numerous advantages and disadvantages compared one another that can depend on the particular states of the brain to be modeled, the range of brain states considered, quality of recordings, feature extraction methods and so on.

While the state of the art of neuroscience has made progress relevant to the development of BMIs, there is still much room for improvement in understanding the basic and advanced mechanisms of normal brain function as well as impaired brain function in various neurological disorders. While the impaired neural functions of interest in the previously described BMI applications may in some cases seem rather straight forward, the specific neural impairment processes of some other neurological disorders are at the present moment less explicitly understood. For such disorders, such as epilepsy, the extraction of suitable biomarkers for any type of advanced therapeutic scheme is hampered by the apparent mysterious nature of the disorder. Epilepsy is a disorder that not only has symptoms that are not fully understood (e.g. the specific cause and purpose of an epileptic seizure), but also the occurrence of seizures often does not appear to follow any known behavioral pattern with a sufficient degree of accuracy. There is much room for improvement.

Establishment of Neural States in Epilepsy

Extensive research has been conducted in the last four decades with the focus of unveiling and modeling the mechanisms that lead up to a seizure. It has been said that only approximately 3% of epilepsy cases present seizures that are initiated by some external stimulus whereas for the vast majority of patients there are no such clear events associated with seizure initiation (Le Van Quyen et al., 2001). However, there is a large body of clinical evidence suggesting that seizures are preceded by a physiologic state change that occurs prior to seizure onset.

Documented clinical changes preceding a seizure include increase in heart rate (Delamont et al., 1999; Novak et al., 1999; Kerem and Geva, 2005), cerebral blood flow (Weinand et al., 1997; Baumgartner et al., 1998), the availability of oxygen (Adelson et al., 1999), magnetic resonance imaging of the blood oxygen-level-dependent signal (Federico et al.,

2005) as well as changes visible in single photon emission computed tomographic patterns (Baumgartner et al., 1998).

Thus, one of the most profound discoveries in this field of research is postulation of a physiologic "preseizure" state (Mormann et al., 2007). This theory is supported by a large volume of documented physiologic changes occurring prior to seizure onset within and outside of the brain. This transition from a "normal" state into a preseizure or "preictal" state is one of the major theories regarding seizure initiation that has affected the direction of epilepsy research. On a neuronal level, the preictal state results in an abnormal synchronized "bursting" involving large populations of neurons in various brain structures. Depending on the type of epilepsy, these discharges can begin locally and possibly spread to various regions of the brain or can begin multiple regions nearly simultaneously.

Dynamical Disorders in Neurology

The epileptic disorder exhibits traits similar to a class of diseases termed "dynamic diseases" which demonstrate particular complex behavior patterns that evolve over time. Specifically, these "dynamic diseases" have been broadly described as a class of diseases which undergo a temporal disruption of underlying physiological control mechanisms leading to period of abnormal dynamical behavior (Mackey and Glass, 1977; Mackey and an der Heiden, 1982; Milton and Mackey, 1989; Belair et al., 1995; Milton and Black, 1995; Milton, 2000; Lopes Da Silva et al., 2003; Colijn and Mackey, 2005). Examples of these phenomena include the oscillation of blood cell populations in hematological diseases (Colijn et al., 2006), tremor in Parkinson's Disease (Beuter and Vasilakos, 1994), as well as several neurological disorders such as epilepsy, migraine, and multiple sclerosis (Milton and Black, 1995). Within the perspective of control mechanisms (e.g. feedback or feed forward control systems), dynamical diseases can be viewed as an undesirable alteration of a standard biological control scheme (Mackey and Glass,

1977; Mackey and an der Heiden, 1982; Milton and Mackey, 1989; Belair et al., 1995; Milton and Black, 1995; Milton, 2000; Lopes Da Silva et al., 2003). Such dynamical disorders often undergo state transitions that bear resemblances to bifurcations in mathematical systems, for example. The overall significance of identifying dynamic diseases is that it may be possible to develop therapeutic approaches based on the manipulation of the identified critical control parameters (Mackey and an der Heiden, 1982; Milton and Black, 1995). Numerous studies present models utilizing linear and nonlinear dynamical EEG time series analysis measures to model the transition into a seizure (Iasemidis and Sackellares, 1991; Iasemidis et al., 1993; Lehnertz and Elger, 1995; Casdagli et al., 1996; Lehnertz, 1999; Le Van Quyen et al., 2001; Osorio et al., 2001; Iasemidis et al., 2003, 2004; Chaovalitwongse et al., 2005). Often the long-term goal is to utilize these measures to serve as inputs for a dynamical disease model used in a closed-loop therapeutic control device (Iasemidis et al., 2003; Good et al., 2004, 2005; Fountas and Smith, 2007). Thus, if a seizure represents a period of aberration in a dynamical epileptic disorder which is characterized by nonlinear EEG measures such as STLmax (Iasemidis et al., 2000), then nonlinear dynamical measures (such as STLmax) could conceivably provide a useful framework for characterizing the effect of therapeutic intervention (Good et al., 2004, 2005; Ghacibeh et al., 2005).

Aside from such practical applications, quantitative EEG analysis from a non-linear dynamical framework has also helped provide some novel insight towards defining a physiological role of seizures in epileptic disorders. For example, one theory states that a seizure is the manifestation of the brain's mechanism for "resetting" the brain when it enters an undesirable state. Such a state has been characterized by an unhealthy similarity in the rate of information production among critical brain sites, a process referred to as "dynamical

entrainment" (Iasemidis et al., 2004). Physiologically, such a resetting effect may follow a proposed therapeutic mechanism similar to that of ECT induced seizures (Fink, 2000; Gwinn et al., 2002; Taylor, 2007).

The theorized existence of neural states that are indicative of the current status of the epileptic disorder forms the basis for many model-based seizure control therapy research projects. A common belief of researchers in this field is that a therapeutic dosage of drug or electrical stimulation can be applied at the proper location of the central nervous system and at the proper time to mitigate and possibly prevent seizure occurrence. In essence, this line of therapy embraces a philosophy that a well-timed, "minor" therapeutic action in the proper location will abort a seizure by means of fulfilling the therapeutic action for which the seizure was intended.

Much like the cardiac pace maker described earlier, a "brain pacemaker" is becoming more of a realistic possibility (Savit, 2003) for providing a means to dispense localized electrical stimulation or drug dispensing treatment "on demand" when preictal transition state changes are detected (Stein et al., 2000; Theodore and Fisher, 2004; Good et al., 2004, 2005; Morell, 2006).

Objectives and Contributions of this Dissertation

A team of leading scientists, health care providers, and leaders of voluntary health organizations came together to discuss what it would take to find a cure for epilepsy in March, 2000. The milestone White-House initiated conference, "Curing Epilepsy: Focus on the Future," was sponsored by the National Institute of Neurological Disorders and Stroke in collaboration with the American Epilepsy Society, Citizens United for Research in Epilepsy, Epilepsy Foundation, as well as the National Association of Epilepsy Centers. The conference stressed the importance of scientists throughout the nation to investigate methods of studying and treating

seizures. The conference produced a national agenda for epilepsy research which has served as a community guide towards a cure.

Since then, the epilepsy research community has progressed substantially in updating the research benchmarks to be aligned with current research developments. As a result, a primary goal of the 2007 conference was to assess the original benchmarks and discuss new research directions. The attendees voted on which areas were most promising, as well as those in need of attention. The Epilepsy Benchmark Stewards gathered in October 2007 to finalize a hierarchy of epilepsy research benchmarks. Of particular interest to this dissertation are the following specific benchmarks:

- Develop valid screening strategies and biomarkers and surrogate markers (e.g., genetic, pharmacogenomic, electrophysiologic, imaging, biochemical) to identify patients who are likely to respond to, or develop adverse effects from specific therapies.
- Develop higher-throughput cost-effective models for screening pharmacotherapies for specific types of epilepsy.
- Optimize existing therapies

The main goal of this dissertation is to extract useful features from the EEG signal of patients afflicted with epilepsy in order to further the understanding of the disorder and work towards improvements to existing therapies. The first portion of this research addresses the desire to identify EEG markers of optimal VNS therapy for the purpose of expediting the parameter adjustment phase in newly-implanted patients. The final chapter introduces a novel approach to seizure detection and stratification algorithm which may provide a useful tool for evaluation drug efficacy.

Organization of Chapters

The research presented in this dissertation is organized into seven chapters. Chapter one provides an overview of the document. The overview consists of a brief introduction to the field

of quantitative EEG analysis in epilepsy as well as the scope of research presented in this dissertation from the context of federally-established epilepsy research guidelines.

Chapter two describes an extensive overview of various epileptic disorders, symptoms, diagnosis, and a range of relevant clinical and biological information. In addition, an overview of diagnostic tools and current treatment modalities is presented as well the direction of future treatment research.

Chapter three overviews the broad range of methods utilized in quantitative EEG analysis. The described methods are broadly classified as time series analysis and data mining methods. Relevant mathematical theory is and biological interpretations in experimental situations are explained.

Chapter four begins with a description of epilepsy from a dynamical disorder perspective and outlines some key EEG data mining analysis methods applied within this framework. Based on these observations from scientific literature, the aforementioned dynamical EEG analysis methods are employed to study the effect of vagus nerve electrical stimulation therapy in order to characterize the relationship of the stimulation parameters with the EEG behavior in terms of dynamical measures. The results are discussed in terms of their relationship to relevant clinical research observations and the underlying biological processes. The work described in chapter four is has been published in three journal articles:

- “Biclustering EEG data from epileptic patients treated with vagus nerve stimulation”, authored by Stanislav Busygin, Nikita Boyko, Panos Pardalos, Michael Bewernitz, and Georges Ghacibeh (Busygin, 2007).
- “Quantification of the Impact of Vagus Nerve Stimulation Parameters on electroencephalographic Measures” with authors Michael Bewernitz, Georges Ghacibeh, Onur Seref, Panos Pardalos, Chang-Chia Liu, Basim Uthman (Bewernitz, 2007).
- "A Data Mining Approach to the Investigation of EEG Biomarker Existence for Vagus Nerve Stimulation Therapy Patients", with authors Nikita Boyko, Michael Bewernitz,

Vitaliy Yatsenko, Panos Pardalos, Georges Ghacibeh, Basim Uthman, submitted to Computing and Optimization in Medicine and Life Sciences Vol. 3, (Boyko et al., 2008).

Chapter five provides additional quantitative EEG analysis in patients undergoing VNS therapy for epilepsy. This chapter closely examines the interstimulation EEG dynamics using numerous EEG dynamical measures commonly applied in neural state classification studies. Specifically, this chapter assesses the nonlinearity of EEG dynamics and characterizes time-dependent dynamical behavior and compares these features to stimulation parameters.

The results are discussed in the context relevant clinical research findings as well as relevant physiologic processes. The potential application of such results for use in real-time seizure control applications and rapid parameter tuning apparatus is presented. A paper related to these interstimulation dynamics studies was published under the title "Optimization of epilepsy treatment with vagus nerve stimulation" with authors Basim Uthman, Michael Bewernitz, Chang-Chia Liu, and Georges Ghacibeh (Uthman et al., 2007).

Chapter six begins with an introduction into generalized absence epilepsy. A novel seizure detection and stratification algorithm is presented as a means to help physicians and researchers rapidly annotate EEG signals as well as provide online diagnostic tools. In particular, such a seizure stratification algorithm may provide a clinically interesting measure of therapeutic efficacy for drug evaluation studies (e.g. the distribution of seizure duration distribution before and after drug therapy may provide clinically relevant information which a raw seizure count would miss). A manuscript related to this work was published under the title "Support vector machines in neuroscience" with authors Onur Seref, O. Erhun Kundakcioglu, and Michael Bewernitz (Seref et al., 2007).

Chapter seven summarizes the findings of this dissertation. Concluding remarks regarding the overall significance of the findings are discussed. Future research directions in light of these results are presented.

CHAPTER 2
AN OVERVIEW OF EPILEPTIC DISORDERS AND EPILEPSY RESEARCH DIRECTIONS

Introduction

The term epilepsy is derived from the Greek word epilamvanein which means "to be seized", "to be attacked", "to be taken hold of". This disorder has been well documented throughout historical texts for thousands of years in numerous civilizations. Ancient Greeks referred to people "being seized" and "having an attack" as if the person were under the influence of a supernatural force. This idea comes from the ancient notion that disease was a form of punishment from the gods or evil spirits (Engel, 1989). These descriptions likely refer to the abrupt, complex timing of seizure onset and how the symptoms could be described as almost a supernatural "seizing" of the individual for certain types of seizure. Hippocrates was the first person documented as having suggested that epilepsy was a disorder of the brain around 400 B.C. (Parker and Parker, 2003).

Epilepsy is not a disease, though, but rather a symptom of a disorder of the brain. Normally, the tens of billions of brain cells making up the brain communicate with one another via small bursts of electrical activity. An unexpected, erratic electrical discharge of a group of brain cells is referred to as a seizure. A seizure can be brought on by a variety of insults such as toxins, drugs, metabolic disturbances, or trauma, flashing lights, or hyperventilation (Wilner, 2003). Such a provoked seizure is separate from Epilepsy, which is a disorder distinguished by recurrent seizures (Lothman et al., 1991).

The epileptic condition can arise from numerous causes. Typically, the common element in all causes of epilepsy are events that result in a disturbance of neuronal functionality such as extreme illness, chemical or physical brain damage, or abnormal brain development resulting from genetic or other triggers (Parker and Parker, 2003). Specific brain features resulting from

such brain alterations that could be responsible for epilepsy include altered neuronal connectivity, excessive levels of excitatory neurotransmitters, deficiencies of inhibitory neurotransmitters, or possibly a combination thereof. It has also been observed that the brain's attempts to repair itself after injury can lead to irregular nerve connectivity patterns which eventually lead to epilepsy (Parker and Parker, 2003). Recent estimates of world-wide epilepsy prevalence for a wide range of age groups indicated between 3 and 8 reported cases of epilepsy per 1000 people (Shorvon et al., 2004).

The hallmark of epilepsy is recurrent seizures caused by the sudden development of synchronous neuronal firing. Seizure symptoms can include uncontrollable shaking, loss of awareness, visual and aural hallucinations, phantom odors, and other sensory disturbances depending on the location and spread of electrical activity in the brain (Weaver, 2001; Wilner, 2003).

Electroencephalogram (EEG) recordings show that these discharges begin either locally in one or more portions of a cerebral hemisphere or simultaneously in both cerebral hemispheres (Binnie et al., 1997; Niedermeyer et al., 1993). These seemingly unpredictable seizures can cause a variety of motor symptoms and have a major effect on the patient's quality of life by imposing restricted driving privileges, adverse effects on social and career opportunities, self-esteem, education, and psychiatric issues (Goldstein and Harden, 2001; Manford, 2003; Wilner, 2006). In addition, recurrent seizures may cause progressive neuronal damage, leading to impaired memory and cognition. A 1995 study estimated that epilepsy imposed an economic burden of $12.5 billion in associated health care costs and losses in employment, wages, and productivity in the U.S. (Begley et al., 2000).

Classification of Seizure Types

All types of seizures are broadly classified depending on whether the seizure arises in a restricted portion of the brain within one hemisphere or if the onset involves both hemispheres (Shorvon et al., 2004). Seizures that do not fit into these categories are referred to as unclassified. Figure 2-1 outlines a basic framework for seizure classification as designated by the Epilepsy Foundation (2008).

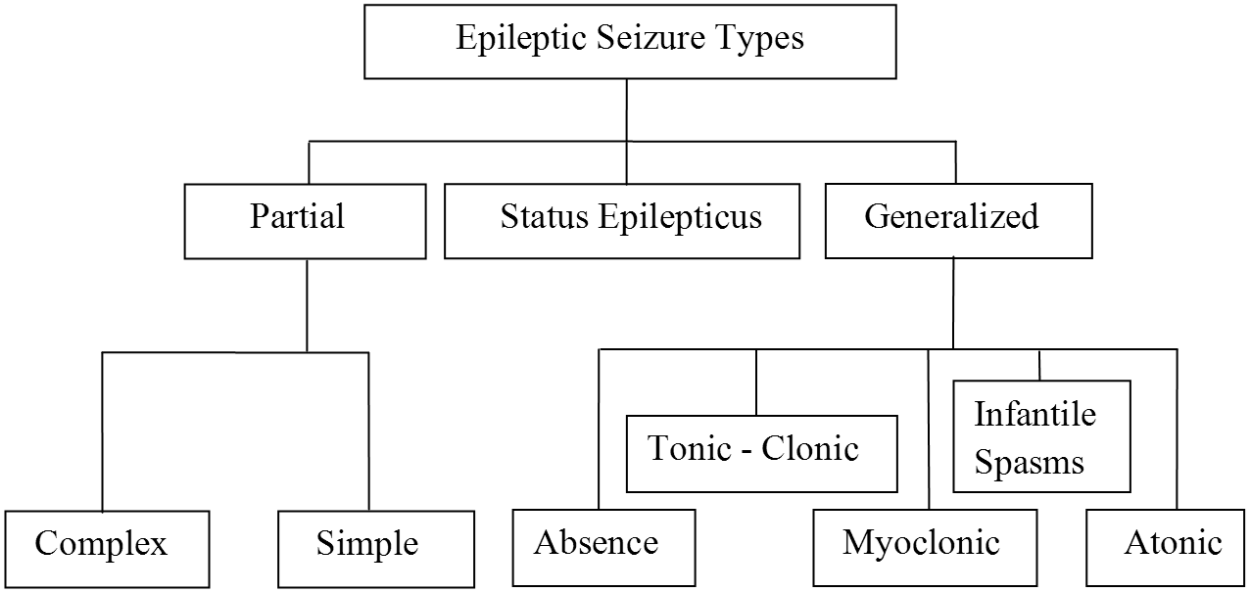

Figure 2-1. Seizure classification ruling as designated by the Epilepsy Foundation (2008).

Partial Seizures

Partial seizures are those that occur in a localized region of the brain known as a "focus". Partial seizures can be roughly broken down into simple partial, complex partial, and secondary generalized seizures.

A simple partial seizure may materialize with rhythmic twitching of a limb, cessation of speed, strange sensations in the body, or hallucinations (Shorvon et al., 2004). The particular symptoms vary from patient to patient and depend on the region of the brain in which the seizure

is occurring. Simple partial seizures begin suddenly, cease quickly, and do not involve an impairment of consciousness.

In a complex partial seizure a person will temporarily undergo an impairment of consciousness are often preceded by a premonitory sensory or psychic aura (Shorvon et al., 2004). During the seizure the person appears unresponsive and may make purposeless limb movements called "automatisms". Automatisms can include such behavior as eye blinks, twitches, chewing motions of the mouth, and possibly walking in a circular pattern (Parker and Parker, 2003). Patients can often be amnesic about the events occurring in complex partial seizures.

Some partial seizures can spread to both hemispheres resulting in tonic (muscle tensing) and clonic (rhythmic muscle twitching) symptoms. This type of spreading of seizure activity after focal onset is referred to as secondary generalization. These seizures were once referred to as "grand mal" seizures, though this terminology is now discouraged. Conversely, atonic seizures produce a sudden reduction in muscle tone.

Generalized Seizures

Generalized seizures refer to seizures initiate in both brain hemispheres simultaneously. These seizures are often accompanied with impaired consciousness. Two important types of generalized absence seizures are absence seizures and status epilepticus.

Absence seizures

Absence seizures are a type of generalized seizure where seizures are initiated by an abrupt rapid onset as well as an abrupt rapid offset. These seizures have an off and on nature where the duration of the seizure is rarely longer than 30 seconds in duration and most often less than 5 seconds in duration (Shorvon et al., 2004). Often the patient will not provide explicit symptoms of having experienced a seizure, but rather may continue the behavior or movement pattern that

was active at seizure onset. The impaired consciousness combined with a general amnesia about the experience means that absence seizures can interfere with schooling and may even be misinterpreted as daydreaming.

Status epilepticus

Status epilepticus is a serious, potentially fatal condition in which seizures persevere for significantly longer durations than other seizure types. One of the challenges in diagnosing status epilepticus is to provide a definition that is theoretically sound as well as useful in the emergency room as neuronal damage can occur after sufficient time (Costello and Cole, 2007). In addition to the brain, prolonged seizures can damage to numerous body systems including heart, lung, and kidney tissue (Wilner, 2003). A recent review article suggests a hybrid of operational definitions including 5 minutes of persistent, generalized, convulsive seizure activity or two or more distinct seizures between which there is incomplete recovery of consciousness (Lowenstein et al., 1999) where the seizure activity also persists after sequential administration of appropriate doses of appropriate first and second line-AEDs (Costello and Cole, 2007).

Nonconulsive status epilepticus (NCSE) refers to the cases of status epilepticus associated with ictal EEG activity yet without convulsive motor activity (Uthman and Bearden, 2008). Patients in the NCSE state may appear to be in a confused stuporous state or a comatose-like state (Costello and Cole, 2007). While status epilepticus can take on many electroencephalographic characteristics, "clear cut" nonconvulsive status epileptic cases will present the following properties:

- Frequent or continuous focal electroencephalographic seizures demonstrating changes in amplitude, frequency, or localization
- Frequency or continuous generalized spike and wave discharges (SWDs) in patients whom do not have a history of epilepsy

- Frequent or continuous generalized SWDs which show significant amplitude or frequency differences in relation to previous SWDs (in patients with a history of epileptic encephalopathy)
- Periodic lateralized epileptiform discharges (PLEDs) in patients which have become comatose after convulsive status epilepticus

(Korff and Nordli, 2007).

The challenge of treating NCSE cases is that both the electroencephalographic characteristics and the clinical symptoms can appear very similar to those exhibited by metabolic disorders. For example, cases of positive NCSE diagnosis have been reported where patients initially demonstrated extended periods of diffuse rhythmic delta activity before any ictal waveforms were presented (Uthman and Bearden, 2008).

Triphasic waves can be present in both NCSE as well as the non-epileptic encephalopathies such as metabolic encephalopathies, though triphasic-like waves must be highly persistent to be considered as possibly arising from NCSE (Kaplan and Birbeck, 2006).

Currently, one of the most reliable diagnostic strategies is to administer a dosage of a benzodiazepine class drug and to observe any changes in the EEG signal. Though a small portion of patients (~15%) will be resistant to benzodiazepine therapy, the drug will often result in improved mental status and suppression of ictal waveforms in patients that were undergoing NCSE (Shneker and Fountain, 2003). The absence of clinical improvement after benzodiazepine dosage does not necessary rule out NCSE.

Epilepsy Treatment

Surprising as it may be the plethora of modern medical imaging technologies that have developed in the recent decades, though useful for supplementing available information about the brain, are no substitute for a medical imaging modality invented over 80 years ago. EEG

recordings are relatively cheap to acquire, relatively safe, are often noninvasive (except in more severe epilepsy cases), and provide exceptional time resolution.

The Electroencephalogram as a Diagnostic Tool

EEG recordings as well as other related electrophysiological measures are the most commonly used diagnostic tools for the treatment of epilepsy. Though numerous people made significant technological contributions, Richard Caton is established as the first physician to observe the brain's continuous spontaneous electrical activity in 1875 (Goldensohn, 1997). Hans Berger is credited as the father of electroencephalography due to his 1932 report containing four photographic EEG segments of a patient's postictal recovery (Goldensohn, 1997).

The measurement of the brain's electrical field potentials via EEG is the cornerstone for epileptic diagnosis and classification of epileptic seizures (Speckmann et al., 1997). Field potentials are detectable in the space surrounding nervous system tissue. Field potentials arise from the changes in membrane potential of neurons and glial cells. An excitatory post synaptic potential (EPSP) occurs when an excitatory afferent fiber is stimulated and the resulting inflow of cations (e.g. sodium) lead to a membrane depolarization. The spread of the membrane depolarization results in an intracellular current as well as an extracellular current. The extracellular current induces the field potential which is perceived by a nearby electrode as a negative charge (due to the influx of cations) and a distant electrode perceives a positive charge (due to the out flux of cations) (Speckmann et al., 1997). A similar yet opposing process occurs for an inhibitory post synaptic potential (IPSP), where the stimulation of an inhibitory afferent fiber induces an outflow of cations perceived by a nearby electrode as a local positive charge.

Field potentials generated by epileptic processes exceed the potentials generated by nonepileptic processes because the epileptic activity is highly synchronized (and thus have relatively elevated amplitude due to a summation effect). Furthermore, experiments have

demonstrated a close temporal relationship between the paroxysmal depolarization of a neuron in superficial cortex and EEG sharp waves (an indicator of epileptic activity) during the development of an epileptic focus in a seizure model (Speckmann et al., 1997). Due to the large degree of synchrony in epileptic outbursts the behavior of this neuron can be extrapolated to provide a suitable representation of the epileptic neuronal network. Though sharp waves have an important role in epilepsy diagnosis, there are numerous types of epilepsy with differing characteristic EEG patterns. For example, absence seizures are often associated with 3-hz generalized spike and wave patterns yet tonic-clonic seizures are often associated with a variety of rhythms of generalized spiking and polyspike bursting (Chabolla and Cascino, 1997). Beyond the handful of examples of epileptiform EEG patterns listed here, there are numerous EEG properties that the trained electroencephalographer takes into consideration before arriving at a diagnosis. Such diagnostic details are beyond the scope of this dissertation, however, an excellent overview can be found in Chabolla and Cascino (1997).

Once the proper diagnosis is made, there are numerous methods used to treat epilepsy. The methods are treating a specific cause (if one can be identified), avoiding precipitants of seizures (if any can be identified), antiepileptic drugs (AED), behavior modification, surgery, electrical stimulation, and diet control (Oxley and Smith, 1991). Use of AEDs is the most common form of treatment.

Antiepileptic Drugs

AEDs can treat seizures in numerous ways. Some AEDs make brain cells less excitable. Others make brain cells less likely to pass messages. Still other AEDs increase the amount of a inhibitory neurotransmitters such as gamma amino butyric acid (GABA) (Oxley and Smith, 1991). One way to classify AEDs is by their main therapeutic mechanism (though there are some drugs that utilize numerous mechanisms and others may even have unknown mechanisms).

From this organizational framework, the main groups include sodium channel blockers, calcium current inhibitors, gamma-aminobutyric acid (GABA) enhancers, glutamate blockers, carbonic anhydrase inhibitors, hormones, and drugs with unknown mechanisms of action (Ochoa and Riche, 2007). While an in-depth review of antiepileptic drugs is beyond the scope of this dissertation, an executive summary of some of the basic antiepileptic drug categories will be outlined.

Sodium channel blockers

This class of drug is well characterized. As the name implies, sodium channel blocking drugs inhibit sodium channel operation which prevents the affected neuron from depolarizing and thus inhibits neuronal firing (Ochoa and Riche, 2007). Prominent examples of sodium channel blockers include carbamazepine, lamotrigine and zonisimide. Lamotrigine is a drug commonly used to treat absence seizures.

GABA agonists, reuptake inhibitors, and transaminase inhibitors

γ-aminobutyric acid (GABA) is an inhibitory neurotransmitter and popular target for antiepileptic drug action. This is because there are numerous ways to enhance the functionality of the GABA system, many of which demonstrate a clinically useful antiepileptic effect. GABA-A receptors control the influx of Cl- ions and GABA-B receptors are connected with potassium channel function (Ochoa and Riche, 2007). The effect of GABA can be enhanced several ways:

- direct binding to GABA-A receptors,
- blocking presynaptic GABA uptake,
- inhibiting the metabolism of GABA by GABA transaminase,
- increasing the synthesis of GABA

(Ochoa and Riche, 2007). Benzodiazepines (BZDs) are an important class of short-acting drugs whose anticonvulsant effect is due to binding with GABA-A receptors, where they then

enhance inhibitory neurotransmission (Shorvon et al., 2004). BZDs are commonly used in epilepsy treatment as well as anesthetic applications. They are most often used for treating status epilepticus and clusters of seizures rather than long term treatment. For example, the BZD midazolam has demonstrated effectiveness the treatment of convulsive status epilepticus in patients for whom phenytoin, and/or phenobarbital had failed (Kumar and Bleck, 1992). One difficulty in with this drug class is the sedative effects which are a major factor limiting the use of benzodiazepines in long term seizure therapy. Thus, benzodiazepines tend to be used most often for acute seizure treatment.

Glutamate blockers

Glutamate is more of the most important excitatory neurotransmitters in the brain (along with aspartate). The glutamate neurotransmission system is highly intricate and the major classification scheme for ionotropic glutamate receptors is to name them after the agonist that activates the binding site (e.g. AMPA, kainite, and NMDA). AMPA and kainite sites control channels that pass sodium and a small amount of calcium. NMDA sites control channels that pass large amounts of calcium in addition to sodium (Ochoa and Riche, 2007). Felbamate and Topiramate are examples of antiepileptic drugs that mitigate glutamate excitatory transmission.

Pharmacologically-resistant epileptic seizures

AED therapy can be very effective in preventing seizures. Primary generalized epilepsy and benign partial epilepsy are two classes of epilepsy that respond well to AEDs. Patients with temporal lobe epilepsy are not so fortunate, though. These unfortunate people can usually expect to take AEDs their entire life. The odds of gaining complete control over temporal lobe epilepsy seizures are not as good as primary generalized or benign partial epilepsy (Oxley and Smith, 1991). Approximately 30% of patients with epilepsy have seizures that are resistant to AED therapy, and must resort to alternative therapies (Theodore and Fisher, 2004).

Epilepsy Surgery

Surgical treatment may be considered in extreme cases where the patient does not achieve adequate benefit from AED therapy (Engel et al., 1993). The mean duration of in-patient hospital stay for pre-surgical EEG monitoring ranges from 4.7 to 5.8 days and costs over $200 million each year (Begley et al., 2000). In order to be a candidate for surgery, the first criterion is that the patient must have seizures arising from a single seizure focus in the brain. In addition, the excision procedure cannot be performed on brain regions that are essential for normal functioning of the patient (Roper, et al., 1993; Velasco et al., 2000; Durand and Bikson, 2001). Even if as many as 50% of these patients were to benefit from surgical resection (an optimistic estimate), many patients still require new therapeutic approaches (Theodore et al., 2004).

Gene Therapy

Gene therapy is an innovative approach to providing antiepileptic therapy to patients with pharmacologically resistant seizures. From the perspective of treating epilepsy by correcting an imbalance in excitatory and inhibitory neuronal transmission, a vector can be used to insert neuropeptide genes in certain brains which lead to intracranial creation of therapeutic peptides. For example, the neuropeptide Y gene inserted into rat hippocampus with adeno-associated viral vectors resulted in reduced generalization, delayed seizure initiation, and provided neuroprotection in a rat seizure model (Noe' et al., 2007). Additionally, the lentivirus may be used as a vector, or to graft genetically engineered cells which produce therapeutic substances (Vezzani, 2004). Though these as well as other results are very promising, gene therapy for epilepsy treatment is still at the pre-clinical research stage.

Electrical Stimulation Therapy

Brain stimulation is becoming one of the main alternative therapeutic approaches for patients whom are suffering for pharmacologically intractable epilepsy and are not surgical

candidates. While the force can have a strong influence on the weak-minded (Kenobi, 1977), conventional electrical stimulation therapy remains a more widely-used form of brain stimulation. Numerous forms of electrical stimulation therapy have been utilized for the treatment of epilepsy. One such method of brain stimulation is membrane polarization by uniform direct current (DC) electric fields.

This form of stimulation comes from the basic principle that electrical current can generate an electric field when then results in generation of electric current. Specifically, electric fields generated by the nervous system can directly modulate the activity of neurons and often can recruit neighboring cells. DC electric fields have a unique property compared to other stimulation paradigm in that they can cause either excitation or inhibition of neuronal activity depending on the orientation of the field with respect to dendrite. (Durand and Bikson, 2001).

While DC field stimulation utilizes a relatively low current amplitude (only a few microamperes), there are several drawbacks to this method: 1) irreversible chemical reactions can result the dc field which often result in tissue and/or electrode damage; 2) the efficacy of stimulation is highly sensitive on DC field orientation; 3) either excitation or inhibition can be induced depending cell location and orientation (thus, improper DC field orientation can induce the "opposite" of the intended effect); 4) the termination of the DC pulse induces an excitation which results in a rebound of spontaneous activity; and 5) DC fields application must typically be applied for the entire duration of an ictal event for desired efficacy and thus may require long pulses (Durand and Bikson, 2001).

Low frequency stimulation paradigms (e.g. stimulation frequencies less than 10 Hz) provide robustness over DC electric field stimulation. Unlike DC field stimulation, low frequency stimulation is not orientation dependent and thus its effects are less variable. In

addition, low-frequency and single pulse stimulation have long-lasting effects which remain long after the duration of the pulse. This after effect helps minimize the electrochemical damage as well as the amount of energy required for stimulus.

Periodic low frequency stimulation applied via transcranial magnetic stimulation (TMS) is a noninvasive method to induce electric fields in the brain. A study investigating the susceptibility of amygdala for kindling in rats demonstrated a 55% higher threshold for the induction of epileptic after discharges two weeks after a single TMS train (120A/μs, 20 Hz for 3 s) (Ebert, 1999). The mechanism underlying this type of antiepileptic effect for low-frequency stimulation is unknown, but suspected to be long-term depression (LTD). LTD is a persistent decrease in synaptic strength caused by low frequency (e.g. 1 Hz) stimulation (Purves et al., 2004). Low-frequency stimulation paradigms for establishing LTD could decrease neuronal firing rate which may in an antiepileptic effect (Durand and Bikson, 2001).

Deep brain stimulation

Deep brain stimulation (DBS) attracted great attention in 1996 for its use in the treatment of tremor related to Parkinson's disease and essential tremor (Gross, 1994). DBS offers several advantages over PNS (e.g. vagus nerve) stimulation. Specifically, electrodes implanted in the brain can directly stimulate the targeted structure with far greater accuracy than PNS stimulation. Also, the coarse action of PNS stimulation risks activation of afferent (such as pain or sensory) and efferent fibers (such as those modulating cardiovascular and abdominal visceral functions) (Durand and Bikson, 2001). Naturally, a major DBS disadvantage is that the implantation of intracranial electrodes has a greater extent of invasiveness and associated risk than PNS stimulation.

There are presently four general hypotheses explaining the therapeutic mechanism of DBS: 1) stimulation-induced alterations in the activation of voltage-gated currents block neural output

near the stimulating electrode; 2) indirect inhibition of neuronal output by means of activation of axon terminals that make synaptic connections with neurons near the stimulating electrode; 3) synaptic transmission failure of the efferent output of stimulated neurons as a result of transmitter depletion; 4) stimulation-induced disruption of pathologic network activity (McIntyre et. al, 2004). Additional research utilizing microdialysis, neural recordings, modeling, and functional imaging will likely need to be conducted in order to fully characterize the effects of DBS (McIntyre et. al, 2004).

Since DBS therapy relies on accurate positioning of electrodes, surgical implantation is assisted with several guiding tools. DBS electrodes are implanted into the brain using stereotaxic methods, MRI targeting, recording of extracellular unit activity, and electroencephalographic monitoring. Some typical stimulation parameters are 1-10 volts, 90 μs pulses in trains of 100-165 Hz, running either continuously or in intervals of 1 minute on and 5 minutes off (Theodore and Fisher, 2004). Clinically useful and tolerable stimulation parameters can vary from patient to patient as well as across different sections of the brain. Thus, a common strategy of DBS is to exploit the natural behavior of various brain structures in a manner to most effectively produce an anti-seizure effect.

Cerebellum

Cerebellar stimulation can be performed to capitalize on the inhibitory outflow which is present in nearly all patients. Anterior stimulation decreased hippocampal formation discharges. However, cerebellar stimulation has had variable effects in animal models, which may have been related to variable stimulation parameters (Theodore and Fisher, 2004). An interesting phenomenon discovered in controlled DBS studies is the placebo effect. For example, in a controlled study of cerebellar DBS involving 14 control patients, 2 of the 14 patients showed improvements in seizure frequency (Hodaie et al., 2002). This placebo effect, defined as a

reduction (or abolition) of symptoms with insertion of DBS alone, might be due to an initial lesioning resulting from the implantation procedure.

Subcortical structures

Interest in subcortical stimulation comes from its widespread, non-specific, anterior and intralaminar nuclear connections to the mesial frontal, temporal, and limbic structures. In addition, it demonstrates progressive recruitment of substantia nigra, subthalamic nucleus, and midline thalamic nuclei in animal models of epilepsy. Stimulation of the subthalamic nucleus, anterior, thalamus, and substantia nigra have been shown to inhibit limbic seizures in animal models of epilepsy (Theodore and Fisher, 2004). In addition, stimulation of the basal ganglia structure may modify propagation of seizures (Deransart et al., 1998). Some of the most important subcortical structures will now be discussed.

Caudate nucleus

The effect of caudate nucleus stimulation has demonstrated antiepileptic effects in an aluminum-hydroxide seizure focus model, though the efficacy is highly dependent on stimulation frequency (Theodore and Fisher, 2004). An inhibitory seizure protection effect was demonstrated for stimulation at 10-100 Hz, whereas 100 Hz stimulation increased seizure frequency. The anti-seizure effects of the caudate-nucleus are hypothesized to be due to activation of the substantia nigra under the presumption that low-frequency stimulation is excitatory and high frequency stimulation is inhibitory (Theodore and Fisher, 2004). Since these results are from uncontrolled studies, it is uncertain if "micro ablation" resulting from electrode implantation is contributing to the anti-seizure effect.

Thalamus

The thalamus is seen as a strategic stimulation site on the basis that it is the pacemaker of the cortex, with widespread connections between the two structures. There is electrophysical

and anatomical evidence suggesting that midline thalamic nuclei may participate in modulation and spread of limbic seizures. Experimentally, thalamic stimulation has been shown to terminate seizures in a primate epilepsy model. Studies of human thalamic stimulation have been published with favorable results (Theodore and Fisher, 2004).

Centromedian nucleus

The centromedian nucleus (CN) has been classified as part of the non-specific thalamus. The CN's major difference from the thalamus in terms of stimulation for epileptic seizures is that the CN's output is more strongly related with the caudate nucleus than with the cortex (Theodore and Fisher, 2004). In a placebo-controlled double-blind study involving 7 patients, CN stimulation resulted in a 30% decrease with respect to baseline when the stimulator was on versus an 8% decrease when the stimulator was off (Fisher et al., 1992). CN stimulation appeared safe and well tolerated by the patients.

Anterior thalamic nucleus

The anterior nucleus of the thalamus (ATN) may help influence the propensity of seizures due on its connectivity and functional relations with the cortex and limbic structures. High frequency stimulation of the ATN leads to EEG desynchronization, which is believed to render the cortex less susceptible to seizures (Hodaie et al., 2002). Specifically, 100 Hz had an anti-seizure effect whereas stimulation at 10-50 Hz lowered the seizure threshold. A controlled study of 5 patients resulted in a mean seizure reduction of 54%. An interesting observation was that the results did not differ from the stimulation on and stimulation off periods (Theodore and Fisher, 2004). This is thought to be due to a "microthalamotomy" placebo-effect. This phenomenon of a reduction or abolition of symptoms due to insertion of DBS electrodes alone has been seen in over 53% of DBS electrode implantations for tremor, and can last up to a year in some cases (Hodaie et al., 2002).

Subthalamic nucleus

The subthalamic nucleus (STN) was chosen based on encouraging responses in patients with movement disorders as well as high-frequency stimulation in animal epilepsy models. In a study utilizing STN high frequency stimulation in 5 patients, 3 patients showed reduction in seizure frequency of 67-80%, one patient had approximately 50% seizure reduction, and the fifth showed no improvement. In this study, the recording of epileptiform activity in the STN suggests that it is part of a cortico-subcortical network involved in the epileptogenic process (Chabardes et al., 2002).

Hippocampus

Human studies of hippocampal stimulation have demonstrated that high-frequency stimulation, rather than low frequency, can be inhibitory. This is contradictory to several preclinical investigations of hippocampal stimulation. One theory for this phenomenon is that the anti-seizure effect is due to the activation or inhibition of downstream structures (as opposed to the hippocampus itself). Nevertheless, 7 patients that participated in a hippocampal stimulation study involving 2-3 weeks of 130 Hz electrical stimulation for 23 hours per day responded very well. Stimulation halted clinical seizures and decreased the number of interictal EEG spikes at the focus after 5-6 days. However, no observable antiepileptic effects (or no effects at all) were found in three patients when stimulation was either interrupted or given elsewhere just outside of the hippocampus (Theodore and Fisher, 2004).

Vagus nerve stimulation

VNS therapy has been the subject of many studies before and after its approval for treatment of intractable seizures in 1997 (Uthman et al., 1993; Ben-Menachem et al., 1994; Theodore et al., 1997; Schachter et al., 2002; Cyberonics®, 2006; Ardesch et al., 2007; Ramani, 2008). VNS is licensed in several countries as an adjunctive epilepsy therapy with a rare

occurrence of serious side effects. Studies suggest that VNS treatment results in a much lower incidence of adverse cognitive, neurological, and systemic effects than AED treatments (George, 2001). Over 40,000 epilepsy patients have VNS therapy® implants (Cyberonics®, 2008). VNS is a useful therapy for patients with medically refractory and localization-related epilepsy characterized by complex partial and secondary generalized seizures (Theodore and Fisher, 2004). The apparatus consists of an electric stimulator which is implanted subcutaneously in the left side of the chest and connected to the left cervical vagus nerve using subcutaneous electrical wires. The device is programmed to provide neurostimulation at a set duration, frequency, intensity, and pulse width for the treatment of epilepsy. Figure 2-2 provides an example of the VNS pulse sequence.

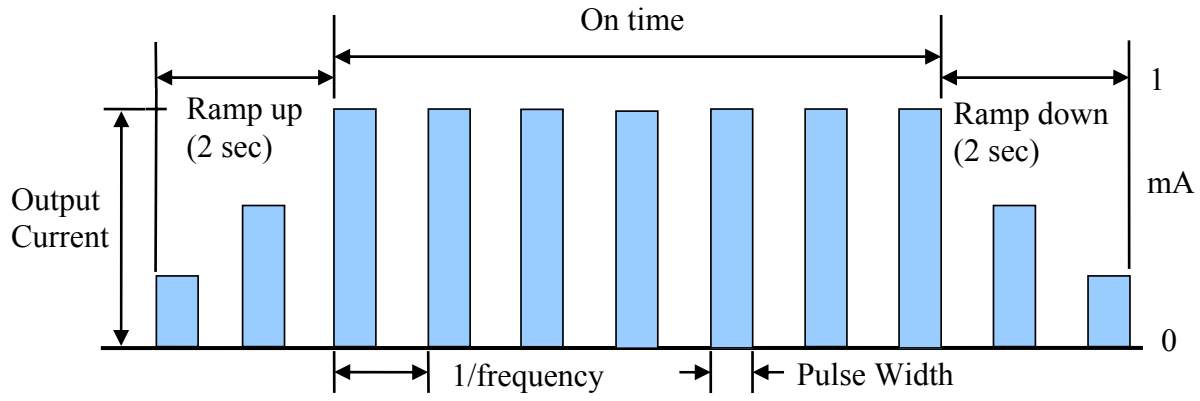

Figure 2-2. VNS pulse sequence.

The vagus nerve was chosen as the site for stimulation because of its diffuse and widespread projections to the thalamus, amygdala, and forebrain through the nucleus tractus solitarius and to other cortical areas via the medullary reticular formation.

Though VNS therapy has demonstrated seizure treatment efficacy, the therapeutic mechanism is still uncertain (Ben-Menachem et al., 1994; Fisher et al., 1999; Groves, 2005; Ramani, 2008). However, a physiologic framework for the VNS therapy mechanism has been

described (Upton et al., 1991; Ramani, 2008). The vagus nerve is the 10th cranial nerve and is comprised of approximately 80% afferent fibers, which carry sensory information to the brain. The vagus nerve is highly involved in the regulations of numerous autonomic systems such as the heart, the intestines, and provides and integral role in respiration.

Studies suggest that the metabolic activation of thalamic, brainstem, and limbic regions may be integral in the mediation of VNS effects (Fisher et al., 1999). It has been shown that depletion of norepinephrine in the locus coeruleus attenuates the AED-like effect of VNS (Krahl et al., 1998). Recent studies also suggest that the VNS may exert its effect through the locus coeruleus (Groves, 2005; Ramani, 2008).

Experiments in which cat vagus afferent neurons were stimulated were able to produce either cortical synchronization or desynchronization, depending on the fibers' conduction velocity (Upton, 1991). Recent studies have determined that vagus A and B fiber activation can lead to EEG synchronization whereas vagus C fiber activation results in EEG desynchronization (Groves, 2005). Electrical stimulation of the vagus nerve resulted in a reduction of interictal epileptiform spike frequency during and up to three minutes after stimulation in a rat seizure model (McLachlan, 1993). Overall, in lieu of these and other reported VNS effects there is no consensus as to how these empirical effects relate to epilepsy. Though studies have examined how vagus A, B, and C fiber stimulation affects synchronization, the overall VNS-induced effects of these fibers and other relevant brain structures on EEG, reports suggest that these effects not explicitly visible in the time domain (Fisher et al., 1999) or in frequency domain (Salinsky et al., 1993). Numerous studies report little success in quantifying immediate EEG effects corresponding with VNS (Hammond et al., 1992; Salinsky et al., 1993; Koo, 2001; Rizzo et al., 2004; Marrosu et al., 2005). The only reported scalp-EEG effects of VNS are reported to

occur numerous months after VNS implantation. Studies involving long-term EEG monitoring have shown that long-term VNS produces a delay in interspiking activity and a reduction in the occurrence of epileptic interictal spikes (Koo, 2001; Olejniczak et al., 2001). Marrosu et al. reported no noticeable changes after one month but an increase in gamma activity and desynchronization one year after VNS implantation compared to baseline recordings (2005). Studies have demonstrated VNS effects on interictal epileptiform discharges (Santiago-Rodriguez and Alonso-Vanegas, 2006) and that the absence of bilateral interictal epileptiform discharges may be an electroencephalographic predictor of seizure freedom (Janszky et al., 2005). In addition, long-term VNS effects have been reported on the spectral content of sleep EEG after 10-18 months of VNS compared to a baseline at 3 months prior to implantation (Rizzo et al., 2004).

Future Therapeutic Directions

One major epilepsy research direction is to enhance therapeutic effectiveness of electrical stimulation or drug therapy though the application of implantable controlled therapy systems. For patients which are currently undergoing therapy from the available electrical stimulation implants (such as the vagus nerve stimulator), research in this direction may help to enhance efficacy, mitigate side effects, reduce therapeutic tolerance, and prolong battery life. Along these lines, such a framework could be adapted to an implantable drug delivery system that would dispense drug at "right" and the right place (e.g. in proximity of a seizure focus or in a location to rapidly circulate medication such as the ventricles).

One framework from which this strategy can be visualized is from a system control perspective. Thus, the basic theory behind this strategy is that the transition from a normal interictal state into a preictal state can be conceptualized as a deviation of a control parameter from its set point. Numerous researchers have invested in this idea using EEG signals as

controlled measure (Osorio et al., 2001; Iasemidis, 2003; Iasemidis et al., 2003; Osorio et al., 2005).

While the basic example of deviation from a set point does not do justice to the enormous complexity of the brain's electrical activity, recent advances in mathematical theory of complex nonlinear dynamical systems provide an interesting perspective from which to examine and interpret EEG signals.

Complex nature of epileptic dynamics

One of the most challenging aspects of epilepsy treatment is that despite the major milestones in biological research, there is still an inadequate knowledge of the underlying biological processes governing the epileptic condition that describes how, where, when, and for what purpose a seizure will occur. One perspective is that the epileptic brain is exposed to at least two states, a normal (interictal) state and a seizure imminent (preictal state).

A natural approach for studying any aspect of brain behavior is to create mathematical model of some brain function using measurable quantities, such as electrical signals. Such models allow predictions to be made about the behavior of sections of the brain. Due to the massive complexity of the interacting neurons in the brain, direct models are most often achieved for small groups of neurons and small brain structures (Hodgkin and Huxley, 1952; Breakspear, 2001; Chauvet and Berger, 2002). The enormous complexity of electrical brain signals often means exact modeling approaches are insufficient. However, despite the observed dynamical complexity of the epileptic brain there certain behavioral characteristics it possess which can provide analytical guidance.

Dynamical diseases and disorders

One important diagnostic aspect of many diseases and disorders is the physiologic behavior in the temporal dimension. In the 1980's many studies addressed the temporal behavior

of biological systems with and without a disease state. Experts within this field often focused their attention on the time scales involved in the clinical aspects of the disorder. This includes characterization of the disease or disorder onset (acute or subacute) as well the succeeding clinical course (self-limiting, relapsing-remitting, cyclic, or chronic progressive) (Belair et al., 1995).

The term Dynamical Disease or Dynamical Disorder refers to the general class of diseases and disorders that are characterized by sudden changes in physiological dynamics that lead to state of morbidity characterized by abnormal dynamics (Belair et al., 1995). Such dynamical disorders arise as a result of abnormalities in underlying physiological control mechanisms. There are many instances of disease and disorder models where the apparent shift of control parameters to region results in pathological behavior of an observable which bears a resemblance to experimental data. Mackey and Glass demonstrated adaptive respiratory disease behavior that displayed a wide range of behaviors such as limit cycle oscillations with aperiodic chaotic solutions (Mackey and Glass, 1977). This particular example exhibited a bifurcation in the systems dynamics that was associated with disease onset. The unstable dynamical realm achieved by altering a "normal" hematopoiesis model bears qualitative similarities to actual hematopoietic data from a leukemia patient (Mackey and Glass, 1977). Thus, there are biological examples to support the claim that mathematical models of physiologic systems may be able to predict the existence of dynamical regimes corresponding to the status of a dynamical disease. Whether the dynamical behavior is periodic, irregular, or apparently random, the significance of dynamical disease identification is that it may be possible to develop therapeutic strategies based on manipulation of critical control parameters (Milton and Black, 1995). Taking into account the temporal rhythm of the disorder as well as an understanding that certain

dynamical rhythms may respond better to some treatments rather than others can help provide a foundation for a suitable therapy (Belair et al., 1995).

Epilepsy as a dynamical disorder of brain systems

Neurological disorders can take on a wide range of complex and abnormal rhythmic behavior over time (Milton et al., 1989). Milton and Black reported observations of recurring sets of symptoms and oscillatory behavior in 32 "periodic" diseases of the nervous system including, ankle clonus in corticospinal tract disease, movement disorders such as essential tremor and Parkinson's disease, as well as paroxysmal oscillations in neuronal discharges in epileptic seizures (Milton and Black, 1995). The cluster of symptoms occurring with a distinct temporal pattern could represent the clinical manifestation of dynamical state changes in these patients. In the context of neural tissue, one view of the abnormal dynamical behavior in neurological patients may arise because of altered control parameters (e.g. nerve conduction time, number of receptors, etc.) and/or alterations in neuronal network structure (Milton et al., 1989).

Compensating for impaired neural control mechanisms: system control therapy

Currently, the biological mechanisms driving transitions into and out of dynamical rhythms (e.g. oscillatory behavior) in neurological disorders are in general poorly understood. A study examining a tremor simulation by inducing delay and amplification in a visual motor task suggests there tremor could be an alteration of numerous interacting control loops or possibly a time-delay state-dependent control system (Milton et al., 1989). One major difficultly whether dealing with tremor or other neurological disorders is to uncover the complex interactions of various interconnected control loops and determine how each contributes to the observed dynamical behavior. Understanding the origins of the dynamical behaviors seen in neurological

disorders can provide a foundation for designing any type of patient-specific therapeutic control system. An example of such a device is shown in figure 2-3.

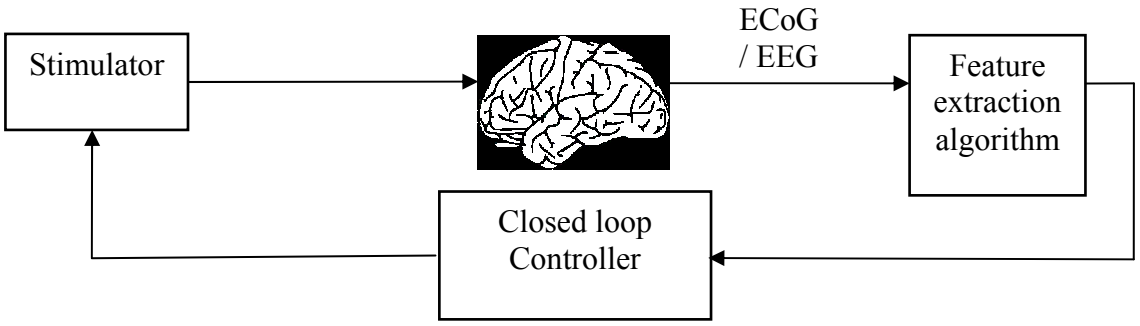

Figure 2-3. Closed-loop seizure control device using electroencephalogram or electrocorticogram signals as an input to a feature extraction algorithm, which supplies the extracted features to a controller which makes a decision regarding the action of a stimulator.

One of the major themes of quantitative EEG analysis in epilepsy as well as other neurological disorders is the identification of signal features that are sensitive to neural state changes. Chapter 3 provides an overview of the rich spectrum of feature extraction strategies employed for quantification of brain dynamics in neurological disorders such as epilepsy.

CHAPTER 3
TIME SERIES ANALYSIS AND DATA MINING TECHNIQUES: THEORY AND APPLICATION

The wealth of epilepsy research conducted via quantitative analysis of EEG signals comprises a rich history. Numerous mathematical models have been applied for the purpose of modeling the progression of disease and inferring the biological significance of the underlying the observed EEG signal patterns. The EEG is a time series of voltage measurements acquired between a scalp or intracranial location of interest and a reference electrode point (e.g. an electrode placed on the ear). Naturally, time series analysis techniques were among the first methods applied for quantifying brain dynamics and constitute a significant portion of quantitative EEG research. In addition, data mining tools are becoming increasingly popular for the extraction and classification of patterns in biological datasets such as EEG signals. The following literature review provides a general overview of the tools used in quantitative EEG research.

Glossary of Terms

Attractor. An attractor is defined as a set of points mapped into a phase space representation which is a target region which adjacent states within a neighborhood (see: basin of attraction) will converge towards as the system evolves towards infinity. An attractor is established to be the smallest region for which the entire volume cannot be further split into two or more attractors having corresponding basins of attraction (as a system may have multiple attractors each with a basin of attraction).

Basin of Attraction. A set of points in phase space such that initial conditions existing in this set evolve over time into a corresponding attractor.

Bifurcation. A bifurcation is defined as a sudden appearance of a qualitative change in dynamics resulting from an alteration in a parameter of a nonlinear system. Bifurcations can occur in both continuous systems as well as discrete systems.

Degrees of Freedom. The dimensions of a phase space mapping.

Limit Cycle. In a phase space, a limit-cycle is a closed trajectory which possesses the characteristic that at least one other trajectory will traverse into it as time approaches infinity.

Phase Space. Phase space is the group of potential states for a dynamical system. Phase space is typically identified with a topological manifold. Each point in the phase space represent an instantaneous and unique state of the system.

Strange Attractor. Strange attractors have a non-integer dimension. The descriptive term 'strange' refers to the geometrical structure of the attractor, whereas the term 'chaotic' refers to the dynamics on the attractor (Grebogi, 1984).

Trajectory. The trajectory of a dynamical system is the orbit connecting points in chronological order in the phase space that is traversed by a solution of an initial value problem. If the state variables are within a real-valued continuum, then the orbit of a continuous time system is a curve. Discreet system trajectories consist of a sequence of points.

Time Series Analysis

Time series analysis is the field of study that aims to extract useful information from time series datasets. A time series is a series of measurements that are acquired at successive times often with a constant time interval. Many aspects of our universe can be represented and studied as time series datasets. This field of study has been extensively applied to financial decision making as well as numerous scientific disciplines. One major goal of time series analysis is to extract useful information about the system that generated the time series dataset. An additional

aim of time series analysis is to model the system dynamics in order to make predictions about future behavior.

Methods Applied in the Time Domain

Numerous linear EEG processing techniques have been implemented in the history of quantitative analysis. This section reviews some of the most utilized measures for the analysis of discrete time series data within the time domain.

Autoregressive moving average modeling

The autoregressive moving average model (ARMA) is standard time series analysis tool used to model univariate datasets. This method is also known as the Box-Jenkins model as the iterative Box-Jenkins procedure it often used to estimate model coefficients (Box and Jenkins, 1976). The model is comprised of two parts, an autoregressive component and a moving average component. For a univariate time series dataset X_t, autoregressive component at time t is defined as:

$$X_t = C + \sum_{i=1}^{p} \phi_i X_{t-i} + \varepsilon_t \tag{3-1}$$

where C is a constant, $\phi_i ... \phi_p$ are the parameters of the model of order p and ε_t is the error term. The moving average component is defined as:

$$X_t = \sum_{i=1}^{q} \theta_i \varepsilon_{t-1} + \varepsilon_t \tag{3-2}$$

where $\theta_i ... \theta_p$ are the parameters of the model of order q, and ε_{t-1} and ε_t are the previous and current error terms, respectively. Combining the autoregressive term with the moving average term produces the ARMA model of order p (autoregressive terms), and q (moving average terms):

$$X_t = \sum_{i=1}^{p} \phi_i X_{t-i} + \sum_{i=1}^{q} \theta_i \varepsilon_{t-1} + \varepsilon_t \quad . \tag{3-3}$$

Such methods have been utilized in modeling functional brain network organization using spectral analysis of local field potentials (Bressler et al., 2007).

Autoregressive integrated moving average modeling

The autoregressive integrated moving average (ARIMA) process is a well-known method for making predictions in nonstationary time series datasets (Box and Jenkins, 1976). As the name implies, this measure is a generalization of the ARMA process. The ARIMA approach to working with nonstationary time series works by utilizing the d^{th} difference to convert the nonstationary time series to a stationary ARMA process. Naturally, the ARIMA method assumes that a time series can be reduced to a stationary time series through the process of differencing. The statistical properties of the stationary time series remain constant in time, and residuals (errors between the original time series and the ARIMA model) are assumed to be the result of noise.

Let $\{y_t\}$ be an ARIMA process of order p,d,q where the d^{th} difference of y_t is a stationary ARMA process of order p,q. The model ARIMA model is then expressed as:

$$\Phi(B)(1-B)^d y_t = \Theta(B) z_t \tag{3-4}$$

where Φ and Θ are polynomials of degree p and q (respectively) having roots outside the unit circle, B is the backward shift operator, and z_t is white noise.

Cross correlation

Cross-correlation analysis is one of the oldest and most standard time series analysis techniques (Bendat and Piersol, 1986). This method measures the linear coupling between two signals.

Let X be some represent an identically distributed stationary stochastic process where $X(t)$ is the value of X at time t. Cross-correlation function representing the coupling between two time series functions $X(t)$ and $Y(t)$ is defined with a time lag, τ, as follows:

$$\hat{C}_{xy}(\tau) = \int_{-\infty}^{\infty} x(t+\tau)y(t)dt \,. \tag{3-5}$$

Cross-correlation is often applied to data from a physical system which typically takes on a discrete form. Let $x_0,...,x_{M-1}$ and $y_0,...,y_{M-1}$ represent two simultaneously acquired stationary time series of length M, zero mean, and unit standard deviation. The discrete unbiased estimate of the cross correlation function is then defined as a function of time lag , $\tau = -(M-1),...,0,...,M-1$ as follows:

$$\hat{C}_{xy}(\tau) = \begin{cases} \dfrac{1}{N-|\tau|}\displaystyle\sum_{i=1}^{N-\tau} x_{i+\tau}y_i, & \tau \geq 0 \\ \hat{C}_{xy}(-\tau), & \tau < 0 \end{cases} . \tag{3-6}$$

The normalized cross-correlation function outputs values within the range of negative one (maximum anti-synchronization) to one (complete synchronization). The maximum τ of equation 3.5 is understood to be an estimation of the delay between two signals (assuming this signals have a linear relationship to one another). The cross-correlation of a function to itself is called autocorrelation.

As the cross-correlation value approaches zero, the signals of interest are increasingly linearly independent. Often a significance threshold is applied to prevent the possible occurrence of a non-zero cross-correlation value for two linearly independent systems (Box and Jenkins, 1976).

Methods Applied in the Frequency Domain

Frequency representation is a standard format for visualizing signal characteristics. This perspective provides a clear visualization of a signal's periodic behavior which may not be evident in the time domain. Thus, frequency domain analysis can help uncover important properties of the system of interest.

Coherence

Coherence is a measure of coupling between two signals as a function of frequency. The signal coherence can take on values between zero and one that provide a relative indicator of how well the signal X corresponds to signal Y at each frequency. The Fourier transform is performed on each signal to convert the signal into the frequency domain (calculate the power spectral density). The cross power spectral density is calculated by multiplying one signal by the complex conjugate of the other signal. The coherence measure is a function of the power spectral density of the individual signals and the cross power spectral density. This measure is typically expressed in terms of its square magnitude and is derived by normalizing the cross power density by the product of power spectral density for the two signals,

$$C_{xy}^2(f) = \frac{\left|P_{xy}(f)\right|^2}{P_{xx}(f)P_{yy}(f)}, \tag{3-7}$$

where P_{xx} and P_{yy} represent the power spectral densities for signals X and Y respectively and P_{xy} is the cross power spectral density (Fuller, 1976). A coherence of zero indicates no coupling between the two signals at the particular frequency whereas a coherence of one implies linear relationship with constant phase shifts between each frequency component. Coherence has been implemented in electrophysiology experiments for several years and more information can be found in literature (Shaw, 1984; Leocani, 1999).

Discrete Fourier transform

The Fourier transform has been implemented in extensively in numerous fields such as mathematics, physics and natural sciences. The Fourier transform is an especially attractive algorithm due to the development of the streamlined Fast Fourier Transform (FFT) (Cooley and Tukey, 1965). In recent years, additional developments have been implemented in the FFTW subroutine library developed by a team of MIT researchers (Frigo and Jonhnson, 2005). This free software package provides a means to optimize the FFT algorithm using various heuristic approaches for each unique problem and platform combination. This subroutine library has been utilized by many researchers and is even implemented in the Matlab® function library.

Fourier analysis decomposes a signal into linear component parts. The analysis involves to concepts:

- Linear combination of different waveforms.
- A time series of any shape can be sufficiently represented by the summation of ample simple sine waves of different frequencies, phases, and amplitudes.

Given a signal $x(t)$, Fourier analysis models the signal as a linear combination of sine and cosine waves for frequency f where:

$$x(t) = \int_{-\infty}^{\infty} X(f) e^{i2\pi ft} df \tag{3-8}$$

and

$$X(f) = \int_{-\infty}^{\infty} x(t) e^{-i2\pi ft} dt \,. \tag{3-9}$$

Equation (3-8) is the continuous Fourier transform which is comprised of the complex coefficients representing the contributions of each frequency, f, to the overall representation of the original time series $x(t)$. Equation (3-7) is often referred to as the inverse Fourier transform.

For a discrete signal,

$$x = \{x_0, ..., x_{N-1}\}, \tag{3-10}$$

where x_n is sampled at the time $t_n = t_0 + j\Delta$, the discrete Fourier transform (DFT) is represented as:

$$X(k) = \sum_{n=0}^{N-1} x(n) e^{\frac{-i2\pi kn}{N}}, \tag{3-11}$$

for the discrete frequencies

$$f_k = \frac{k}{N\Delta}, \tag{3-12}$$

where the inverse Fourier transform is expressed as:

$$x(n) = \frac{1}{N} \sum_{k=0}^{N-1} X(k) e^{\frac{i2\pi kn}{N}}. \tag{3-13}$$

While Fourier analysis is useful for capturing periodic waveforms in non-transient signals, this measure is not suited for extracting transient features. This is because time information is no longer available in the frequency domain as the DFT coefficients are representative of the entire signal duration.

The Fourier transform has been extensively applied to the analysis of EEG waveforms in epileptic patients. Diagnostically, it can help determine the presence of specific brain wave rhythms which may be indicative of certain types of epileptic behavior. Often the time series of interest is broken down into non-overlapping segments in which the Fourier transform is calculated to give a rough estimate of the frequency behavior over time. An example of an a single channel of EEG acquired during an absence seizure and its corresponding windowed Fourier transform is shown in figures 3-1 and 3-2, respectively.

In figure 3-2, the absence seizure onset is characterized by a sudden energy increase in the 0-30 Hz frequency band with the strongest effect around 3 Hz (which is the typical rhythm of spike wave discharges in absence seizures).

Wavelet analysis

Wavelet analysis is a signal processing tool which models a times series signal in terms of shifted and scaled "mother" wavelet. Wavelet analysis is similar in some aspects to Fourier analysis, which models a signal using sinusoids. Instead of sinusoids, wavelet analysis models a signal using an application-specific waveform called a wavelet which has an effectively limited duration and a mean value of zero (Misiti et al., 1996). Wavelet analysis is very useful for performing localized analysis in a subregion of a larger signal. In addition, wavelet analysis is capable of revealing aspects of data that traditional signal analysis techniques may miss such as trends, breakdown points, discontinuities in higher derivatives, and self-similarity (Misiti et al., 1996). For a particular mother wavelet function $\Psi(t)$, the subspace at time t for a scale, a, and a position, b is represented by

$$\Psi_{a,b}(t) = \frac{1}{\sqrt{|a|}} \Psi\left(\frac{t-b}{a} \right). \tag{3-14}$$

If $x(t)$ represents the time series signal, then the continuous wavelet transformation at scale, a, and position b is defined as:

$$C_{a,b} = \int_{-\infty}^{\infty} x(t) \frac{1}{\sqrt{|a|}} \overline{\Psi}\left(\frac{t-b}{a} \right) dt, \tag{3-15}$$

where $\overline{\Psi}$ denotes the complex conjugate of the wavelet and $a, b \in R, a \neq 0$. For low values of the scaling factor a, the wavelet becomes compressed and becomes sensitive to rapidly-changing details and high frequency waveforms. For high values of a, the wavelet becomes stretched and

is more sensitive to coarse slowly-changing features and low frequency waveforms. The parameter b localizes the wavelet function in time. Wavelet analysis has demonstrated utility for the analysis of nonstationary signals such as EEG (Geva et al., 1998, Güler and Ubeyli, 2005; Glassman et al., 2005).

Information Based Methods

Information theory is based on the 1948 publication by Claude Shannon which was the first paper to quantify the concepts involved in communication. Information quantified in units of bits and concepts such as entropy and mutual information were used to describe the transfer of information (Shannon, 1948). Information theory concepts have been extended to time series analysis in biological series such as the EEG. Under the proper statistical conditions, these measures provide useful information about the behavior of the brain.

Approximate Entropy

Approximate entropy (ApEnt) is a statistical measure used to quantify system regularity/complexity from a time series dataset. This measure has been extensively utilized in physiological time series data (Pincus, 1995). The ApEnt measure has been utilized to study the EEG signals acquired from Alzheimer's disease patients (Abásolo et al., 2005), as a measure of anesthetic depth (Bruhn et al., 2000, 2001, 2003), epileptic seizures detection (Abásolo et al., 2007; Srinivasan, 2007), and studies characterizing EEG nonlinearity patterns (Thomasson et al., 2000; Burioka et al., 2003,2005; Ferenets et al., 2006).

The ApEnt measure has demonstrated the ability to quantify system complexity using as few as 1000 data points based on theoretical analyses of stochastic and deterministic chaotic processes (Pincus, et al., 1991; Pincus and Keef, 1992) as well as clinical and clinical applications (Pincus 1995; Bruhn et al., 2000). In this dissertation, ApEnt is used as a measure for quantifying the VNS effect on EEG recordings.

Let U be a signal of length N. For positive integer m and a positive real number r_f, extract $N-m+1$ create vectors $x_m(i)=\{u(i),u(i+1),...,u(i+m-1)\}$. For all i, $1 \le i \le N-m+1$, the quantity C_i^m is computed as follows: number of j such that

$$C_i^m(r_f)=\frac{\text{number of j such that d}[x_m(i),x_m(j)] \le r_f}{N-m+1} \tag{3-16}$$

where d is the maximum absolute difference between the respective scalar components of the two vectors $x_m(i)$, $x_m(j)$ defined as :

$$d(x_m(i),x_m(j))=\max_{k=1,...,m}(|x_m(i+k-1)-x_m(j+k-1)|) \tag{3-17}$$

Using these results, the value of Φ^m can be calculated as:

$$\Phi^m(r_f)=\frac{1}{N-m+1}\sum_{i=1}^{N-m+1}\log C_i^m \tag{3-18}$$

.

ApEnt is calculated as:

$$ApEn(m,r_f,N)=\Phi^m(r_f)-\Phi^{m+1}(r_f). \tag{3-19}$$

In this manner, the value of the positive real number r_f corresponds distance between the neighboring point that is often designated as some fraction of the signal's standard deviation. For this reason, the positive real number r_f can be thought of as a filtering level for the process. The parameter m is the dimension at which the signal is embedded for calculation.

Pattern Match Regularity Statistic

Pattern match regularity statistic (PMRS) is a method used to extract the nonlinear characteristics (complexity) of a time series over time. This measure has been for the quantifying the complexity of an input EEG signal and further detecting EEG state changes such as seizure onset (Shiau, 2001; Shiau et al., 2004). This measure estimates the likelihood of

pattern similarity for a given time series. PMRS has the attractive feature that it can be interpreted in both stochastic and chaotic models. The steps to calculate PMRS include reconstruction of the state space, searching for the pattern matched state vectors, and the estimation of pattern match probabilities. Specially, given an EEG signal $U = \{u_1, u_2, \ldots, u_n\}$, let $\hat{\sigma}_u$ be the sample standard deviation for *U*. For an integer m (embedding dimension), phase space vectors *U* are reconstructed as

$$x_i = \{u_i, u_{i+1}, \ldots, u_{i+m-1}\},\ 1 \le i \le n-m+1 \tag{3-20}$$

then for a given positive r_f, x_i and x_j are considered pattern match to each other if:

$$|u_i - u_j| < r, |u_{i+m-1} - u_{j+m-1}| < r, \text{ and } sign(u_{i+k} - u_{i+k-1}) = sign(u_{j+k} - u_{j+k-1}) \text{ for } 1 \le k \le m-1 \tag{3-21}$$

where r_f corresponds distance between the neighboring point that is often designated as some fraction of the signal's standard deviation. PMRS can then be calculated as:

$$PMRS = -\frac{1}{n-m}\sum_{i=1}^{n-m} \ln(\hat{p}_i), \tag{3-22}$$

where

$$p_i = \Pr ob\{sign(u_{i+m} - u_{i+m-1}) = sign(u_{j+m} - u_{j+m-1}) \mid x_i \text{ and } x_j \text{ are pattern matched}\} \tag{3-23}$$

Mutual Information

Information theory measures such as mutual information have shown utility for estimating high order statistical dependencies between signals. In contrast to linear coupling measures (e.g. cross-correlation), mutual information is sensitive to nonlinear dependencies.

For continuous variables X and Y with probability density function of $f(x)$ and $f(y)$, respectively, and $f(x,y)$ is the joint density function, mutual information can be calculated as follows:

$$I(X,Y) = \int_Y \int_X f(x,y) \log \frac{f(x,y)}{f(x)f(y)} dxdy \tag{3-24}$$

Mutual information between two discrete random variables having marginal probabilities $p_X(x)$ = prob(X=x) and $p_Y(y)$ = prob(Y=y) and joint probability $p_X(x) = prob(X = x, Y = y)$ is defined as:

$$I(X,Y) = \sum_{x,y} p(x,y) \log \frac{p(x,y)}{p_x(x)p_Y(y)}. \tag{3-25}$$

A common approach to calculating mutual information is to first partition X and Y into bins (e.g. a histogram). An estimation of $I(X,Y) \approx I_{bin}(X,Y)$ is obtained by replacing the probability functions $f(x)$, $f(y)$, and $f(x,y)$ with an approximations based on the histogram. Thus, if b_x and b_y are the number of points from X within the x-th bin and number of points from Y within the y-th bin, respectively, and b_{xy} is the number of points in the intersection of the two bins, then $p_x(x) \approx b_x / N$, $p_Y(y) \approx b_y / N$, and $p(x,y) \approx b_{xy} / N$.

Mutual information has been successfully used to quantify statistical couplings in biological applications such as sleep studies (Na et al., 2006) Alzheimer's disease (Abásolo et al., 2007) and epileptic seizures (Varma et al., 1997; Palus et al., 2001; Netoff et al., 2002).

Chaotic System Analysis Techniques

One approach for quantifying the behavior of a complex system such as the brain is to create a mathematical model of the system behavior using measurable quantities. Electrical signal measurements are often used to model the brain modeling the brain's behavior. Such

models allow predictions to be made about the behavior of sections of the brain. Due to the massive complexity of the interacting neurons in the brain, direct models have only been achieved for small groups of neurons and small brain structures (Breakspear et al., 2001; Chauvet and Berger, 2002; Hodgkin and Huxley, 1952). The enormous complexity of electrical brain signals often means exact modeling approaches are insufficient.

Edward Lorenz is often credited as the discoverer of chaos for the fruits of his efforts to devise a long-term weather prediction scheme (Lorenz, 1963). Though Lorenz's model did not turn out to aid in forecasting weather, his results directed his attention to research which helped give rise to research in the area of chaos theory.

Chaotic systems have the interesting property of displaying apparent random behavior but are actually governed by deterministic laws. Specifically, chaotic systems demonstrate a large degree of sensitivity to initial conditions to the point at which minor fluctuations in initial parameters give rise to extremely altered outcomes (to the extent that prediction of such events may even be hampered by sensitivity to computer precision rounding). Since chaotic systems have characteristic similar to noise as well as a broad range of frequency components, linear measures may fail to provide meaningful results.

When exact knowledge of the system governing dynamics is unknown, such as in the brain, an alternative method is a macroscopic modeling approach based on empirical measures of the system as a whole (Iasemidis et al., 1996). After such information is extracted, it may be possible to derive useful empirical models of the global behavior of the system as a whole.
A well-known method to study complex system behavior is to observe the system from a phase space representation (Hively et al., 2005; Iasemidis et al., 1996). Phase space mapping is a process of applying some transformation on a dataset, often into a higher dimensional space,

from which system behavior characteristics can be quantified. Some classic transformations applied in EEG analysis include time delay mapping, (Breakspear, 2001; Hively et al., 2005; Iasemidis et al., 1996; Da Silva et al., 2003; Marino et al., 2003) derivative mapping (Aksenova et al., 1999, 2003; Letellier et al., 1998; Sceller et al., 1999; Tetko et al., 1999). Phase space mapping provides a means to help distinguish random, noisy signals from signals generated from a system governed by deterministic chaos.

Phase Space Mapping

Generate of a time-delay phase space portrait of the system is one of the most established methods for visualizing the dynamical behavior of a multivariable system such as the brain (Iasemidis et al., 1996; Hively et al., 2005). Time-delay phase space maps are a particularly useful phase space mapping variant and are often used for the study of nonlinear deterministic systems. The phase space portrait is created by assigning each time-dependent variable of the observed from the system as a vector element in a multidimensional phase space. Each vector mapped into the phase space represents a unique and instantaneous state of the system. By plotting the phase space vectors in chronological order a representation of the temporal evolution of a discrete system can be visualized.

In principle, the analysis of an individual measured variable can provide dynamical information about other system variables which are related to the measured variable (Iasemidis et al., 2003). A relevant example of this concept is that EEG recorded from one electrode can be related to the activities located at distant electrode sites. Thus, important features of a dynamical system can often be quantified through analysis of a single variable's behavior over time in terms of geometrical attractor properties.

From the reconstructed phase space, measurements can be made to extract useful system information from a single variable (Iasemidis et al., 1996; Pardalos et al., 2003; Chaovalitwongse

et al., 2006). Such information can often be used in data classification algorithms for determining neural state (Tetko et al., 1999, Hively et al., 2005). The method of quantifying phase space properties has been extensively applied to EEG signals analysis for the purpose of studying neurological disorders (Chaovalitwongse et al., 2006; Hively et. all, 2000, 2005; Iasemidis et al., 1996, 2004, 2005; Pardalos et al., 2003, 2004).

The Method of Delays

Time-delay embedding is performed as follows:

$$x_n = \begin{Bmatrix} x(t_n) \\ x(t_n - \tau) \\ x(t_n - 2\tau) \\ . \\ . \\ . \\ x(t_n - (m-2)\tau) \\ x(t_n - (m-1)\tau) \end{Bmatrix} \tag{3-26}$$

where τ is the time delay and *m* is the embedding dimension (Takens, 1981). For a discrete system, every instantaneous state of the system is represented by the vector x_n in *m* dimensional phase space.

Numerous studies have addressed the problem of determining proper parameters for the embedding dimension *m* and τ. The first zero of the autocorrelation function (Rapp et al., 1988) or the first minimum of the mean automutual information (Fraser et al., 1986) are two of the most common approaches to obtain the time delay, τ. Takens recommended a minimum embedding dimension *m* = (2D+1) to ensure complete unfolding of the attractor, where D is the fractal dimension (Takens, 1981).

Fractal Dimension

The term "fractal" was coined by Benoit Mandelbrot in 1975 to describe self-similarity characterized as a jagged geometric shape which can be split into parts which are approximately reduced-size copies of a whole (Mandelbrot et al., 1983). The fractal dimension is a statistical measure of the extent to which a fractal appears to fill space. A non-integer fractal dimension is said to originate from fractal geometry. Strange attractors often have a complex structure with fractal-like properties. Thus, the fractal dimension is a logical measure to use for quantifying strange attractor dimension.

Determining the dimension of an attractor is an important step in the characterization of a system's properties. A proper dimensionality estimate can enhance the accuracy at which the location of a point on an attractor can be specified. Furthermore, the dimension value provides a lower bound on the number of variables required to model the system dynamics.

A standard technique for estimating attractor dimension is from the framework of measuring the changes in the number of points occupying a sphere of radius r as it approaches zero (Grassberger and Procaccia, 1983a; 1983b). Geometrically, the relevance of this observation is that volume occupied by a sphere of radius r in dimension d behaves as r^d. For most attractors the dimension d would be the dimension of the attractor, regardless of the origin of the sphere.

For a chaotic attractor, however, the dimension will vary depending on which point is selected for the estimation. If the particular system's dynamics do not result in dimensional variation, then the mean of the surrounding points can be used. Obtaining the dimension in this method can be obtained by determining the number of point $y(k)$ within a sphere positioned at the phase space location x as follows:

$$n(x,r)=\frac{1}{N}\sum_{k=1}^{N}\Theta\left(r-\left|y(k)-x\right|\right), \tag{3-27}$$

where Θ represents the Heaviside Step Function where:

$$\Theta(n)=\begin{cases}0, & n<0\\ 1, & n\geq 0\end{cases}. \tag{3-28}$$

Equation (3-26) returns a counts of all the points on the orbit *y(k)* located within a radius *r* from point *x* and normalizes this quantity by *N*, the number of points in the dataset. The point density, *ρ(x)*, on an attractor does not need to be uniform to utilize this method (for a strange attractor). If equation (3-27) is raised to the power of *q-1*, the function *C(q,r)* is established in terms of *q* and *r* and the mean of $n(x, r)^{q-1}$ over the attractor weighted with the natural density ρ(x) as:

$$C(q,r)=\int d^{x}x\rho(x)n(x,r)^{q-1}=\frac{1}{M}\sum_{k=1}^{M}\left[\frac{1}{M}\sum_{n=1,n\neq k}^{M}\Theta\left(r-\left|y(n)-y(k)\right|\right)\right]^{q-1}. \tag{3-29}$$

This quantity is referred to as the correlation function or correlation integral. This function estimates the probability that two points on the attractor lie within a distance *r* of each other. M and K are large in value (but not infinite). Though this function is invariant on the attractor, it is conventional to only look at the variation of $C(q,r)$ when r is small. At that scale, it is assumed that:

$$C(q,r)\approx r^{(q-1)D_q}, \tag{3-30}$$

which defines the fractal dimension D_q. The quantity D_q is estimated in the case of small r as:

$$D_q=\lim_{r\to 0}\frac{\log\left[C(q,r)\right]}{(q-1)\log(r)} \tag{3-31}$$

Using this method, $C(q,r)$ needs to be calculated over a small range of *r* in order to achieve a near-linear range for selection of the slope of $\log[C(q,r)]$ over $\log(r)$.

Box counting dimension (D0)

Box counting dimension (*D0*) is the title given to the measure when q=0. *D0* can be estimated as the amount of spheres of radius *r* or the number of "boxes" required to envelop all points in the dataset. If N(r) represent the amount of D-dimensional spheres needed to cover the attractor for relatively small values of r, then the box counting dimension can be estimated as:

$$D_0 = \lim_{r\to 0}\frac{\log[N(r)]}{(q-1)\log(r)} = -\lim_{r\to 0}\frac{\log[N(r)]}{\log(r)}. \tag{3-32}$$

Equation (3-31) is often represented as:

$$D_0 = \lim_{q\to 0} D_q\,. \tag{3-33}$$

Information dimension (D1)

Information dimension (*D1*) is the name of the measure when q=1. *D1* is a generalization of the box counting dimension that takes into account the relative probability of cubes used to cover the dataset. Let *I* represent the information function:

$$I = -\sum_{i=1}^{N} P_i(r)\log[P_i(r)] \tag{3-34}$$

and $P_i(r)$ represent the probability that an element *i* is populated, normalized such that:

$$\sum_{i=1}^{N} P_i(r) = 1\,. \tag{3-35}$$

Information dimension is thus defined as:

$$D_1 = \sum_{i=1}^{N}\frac{P_i(r)\log[P_i(r)]}{\log(r)}. \tag{3-36}$$

Correlation dimension (D2)

Correlation dimension (*D2*) is title of the measure when q=2 (Grassberger and Procaccia, 1983a, 1983b; Kantz and Schreiber 1997). Under this condition, *Dq* takes on special form which tends towards reliable computation. Correlation dimension is estimated as the slope of the log-log plot generated by:

$$D_2 = \lim_{r \to 0} \frac{\log[C(2,r)]}{\log(r)}. \tag{3-37}$$

The correlation dimension can be challenging to quantify in time series data as it can result in highly nonlinear slopes for small r. Correlation dimension has been extensively utilized for neural state classification studies using EEG (Tirsch et al., 2000; 2004) and has been utilized extensively in analysis of physiological data (Kantz and Schreiber, 1995) such as seizure prediction applications (Elger et al., 1998; Martinerie et al., 1998). As correlation sum can demonstrate a high sensitivity to EEG amplitude when using a fixed radius (Osorio, 2001), many authors have implemented a relative radius (with respect to the dataset diameter in vector space) to strengthen their findings (Casdagli et al., 1996, 1997, Merkwirth et al., 2002).

The Lyapunov Exponent

The Lyapunov exponent is an important measure for the quantification of dynamical systems. This measure quantifies the degree of system chaoticity by quantifying the rate of divergence or convergence between two points initially in close proximity (Iasemidis et al., 1999). Lyapunov exponents provide a generalization of linear stability analysis due to steady-state solution perturbation to time-dependent solution perturbations. The measure also provides a meaningful characterization of asymptotic behavior in nonlinear dynamical systems.

Lyapunov exponents are a collection of invariant geometric measures that characterize describe a system's dynamics. Specifically, they provide a measure of predictability for the

particular system. Lyapunov exponents provide a global measure of the rate of convergence or divergence or of two trajectories initially in close proximity to one another for a dynamical system. Positive Lyapunov exponents measure represent the mean exponential divergence rate of two trajectories, whereas negative Lyapunov exponents measure represent the mean exponential convergence of two trajectories. As Lyapunov exponents becomes more positive, trajectories move apart more rapidly. Similarly, as Lyapunov exponents become more negative, the trajectories move together more rapidly. A system with positive exponents has positive entropy as trajectories that are initially in close proximity to one another separate over time.

If a discrete nonlinear system is dissipative then the sum of all the Lyapunov exponents is zero. A system with both a positive and negative Lyapunov exponents is said to be chaotic. Thus, Lyapunov exponents provide a measure of linear stability (or instability) of the attractor or an asymptotically long orbit for a dynamical system.

For a chaotic system with initial conditions *a* and *b* which are initially in close proximity, the distance between these two trajectories at successive time points will exponentially increase over time. If this is written as $e^{n\lambda}$ for a time duration of *n* iterations, then λ is the Lyapunov exponent. For a system to be chaotic, at least one Lyapunov exponent needs to be positive. Thus, at each point in the series the derivative of the time-advanced equation is evaluated. The Lyapunov exponent is expressed as the mean value of the log of the derivative. If the Lyapunov exponent is negative, the iteration is stable. It is important to note that by summing the logs of the derivatives the result corresponds to multiplying the derivatives. Thus, if the product of the derivatives has magnitude less than 1, points will attract together as they go through the iteration.

Though an *n*-dimensional system will produce *n* Lyapunov exponents, the maximum exponent is usually most important. The maximum Lyapunov exponent represents the time

constant, ,, in the expression for the change in distance between the two initial orbits, $e^{n\lambda}$. If ¸ is negative, then the orbits converge over time, and thus the dynamical system is insensitive to the choice of initial conditions. However, if ¸ is positive, then the distance between the initial orbits increases exponentially over time and the system displays sensitivity to initial conditions.

Calculation of the spectrum of Lyapunov exponents can be derived analytically for systems in which process dynamical equations are known aprioi (Shimada et al., 1979). Numerous algorithms have been developed which compute this measure on experimental datasets. One of the most well-known algorithms was developed by Wolf et al. (1985), though other algorithms have been established (Eckman et al., 1986; Ellner et al., 1991).

Short comings of the Wolf algorithm have been identified as sensitivities to the number of observations as well as measurement noise. Numerous researchers have proposed updated versions of Wolf's algorithm with increased robustness to the number of observations (Ellner et al., 1991; Iasemidis et al., 1991; Iasemidis and Sackellares, 1992; Abarbanel, 1996). The following section will provide an executive overview of the Lyapunov exponent estimation. Additional details can be found in (Iasemidis et al., 1991, 2000; Wolf et al., 1985).

Computing Short-Term Maximum Lyapunov Exponents

A phase space mapping is performed by embedding a signal x(t) of duration T using the method of delays (3-26). The phase space representation provides the proper perspective for measuring the degree of chaoticity of the attractor. An attractor is chaotic if on average the two trajectories with similar initial conditions (two points in close proximity in phase space) diverge at an exponential rate (expansion process). If these trajectories are members of a finite attractor, they will fold back into the attractor as time progresses (folding process). A result of these two processes may be the generation of a stable and topologically layered attractor. If the expansion

process outweighs the folding process in some of the attractor's eigen-directions, the attractor is said to be chaotic. If the phase space is D-dimensional then theoretically up to D Lyapunov exponents can be estimated. However, as expected, only (D +1) of them will be real (Abarbanel, 1996).

If L represents the short term largest Lyapunov exponent estimate STLmax, then:

$$L = \frac{1}{N_a \Delta t} \sum_{i=1}^{N_a} \log_2 \frac{\left|\delta X_{i,j}(\Delta t)\right|}{\left|\delta X_{i,j}(0)\right|}, \tag{3-38}$$

where

$$\delta X_{i,j}(0) = X(t_i) - X(t_j), \tag{3-39}$$

$$\delta X_{i,j}(\Delta t) = X(t_i + \Delta t) - X(t_j + \Delta t) \tag{3-40}$$

for the following conditions:

1. $X(t_i)$ is the point of the fiducial trajectory $\phi_t'[X(t_i)]$ having $t = t_i$, $X(t_0) = [x(t_0),...,x(t_0 + (D-1)\tau)]^T$, T denotes the transverse, and $X(t_j)$ is a properly chosen vector adjacent to $X(t_i)$ in the phase space.
2. $\delta X_{i,j}(0) = X(t_i) - X(t_j)$ is the displacement vector t_i i.e., a perturbation of the fiducial order at t_i, and $\delta X_{i,j}(\Delta t) = X(t_i + \Delta t) - X(t_j + \Delta t)$ is the evolution of this perturbation after time Δt.
3. $t_i = t_0 + (i-1)\Delta t$ and $t_j = t_0 + (j-1)\Delta t$, where $i \in [1, N]$ and $j \in [1, N]$ for $j \neq i$.
4. Δt is the evolution time for $\delta X_{i,j}$ (the time provided for $\delta X_{i,j}$ to evolve in phase space). If the evolution time Δt is given in seconds, then the Lyapunov exponent is measured in bits/sec.
5. t_0 is the initial time point of the fiducial trajectory and coincides with the time point of the first data in the data segment of analysis. In the estimation of L, for a complete scan of the attractor, t_0 should move within $[0, \Delta t]$.
6. N_a is the number of local $L_{\max}$'s that will be estimated within a duration T data segment. Therefore, if t_s is the sampling period of the time domain data, then $T = (N-1)t_s = N_a \Delta t + (D-1)\tau$.

The method proposed by Iasemidis et al. (Iasemidis et al., 1999) was used to estimate the short term maximum Lyapunov exponent (STLmax). This method is a modification of Wolf's algorithm (Wolf et al., 1985). The measure is denoted as "short term" to distinguish it from the variants used to study autonomous dynamical systems. Modification of Wolf's algorithm is

necessary to enhance STLmax estimate robustness to transients in small data segments such as interictal spikes. The main modification is in the replacement vector searching procedure along the fiducial trajectory. One of the most crucial parameters affecting STLmax's ability to distinguish interictal from preictal states is the adaptive estimation in time and phase space of the magnitude bounds of the candidate displacement vector (Iasemidis 1999), though evolution time Δt, and the angular separation $V_{i,j}$ between the evolved displacement vector $\delta X_{i-1,j}(\Delta t)$ and the candidate displacement vector $\delta X_{i-1,j}(0)$ are important components as well (Frank et al., 2005).

The modifications proposed by Iasemidis and Sackellares (1991) can be summarized as follows:

1. To help ensure that L is a reliable estimate of STL_{max}, the candidate vector $X(t_j)$ should be chosen such that the previously evolved displacement vector $\delta X_{i-1,j-1}(\Delta t)$ is nearly parallel to the candidate displacement vector $\delta X_{i,j}(0)$, that is,
$$\left|V_{i,j}\right| = \left|\left\langle \delta X_{i,j}(0), \delta X_{i-1,j-1}(\Delta t)\right\rangle\right| \le V_{\max} \tag{3-41}$$
where V_{max} should be relatively a small value and $\left|\langle \gamma, \theta \rangle\right|$ denotes the absolute value of the angular separation between two vectors γ and θ in phase space.
2. Also, $\delta X_{i,j}(0)$ should also be relatively small in magnitude. This constraint helps avoid computer overflow in the future evolution within very chaotic regions and also reduces the probability of starting up with points on separatrices (Wolf et al., 1986). Mathematically, this corresponds to,
$$\left|\delta X_{i,j}(0)\right| = \left|X(t_i) - X(t_j)\right| \le \Delta_{\max}, \tag{3-42}$$
where $\Delta_{\max}$ takes on a small value.
Thus, the parameters involved in the estimation of L are:
(i) The embedding dimension p and the time lag τ for the reconstruction of the phase space
(ii) The evolution time Δt
(iii) The constraint parameters for selecting $X(t_j;\ V_{\max}$ and $\Delta_{\max})$
(iv) The duration of the data segment T

It is worth nothing that since only vector differences are involved in the estimation of L, any direct current (DC) present in analyzed data segment does not influence the value of L. In addition, only vector difference ratios participate in the estimation of L. Thus, L is not influenced by data scaling (provided the parameters involved in the estimation procedure, i. e. $\Delta_{\max}$, are

expressed in values relative to the scale of each analyzed data segment). Both of the above points are consistent with the fact that *L* is related to the entropy rate of the data (Palus et al., 1993).

Selecting D and τ. The selection of the embedding dimension D is such that the dimension of the epileptic attractor in phase space is clearly defined. For an epileptic attractor, $v \approx 3$ (Iasemidis et al., 1988, 1990; Iasemidis, 1991). Thus, according to Takens theorem a value of $D \geq (2 * 3 + 1) = 7$ can be viewed as adequate for the embedding of the epileptic attractor in the phase space. This value of D may not provide a large enough phase space to embed all interictal brain states, but has demonstrated success in detecting the transition of the brain toward the ictal stage (Iasemidis and Sackellares, 1991).

The parameter τ should be small enough to characterize the shortest signal changes (i.e., highest frequency component) in the data. However, τ should be large enough to result in the maximum feasible independence between the vectors components in the phase space (with the method of delays). These two conditions are typically addressed by selecting τ to be the first minimum of the mutual information or as the first zero of the time domain autocorrelation function of the data (Abarbanel, 1996). Since the time span (D-1) τ of each vector in the phase space theoretically represents the duration of a system state, (D-1) τ has been recommended to be (at the greatest) equal to the period of the maximum (or dominant) frequency component in the data (Abarbanel, 1996). As an example, a sine wave (or a limit cycle) has $v = 1$, then $D = 2 * 1 + 1 = 3$ is required the phase space embedding and $(D-1)\tau = 2\tau$ should equal the sine wave's period. In such a case, the value of τ would then correspond to the Nyquist frequency of the sine wave. In addition, for the epileptic attractor the highest frequency considered is 70 Hz (as EEG data are often low-pass filtered at 70Hz) which would require a maximum τ of about 7 ms according to the above rationale for D = 3. However, since a typical epileptic attractor (i.e.,

during the ictal period) in temporal lobe epilepsy has described to have a maximum dominant frequency of about 12 Hz (Iasemidis and Sackellares, 1991), according to the above rationale, an adequate τ value for phase space reconstruction of the epileptic attractor is (7 - 1) $\tau \approx 84$ ms, and thus, τ should be about 14 ms (for additional details see Iasemidis and Sackellares, 1991).

Selecting Δt. If the evolution time Δt is too large, the folding process within the attractor distorts L. If Δt is too small, $\delta Xi,j(0)$ may not follow the direction of the maximum rate of information change. One option is to obtain Δt as a fraction of time-delay mapping of the maximum frequency component of interest in the data, f_0. Specifically, the Δt is usually chosen to correspond to $0.5*f_0$ (Iasemidis and Sackellares, 1991). Therefore, according to the previous discussions about the selection of D and τ , $\Delta t \approx ((D - 1)\tau)/2$, which results in $\Delta t \approx 42$ ms which is within a range that can distinguish the ictal state from the pre-ictal state (Iasemidis and Sackellares (1991).

Selecting Δ_{max}. In Wolf's algorithm (1986), Δ_{max} is selected as

$$\Delta_{\max} = \max_{i,j} \left| \delta X_{i,j}(0) \right| \tag{3-43}$$

where j = 1,…,*N* and i = 1,…,N_a

Thus, Δ_{max} represents the global maximum distance between any two phase space vectors in a segment of data. This value suffices as long as the data is stationary and distributed relatively uniformly in phase space. Rarely is this the case with real data, especially with the brain's electrical activity which is strongly nonstationary and nonuniform (Barlow et. al, 1985; Feber et. al, 1987; Jansen and Cheng, 1988). Such statistical fluctuations combined with noise may adversely influence the predictive power of STLmax (Lai et al., 2003, 2004). Thus it is essential to perform a searching procedure modification in order to locate the proper $X(t_j)$. The first step is obtain an adaptive estimation of Δ_{max} for each point $X(t_i)$ as

$$\Delta_{i,\max} = \max_{j} \left| \delta X_{i,j}(0) \right|, \tag{3-44}$$

where j = 1,…,*N*. Estimating Δ_{max} in this manner can help compensate for the nonuniformity of phase space (Δ_{max} is now a spatially local quantity of the phase space at a point $X(t_i)$). Another technique for managing nonstationary data is to estimate Δ_{max} with a temporal constraint on top of the spatial constraint. From this perspective, Δ_{max} is

$$\Delta_{i,\max} = \max_{IDIST_1 < |t_i - t_j| < IDIST_2} \left| \delta X_{i,j}(0) \right|; j \neq i \tag{3-45}$$

for which

$$IDIST_1 = \tau \tag{3-46}$$

$$IDIST_2 = (D-1)\tau \tag{3-47}$$

where $IDIST_1$ and $IDIST_2$ upper and lower bounds for $\left| t_i - t_j \right|$, which help enforce temporal constraints when searching for a maximum spatial distance. In other words, these parameters establish a neighborhood in time around each point in the fiducial trajectory for the estimation of the parameter $\Delta_{i,max}$, which establishes a spatial search neighborhood around this point in the phase space. Thus, the search for $\Delta_{i,max}$ is always made temporally about the state $X(t_i)$ and its changes within a period of the time span (D - 1) τ of a state. According to the previous formulae, the values for the parameters involved in the adaptive estimation of $\Delta_{i,max}$ for the neural state classification studies are: $IDIST_1$ = τ = 14 msec and $IDIST_2$ = (D - 1) τ ≈ 84 msec.

Selecting V_{max}. Starting with an initial $V_{max,initial}$ = 0.1 rad, if a replacement vector $X(t_j)$ is not found with $0 \leq \left| V_{i,j} \right| < V_{max,initial}$ and $\left| \delta X_{i,j}(0) \right| < 0.1 * \Delta_{max}$, the bound is relaxed for $\left| \delta X_{i,j}(0) \right|$. At this point the process is repeated with bounds up to 0.5* Δ_{max}. If it is not successful, we relax the bounds for $\left| V_{i,j} \right|$ by doubling V_{max} and then repeat the process with bounds for V_{max} up to 1

rad. It should be noted that values of V_{max} larger than 0.8 rad did not occur in the reported results (Iasemidis and Sackellares, 1991). If V_{max} does grow this large, the replacement procedure halts, a local $L(t_i)$ is not estimated at time t_i the entire procedure beings again at the next point in the fiducial trajectory.

Selecting $X(t_j)$. It is important that the replacement vector $X(t_j)$ should be spatially close to X(ti) in phase space (with respect to angle deviation and magnitude), yet with sufficient temporal distance from $X(t_i)$ to allow selecting $X(t_j)$ from a nearby (but not the same) trajectory. Otherwise, by replacing one state with one that shares "too many" common components would lead to a false underestimation of L. The arguments described above are represented by the following expressions:

$$0 \le \left|V_{i,j}\right| < V_{i,j,initial} = 0.1rad \tag{3-48}$$

$$b\Delta_{i,\max} \le \delta X_{i,j}(0) \le c\Delta_{i,\max} \tag{3-49}$$

$$\left|t_i - t_j\right| > IDIST_3 \approx (D-1)\tau \tag{3-50}$$

The parameter c at a value of 0.1 and increases with a step of 0.1 up to 0.5 in order to locate a replacement vector $X(t_j)$ satisfying (3-48) through (3-50). The parameter b (which must be less than parameter c) is used to account for possible noise contamination of the data. Thus, b is the distance below which the estimation of L is considered to be inaccurate. A value of b = 0.05 provided is recommended (Wolf et al., 1985; Iasemidis and Sackellares, 1991). To clarify, the temporal bound IDIST2 should not be confused with the temporal bound IDIST3. The variable IDIST2 places an upper temporal bound for locating an appropriate $\Delta_{i,max}$ at each point $X(t_i)$, whereas IDIST3 is a lower temporal bound for locating an appropriate $X(t_j)$ within a $\Delta_{i,max}$ spatial distance from $X(t_i)$.

Selecting T. For data obtained from a stationary system state, the time duration T of the analyzed data segment may be large for estimating of L. For nonstationary data, there are two competing requirements: T is desired to be as small as possible to provide local dynamic information yet the algorithm requires a minimum length of the data segment to stabilize the STLmax estimate. Previous studies have deemed that for 200 Hz, a window of 2048 points (corresponding to 10.24 seconds) is a sufficient length for the algorithm to converge and yet is able to distinguish the two extreme cases (pre-ictal and ictal) (Iasemidis, 1991; Iasemidis and Sackellares, 1991; Iasemidis et al., 2000). These studies also point to the IDIST2 parameter as being the most critical parameter in the above algorithm.

The STLmax seizure prediction algorithm identifies progressively increasing similarity in the information production rate (termed "dynamical entrainment") between critical electrode sites prior to seizures. In other words, long before the onset of an epileptic seizure, critical brain sites begin to display similar dynamics. The progressive STLmax convergence prior to a seizure is thought to reflect dynamical dependence because 1) the critical sites share direct or indirect anatomical connections that are conducive to physiologic interaction, and 2) occurrence of the progressive STLmax entrainment prior to a seizure (Iasemidis et al., 2004). This concept is indirectly supported by the therapeutic effect of neurostimulation therapies such as ECT-induced seizures and the potential long-term anticonvulsant effect (for a recent review of ECT therapy see Taylor, 2007). A potential physiologic basis for brain resetting could be a release of neuromodulators after seizures (Gwinn et al., 2002). In addition, Iasemidis et al. (2004) suggest that the lack of an observed time-reverse of the resetting phenomenon is consistent with hysteresis, a characteristic observed in epilepsy as well as other dynamical disorders (Lopes Da Silva et al., 2003).

Mean Angular Frequency in Phase Space

One modification of the Lyapunov exponent was proposed by Iasemidis to measure a quantity related to the STLmax measure (Iasemidis et al., 2002, 2003). The mean angular frequency in phase space ($\overline{\Omega}$) measure quantifies the angular frequency of the phase space evolution of two nearest neighbor points relative to a reference point. Conceptually, this measure quantifies the rate of change in stability of a dynamical system. The measure is related to the Lyapunov exponent, which measures the local stability of a system. Consider the vectors $X(t_i)$ and $X(t_i + \Delta t)$ as two states in phase space separated by the time delay Δt. The difference in phase between these two states in phase space is $\Delta\Phi_i$ (Iasemidis et al., 2002). The mean ($\Delta\Phi$) of the local phase changes $\Delta\Phi_i$ in state space is denoted as:

$$\Delta\Phi = \frac{1}{N_\alpha} \cdot \sum_{i=1}^{N_\alpha} \Delta\Phi_i \,, \tag{3-51}$$

where N_α is the total number of phase differences calculated from the evolution of $X(t_i)$ to $X(t_i + \Delta t)$ in state space, according to:

$$\Delta\Phi_i = \left| \arccos \frac{X(t_i) \cdot X(t_i + \Delta t)}{\|X(t_i)\| \cdot \|X(t_i + \Delta t)\|} \right| . \tag{3-52}$$

The mean angular frequency in phase space $\overline{\Omega}$ can then be defined as:

$$\overline{\Omega} = \frac{1}{\Delta t} \Delta\Phi \,. \tag{3-53}$$

If the units of Δt are seconds, $\overline{\Omega}$ has units of radians per second (an alternative is to divide by 2π resulting in units of $\sec^{-1}$ or Hz for expression of rate of system state change). Figure 3-3 illustrates the concept of the phase change measure as it is applied to data with the same phase

space mapping with STLmax where $\Delta t = k \times dt$ is the evolution time allowed for the vector $X(t_i)$ to evolve to $X(t_i + \Delta t)$ where *dt* is the sampling period of the original time series.

Data Mining

Data mining refers to the application of algorithms to extracting patterns from and modeling large databases (Flexer et al., 2000) and provides reasonable tools for extracting useful patterns in datasets from complex systems. Data mining techniques have demonstrated successful detection of scalp EEG patterns which may be difficult for the human eye to visualize (Acir et al., 2005; Chaovalitwongse et al., 2006; Thulasidas et al., 2006). Often such algorithms or the patterns they reveal can be utilized in real time applications, providing a basis for real-time EEG analysis tools (Chaovalitwongse et al., 2005; Iasemidis et al., 2005; Sackellares et al., 2006; Thulasidas et al., 2006).

Typical data mining tasks are described by the following categories:

- Dimensionality reduction: the process of mapping of a high-dimensional data set into a lower-dimensional space in order to facilitate data exploration
- Reduction of noise: correction or removal of measurement artifacts and significantly atypical samples from the data set.
- Clustering: creation of a partition of a given set of samples into classes according to similarities that are relevant to the particular analysis

One of the more important instances of dimensionality reduction is called feature selection. This process results in the generation of a lower-dimensional space by eliminating a subset of dimensions from the original space. Feature selection is an important process for reducing computation time as well potentially improving accuracy. Reduction of noise is an important procedure which is universally applied in applications spanning numerous disciplines. Finally, clustering refers to a broad class of data mining applications which are highly relevant to the work done in this dissertation.

Clustering

Clustering problems can be subdivided into unsupervised or supervised clustering. Unsupervised learning methods divide data into natural groupings. Supervised clustering methods are also referred to as classification, which is described later in this chapter. The following represents a non-exhaustive listing of some basic clustering techniques.

K-means clustering

The k-means algorithm is one of the most basic and commonly applied cluster algorithms. The method clusters a set of N data points into K partitions based on the similarity between the pattern and the cluster centers, where K< N (Jain et al., 1999). A random initial partition is selected after which the patterns are repeatedly reassigned some convergence (e.g. squared error threshold) is achieved.

The k-means algorithm is especially attractive due to its O(n) complexity as well as its ease of implementation (Jain et al., 1999). One deficit of this method is a high sensitivity to initial conditions, which can result in convergence at local minima.

Biclustering

Biclustering is a data mining technique which provides the ability to not only cluster data samples, but also the data features. The procedure is performed in a manner that each class of data features created within the biclustering is related to a class of data samples by a particular property that distinguishes it from samples in other classes and is said to be the "cause" of its creation. In other words, the biclusters are subsets of samples which exhibit similar characteristics across a subset of features, or vice versa.

The biclustering methodology has been used extensively in numerous biomedical research applications such as DNA microarray analysis and drug design as well as others (Madeira and Oliveira, 2004; Shamir et al., 2005; Busygin et al., 2006). The output of biclustering algorithms

is especially useful for feature extraction, a crucial procedure in many biomedical studies. Analogous to the ability of biclustering to reveal up regulation and down regulation of genes in dna microarray datasets, biclustering is a data mining tool well-suited for revealing spatial and temporal subsets of EEG features that are indicative of neural states (Busygin, 2007).

A dataset containing *m* features and *n* samples is arranged as a rectangular matrix $A = (a_{ij})_{m \times n}$, where a_{ij} represents the *i*-th feature of the *j*-th sample. Consider the assignment of the samples into classes as follows

$$S_1, S_2, ..., S_r, S_k \subseteq \{1, ..., n\}, k = 1, ..., r,$$
$$S_1 \cup S_2 \cup ... \cup S_r = \{1, ..., n\},$$
$$S_k \cap S_l = \varnothing, k, l = 1, ..., r, k \neq l$$

This method intends to assign samples such that samples from the same class share specific common properties. Similarly, a feature *i* may be assigned to one of the features classes

$$F_1, F_2, ..., F_r, F_k \subseteq \{1, ..., m\}, k = 1, ..., r,$$
$$F_1 \cup F_2 \cup ... \cup F_r = \{1, ..., m\},$$
$$F_k \cap F_l = \varnothing, k, l = 1, ..., r, k \neq l$$

in such a manner that the features of class F_k are "responsible" for the creation of the class of samples S_k. Such a simultaneous classification of samples and features is termed biclustering.

Definition 1: *A biclustering of a dataset is a group of sample / feature pair subsets* $B = ((S_1, F_1), (S_2, F_2), ..., (S_r, F_r))$ *such that the group* $(S_1, S_2, ..., S_r)$ *forms a partition of the set of samples, and the collection* $(F_1, F_2, ..., F_r)$ *forms a partition of the set of features. A pair* (S_k, F_k) *will be called a bicluster.*

Various criteria may be used for relating sample clusters to feature clusters. Most commonly, it is required that the subset corresponding to a bicluster is either includes a certain

amount of values above the mean of the dataset, or has a lower variance than that of the dataset. In general, it is acceptable for biclustering to rely on any type of common pattern among the elements of the bicluster.

Consistent biclustering: The following biclustering framework utilizes feature selection based on 0-1 fractional programming (Busygin, 2005). Let each sample *j* be arbitrarily assigned to one of the classes $S_1, S_2, ..., S_r$. A 0-1 matrix $S = (s_{jk})_{n \times r}$ is introduced such that $s_{jk} = 1$ if $j \in S_k$ and $s_{jk} = 0$ otherwise. The sample class centroids are represented by the matrix $C = (c_{ik})_{m \times r}$:

$$C = AS\left(S^T S\right)^{-1} \tag{3-54}$$

whose *k*-th column represents the centroid of class S_k.

Consider a row *i* of the matrix C. Each element in the row is the mean expression of the *i*-th feature in one of the sample classes. Each feature is then assigned to the class where it is among the largest number of features with a similar value as is shown in figure 3-4. Let the *i*-th feature be classified as a member of the class $\hat{k}$ with the maximal value $c_{i\hat{k}}$:

$$i \in F_{\hat{k}} \Rightarrow \forall k = 1,...,r, k \neq \hat{k} : c_{i\hat{k}} > c_{ik} \tag{3-55}$$

Using the acquired feature classification $(F_1, F_2, ..., F_r)$, let a classification of samples be constructed using the same principle of maximal average expression and test whether this arrives at the same classification as when using features. This is performed by constructing a 0-1 matrix $F = (f_{ik})_{m \times r}$ such that $f_{ik} = 1$ if $i \in F_k$ and $f_{ik} = 0$ otherwise. The feature class centroids can be represented by a matrix $D = (d_{jk})_{n \times r}$:

$$D = A^T F\left(F^T F\right)^{-1}, \tag{3-56}$$

whose *k*-th column represents the centroid of the class F_k. The requirement for sample classification is

$$j \in S_{\hat{k}} \Rightarrow \forall k = 1,...,r, k \neq \hat{k} : d_{j\hat{k}} > d_{jk} \qquad (3\text{-}57)$$

The feature selection and supervised biclustering framework proposed in (Busygin, 2005) is grounded in the following definition.

Definition 2: *A biclustering B will be called consistent if both relations (3-55) and (3-57) hold, where the matrices C and D are defined as in (3-54) and (3-56).*

Unlike other biclustering schemes, this definition of consistent biclustering is justified by the fact that consistent biclustering implies class separability with convex cones (Busygin, 2005).

Theorem 1: *Let B be a consistent biclustering. Accordingly, there exist convex cones* $P_1, P_2, ..., P_r \subseteq \Re^n$ *such that every sample from* S_k *belongs to the cone* P_k *and no other sample belongs to it,* $k = 1,...,r$.

Similarly, there exist convex cones $Q_1, Q_2, ..., Q_r \subseteq \Re^n$ *such that every feature from* F_k *belongs to the cone* Q_k *and no other feature belongs to it,* $k = 1,...,r$.

It follows from the theorem of conic separability that convex hulls of the classes are separated and thus do not intersect. The term *biclustering-admitting* is used to describe a dataset for which some consistent biclustering exists. In addition, the data set will be called *conditionally biclustering-admitting* with respect to a given (partial) classification of certain

samples and / or features if a consistent biclustering exists which preserves the given (partial) classification.

Given a training set $A = \left(a_{ij}\right)_{m\times n}$ where the samples are assigned to classes $\left(S_1, S_2, ..., S_r\right)$ the corresponding classification of features can be constructed according to expression (3-55). If the obtained biclustering is not consistent, features are then excluded from the dataset so that the biclustering with respect to the cropped feature set is consistent.

Let a vector of 0-1 variables $x = \left(x_i\right)_{i=1,...,m}$ be introduced where the *i*-th feature is selected if $x_i = 1$ and is not selected otherwise. When only the selected features are applied, the condition of biclustering consistency in expression (3-57) becomes

$$\frac{\sum_{i=1}^{m} a_{ij} f_{i\hat{k}} x_i}{\sum_{i=1}^{m} f_{i\hat{k}} x_i} > \frac{\sum_{i=1}^{m} a_{ij} f_{ik} x_i}{\sum_{i=1}^{m} f_{ik} x_i}, \forall j \in S_{\hat{k}}, \hat{k}, k = 1,...,r, \hat{k} \neq k \,. \tag{3-58}$$

The expressions in (3-58) are utilized as constraints of a feature set optimization problem. Though the objective function may take on various functions of x depending on the desirable properties of the features, a general choice is to aim for the maximal number of features. This formulation helps minimize the amount of lost information provided during training. In this scenario, the objective function is expressed as

$$\max \sum_{i=1}^{m} X_i \tag{3-59}$$

Expressions (3-58) and (3-59) comprise a specific type of fractional 0-1 programming problem which can be solved using the approach laid out in (Busygin et al., 2005).

Data Classification

Classification can be described as the process of categorizing an unknown dataset. First, a so-called training set of samples wherein sample classes are known a priori is provided to the algorithm. The pre-classified training data is used to train the algorithm to recognize the specified patterns. Training is typically an iterative process where the parameters affecting classification are systematically adjusted until the classification error bound is decreased below a specified threshold. This specific process is referred to as machine learning.

Machine learning

Machine learning refers to a collective group of methods which are utilized to enable computers to "learn". There have been very successful implementations such as finding genes in a DNA sequence, filtering email, financial analysis, detecting or recognizing objects in machine vision, language processing, and medical diagnosis (Cristianini and Shawe-Taylor, 2000). Many of these applications rely on pattern recognition which is essentially concerned with object classification based on characteristics. An object's characteristics or features can be described as the qualitative and quantitative measures which can distinguish it from other objects. The amount of similarity between two objects can be quantified as a function of the differences in the objects' set of features. Object similarity can be used as a basis for grouping objects into classes. Please note, while the content of a person's character may be a useful feature of a person, the color of a person's skin is not a good feature for classification. Classes may be represented in various ways such as approximation functions or functions that define borders between classes. Arranging objects into classes based on their location relative to these functions is referred to as classification.

Machine learning from the classification perspective can be organized into two main categories. Supervised learning refers to the process where a system learns from an example data

set in the form of input/output pairs. In such an example dataset, the input is typically a vector of representing an object's features and the output is the object's class label. A set of objects each with a corresponding feature vector and class label is more formally referred to as a training set. The training set is used to derive a classification function. Once trained, a classification function is capable of predicting an object's label. The term "supervised" stems from the nature of the training scheme where the training set's object labels are determined by an outside source and provided as an input. Therefore, this training method requires supervisory guidance to train the classifier. Unsupervised learning is the other machine learning category where objects are not labeled with any class information a priori. Thus, unsupervised learning forms object classes based on inherent feature similarities determined during training.

Supervised learning systems applications have found extensive use in biological applications (see Tarca et al., 2007 for a review). Briefly, some biological and medicinal applications include detection of cancer prone tissues, mapping tissue gene expression profiles to disease groups, and protein folding based on the DNA sequence. In addition, a broad range of machine learning algorithms have provided a means for successful neural state classification and neurological disorder diagnosis using EEG signal features (Flexer, 2000; Lotte et al., 2007; Seref et al., 2007).

There are several well-known machine learning algorithms, including decision trees, neural networks, and support vector machines. These base algorithms can be used in combination with other algorithms for improved accuracy often at the cost of hindered performance. One of the most widely used measures in classification problems is the Mahalanobis distance metric.

Mahalanobis distance classification

Mahalanobis distance is a statistical distance measure which factors in correlations between variables. The mahalanobis distance is a useful method of quantifying similarity of an

unknown sample set to a known sample set. The square of the mahalanobis distance measure has been applied to the classification of neural states using EEG signal patterns (Scher et al., 2003; Le Van Quyen et al., 2005; Piccini et al., 2005). The squared mahalanobis distance, $D^2_{ref,t}$, between a 25-dimensional EEG data point vector X(t) where

$$X(t) = \left(X_{ch1,t}, X_{ch2,t}, X_{ch3,t}, ..., X_{ch25,t},\right)^T \tag{3-60}$$

and the centroid of the reference class μ_{ref} where

$$\mu_{ref} = \left(\mu_{ch1}, \mu_{ch2}, \mu_{ch3}, ..., \mu_{ch25}\right)^T \tag{3-61}$$

is equal to:

$$D^2{}_{ref,t} = \left(X(t) - \mu_{ref}\right)^T C_{ref}^{-1} \left(X(t) - \mu_{ref}\right) \tag{3-62}.$$

The C_{ref} term is the covariance matrix for the reference class.

The mahalanobis distance measure $D^2_{comparison,t}$ refers to distance between the same EEG data point, X(t), and the centroid of the comparison class, $\mu_{comparison}$. The EEG data point X(t) is assigned to the class with the closest centroid (e.g. the class from which the point is at the minimum Mahalanobis distance) to X(t) (Le Van Quyen et al., 2005). If the EEG data point is equidistant between the two classes, the point is considered misclassified. The accuracy of the minimum Mahalanobis distance classifier is equal to the number of correctly classified points divided by the total number of points.

Support vector machines

Support Vector Machines (SVMs) are a class of data classification algorithms first introduced by Vapnik and Lerner (1963) which are used to model and classify large volumes of multivariate data. The SVM algorithm determines the optimal separating hyper surface between two multidimensional datasets (Burgess et al., 1998). SVMs have been demonstrated success in numerous biomedical applications such as magnetic resonance imaging (MRI), functional MRI

(fMRI), positron emission tomography (PET), and Single-photon emission computed tomography (SPECT) (Seref et al., 2007) in addition to applications where neural states were classified from EEG data (Acir et al., 2005; Chaovalitwongse et al., 2006; Lehmann et al., 2007; Thulasidas et al., 2006).

The SVM formulation for linearly separable data quantifies the distance from the hyper surface for each data point in the positive class and each data point in the negative class. In this context, the term "margin" will refer to the distance between the separating hyper surface and the nearest point for a class. The margin of the function output is referred to as the functional margin. The geometric margin is the functional margin of a normalized weight vector. Hence the geometric margin can be optimized by fixing the functional margin to be equal to one and then minimizing the norm of the weight vector (Cristianini and Shawe-Taylor, 2000). If w is the weight vector for a functional margin of distance equal to one from a positive (reference) class point, x+ and a distance equal to one from a negative (comparison) class point, x-, then the geometric margin can be determined as follows. For a functional margin equal to one:

$$\left\langle w, x^{+} \right\rangle + b = +1 \tag{3-63}$$

$$\left\langle w, x^{-} \right\rangle + b = -1 \tag{3-64}.$$

To calculate the geometric margin, w must be normalized. The geometric margin, γ, is then the functional margin of the resulting classifier

$$\begin{aligned} \gamma &= \frac{1}{2}\left(\left\langle \frac{w}{\|w\|_2}, x^{+} \right\rangle - \left\langle \frac{w}{\|w\|_2}, x^{-} \right\rangle \right) \\ &= \frac{1}{2\|w\|_2}\left(\left\langle w, x^{+} \right\rangle - \left\langle w, x^{-} \right\rangle \right) \\ &= \frac{1}{\|w\|_2} \end{aligned} \tag{3-65}.$$

Thus, the interclass margin is maximized by

$$\min_{w,b} \|w\|_2 \tag{3-66}$$

$$\text{subject to} \qquad y_i\left(\left\langle w, x^+ \right\rangle + b\right) \geq 1 \qquad \forall i = 1, \cdots, n \tag{3-67}$$

where the constraints are that all points are properly classified for positive and negative classes, as stated in (3-67). For non-separable data, the objective function (3-68) combines the term for maximizing interclass margin with a term for minimizing misclassification error (Cristianini and Shawe-Taylor, 2000).

$$\min_{w,b,\xi} \|w\|_2 + C\sum_{i=1}^{n} \xi_{2,i} \qquad \forall i = 1, \cdots, n \tag{3-68}$$

$$y_i\left(\left\langle w \cdot x_i \right\rangle + b\right) \geq 1 - \xi_i \qquad \forall i = 1, \cdots, n \tag{3-69}$$

$$\xi_i \geq 0 \qquad \forall i = 1, \cdots, n \tag{3-70}$$

The cost term, C, in (3-68) is the weight assigned to the error. Expressions (3-69) and (3-70) represent the constraints that each misclassified point is assigned a linear penalty (slack variable) and that all slack variables are non-negative, respectively. An example of such a soft margin classifier is shown in figure 3-5.

The SVM formulation in equations (3-68), (3-69), and (3-70) utilizes a linear hyper surface for discrimination. A common practice for improving separation accuracy is to perform a transformation to remap the data from input space into feature space using a kernel function. The inner product is then performed on the transformed feature space data (see equation (3-71)).

$$K\left(x_i, x_j\right) = \left\langle \phi\left(x_i\right), \phi\left(x_j\right) \right\rangle \tag{3-71}$$

The concept of a kernel function is identical to that of phase space mapping. The purpose is to view the data in a transformed space to unmask patterns which may have been hidden in

input space. The radial basis function (RBF) is a standard choice as a kernel function in neuroscience applications (Acir and Güzelis, 2005; Bewernitz et. al., 2006; Lehmann et. al., 2007; Thulasidas et. al., 2006; Seref et al., 2006). The RBF function is expressed as

$$K\left(x_i, x_j\right) = \exp\left(-\frac{\left\|x_i - x_j\right\|^2}{\sigma}\right) \tag{3-72}$$

The SVM is trained using a set of data features with a known classification. The SVM's performance is measured in terms of the accuracy at which it is able to classify a test data set.

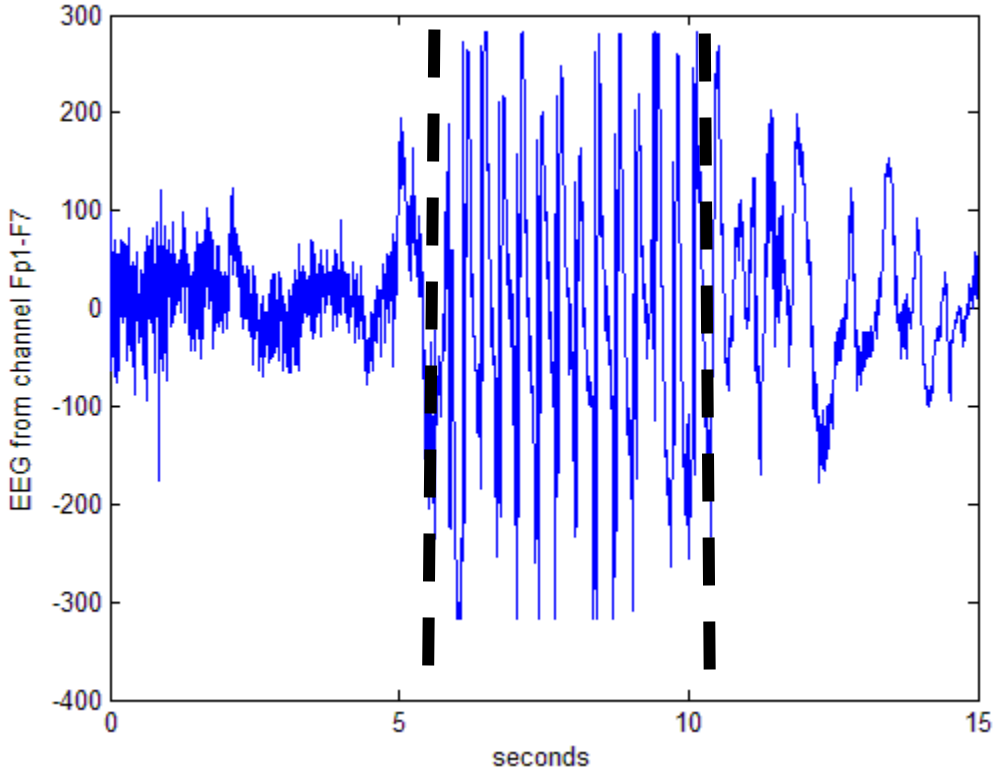

Figure 3-1. A 15 second segment depicting the 200 Hz EEG of an absence seizure viewed from channel Fp1-F7.

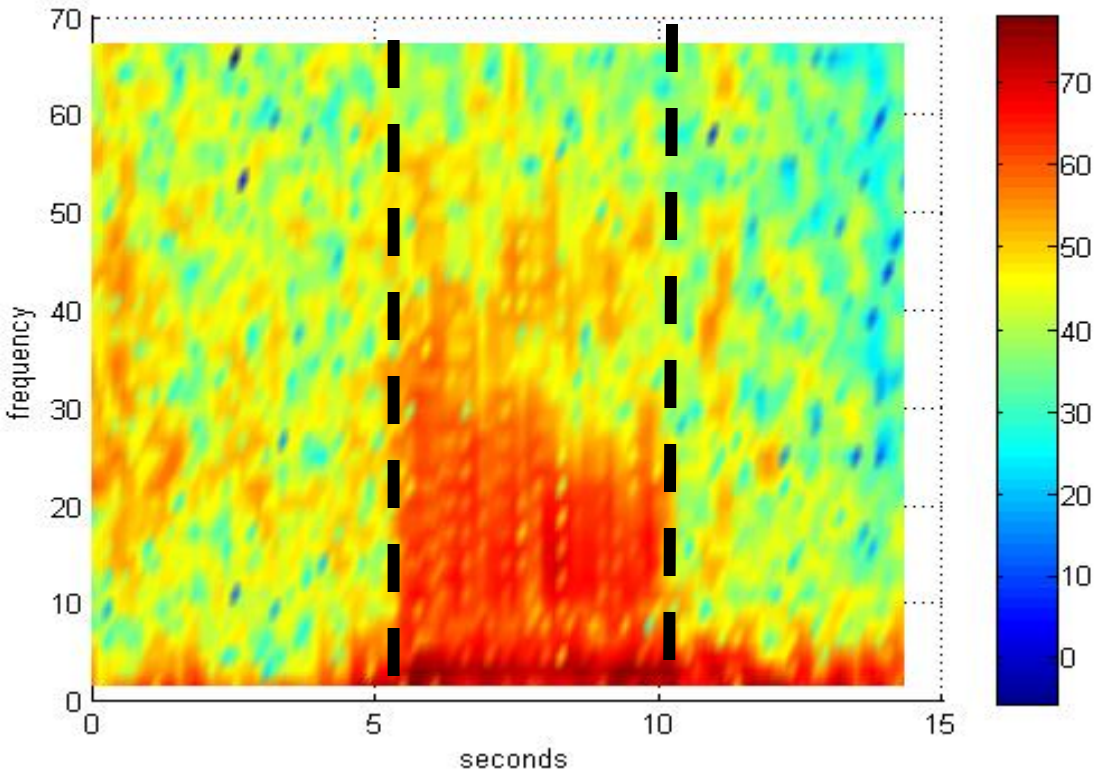

Figure 3-2. A 15 second segment depicting the spectrogram of an absence seizure viewed from channel Fp1-F7. The vertical lines represent the onset and offset of the seizure.

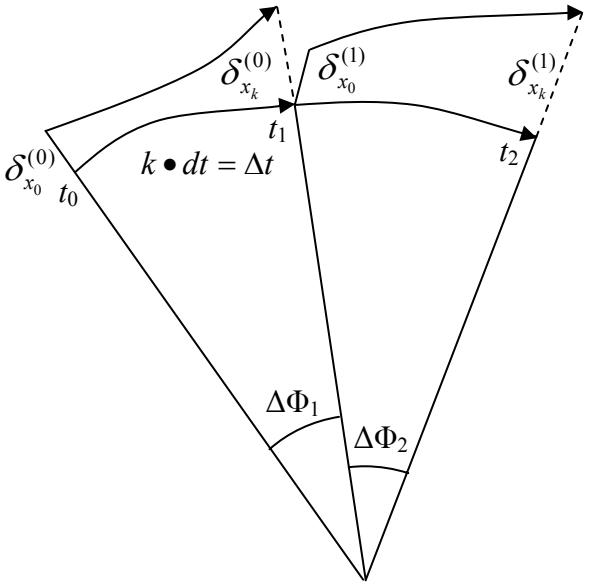

Figure 3-3. Example angular frequency evolution in phase space.

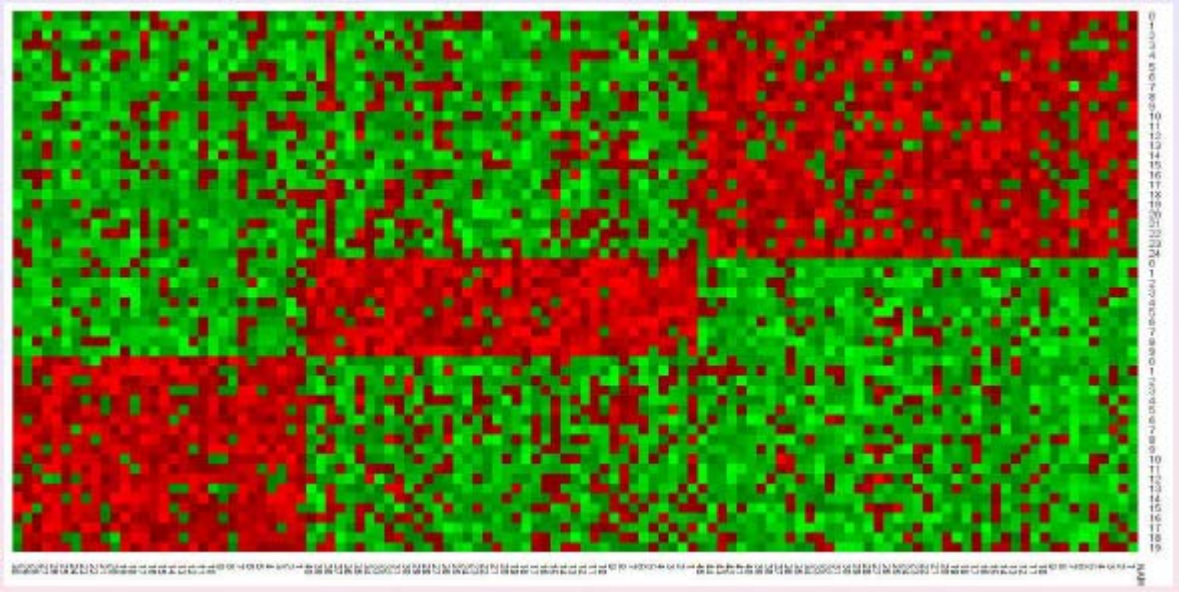

Figure 3-4. Biclustering result of a toy dataset. The dataset produced three distinct classes.

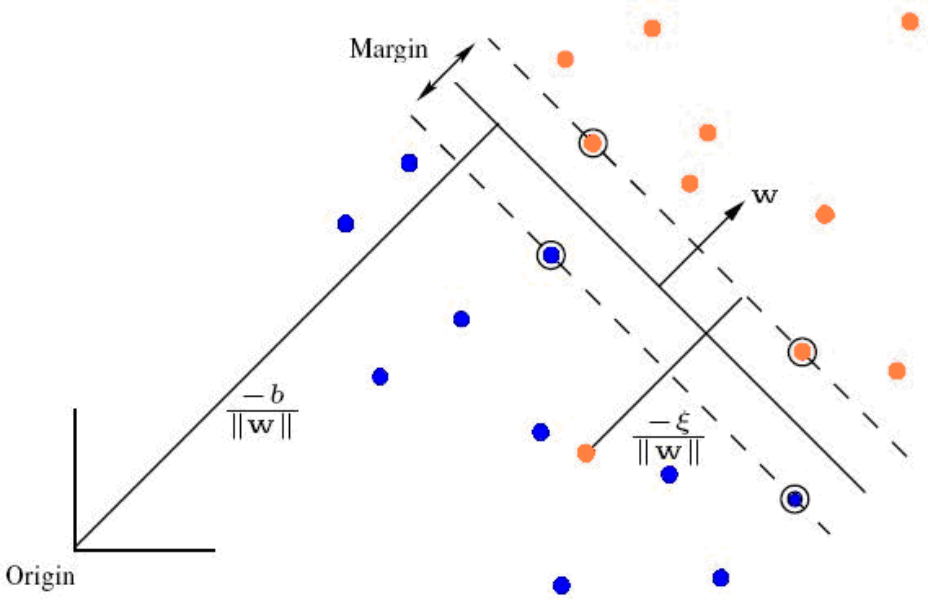

Figure 3-5. Linear hyperplane classifier applied to non-separable data.

CHAPTER 4
INVESTIGATION OF EEG BIOMARKER EXISTENCE FOR VAGUS NERVE STIMULATION THERAPY: A DATA MINING APPROACH

Patients with newly implanted vagus nerve stimulation (VNS) systems in VNS therapy ® undergo a calibration period of several months. With little knowledge of the mechanism of action (see chapter 2) or a rapid measure of efficacy, the current process of tuning VNS stimulation parameters in newly implanted patients is essentially based on the physician's experience and trial-and-error. This process consists of setting initial stimulation parameters then iteratively adjusting stimulation parameters based on patient reports of clinical efficacy (seizure frequency) and tolerability since the previous visit to the doctor. It is known that "high" settings for stimulation parameters (such as output current, frequency, and pulse width) are shown to result in greater seizure reduction than "low" settings (Ben-Menachem et. al, 1994), but there is no available means for determining the proper set of stimulation parameters for a particular patient without numerous visits to the neurologist. This period involves numerous medical check-ups to fine tune the electrical stimulation parameters based on clinical response. This sub-optimal adjustment method leaves the patient at risk of seizures and imposes financial burden. The purpose of this study is to address this problem using data mining analysis.

This chapter is organized as follows. First, the rationale for this study is introduced in terms of clinical relevance. Next, the experimental strategy is outlined and justified with examples from the literature. Afterwards, the four experiments comprising this chapter are presented in the following format: introduction, data description, experimental setup, results, and discussion. Finally, an overall conclusion is presented which comments on all the findings as a whole.

Motivation for VNS Therapy Improvement

It is desirable to establish a method to rapidly predict the efficacy of the various combinations of VNS parameters newly-implanted patients in order to mitigate doctor's visits and perhaps expedite the process of optimizing therapeutic efficacy. A first step towards this goal is to investigate the existence of a physiologic metric that is sensitive to the EEG stimulation parameters and then the patient's clinical response to VNS therapy. Such an effect could be present in the EEG signal.

EEG Markers for Treatment of Neurological Diseases and Disorders

The utility of electroencephalogram (EEG) markers in treatment of neurological disorders motivates the examination of this treatment modality in terms of EEG effect (see chapters 2 and 3 for additional details). Electroencephalographic markers have demonstrated robust utility for the diagnosis, treatment, and evaluation of treatment for epilepsy (Iasemidis et al.,1996; Pardalos et. al, 2003, 2004; Chaovalitwongse et al., 2005, 2006; Ding et al., 2007; Schevon et al., 2007) as well as other neurological disorders (Krystal et al., 1996, 1997, 2000; Asyali et al., 2007; Ding et al., 2007; Quintana et al., 2007). Specifically, there is has been an interest in the application of such analysis to the EEG signals of VNS patients to provide a better understanding of the therapy (Uthman et al., 2007). Recent studies have produced interesting findings of long-term VNS effects on epileptic interictal spikes (Koo, 2001), epileptiform sharp waves in the hippocampus (Olejniczak et al., 2001), interictal epileptiform discharges (Janszky et al., 2005; Santiago-Rodriguez and Alonso-Vanegas, 2006), gamma activity and desynchronization (Marrosu et al., 2005), and spectral content of sleep (Rizzo et al., 2004).

The effects on interictal epileptiform discharges such as the studies by Koo and Olejniczak et al. suggest the presence of brain dynamical changes and further motivate the desire to examine VNS-induced EEG changes from the perspective of nonlinear dynamics since the

existence dynamical changes are implied by changes in spiking patterns. In addition, no studies could be located which aimed to relate the EEG effects of VNS to the stimulation parameters.

Aside from long-term epileptiform effect (Koo, 2001) or effects observed in hippocampal depth electrodes (Olejniczak et al., 2001), the lack of readily-available short-term scalp electroencephalographic VNS effects reported in the literature (Hammond, 1992; Salinsky et al., 1993; Fisher et al., 1999; Koo, 2001; Rizzo et al., 2004; Marrosu et al., 2005), the benign non-invasiveness of scalp-EEG, state of the art techniques of modern knowledge discovery in database techniques (Flexer, 2000), and the potential for real-time application due to modern computer technology make EEG data mining analysis a desirable approach to studying VNS effect. These reasons motivate the current study which aims to identify electroencephalographic markers which are sensitive to VNS stimulation parameter configuration. If such electroencephalographic markers are identified, and if the electrographic markers are found to correlate with clinical efficacy then these findings could be applied to determine optimal VNS stimulation parameters on a patient-by-patient basis.

Modeling Brain Disorder Dynamics

One approach for studying the brain's behavior is to generate a mathematical model of some subset the brain's activity using observable quantities, such as EEG recordings. Such models provide a means to make predictions about the behavior of one or more sections of the brain in response to various inputs. Due to the high degree of complex neuronal interaction in the brain, direct models have only been achieved for small neuronal networks small brain structures (Breakspear, 2001; Chauvet and Berger, 2002). The enormous complexity of electrical brain signals often means exact modeling approaches are insufficient. The challenge of direct modeling is compounded by the fact that no consistent immediate or short-term VNS-induced effects have been identified in the raw EEG or its time-frequency profile (Salinsky et al., 1993;

Fisher, et al., 1999; Koo, 2001; Rizzo et al., 2004; Marrosu et al., 2005). However, suppression of epileptiform sharp waves in the hippocampus has been observed (Olejniczak et al., 2001). This provides motivation for searching for dynamical scalp-EEG effects of VNS.

However, in a complex system such as the brain, it is often difficult if not impossible to obtain exact knowledge of system governing the observed dynamical behavior. In such a case, an alternative method to exact modeling is to develop a macroscopic modeling approach based on observable measures of the system in its entirety, such as EEG signals (Iasemidis et al., 1996). Upon extraction of such information, it may be possible to generate useful empirical models of the system's global behavior.

One such modeling scheme treats epilepsy as a dynamic disorder which is a class of disorders characterized by a sudden qualitative change in dynamics in response to an endogenous factor or a clinical maneuver (Milton, 2000). From this perspective, epileptic symptoms occur as a result of modifications to underlying physiologic control system parameters (Mackey and Glass, 1977; Mackey and an der Heiden, 1982; Milton and Mackey, 1989; Belair et al., 1995; Milton and Black, 1995; Milton, 2000; Lopes Da Silva et al., 2003). Such changes may manifest, for example, as a qualitative change in dynamics corresponding to bifurcations in mathematical systems. The importance of identifying a dynamic disorder is that a treatment possibility can focus on manipulating underlying control parameters back into a range of healthy dynamics (Milton, 2000). An example of this is the epileptic seizure control strategy of Iasemidis et al. where the control focuses on maintaining a "healthy" range of STLmax t-index values (associated with seizure transition) by therapeutic intervention (Iasemidis et al., 2003; Good et al., 2004, 2005). An analogous scenario may apply to VNS calibration in newly-implanted patients where the VNS parameters are adjusted in order to elucidate a brain

dynamical response or "state" that has been previously established as indicative of desired and even optimal seizure protection. Thus, the achieved neural state as described by dynamical EEG responses associated with different stimulation parameters over time may serve as "marker" for VNS treatment and facilitate rapid determination of optimal VNS parameters. See figure 4-2 for a three-dimensional conceptual example of such a model.

The example in 4-2 utilizes three measures only for the sake of example. In actuality, a real model may utilize dozens or even hundreds of such EEG features. Determining which EEG measures should be used in such model is a challenging task indeed.

A common approach for revealing complex relationships among the features and samples from large a multidimensional dataset (such as an EEG recording) is to employ data mining methods. Data mining refers to the application of algorithms in order to extract patterns from complex databases (Flexer, 2000) and provides a means for identifying EEG features which may be sensitive to neural stimulation as well as neural stimulation parameters in the VNS implant. Previous work employing data mining techniques has demonstrated successful pattern detection from scalp EEG signals which is often difficult for the human eye to visualize (Iasemidis et al., 1996; Pardalos et al., 2003; Iasemidis et al., 2004; Acir et al., 2005; Iasemidis et al., 2005; Chaovalitwongse et al., 2006; Sackellares et al., 2006; Thulasidas et al., 2006). Thus, such an algorithm may be useful in the case of VNS therapy where short-term stimulation scalp EEG effects are not explicitly visible in the time or frequency domain (Hammond et al., 1992; Salinsky et al., 1993; Koo, 2001; Rizzo et al., 2004; Marrosu et al., 2005). Often such algorithms can be run in real time, providing a basis for an online EEG analysis tool (Sackellares et al., 1997; Chaovalitwongse et al., 2005; Iasemidis et al., 2005; Thulasidas et al., 2006).

The overall goal of this work is to investigate the existence of EEG feature patterns which may be related to clinical and biological aspects of a patient's VNS therapy. The underlying hypothesis of this work (stated as null) is "electroencephalographic effects in patients undergoing VNS therapy for epilepsy do not vary with differing VNS parameters". Expressing VNS-related effects in terms of scalp-EEG recordings is desirable considering its wide availability at medical facilities and utility in epilepsy diagnosis. Such EEG measures may one day find use as markers to help determine optimal VNS parameters more rapidly in newly-implanted patients.

Biclustering Analysis of EEG Dynamics in Patients undergoing VNS Therapy for Epilepsy

Biclustering is a useful method for determining the existence of supervised binary classifications in multivariate datasets. The outputs of biclustering are particularly valuable for feature extraction purposes which are a significant concern in many biomedical studies. One of the most common applications is establishing connections between syndromes (e.g., signs and symptoms in cancer) and their corresponding gene expression patterns (Cheng et al. 2000; Kluger et al., 2003; Yoon et al., 2005). The biclustering algorithm's ability to distinguish two predefined states makes it a potentially useful tool for characterizing EEG dynamical alterations associated with VNS activation using EEG features (such as STLmax) as an input.

Data Description

The scalp-EEG recordings utilized in this study were obtained from patients with functioning VNS implants for the treatment of epilepsy. The recordings were performed at the General Clinical Research Center (GCRC) in Shand's Hospital at The University of Florida. EEG was acquired under GCRC protocol # 614, Institutional Review Board (IRB) protocol #617-2004, "Neurophysiologic Measures of Vagus Nerve Stimulation". EEG data were obtained at 512 Hz sampling rate using 16-bit precision with a 0.16 Hz high pass filter and 105

Hz low pass filter hardwired into the amplifier. The dataset contained 25 scalp-EEG channels arranged in the standard international 10-20 system (see Fig. 4-3).

EEG channels included in the study were: Fp1, Fp2, F3, F4, C3, C4, P3, P4, O1, O2, F7, F8, T3, T4, T5, T6, A1, A2, Fz, Cz, Pz, Leye, Reye, Lmn, and Rmn ("mn" refers to an electrode placed on the mandibular notch positioned between the jaw bone and the skull, which provides information about the temporal lobe).

The CPz electrode, which is positioned between Cz and Pz, is used as the reference for the 25 EEG channels and electrocardiogram (ECG). The ECG electrode was placed near the VNS pulse generator for two reasons. While this position provides a sufficient ECG signal, it is also close enough to the pulse generator to introduce a unique artifact in the ECG channel which corresponds to the pulse generator activation. This explicit VNS signature provides a means to determine stimulation times. Once stimulation times were obtained, the ECG channel was excluded the further study.

This study included two patients. The VNS paradigm is configured to deliver stimulation for 30 seconds and halt stimulation for 5 minutes, a cycle which repeated regularly throughout the entire recording for both Patient A and Patient B. Patient A's VNS parameters were 1.75 mA output current, 30 Hz signal frequency, 500 μsec pulse width, 30 second signal duration, and a 5 minute VNS deactivation duration. Patient B's VNS stimulation parameters were 1.5 mA output current, 20 Hz signal frequency, 250 μsec pulse width, 30 second signal duration and 5 minutes VNS deactivation duration. The VNS implants allow manual activation of the device should the patient require an immediate stimulation (e.g. if the patient senses an imminent seizure). Patient A's manual stimulation parameters were 2 mA output current, 30 Hz signal frequency, 500 μsec pulse width, and a 60 second stimulation duration. Patient A did not experience any seizures

during the recording session, and did not initiate manual stimulations. Patient B's manual stimulation parameters were 1.75 mA output current, 20 Hz signal frequency, 500 μsec pulse width, and a 60 second signal duration. Patient B underwent 14 seizures during the recording session and manually activated the stimulator between 20 to 40 seconds after onset of each seizure (a total of 14 manual activations). Additional information on the patient's clinical status can be found in tables 4-1 and 4-2.

Each patient underwent continuous scalp-EEG recordings approximately 24 hours in duration. For Patient A, a total of 255 VNS were analyzed in this study. For Patient B, a total of 237 VNS cycles were used in the analysis. Some of Patient B's VNS cycles were excluded from the study due to their disruption by a manually-activated stimulation and/or occurrence during a seizure. Finally, the last VNS cycle was excluded from analysis for both patients because it was not a complete cycle (it began closer than a full cycle length to the end of the recording).

STLmax Feature Extraction

Modeling brain activity using chaos measures has been shown to be useful for providing dynamical information about the neural state of the epileptic brain. Studies involving human patients (Iasemidis and Sackellares, 1990; Iasemidis and Shiau et al., 1999; Iasemidis et al., 2001; Iasemidis and Pardalos et al. 2003; Iasemidis and Shiau et al., 2003) and animal models of epilepsy (Nair et al., 2004, 2005, 2006; Talathi et al., 2008) suggest that occurrence of spontaneous seizures correlates with the evolution of the brain to a state of greater spatio-temporal order. This phenomenon manifests as a progressive increase in intra-channel similarity as measured by Lyapunov exponents calculated from multichannel EEG recordings. The reported sensitivity of STLmax to neural state changes in epilepsy make the measure a reasonable choice for attempting to characterize the VNS effects. Additional information can be found on the STLmax measure in chapter 3.

Briefly, as was described in chapter 3, the window duration for calculating STLmax needs to be short to provide temporally local information about the brain's dynamics yet contain enough points for the algorithm to converge. A window length of 2048 points (corresponding to 4 seconds) was selected as it was sufficient for providing a stabilized STLmax estimate in previous neural state classification studies in epilepsy (Iasemidis and Sackellares, 1999). In addition, it is desirable to utilize the shortest window length possible for STLmax estimation in order to provide locally dynamic information. As such, while maintaining a window length of the recommended number of data points for algorithm convergence, the 512 Hz sampling frequency provides improved time resolution over previous studies (which utilized a 200 Hz frequency). Additional parameters for STLmax estimation were selected based on the successful neural state classification studies that utilized them (Iasemidis and Sackallares, 1999): reconstructed dimension D = 7, phase space reconstruction delay τ = 14 msec (7 samples), evolution time ΔT = 41 msec (21 samples).

Experimental Setup

The STLmax time series for 25 EEG channels were analyzed using a consistent biclustering framework to determine separability of EEG fragments corresponding to stimulation times versus VNS deactivation. Since stimulation duration was set to 30 second and a four second time window was used to estimate each STLmax value, each stimulation provided seven data points. In order to help compensate for EEG pattern changes over the recording session which may not be related to VNS, each point in the stimulation class was averaged with the corresponding samples across all other stimulation cycles. This procedure reduces the amount of features to seven STLmax values for each channel to represent the stimulation class.

The non-stimulation class was comprised of ten STLmax points starting 250 seconds after each stimulation to represent the portion of the non-stimulation temporally furthest from the end

of stimulation. This class size was utilized capture as much information about the non-stimulation periods as possible while keep class sizes reasonably close to one another (<50% size difference in classes). Each STLmax point in the non-stimulation class was averaged across all VNS epochs (where an epoch consists of one stimulation and one non-stimulation period). Thus, the non-stimulation class consists of ten averaged STLmax samples from non-stimulation time intervals (see figure 4-4).

Thus, with 25 EEG channels, there total dimensionality of the biclustering input is 25 x 17. This particular input size this problem could be solved without any relaxation using CPLEX (ILOG Inc., 2004). Cross-validation by the leave-one-out method was performed for each sample.

Results

Patient A's data were conditionally biclustering-admitting into a binary supervised classification for the designated non-stimulation and stimulation classes with inclusion of all features (see figure 4-5).

All but one feature (channel P3) were classified into the non-stimulation class. The heatmap indicates that STLmax indicates during the stimulation with respect to non-stimulation for all but the P3 channel. The leave-one-out cross-validation method resulted in consistent classification of all 17 samples for Patient A.

Only five features in patient B were able to fulfill the supervised biclustering-admitting sample class designation with respect to given stimulation and non-stimulation classes. Channels F7 and T6 were designated as belonging to the non-stimulation class, while channels T3, Leye and Reye were classified into the stimulation class. Thus, there is less similarity among the channels during stimulation and non-stimulation, and a less clear distinction between stimulation and non-stimulation in Patient B than Patient A.

Patient A's stimulation parameters (1.75 mA, 30 Hz, and 500 μs pulse width) were all greater than Patient B's (1.5 mA, 20 Hz, and 250 μs pulse width) except for the 30 second on time and 5 minute off time, which were the same for both patients.

Discussion

The successful application of biclustering with Lyapunov exponents demonstrates the potential to distinguish during VNS stimulation from VNS deactivation epochs using the dynamical scalp-EEG measure STLmax.

There is a greater spatial-temporal similarity in EEG dynamics during stimulation in patient A than during non-stimulation. However, this phenomenon was not nearly as well-defined in patient B. It should be noted that Patient A had no seizures during the recording, whereas Patient B underwent seizures which were accompanied by a manually-initiated VNS stimulation. Though epochs containing seizures or manual stimulations were excluded from the analysis, it is possible that the seizures may have affected the results. Studies have demonstrated EEG dynamical transitions (in terms of the STLmax measure) preceding seizures minutes to hours (Iasemidis et al., 1988; Iasemidis, 1991; Iasemidis et al., 1994, 1996, 1997). It may be that EEG dynamical changes leading up to a seizure and/or persisting after the seizure lead to such a small amount of features selected in Patient B.

Despite the seizures and manual stimulations, the signals arising from the frontal lobe (f7, leye, and reye) and temporal lobe (t3 and t6) of the brain were sufficiently altered between stimulation and non-stimulation to allow a biclustering of the during the stimulation class (from t3, leye and reye channels) and non-stimulation class (from f7 and t6 channels) for Patient B. This could mean that the EEG effects of VNS are most pronounced in the frontal and temporal lobes. Patient B has a right frontal lobe focus.

The biological significance of these results may be related to study which discovered that VNS-induced acute suppression of epileptiform activity in a hippocampal depth electrode (Olejniczak et al., 2001). While the study by Olejniczak et al. utilized depth electrodes, its possible that scalp EEG recordings may display some manifestation of such an EEG effect observed at a hippocampal depth electrode. From this perspective, perhaps the STLmax behavioral differences between patients A and B are associated with enhanced suppression of epileptiform activity in patient A compared to patient B. Patient A's stimulation parameters were all higher than patient B's parameters, with the exception of stimulation duration and off time, which were 30 seconds and 5 minutes for both patients, respectively. In general, "high" stimulation parameters are associated with a greater clinical response than "low" settings (Ben-Menachem et al., 1994). Thus, any enhancement to epileptiform activity suppression in patient A over patient B is likely attributed to patient A's higher stimulation parameter settings.

This work was published in the paper "Biclustering EEG data from epileptic patients treated with vagus nerve stimulation", authored by Stanislav Busygin, Nikita Boyko, Panos Pardalos, Michael Bewernitz, and Georges Ghacibeh (Busygin, 2007).

SVM Analysis of EEG Phase Space Patterns in Patients undergoing VNS Therapy for Epilepsy

In light of the numerous successful neural state classification applications, often in real time (Chaovalitwongse et al., 2006; Thulasidas et al., 2006) it is possible that SVMs may be able to provide a computationally inexpensive yet robust similarity measure for quantifying stimulation-induced EEG effects. As was stated chapter 3, experimental evidence supports the idea of a therapeutic resetting effect of epileptic seizures in terms of preictal convergence and postictal divergence of the STLmax measure among critical EEG electrodes (Iasemidis et al., 2004). Furthermore, recent experimental evidence suggests that therapeutic interventions such

as neurostimulation and AEDs can mimics the electroencephalographic resetting effect of a seizure (Good et al., 2004, 2005; Ghacibeh et al., 2005). Thus, a reasonable approach for examining VNS therapy is from the framework that it mimics the effect of a seizure by comparing stimulation "artificial seizures" to non-stimulation ("post-ictal" or "interictal"). Thus, the EEG phase space of an EEG segment during VNS stimulation was compared to successive windows spanning the full stimulation / non-stimulation epoch with the intent of comparing the degree of separability to the stimulation parameters and the clinical status of the patient.

The application of support vector machines for obtaining an estimate of EEG similarity during stimulation compared to subsequent EEG segments may provide a rapid means to investigate and quantify electroencephalographic effects of VNS. The goal of this study is to extract EEG patterns which could be used as an electroencephalographic marker of optimal VNS stimulation parameters.

Data Description

Approximately 24 hours of scalp-EEG was recorded and analyzed from six epileptic patients being treated undergoing AEDs and VNS therapy and the control patient. The recording electrode placement scheme is described in figure 4-2. The VNS Patient information is summarized in tables 4-1 and 4-2.

SVM Application Description

SVM training and testing were performed using LIBSVM software package designed for Matlab (Chang et al., 2001). The RBF kernel transform (equation 3-72) is a useful feature space mapping technique successfully utilized in numerous neurophysiological studies (Acir et al., 2005; Lehmann et al., 2007; Thulasidas et al., 2006).The RBF kernel with σ=39 was utilized for the feature space transformation and a cost parameter of C=1000 were employed based on studies utilizing RBF SVMs to classify neural states using scalp EEG data (Kaper et al., 2004;

Acir et al., 2005; Lotte et al. 2007). Thus, In contrast to the traditional SVM application where a typical goal is to obtain maximal separation basis by adapting all parameters, this study fixes the σ and C parameters in order to mitigate subjectivity when comparing stimulation epochs to the non-stimulation epochs. An SVM classification accuracy of 50% implies minimal separation between the reference class and comparison class whereas 100% separation implies maximal separation between the reference and comparison class. These two extremes are interpreted as maximal and minimal similarity, respectively.

Experimental Design

The progression of EEG pattern evolution was quantified as the amount of separation achieved with support vector machines between two EEG segments both mapped into feature space using the radial basis function kernel. This exploratory study aims to examine how the EEG feature space patterns evolve throughout VNS stimulation and to identify potential relationships to stimulation parameters. In addition, the results will be compared to the clinical status of the patient.

The ECG electrode was positioned on the skin over the VNS pulse generator so that VNS stimulation waveform is introduced into the ECG channel (see figure 4-3). The VNS stimulation times were then obtained by examining the ECG channel, which was excluded from further analysis. The following experimental procedure was applied to each stimulation epoch (an epoch defined as a VNS "on" cycle and one "off' cycle) in the continuous EEG recording for each patient (with the exclusion of the final stimulation epoch which began less than one full cycle before the EEG acquisition was deactivated). An EEG segment occurring from 10 seconds to 20 seconds after the start of the VNS stimulation is selected as the positive class (from here on this class will be referred to as the “reference class”). The duration of each class was set at 10 seconds because this time frame is suggested to be long enough to be able to quantify brain

dynamics yet short enough to be sufficiently stationary (Casdagli et al., 1995, 1996, 1997). The reference class segment was selected to start at one full window length after the start of stimulation because that allows the stimulator to have finished the ramp-up phase and be at the steady-state stimulation phase. The first successive EEG window (the segment ranging from 20 seconds to 30 seconds) was selected as the first negative class (from here on this class will be referred to as the "comparison class"). The first preprocessing step was to down sample both classes by calculating the mean value of a moving-average non-overlapping window, a step which decreases SVM classification time often without a significant effect of results (Thulasidas et al., 2006). The smoothing window was set at 10 points in duration based on prior experience. Next, each data point is converted to a z-score by normalizing to zero mean and unit standard deviation. This procedure prevents channels with greater mean amplitudes from dominating the classification decision (Acir et al., 2005).

The trained SVM was tested with a v-fold cross validation scheme, as described in (Hsu et al., 2003). This process applied a resampling technique in which the two classes are first randomly shuffled then divided into v equally-sized subsets. The SVM is trained using v-1 segments and is tested using the remaining subset V. This process is repeated until all v subsets have been tested. The accuracy is the percentage of properly classified points from each of the v trials. Based on prior experience, v=2 folds were utilized for SVM training and testing in this study. Once the training accuracy is obtained for the particular reference class and comparison class combination, the comparison class advances one full window length and the process repeats. The process of calculating SVM accuracy then advancing the comparison class is repeated for all comparison segments which occur within one window length from the next stimulation (into the next VNS epoch). This process is performed for each VNS epoch in the

approximately 24 hour continuous EEG recording for each patient (with the exception for the final stimulation epoch during which the EEG recording ended).

Results

The results for the six patients are shown in figures 4-6 through 4-9 and table 4-3. The vertical line at 30 seconds in figure 4-6 represents the time when the VNS stimulator deactivates. Patients D and F have fewer comparison segments due to their off time of 3 minutes (thus the time between stimuli is less than the rest of the patients, which have a 5 minute off time). Patients E and F are seizure free.

Discussion

The results suggest a correlation may exist between pulse width and SVM separation accuracy (figure 4-8) as well as between stimulation frequency and SVM separation accuracy (figure 4-9). Furthermore, less similarity (greater SVM separation accuracy) is observed between the reference class (10 second EEG segment during stimulation) and all subsequent comparison classes (all non-overlapping 10 second EEG segments prior to the next stimulation) for higher values of pulse width and stimulation frequency than is observed with lower values of pulse width and stimulation frequency.

The biological significance of these results may be related to studies demonstrating differences in cerebral blood flow related to stimulation parameters. Specifically, a study demonstrated that the 250 μs VNS pulse width caused reduced blood flow in significantly more brain regions (e.g. hippocampus and superior temporal lobe) than a 500 μs pulse width (Mu et al., 2004). It is possible that pulse-width-induced blood flow changes in these brain regions may have altered neuronal activity and thus be responsible for covariation of EEG feature space dispersion with pulse width. Another study reported that a 20 Hz stimulation frequency produced significant blood flow increase over 5 Hz in numerous brain regions such as the orbitofrontal

cortex, hypothalamus, and thalamus in VNS patients (Lomarev et al., 2002). These regions may brain regions may be responsible for observed covariation of EEG feature space dispersion with stimulation frequency.

It may seem counterintuitive that output current (figure 4-7) did not appear to demonstrate a trend with the SVM separation measure as a study demonstrated that “higher” stimulation settings (such as output current, frequency, and pulse width) can result in greater seizure reduction than “lower” (Ben-Menachem et al., 1994). However, the output current increase in (Ben-Menachem, et al., 1994) was also accompanied by increases in frequency and pulse width parameters. Thus the outcomes of that study can not be attributed to changes in a single parameter. Fortunately, the other two parameters (frequency and pulse width) mentioned in (Ben-Menachem et al., 1994) may correlate with EEG pattern changes, though more patients are needed to verify such a claim.

It is possible that VNS mimics the seizure effect of "resetting" the brain from an unfavorable preictal state to a more favorable interictal state (Sackellares et al., 1997; Iasemidis et al., 2004) in which case the decrease in EEG similarity (signified by higher SVM separation accuracy) between the reference class and all subsequent comparison classes in an epoch may be an multidimensional analog to the brain dynamical resetting effect. The original effect was described as statistical convergence and divergence of STLmax values among critical electrode pairs (Iasemidis et al., 2004). Thus, one explanation for the observed feature space similarity phenomenon is these measures are electroencephalographic evidence that VNS is in some manner “resetting” the brain more effectively (as denoted by the lower similarity measures after stimulation) in the patients with fewer seizures per month. Perhaps therapies such VNS provide

ongoing gradual therapeutic action which suppresses the need for a large scale brain dynamical transition such as a seizure.

It is worth stating that the time of each patient's last seizure prior to the EEG recording session for this study is not documented. The timing of the last seizure could prove to be important for patients who are not seizure-free (A, C and D). This is because there is a period of heightened seizure resistance during the period immediately following a generalized tonic-clonic seizure. If patients A, C, and D had undergone a generalized tonic clonic seizure shortly before the EEG data were recorded for this study, then they may still have been under the influence of the reduced seizure susceptibility phenomenon. This may explain why they did not experience any seizures during this study. If Patient B had not experienced a generalized tonic clonic seizure recently, then reduced seizure susceptibility phenomenon may have been partially responsible for the large number of seizures reported this patient underwent during the study. These results should be viewed in the context that all six VNS patients are considered responders to the therapy defined as having at least 50% seizure reduction after one year of VNS therapy (Morell et al., 2006).

Drug medication differences could also have an effect on the results. For example, patient D (whom demonstrated the lowest average similarity) is the only patient using either carbamazepine or zonisamide. On the other hand, Patient B (whom demonstrated the highest average similarity) is the only patient taking phenobarbital. Perhaps these differences in antiepileptic medications could have altered the observed electroencephalographic effects.

As all patients have undergone VNS therapy for >1 year it may be regions of their nervous system such as the vagus nerve and/or brain may have adapted to VNS to such an extent that they do not demonstrate a significant acute EEG response to individual stimulations. However, it

is premature to arrive at such a conclusion. The SVM training parameters utilized, though successful in similar studies, are not optimized for this particular application. In addition to non-optimized SVM parameters, it is likely that improvements can be made in terms of feature selection for exposing VNS EEG effects.

This study is published in an article titled "Quantification of the Impact of Vagus Nerve Stimulation Parameters on electroencephalographic Measures" with authors Michael Bewernitz, Georges Ghacibeh, Onur Seref, Panos Pardalos, Chang-Chia Liu, Basim Uthman (Bewernitz, 2007).

Data Mining Analysis of EEG Dynamics Patients undergoing VNS Therapy for Epilepsy

The fact that the resetting effect is described in terms of the STLmax feature motivates the use of the STLmax measure for investigating EEG patterns potentially associated with VNS and VNS stimulation parameters. Inspired by the notion that therapeutic interventions may replicate the therapeutic seizure resetting effect of a seizure without adverse symptoms, the following study computes and compares STLmax values before VNS to values during VNS and utilizes SVMs as well as logistic regression to provide measures of STLmax pattern evolution. The evolution of STLmax values among the EEG channels is one method to track global EEG dynamics over time.

Data Description

This study involved six patients undergoing VNS therapy for intractable epilepsy. The continuous scalp-EEG recordings are ~24 hour in duration and were obtained at the Shands Hospital GCRC protocol # 614, IRB protocol #617-2004, "Neurophysiologic Measures of Vagus Nerve Stimulation" at the University of Florida, Gainesville. Clinical information for all six patients used in this study is summarized in tables 4-1 and 4-2. The electrode placement scheme is illustrated in figure 4-2.The stimulation times were obtained from the ECG channel, which

was recorded in close proximity to the VNS pulse generator. The ECG channel was excluded from the EEG analysis.

Feature Extraction

The behavior of STLmax values calculated from EEG signals for seizure prediction has been extensively researched (see chapter 3). The embedded dimension of the reconstructed space D=7, lag step τ=7 (14 msec), evolution time ΔT=21 (41 msec), and a window size N=2048 (4 sec) have provided useful neural state classification estimates (Iasemidis and Sackellares, 1991; Casdagli1996; Casdagli1997; Iasemidis et al., 1999). The interested reader may find the detailed explanation and justification of the algorithm and parameters in (Iasemidis, 1991), (Iasemidis and Sackellares, 1999) and (Wolf et al., 1985).

STLmax was calculated for all 25 channels for the full EEG recording duration (~ 24 hours) for all six patients.

SVM Analysis of EEG Dynamics

The LIBSVM software package for the Matlab environment was used for SVM training and testing (Chang et al., 2001). An RBF kernel with σ=39 and a cost parameter of C=1000 were utilized based on studies utilizing RBF SVM to classifying neural states from scalp EEG data (Kaper et al., 2004; Acir et al., 2005; Lotte et al., 2007). The SVM parameters C and sigma are held constant in an effort to provide objectivity to this measure which can be used to study EEG signal evolution over time in feature space for all the patients. This study fixes the σ and C parameters in order to mitigate subjectivity when comparing stimulation epochs to the non-stimulation epochs.

An SVM separation accuracy of 50% is interpreted as maximum measureable dynamical feature space similarity between reference class and comparison class features. An SVM

separation accuracy of 100% is interpreted as the minimum dynamical feature space similarity between the reference class and comparison class features.

Results are validated using a v-fold cross validation scheme, as described in (Hsu et al., 2003) using 10 folds. This process applied a resampling technique in which the two classes are first randomly shuffled then divided into v equally-sized subsets. The SVM is trained using v-1 segments and is tested using the remaining subset V. This process is repeated until all v subsets have been tested. The accuracy is the percentage of properly classified points from each of the v trials.

Logistic Regression Analysis of EEG Dynamics

Logistic regression (LR) has seen number applications for the diagnosis of neurological diseases and disorders. Examples include Parkinson's Disease diagnosis using various clinical diagnostic measures (Leentjens et. al, 2002), diagnosis of Alzheimer's Disease (Lehmann et al., 2007), cognitive decline (Prichep et al., 2006), and Schizophrenia using electrophysiological features (Price et al., 2006), and epilepsy using EEG features (Alkan et al., 2005; Subasi et al., 2005). Thus, LR analysis is a suitable candidate for further characterizing the brain dynamics in patients undergoing VNS.

LR is a statistical modeling technique utilized for probabilistic binary classification. As described in Subasi et al., 2005, the probability, $P_{t,ref}$, of a binary outcome event (EEG point at time "t" belonging to the reference class) is related to EEG value of channel "ch" at time "t", $x_{ch,t}$ in the form:

$$LOGIT\left(P_{t,ref}\right) = \ln\left(\frac{P_{t,ref}}{1-P_{t,ref}}\right) = \beta_0 + \beta_1 x_{ch1,t} + \ldots + \beta_{25} x_{ch25,t} = \beta_0 + \sum_{ch=1}^{25} \beta_i x_{ch(i),t} \qquad (4\text{-}1)$$

$$P_{t,ref}(X_t) = \frac{1}{1+e^{-LOGIT(P_{t,ref}(X_t))}} = \frac{1}{1+e^{-\left(\beta_0 + \sum_{ch=1}^{25} x_{ch(i),t}\right)}} \quad (4\text{-}2)$$

In equation (4-1), β0 is the intercept of the model and β1, β2, …, β25 represent the coefficients for EEG channels one through 25. Once the logistic regression model is trained, the probability $P_{t,ref}$ of an EEG data point X_t belonging to the reference class can be calculated in equation (4-2).

The performance of the logistic regression model is measured using the area under the curve (AUC) approach (Komaraek, et al., 2005). The AUC is equal to the area under the receiver operating characteristics (ROC) curve. The AUC metric is simply the ratio of the area of an ROC curve to the area under a perfect ROC curve.

Let "NR" be the number of points in the reference class, and "NC" be the number of points in the comparison class. NR = NC for this study, but do not have to be equal. The ROC curve is generated by first calculating $P_{t,ref}$ for each EEG data point X_t in both the reference class and the comparison class. Then, the $P_{t,ref}$ values are sorted in decreasing order. The ROC curve creation begins at the lower left hand corner of a blank curve plot. Each point with $P_{t,ref} \geq 0.5$ (most likely that the EEG point is from the reference class) results in the creation of an upward line segment of length one unit. Each point with $P_{t,ref} < 0.5$ (most likely that the EEG point is from the comparison class) in the creation of a line segment of length one unit to the right. The AUC metric is the ratio of the area under the generated ROC curve divided by the area under a perfect ROC curve (which climbs from (0,0) to (0, NR), then moves laterally from (0, NR) to (NC, NR) and is equal to one in this case).

An AUC=0.5 (or ROC=0.5) is equivalent negligible dynamical feature space similarity between the reference class and comparison class. AUC=1.0 (or ROC=0) refers to the maximum measurable dynamical feature space similarity between the reference class and comparison class.

Experimental Setup

The following procedure was applied to each stimulation epoch (an epoch defined as a VNS "on" cycle and one "off" cycle) for each patient using SVMs and then repeated for LR. The EEG segment occurring 8 seconds (two window lengths) prior to stimulation start is selected as the "reference class". The reference class was represented as an $n \times m$ array of STLmax values where n is the number of channels and m is one less than the total number of stimulations occurring during the EEG recording. Setting m as one less than the total number of detected stimulations ensures that only complete VNS epochs are included in the analysis (as the last stimulation intersected with the end of the recording for all six patients). For each patient, the reference class utilized STLmax estimates from all n=25 channels from the time period of 8 seconds (two full window lengths) prior to stimulation start, for all m stimulations. The "comparison class" was initially established as an $n \times m$ array of STLmax values occurring at the start of the stimulation for all m stimulations included for each patient. The SVM and LR classifiers are trained and tested for separation of the reference and comparison class combination. Once the accuracies are obtained, the reference class is advanced 4 seconds (one full window length) and the process is repeated throughout the epoch with the last comparison class occurring 200 seconds after stimulation start. The end point corresponds to the end of the 3 minute interstimulation cycle, which is the final endpoint which

Results

Figures 4-10, 4-11, 4-12, and 4-13 as well as table 4-4 demonstrate a similar performance between the LR and SVM results. Using both methods, the same two patients which produced

the greatest STLmax feature separation between non-stimulation and stimulation epochs (patients A and D) also possessed the greatest stimulation frequency, 30 Hz, whereas the patient with the lowest separation (patient B) also possessed the lowest stimulation frequency, 20 Hz. In addition, patient D produced the second greatest separation while possessing highest stimulation frequency of 30 Hz. On the other hand, Patient F also had the greatest stimulation frequency of 30 Hz yet only achieved an intermediate separation value compared to the other patients (though patient F is seizure-free whereas patients A, B, and D are not). The final noteworthy observation the width was the lowest (250 microseconds) and Patient B who demonstrated the least separation. There was no apparent trend regarding the degree of separation using either LR or SVM and output current.

One interesting connection with the clinical status was that the patients whom experienced the greatest amount of separation (patients A and D) were also taking more types of AED medications (patients A and D each were on four medications, patient B was on three medications, all other patients were only taking two medications). Another interesting connection to the clinical status is that the patient with the largest number of monthly seizures (patient B) also demonstrated the least amount of STLmax feature separation between non-stimulation and stimulation.

Discussion

The LR and SVM classification results suggest that EEG dynamical pattern changes (in terms of the STLmax measure) between stimulation and non-stimulation may be related to the stimulation frequency parameter. Lomarev et al. reported that a 20 Hz stimulation frequency produced significant blood flow increase over 5 Hz in numerous brain regions such as the orbitofrontal cortex, hypothalamus, and thalamus in VNS patients (2002). These regions may

brain regions may be responsible for observed covariation of STLmax dispersion with stimulation frequency.

At a first glance it seems counterintuitive that the output current did not appear to demonstrate a similar LR or SVM classification accuracy trend as pulse width and stimulation frequency, as a study demonstrated that "higher" stimulation parameter settings (such as frequency, output current, and pulse width) are associated with greater seizure reduction than "lower" settings (Ben-Menachem et al., 1994). However, the output current increase mentioned in (Ben-Menachem et al., 1994) was accompanied by increases in frequency and pulse width and thus the observed therapeutic effect in that study can not be attributed to changes in an individual parameter. Furthermore, the values of the other two parameters mentioned in the study by Ben-Menachem et al. (frequency and pulse width) did show indications of a connection with EEG dynamical changes, which is encouraging.

Patient B's large amount of seizures accompanying the lowest LR and SVM separation is an interesting observation. It is difficult to draw preliminary conclusions about clinical connections to the brain dynamical behavior as Patient B's stimulator was set at the lowest pulse width and the lowest stimulation frequency of all six patients. However, a potential connection between this patient's clinical behavior and the observed EEG patterns can be viewed from an interesting perspective first described in seizure prediction research studies. Considering the electroencephalographic and clinical effects observed during seizures, it is possible that the VNS therapeutic effect is enacted by artificially replicating the theorized therapeutic seizure mechanism first suggested by Iasemidis et al. (2004).

By adopting this perspective, patient B's seizures could be seen as the result of the VNS failing to replicate the resetting function of a real seizure. Thus, the brain is then "permitted" to

seize in order to reset itself. This observation is congruent with the notion that patient B has the lowest STLmax feature separation for both LR and SVM between the VNS on (which could be considered a VNS 'artificial' seizure) and VNS off class (which from an 'artificial' seizure perspective could be viewed as a 'post-ictal' period for the 'artificial' seizure). It is worth mentioning that all six patients are considered as responders to VNS therapy by a definition of experiencing at least a 50% seizure frequency reduction following one year of VNS therapy (Morell et al., 2006).

The observation that patients A and D were taking the most types of AEDs and demonstrated the highest STLmax feature separation between non-stimulation and stimulation is reasonable. Again, from the view of a seizure's "resetting" mechanism described in the previous paragraph, the two additional AEDs could possibly be enhancing effectiveness of the VNS resetting phenomenon as characterized by increased STLmax separation between VNS on and VNS off.

This study was submitted to Computing and Optimization in Medicine and Life Sciences Vol. 3, under the title "A Data Mining Approach to the Investigation of EEG Biomarker Existence for Vagus Nerve Stimulation Therapy Patients", with authors Nikita Boyko, Michael Bewernitz, Vitaliy Yatsenko, Panos Pardalos, Georges Ghacibeh, Basim Uthman (Boyko et al., 2008).

Conclusions

The interesting results of these studies may be indicative of EEG dynamical effects of VNS and suggest the LR, SVM and biclustering may serve as useful data classification tools for use in an online real-time seizure control application. Biologically, these results may be related to the trait pointed in a study by Olejniczak et al. which discovered a short-term suppression of epileptiform sharp waves following VNS from a hippocampal depth-electrode (2001). While the

scalp electrodes used to collect the EEG data for this chapter cannot achieve the fidelity of hippocampal depth electrodes, it is possible that the scalp EEG data mining analysis results may reflect the same therapeutic effect as observed in the hippocampus by Olejniczak et al. (2001).

The biological significance of the potential covariation of the EEG patterns with the pulse width and stimulation frequency parameters may be related to studies which demonstrated cerebral blood flow patterns corresponding to the pulse width (Mu et al., 2004) and stimulation frequency (Lomarev et al., 2002) parameters in VNS patients.

Additional patients are needed to validate such claims against possible type 1 error. However, additional patients would also provide the opportunity to potentially uncover any VNS-induced EEG dynamical changes which may have been missed in this small sample (thus reducing the chance of type 2 error).

A difficulty for this type of clinical research is recruiting patients with similar clinical situations (e.g. similar stimulation parameter configurations) in order to strengthen any observed connections between EEG behavior and stimulation parameters. For example, if numerous patients with similar stimulation parameters could be recruited, the patients may be taking different medications in different doses, etc. While it may be tempting to consider altering drug paradigms to mitigate inter-subject variability, practical and ethical concerns must be kept in mind at all times when attempting to alter patient treatment regimes for research purposes.

In addition, the impact of epileptic seizures on these EEG features and classification techniques is important for generating a robust stimulation-response model. Thus, as the clinical circumstances such seizure occurrence can affect observed EEG dynamical patterns, it is worth mentioning that each patient's last seizure time prior to this study's EEG recording session is unknown. The time at which the last seizure occurred may be important factor for the patients

which are not seizure free (patients A, B, C, and D) as there exists a period of reduced seizure susceptibility for a period of time following a generalized tonic-clonic seizure. Thus, patients A, C, and D could have experienced generalized tonic clonic seizures prior to the study recording session and thus been influenced by this period of reduced seizure susceptibility. Such an scenario could have contributed to the lack of seizures occurring during the recording session and also influenced seizure dynamics. In addition, if patient B had not experience a generalized tonic-clonic seizure prior to the study recording session then this patient's large number of seizures may have been partially induced due to the lack of said "seizure protection" phenomena following a seizure.

Despite exclusion of stimulation epochs containing seizure activity from analysis, patient B's seizures during the recording session still may have altered the observed EEG patterns. The rationale for such as claim is the observation of dynamical EEG shifts (in terms of the STLmax measure) identified from minutes to hours prior to epileptic seizures (Iasemidis et al., 1988; Iasemidis, 1991; Iasemidis et al., 1994, 1996, 1997). Thus, conclusions about patient B must be carefully considered as the seizures themselves could affect the observed EEG classification results. There is also a possibility of error in the monthly seizure rate as described by the patients. A 2007 study by Hoppe et al. demonstrated documentation inaccuracies in patient seizure counts (Hoppe et al., 2007). Thus, caution must be exercised in any epilepsy study which incorporates seizure information that was documented by patients.

Thus, in an ideal study, additional consideration should focus on recruiting a group of patients with similar epilepsy cases (e.g. similar focus locations). By studying multiple patient groups each with similar variants of epilepsy, experimental findings are strengthened and the findings may help tailor resulting VNS therapy devices.

In order further the understanding of EEG effects accompanying VNS it is important to track EEG feature patterns in patients before, immediately after, and for at least six months after implantation. A longitudinal study starting before VNS implantation and ending 6-12 months after implantation would provide insight into the evolution of EEG dynamical patterns before and after VNS parameter adjustment. In addition, such an analysis would help determine the presence of EEG characteristics present prior to VNS implantation for each individual patient. Thus, such a study design would add strength to post-implantation EEG patterns which are not observed prior to VNS implantation.

In the case that pre-VNS data is not available for a particular patient of interest, patients whom are receiving VNS for depression treatment may serve as useful control subjects. Such patients could help determine how brain dynamics in VNS patients are influenced by epilepsy and seizures. The potential knowledge gained from these suggested studies could lead us one step closer to the creation of an EEG marker for optimal VNS parameters.

In addition, as the relationship of EEG patterns stimulation parameters and clinical outcome in VNS patients is not clearly defined, then it is possible that the EEG measure parameters or perhaps the measures used in data classifiers are suboptimal. Thus, additional EEG features should be utilized for possible improvements in EEG dynamical comparisons. Complexity measures entropy measures have demonstrated success as data mining features for extracting brain dynamical information and classifying neural states (Chaovalitwongse et al., 2006).

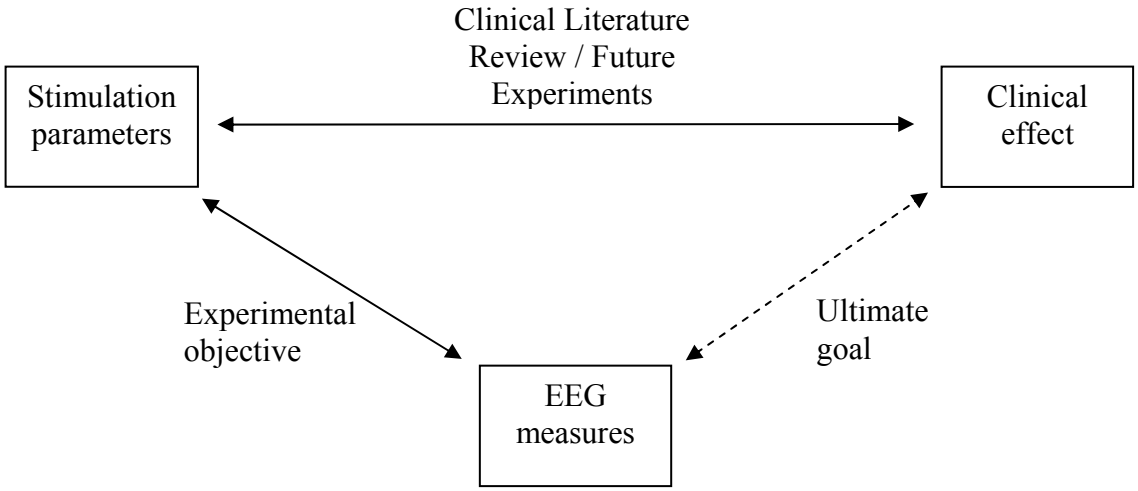

Figure 4-1. Rationale for studying EEG patterns which may be associated with the effect of VNS on the brain.

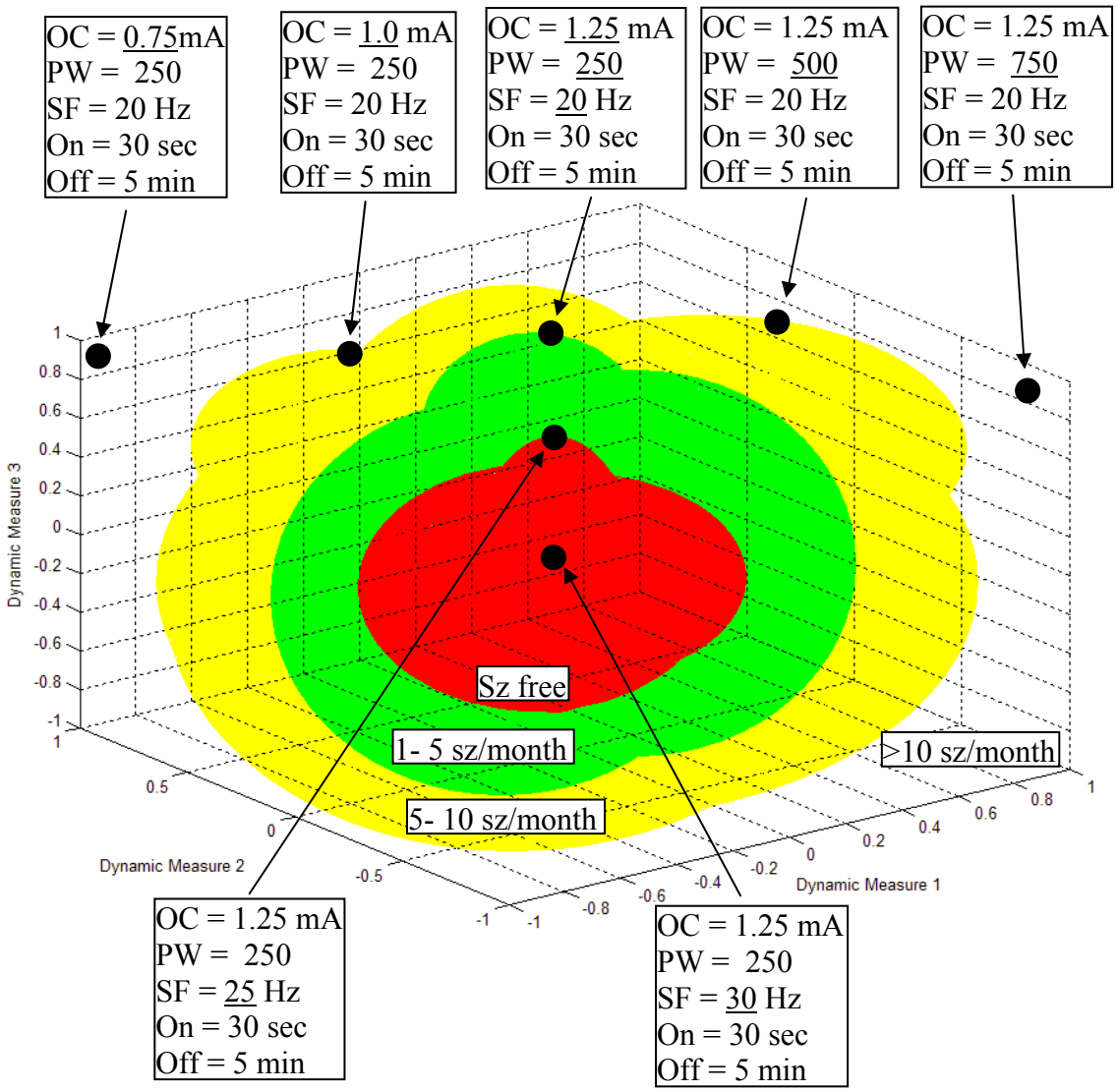

Figure 4-2. Conceptual EEG dynamics model in three-dimensional feature space for testing stimulation parameter configurations in newly-implanted VNS patients. Adjusting the stimulation parameters results in an altered dynamical 'state' of the brain denoted by the coordinates in three-dimensional feature space. The model's colored regions relate the EEG dynamical state to its predicted clinical outcome.

Table 4-1. VNS stimulation parameters

Patient	A	B	C	D	E	F
Output Current (mA)	1.75	1.5	2.5	2	1.25	0.75
Stimulation Frequency (Hz)	30	20	25	30	20	30
Pulse Width (μs)	500	250	500	500	500	750
On Time (seconds)	30	30	30	30	30	30
Off Time (minutes)	5	5	5	3	5	3
Magnet Output Current (mA)	2	1.75	2.75	2	1.5	0.75
Magnet On Time (seconds)	60	60	60	30	60	60
Magnet Pulse width (μs)	500	500	500	500	500	750

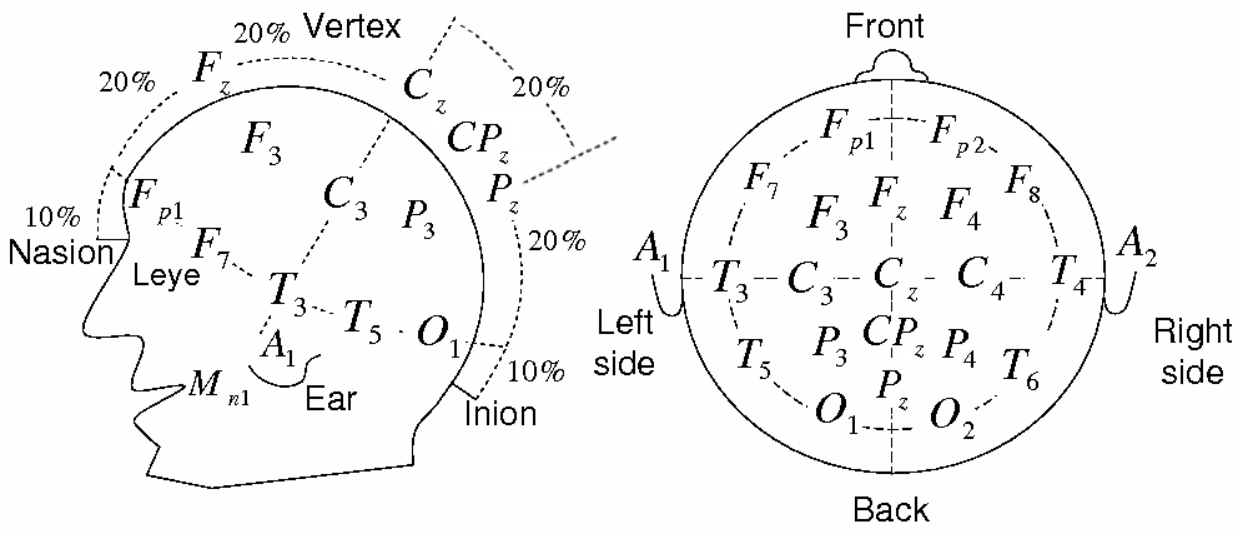

Figure 4-3. EEG electrode placement. Electrodes were positioned according to the 10-20 electrode placement system which assigns locations proportionally spaced locations (e.g. 10%-20%) with respect to the size of the patient's head.

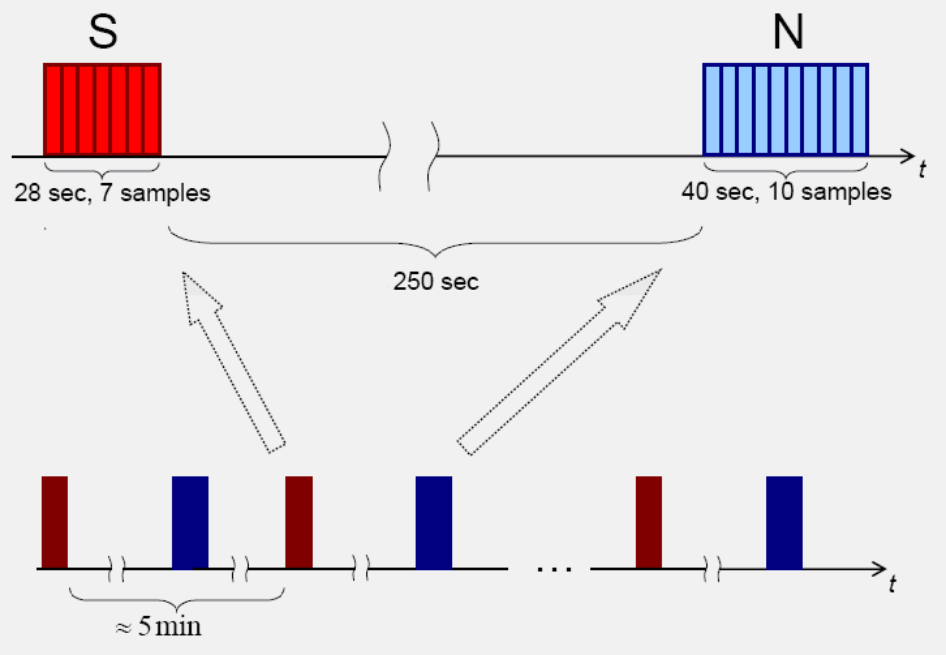

Figure 4-4. STLmax class designation for biclustering analysis.

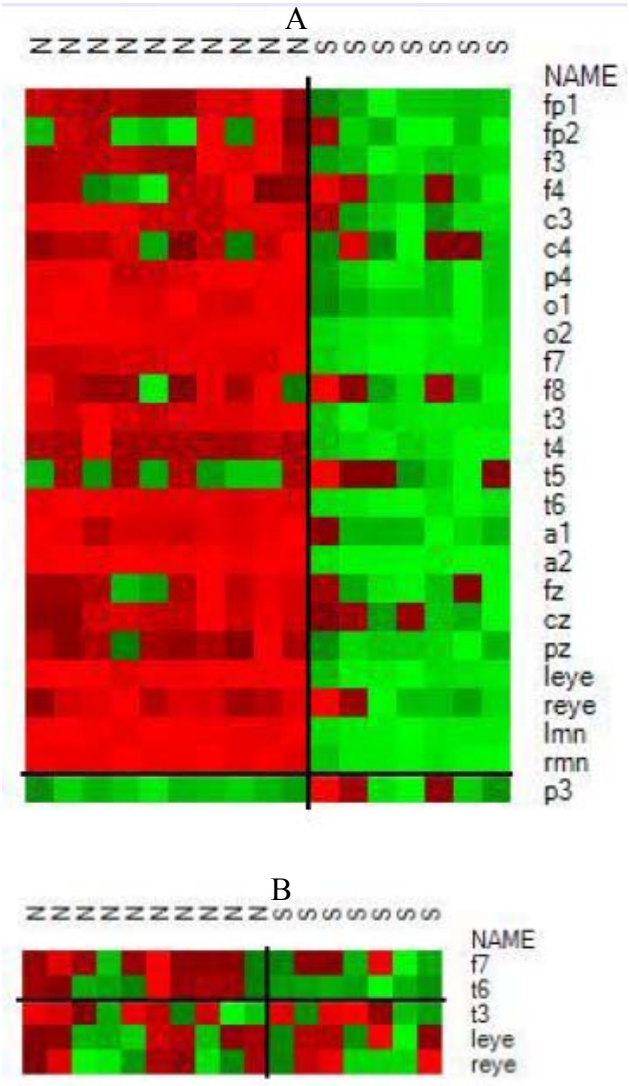

Figure 4-5. Biclustering heatmap of STLmax from A) patient A and B) patient B.

Table 4-2. Patient information for epilepsy patients with the VNS implant.

Patient	A	B	C	D	E	F
Age	38	53	54	29	54	54
Focus	Right frontal Left frontal	Right frontal	Right temporal	Left frontal	unknown	Right temporal Left temporal
Mean seizures per month	3	30	2	3	0	0
# of seizures during recording	0	14	0	0	0	0
Seizure Type	C. Partial with infrequent secondary gen.	C. Partial with infrequent secondary gen.	C. Partial with infrequent secondary gen.	C. Partial with infrequent secondary gen.	C. Partial with infrequent secondary gen.	C. Partial with infrequent secondary gen.
Duration of VNS therapy (years)	> 1 year	> 1 year	> 1 year	> 1 year	> 1 year	> 1 year
Medications*	Gab Lam Lev Preg	Lev Phen Top	Gab Top	Carb Lam Lev	Chlor Gab	Preg Lev

*Gab = Gabapentin, Lam = Lamotrigine, Lev = Levetiracetam, Preg = Pregabalin, Phen = Phenobarbital, Top = Topiramate, Carb = Carbamazepine, Chlor = Chlorazepate

Table 4-3. SVM separation accuracy and seizure information.

Patient	Mean SVM separation	Average monthly seizure rate	Seizures during recording
A	.9284	3	0
B	.7788	30	14
C	.8359	2	0
D	.9807	3	0
E	.9454	0	0
F	.8982	0	0

*Average monthly seizure rate of zero indicates seizure freedom.

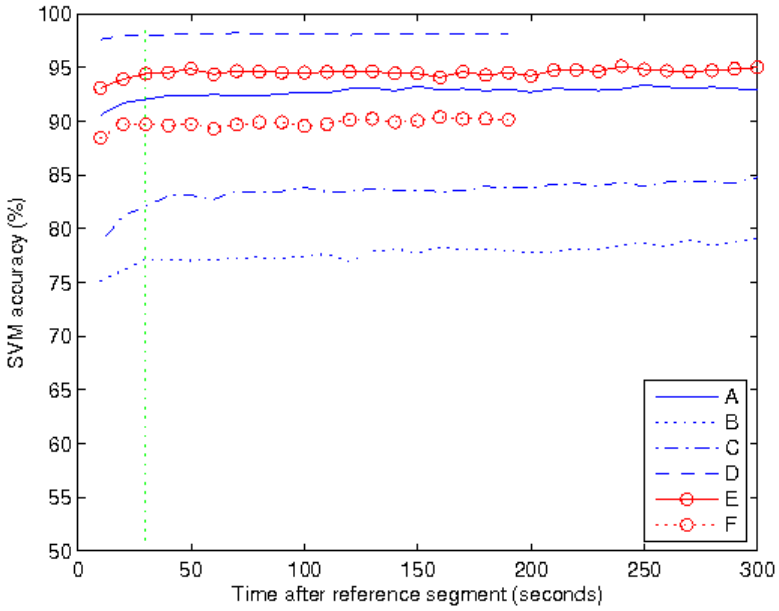

Figure 4-6. Mean SVM separation accuracy value across the stimulations for each individual intra-stimulation window.

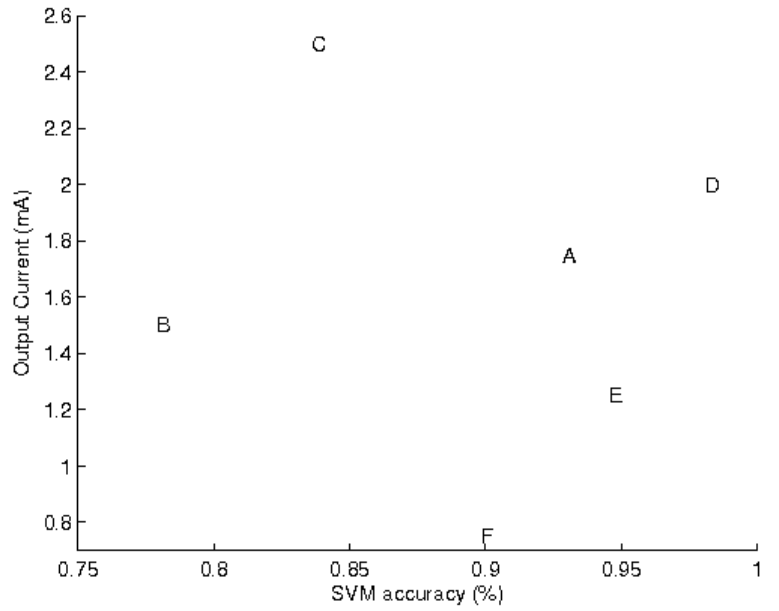

Figure 4-7. VNS output current and the corresponding mean SVM separation accuracy over 24 hours.

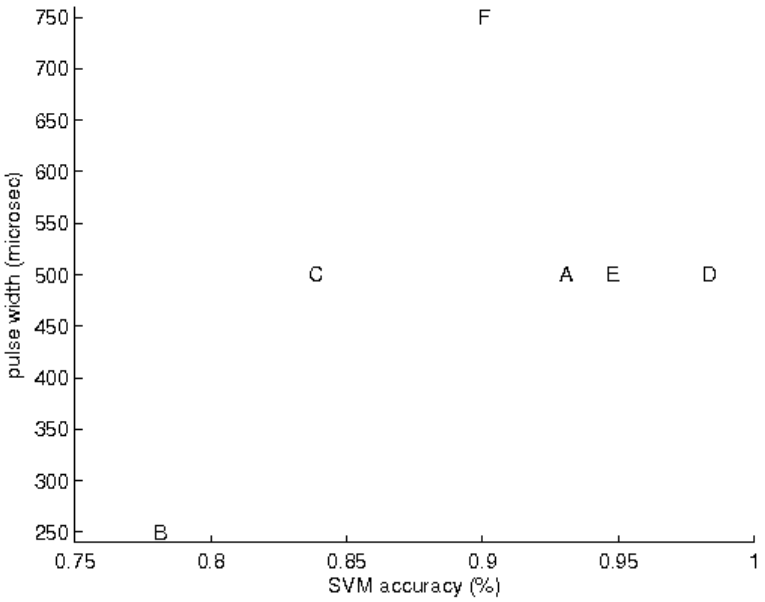

Figure 4-8. VNS pulse width and the corresponding mean SVM separation accuracy over 24 hours.

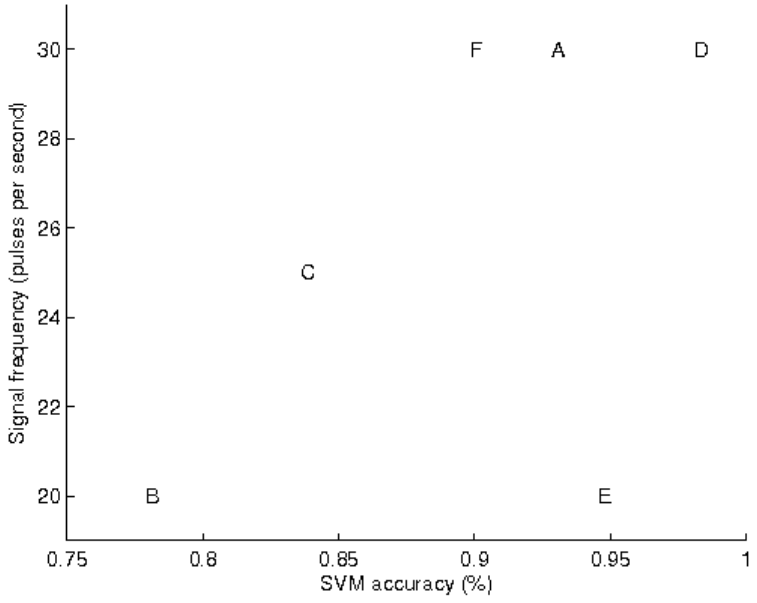

Figure 4-9. VNS signal frequency and the corresponding mean SVM separation accuracy over 24 hours.

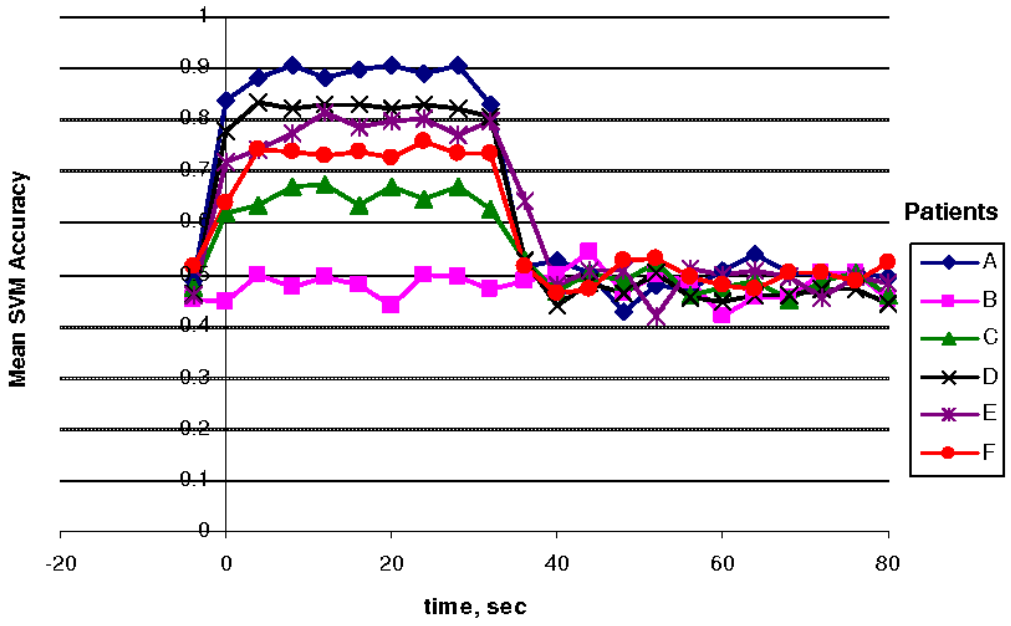

Figure 4-10. SVM Separation accuracy throughout the VNS epoch, averaged across all epochs. Stimulation begins at t=0 seconds.

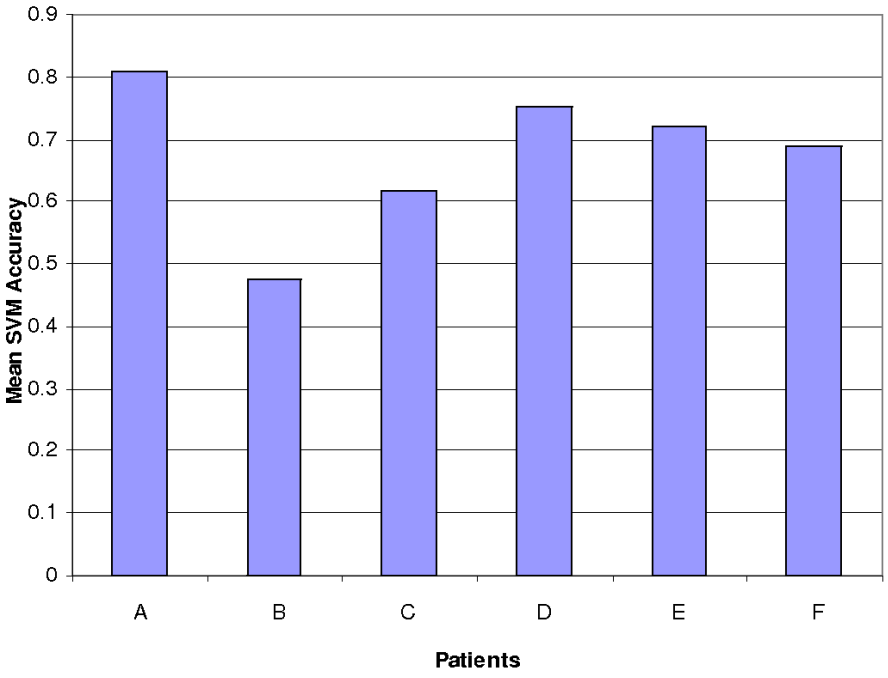

Figure 4-11. Overall mean SVM separation averaged across intra-epoch time points and all epochs.

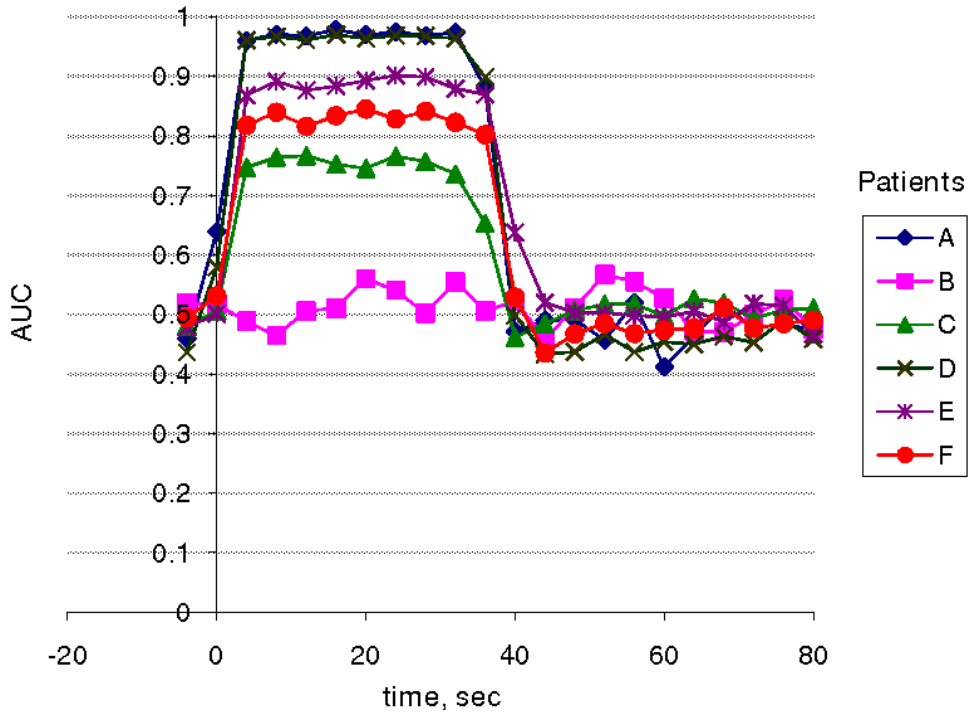

Figure 4-12. LR separation quality throughout the VNS epoch, averaged across all epochs. Stimulation begins at t=0 seconds.

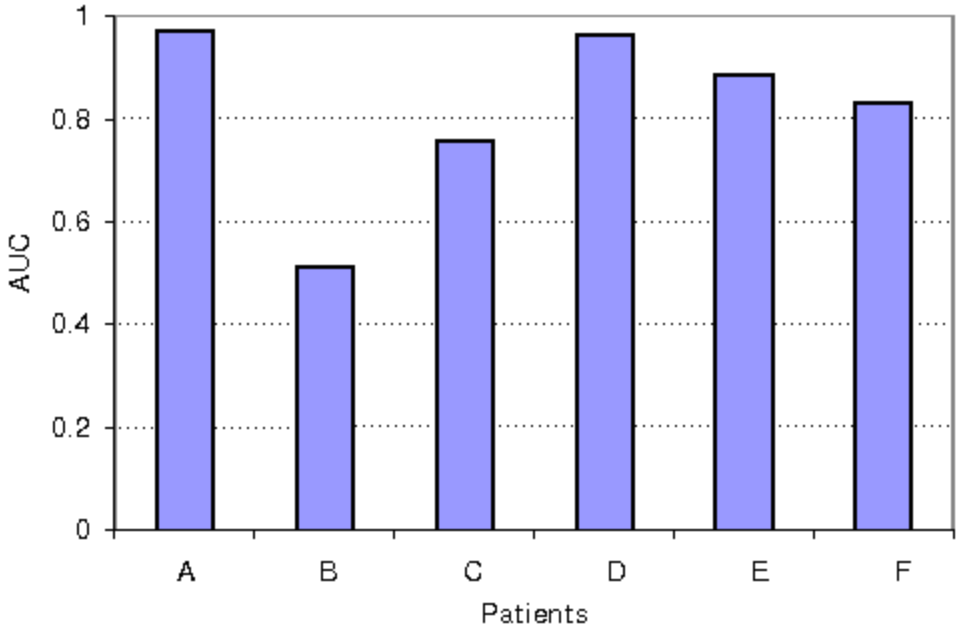

Figure 4-13. Overall mean LR AUC averaged across intra-epoch time points and all epochs.

Table 4-4. Mean SVM and LR separation accuracy and patient seizure information.

Patient	Overall mean SVM separation	Overall mean LR separation	Seizures per month	Seizures during recording
A	0.8082	0.9701	3	0
B	0.4746	0.5104	30	14
C	0.6171	0.7571	2	0
D	0.7536	0.9658	3	0
E	0.7210	0.8878	0	0
F	0.6885	0.8319	0	0

CHAPTER 5
ANALYSIS OF INTERSTIMULATION BRAIN DYNAMICS IN VAGUS NERVE STIMULATION THERAPY

The Identification of a marker of desired VNS operation would greatly expedite the VNS parameter adjustment process in newly-implanted patients. This study faces two significant challenges: 1) the underlying therapeutic mechanism of VNS is still poorly understood, and 2) despite some interesting results reported in innovative research studies, the electroencephalographic effects of vagus nerve stimulation are not clearly defined. From the perspective of dynamical disorder (see chapter 2), there is reason to believe any such potential stimulation-induced EEG effects are likely to be elucidated from dynamical EEG analysis (Uthman et al., 2007).

Further Characterizations/Investigations of EEG-Effects in VNS Therapy

Preliminary data mining results described in chapter four present interesting EEG dynamical phenomena with biological interpretations that are consistent with the theory about the physiological "resetting" role of a seizure. Of additional interest is the behavior of the brain between VNS stimulations. Viewing inter-stimulation brain behavior provides a means to determine how the brain recovers after VNS therapy (or 'artificial seizures'). In addition, this analysis duration also provides information about the brain while is not being actively influenced by a therapeutic action (e.g. VNS or the therapeutic effect of a seizure). Thus, as non-ictal EEG can help provide information about the seizure imminent state, so to may the inter-stimulation EEG intervals provide information additional information about the brain's response to VNS which may not be available while the VNS is active. This chapter focuses on characterizing the temporal dynamical behavior of the EEG signals during the periods when the VNS is inactive.

Building on the successes of the data mining approaches in chapter four, this chapter aims to further characterize EEG patterns which may be related to VNS. The brain's behavior will be characterized during all periods of respite from VNS.

Dynamical EEG Measures as Markers for Neurological Diseases and Disorders

The success of EEG markers for the treatment of neurological disorders is the primary motivation for this study. Such "signature" observations of pathological activity have greatly boosted diagnosis, treatment, and therapeutic evaluation of a range of neurological disorders (Krystal et al., 1996, 1997, 2000; Asyali et al., 2007; Ding et al., 2007; Quintana et al., 2007) including epilepsy (Iasemidis et al., 1996; Pardalos et. al, 2003, 2004; Chaovalitwongse et al., 2005, 2006; Ding et al., 2007; Schevon et al., 2007). Additional details can be found in chapters 2 and 3.

Despite reported interest in the application of such a technique to the EEG signals for improving VNS epilepsy therapy (Uthman et al., 2007), studies have been published which do not support the presence of VNS-induced EEG effects (Hammond et al., 1992; Salinsky et al., 1993; Koo, 2001; Rizzo et al., 2004; Marrosu et al., 2005).

Though long-term VNS-induced EEG changes on epileptic interictal spikes (Koo, 2001) epileptiform sharp waves in the hippocampus (Olejniczak et al., 2001), interictal epileptiform discharges (Janszky et al., 2005; Santiago-Rodriguez and Alonso-Vanegas, 2006), gamma activity and desynchronization (Marrosu et al., 2005), and spectral content of sleep (Rizzo et al., 2004) have been reported, the time frame for observing such an effect renders it less useful the current task of expediting VNS parameter calibration in newly-implanted patients.

Physiological behavior such as alterations in the interitical spiking rate is congruent with the characteristics dynamical diseases and disorders. The class of disorders termed "dynamic disorders" demonstrates complex behavior patterns which evolve over time. Specifically, these

disorders have been broadly described as undergoing a temporal disruption in the underlying physiological control mechanisms which results in a period of abnormal dynamical behavior (Mackey and Glass, 1977; Mackey and an der Heiden, 1982; Milton and Mackey, 1989; Belair et al., 1995; Milton and Black, 1995; Milton, 2000; Lopes Da Silva et al., 2003; Colijn and Mackey, 2005). Thus, studying epilepsy therapy from the vantage point of a dynamical disorder is a rational approach.

Koo's observation of the VNS effect on interictal spiking rate (2001) demonstrates that relatively short-term EEG effects (such as interictal spikes) are the manifestation of long-term modulatory VNS effects (e.g. after several months). Thus, this observation raises the possibility of less obvious short-term manifestations of VNS modulatory effects existing in the EEG. Such EEG effects may be detectable using EEG measures that have demonstrated successful neural state characterization such as preictal transitions in seizure prediction studies (Casdagli et al., 1996; Chaovalitwongse et al., 2005; Iasemidis and Sackellares, 1991; Iasemidis et al., 1993; Iasemidis et al., 2003, 2004; Le Van Quyen et al., 2001; Lehnertz, 1999; Lehnertz and Elger, 1995; Osorio et al., 2001).

The purpose of identifying dynamic disorders is that successful treatment may result from manipulation of some physiologic control parameter into a range associated with healthy dynamics of the observed variables (Milton, 2000). One example of this is a seizure control strategy where the"healthy" range of STLmax t-index values (associated with seizure transition) in maintained by therapeutic intervention (Iasemidis et al., 2003; Good et al., 2004, 2005). An analogous scenario may apply to VNS parameter adjustment in newly-implanted patients where the VNS parameters may be adjusted in order to elucidate a brain dynamical response or "state" that has been previously established as indicative of desired or even optimal seizure protection.

Thus, the achieved neural state as described by dynamical EEG responses associated with different stimulation parameters over time may serve as "marker" for VNS treatment and facilitate rapid determination of optimal VNS parameters.

An example of this concept is illustrated for a brain dynamics model involving three dynamical measures in chapter 4, figure 4-2. Realistically, mapping the clinical outcome to subregions of a multidimensional feature space will likely be very complex and require numerous additional features for adequate characterization. While determining the proper features to best represent the brain behavior and its relationship to stimulation parameters in VNS is a daunting task, this study aims to provide an in-depth evaluation of a number of EEG measures which have demonstrated sensitivity to neural state changes in other studies. For these reasons, the current study aims to identify electroencephalographic markers which are sensitive to the stimulation parameter configuration in patients with the VNS implant. If such electroencephalographic markers are identified, and if the electrographic markers are found to correlate with clinical efficacy then these findings could be applied to determine optimal VNS stimulation parameters on a patient-by-patient basis.

Data Description

This study utilized EEG data from six patients undergoing VNS therapy for epilepsy. Extensive patient information can be found in chapter four. The recordings were acquired under GCRC protocol # 614 / IRB protocol #617-2004, "Neurophysiologic Measures of Vagus Nerve Stimulation" GCRC in Shand's Hospital at The University of Florida. EEG data was acquired from channels Fp1, Fp2, F3, F4, C3, C4, P3, P4, O1, O2, F7, F8, T3, T4, T5, T6, A1, A2, Fz, Cz, Pz, Leye, Reye, Lmn, and Rmn using CPz (located between Cz and Pz) as a reference. The data were acquired at 512 Hz sampling rate using 16-bit precision from an amplifier with 0.16 Hz high pass filter and 105 Hz low pass hardwired filters. The mandibular notch channel near the

location where the jaw and skull contact one another provides information about the nearby temporal lobe. See figure 5-1 for electrode locations.

The ECG electrode was placed near the pulse generator to introduce the VNS waveform in the ECG channel when the stimulator is active. Thus, the VNS signature waveform was introduced into the ECG (see figure 4-4) to provide an effective means to identify stimulation times by modifying a channel that is not used in the quantitative analysis. A summary of patient clinical information can be found in tables 4-1 and 4-2.

Ideally, the baseline recording from each involved patient should be compared to their own EEG after implantation in order to strengthen claims that observed EEG patterns are the result of VNS and thus were not present prior to implantation. However, baseline EEG data was not available for this set of patients. As no baseline data was available for the VNS study, an interictal EEG recording from a temporal lobe epilepsy patient of ~24 hours in duration provided courtesy of the Freiburg Center for Data Analysis and Modeling at the Albert-Ludwigs Universität Freiburg (University of Freiburg), Freiburg, Germany (Winterhalder et al., 2006) was utilized as a control dataset. The interictal EEG data came from patient p012 and was acquired at 512 Hz. The data were acquired from three focal channels (TBa4, TBb6, HR7) and three non-focal channels (TLb2, TLb3, TLc2).

The patient has a right hippocampal seizure focus which gives rise to simple partial, complex partial, and generalized tonic-clonic seizures. The control dataset was utilized with artificial stimulation times based on both a 5 minute interstimulation interval and a 3 minute interstimulation interval.

The Surrogate Analysis Method

The surrogate data analysis method is a statistical approach for identifying nonlinearity in a time series. The best expression of the surrogate data method is from a statistical hypothesis

testing framework (Theiler et al., 1992). This formulation requires a null hypothesis to test against and some test statistic. The null hypothesis is a possible description of system output which is tested to determine how well it models the observed data. The test statistic is a quantity calculated from the sample data to determine whether or not to reject the null hypothesis.

Surrogate data analysis typically defines the null hypothesis such that the time series data are described by a specific process belonging to a broader class of processes (Schreiber and Schmitz, 2000). A common null hypothesis asserts that the time series data are generated by a general Gaussian linear stochastic process (Theiler et al, 1992). However, different realizations that fit within this broad category can result in surrogates with different power spectra and distributions. This scenario and may cause the test statistic may mistake such variations for deviations from the null hypothesis and falsely reject the null hypothesis (Schreiber and Schmitz, 2002). The can be approach using pivotal statistics or using constrained realizations (Theiler and Prichard, 1996). Pivotal statistics are measure created such that do not depend on mean or standard deviation under the null hypothesis. The "constrained realization" method enforces a requirement that all surrogates display the same power spectrum and distribution of values as the original data (Theiler and Prichard, 1996; Schreiber and Schmitz, 2000). Under the constrained realization approach the randomization method covers the "pivotal" requirement and thus opens up the possibility to use numerous non-pivotal test statistics for testing the null hypothesis.

While the surrogate method is useful for suggesting the presence of nonlinear signal components, this technique cannot be used to characterize the specific type of observed nonlinear behavior. For example, while it is valid to utilize a Lyapunov exponent to test the null hypothesis, surrogate analysis cannot indicate that an observed nonlinear signal is the result of low-dimensional chaos (Pritchard et al., 1995; Palus, 1997; Schreiber and Schmitz, 2000).

Surrogate data sets were generated using the algorithm proposed by Schreiber and Schmitz to produce same power spectrum and amplitude distribution as the original dataset (1996). The algorithm runs as follows. Let $\{s_n\}$ represent an EEG signal of length n. Store sorted list of the raw EEG values, $\{s_{n,sort}\}$, and the absolute value of the amplitudes of the discrete Fourier transform (equation 3-11) of $\{s_n\}$ which is denoted as $\{S_k\}$. First the original data $\{s_n\}$ are randomly shuffled $\{s_n^{(0)}\}$. Each iteration consists of two actions. At iteration step i, the signal from the previous iteration $\{s_n^{(i-1)}\}$ is brought to the desired power spectrum by computing the Fourier transform and replacing the amplitudes $\{S_k^{(i-1)}\}$ with those of the original signal $\{S_k\}$, and performing the inverse Fourier transform. The original complex Fourier phase values of the signal from the previous iteration $\{s_n^{(i-1)}\}$ remain unchanged when reconstructing the signal $\{s_n^{(i)}\}$ having the desired power spectrum. While this step enforces the correct power spectrum, it usually disrupts the signal amplitude distribution. Thus, the second step in an iteration is to rank order the resulting time series $\{s_n^{(i)}\}$ and replace the ranked indices with the ranked amplitudes from the original signal $\{s_{n,sort}\}$. Performing the rank ordering will thus alter the power spectrum calculate in step i+1, thus requiring the entire procedure to repeat. After each iteration, the deviation from the original power spectrum is checked and the process repeats until a given accuracy is achieved.

The Role of Surrogate Data Analysis in EEG studies

Nonlinear measures such as complexity, chaoticity, and information-based measures can be useful in the analysis of the output of complex systems such as the brain (Lehnertz and Elger, 1995; Pincus, 1995; Lehnertz, 1999; Le Van Quyen et al., 2001; Osorio et al., 2001; Iasemidis et al., 2003, 2004). However, analysis of less complex systems may not require the application of

nonlinear methods as they may provide the same (or perhaps less) information about the system at hand while often resulting in increased computational cost. Thus, an original application of surrogate analysis was to provide partial justification for the use of nonlinear analysis methods in EEG studies. Surrogate data analysis has provided support for the presence of nonlinear components of EEG signal in various types of epilepsy (Casdagli et al., 1995; 1996, 1997; Lopes Da Silva et al., 1999; Jung et al., 2003; Liu et al., 2007). Additionally, observations have been made regarding the different neural states in epilepsy such as interictal, preictal, ictal, and postictal the corresponding occurrence of significant nonlinearity (Pijn et al., 1997; Jung et al., 2003) as well as a measure of the "amount" of nonlinearity (e.g. the magnitude of the p-value when comparing original to surrogate data) (Liu et al., 2007). In addition, surrogate data analysis has demonstrated changes in nonlinear signal component expression following various brain stimuli such as transcranial magnetic stimulation (Jing and Takigawa, 2002), drug treatment (Ferenets et al., 2006) compared to baseline EEG. As any similar studies regarding VNS was could not be located, such an analysis may provide a means for quantifying EEG effects related to VNS parameters and perhaps clinical outcome. In addition the following analysis may provide an improved understanding of the brain's EEG response to VNS and potentially provide insight into how it delivers its therapy.

Nonlinearity Analysis of Interstimulation EEG

The following study is motivated by a desire to characterize the interstimulation EEG dynamics in VNS patients and identify potential covariation with stimulation parameters using surrogate EEG analysis. The underlying hypothesis (stated as null) which motivates this study is "EEG dynamics during the interstimulation period are unrelated to the stimulation parameters in VNS patients". The interstimulation period is targeted in order to track the brain's post

stimulation response which may contain useful EEG dynamical information relating to the stimulation parameter configuration.

Under this experimental setup, it is logical to compare to the results to a control patient which utilizes artificial stimulation times. Resulting EEG dynamical differences between the VNS patient interstimulation epochs and the control patient artificial interstimulation epochs could provide convincing support for the existence of VNS-induced EEG effects which may be related to the VNS parameters.

Choosing a Test Statistic

By utilizing the "constrained realization" approach to surrogate data analysis, the options for a test statistic become more plentiful as the requirement for a pivotal test statistic is now relinquished (Theiler and Prichard, 1996). Based on the successful application of entropy measures in EEG nonlinearity test studies (Thomasson et al., 2000; Burioka et al., 2003,2005; Ferenets et al., 2006), as well as the general success in classifying neural states from EEG (Bruhn, 2000; Bruhn, 2001; Bruhn, 2003; Abásolo, 2005; Ferenets et al., 2006), the approximate entropy (ApEnt) measure will serve as the test statistic.

The ApEnt measure was calculated within non-overlapping windows of size 2048 points (4 seconds). A window of this size falls within a reasonable range utilized for computing ApEnt in terms of clinical and theoretical relevance (Pincus, 1995). The noise threshold r=0.2*std was selected as a result of studies which successfully correlated the ApEnt EEG measure to clinical drug anesthesiology levels (Bruhn, 2000; Bruhn, 2001; Bruhn, 2003; Ferenets et al., 2006), as well as a study which used ApEnt to characterize background EEG in patients with Alzheimer's Disease (Abásolo, 2005). The phase space mapping process utilized an embedding dimension of 7 is used based on previous EEG complexity studies quantifying neural state transitions in patients with mesial temporal lobe epilepsy (Iasemidis et al. 1988; Iasemidis et al., 1990;

Iasemidis et al., 1999). The time delay embedding process utilized a delay τ=7 corresponding to14 ms (Iasemidis et al., 1990; Zaveri et al., 1993; Iasemidis et al., 1996).

Experimental Design

The amount of surrogates were selected based on a model proposed by Schreiber and Schmitz which considers a residual probability α of a false rejection by random chance with a corresponding significance level of $(1-\alpha)\times 100\,\%$ (2000) The proposal suggests creating an amount of surrogates M=2*K/α -1 such that the probability that the data will reject the null hypothesis by chance is α for a two-tailed test (Schreiber and Schmitz, 2000). Due to the intensive computational complexity of this procedure, this preliminary analysis utilizes K=1 and α=0.1 for the purposes of selecting the amount of surrogate data copies. Thus, this study uses 19 surrogates.

EEG surrogates were calculated in non-overlapping windows of length 2048 points (4 seconds). This window size is considered to be within a reasonable range for surrogate data generation (Schreiber and Schmitz, 1996). This is also used as the window length utilized in the calculation of the ApEnt measure used as the test statistic.

The mean value of each ApEnt point across all 19 surrogates is computed to the surrogate datasets to a single time series which is then compared to the original signal (Casdagli et al., 1996; 1997; Liu et al., 2007). For patients with a 5 minute interstimulation time a window of 73 points represented the interstimulation period. For patients with a 5 minute interstimulation time a window of 73 points represented the interstimulation period. For patients with a 3-minute interstimulation time, a 43 point window represented the interstimulation time. Statistical testing was performed using a two-tailed paired-t test. For 95% certainty and 72 degrees of freedom and 42 degrees of freedom the critical t-values are t= 1.993 and t=2.018, respectively.

This preliminary study assesses the dynamical structure of EEG signals during VNS interstimulation periods. The dynamical structure is evaluated by testing each interstimulation epoch against a null hypothesis of a Gaussian linear process using surrogate datasets for all epochs for all six patients. The hypothesis, stated as null is:

- H0: EEG dynamics during an interstimulation epoch are described by a Gaussian linear stochastic process.

Results

For each patient and for each channel, the hypothesis was tested using approximate entropy of the EEG of VNS deactivation epoch (see figure 5-3 through 5-12 and tables 5-1 through 5-3). Patients A and B showed a notable increase in the amount of interstimulation epochs demonstrating a nonlinear signature occurring across most channels occurring between 11 pm until 7 am. The control patient showed a decrease in a nonlinear fingerprint occurrence in non-focal channels during the same time of day.

The fraction of epochs across the entire recording and all channels which displayed a nonlinear signature (could reject H0 at the given significance) displayed a potential negative correlation with the pulse width parameter for all six patients.

In addition, patient F showed nonlinear signatures in fewer epochs than any other patient (35.1% of all epochs could reject H0 at the given significance), followed by patient E (39.0%). Both of these patients are seizure free. Patient B's EEG showed the most nonlinear fingerprints having 52.3% of the epochs rejecting H0 at the given significance level. While patient F showed the most nonlinearity, patient F had the greatest stimulation frequency (30 Hz) and the greatest pulse width (750 μs). Patient B had the lowest stimulation frequency (20 Hz) and the shortest pulse width (250 μs). The fraction of epochs which displayed nonlinear signatures for the

control patient with 5-minute and 3-minute interstimulation times were 42.5% and 37.2%, respectively.

In general, the lower the monthly seizure rate, the less nonlinear signatures were observed. According figure 5-3, patient F (seizure-free) produced a smaller fraction of nonlinear interstimulation epochs than the 3-minute control whereas patient D (~3 seizures per month) produced a larger fraction of nonlinear epochs than the 3-minute control. A similar trend was observed in the patients with the 5-minute interstimulation time. Patients C and E (seizure free and ~ seizures per month, respectively) generated a smaller fraction of nonlinear epochs than the 5-minute control whereas patients A and B (~3 seizures per month and ~30 seizures per month, respectively) displayed a larger fraction of nonlinear epochs than the 5-minute control.

Patients A, B, D, and F showed noticeably higher expressions of nonlinearity in channels located near foci than non-focal channels. The control patient demonstrated a high density of nonlinear behavior in non-focal channels during waking hours which is diminished around 11 pm – 7 am, except for the TLc2 channel which shows a greater fraction of epochs demonstrating nonlinear signatures than other channels.

Discussion

In regards to the connection of EEG patterns stimulation parameters, the most obvious observation was the potential relationship between the fraction of epochs which displayed nonlinearity and the pulse width parameter. In addition, Patient F produced the smallest fraction of epochs presenting a nonlinear signature (35.1% of epochs could reject H0 at the given significance level) and patient had the highest stimulation frequency (30 Hz) and the highest pulse width (750 μs) of all six VNS patients. Patient B's EEG presented the greatest fraction of epochs presenting a nonlinear fingerprint (52.3% of epochs could reject H0) whereas the patient

had the lowest stimulation frequency (20 Hz) and the lowest pulse width (250 μs) of all six VNS patients.

The underlying biology driving this EEG behavior could be related to a study which demonstrated an acute suppression of epileptiform activity in the hippocampus during VNS (Olejniczak et al., 2001). Perhaps enhanced suppression of epileptiform activity is responsible for the diminished nonlinearity in patients with fewer seizures.

Also, a study has demonstrated that the 250 μs pulse width parameter results in blood flow mitigation to significantly more brain regions (e.g. hippocampus, sup. temp. lobe) than a 500 μs pulse width in VNS patients (Mu et al., 2004). Perhaps pulse width related blood-flow reductions reported by Mu et al. are responsible for any such changes in epileptiform activity suppression which may have been detected by the surrogate data analysis.

In addition, patients E and F demonstrated the lowest fraction of epochs presenting a nonlinear signature (39% and 35.1%) and also happen to be the only two patients which are seizure-free. This may be aligned with the clinical observation that the absence of bilateral interictal epileptiform discharges was the only EEG predictor of seizure freedom (Janszky et al., 2005). Future studies should include characterizing the profile of interictal epileptiform discharges for relationship to linear and nonlinear measures.

In patients A and B there was a notable increase in the amount of interstimulation epochs demonstrating a nonlinear signature occurring across most channels at times around 11 pm until 7 am. The increase in the occurrence of nonlinear signature may have been partially resulted from the patient being drowsy or asleep. A surrogate analysis study by Shen et al. demonstrated a considerable number of EEG segments displaying a nonlinear signature during stage 2 sleep and may be the result of K-complexes (Shen et al., 2003).

The control patient demonstrated a high density of nonlinear behavior in non-focal channels during waking hours which is diminished around 11 pm – 7 am, except for the TLc2 channel which shows a greater fraction of epochs demonstrating nonlinear signatures than other channels.

Patients A, B, D, and F showed a greater fraction of epochs presenting nonlinear signatures in channels located near foci than non-focal channels. This observation is aligned with the literature where focal electrodes demonstrated higher nonlinearity than non-focal electrodes (Casdagli et al., 1995, 1996, 1997).

While the control patient provides information from a patient with a similar epileptic condition and recorded at the same frequency as the VNS patients, the depth electrode recordings from the control patient provide limits to what can be suggested to conclusions about VNS-induced scalp-EEG patterns. The ideal control would be use baseline from each patient using an identical electrode setup.

The fraction of epochs rejected the null hypothesis is a necessary condition for nonlinear dynamical, however, these results are not sufficient to suggest a particular type of nonlinearity (e.g. surrogate analysis cannot prove the existence of low-dimensional chaos). Changing parameters (e.g. the dimensionality or noise threshold) for ApEnt may improve sensitivity to potential VNS-induced EEG effects and thus provide the possibility to relate said effects to stimulation parameters and ultimately to the clinical outcome. The results, combined with studies documenting the ability of various nonlinear measures to quantify neural states motivates the usage of nonlinear as well as linear measures to examine EEG dynamical behavior which could be associated with VNS stimulation.

Temporal Evolution of Interstimulation EEG Dynamics

The results of the previous experiment characterized the presence of nonlinear EEG signal components throughout each of the interstimulation epochs for each of the six patients undergoing VNS therapy for epilepsy. However, as surrogate analysis does not provide characterization of nonlinear signal components, it is possible that the properties of the detected nonlinear components may distinguish the control patient from the VNS patient. Thus, additional characterization signal dynamics would enhance the findings from the surrogate analysis.

This experimental perspective aims to analyze the observed nonlinear signal components and further characterize how brain dynamical patterns behave during the period between stimulations. This study is motivated by an underlying hypothesis (stated as null) "H0: Interstimulation EEG dynamics are time invariant in patients undergoing VNS therapy for epilepsy". While VNS is believed to induce its therapeutic effect via long-term modulation (Koo, 2001), this long-term effect may manifest as changes in short-term temporal dynamical behavior compared to baseline which would be consistent with the traits of a dynamical disorder such as epilepsy (Mackey and Glass, 1977; Mackey and an der Heiden, 1982; Milton and Mackey, 1989; Belair et al., 1995; Milton and Black, 1995; Milton, 2000; Lopes Da Silva et al., 2003).

Thus, it is possible that the brain dynamics during the interstimulation epochs in VNS patients will be distinguishable from a control patient, which would provide support for the use of EEG dynamical analysis for the study of VNS effects. Furthermore, EEG dynamical behavior during the interstimulation period may be related to stimulation parameters.

Data Description

Six patients undergoing VNS therapy for intractable epilepsy were analyzed in this study. The continuous scalp-EEG recordings are approximately 24 hours in duration and were obtained

at the Shands Hospital GCRC protocol # 614, IRB protocol #617-2004, "Neurophysiologic Measures of Vagus Nerve Stimulation" at the University of Florida, Gainesville. Available clinical information for the six patients is summarized in tables 4-1 and 4-2. The electrode positions are described in figure 5-1. VNS activation times were obtained from the ECG channel, which was recorded from an electrode placed in close proximity to the VNS pulse generator. The ECG channel was otherwise excluded from this study.

EEG Dynamical Measures

Quantitative EEG analysis is a broad field incorporating numerous methods for quantifying various properties of EEG signals (see chapter 3). In order to improve the characterization of the dynamical evolution, this study utilized multiple EEG measures. Each of the EEG analysis techniques first applies a phase space transformation after which the relevant information is extracted. The phase space mapping procedure of Takens (1981) was applied using an embedding dimension of 7 is used based on previous studies in which the epileptic attractor was characterized from EEG recordings of patients with mesial temporal lobe epilepsy (Iasemidis et al. 1988; Iasemidis et al., 1990; Iasemidis et al., 1999). For an embedding dimension of 7, a time delay of τ=7 samples corresponding to14 ms is applied. This time delay value has demonstrated success in characterizing the rhythm of a typical seizure in temporal lobe epilepsy (Iasemidis et al., 1990; Zaveri et al., 1993; Iasemidis et al., 1996;).

Approximate entropy

This ApEnt measure (see equations 3-16 to 3-19) has been utilized to study EEG patterns in Alzheimer's disease patients (Abásolo, 2005), as a surrogate marker for anesthesia depth (Bruhn 2000, Bruhn 2001, Bruhn 2003), detecting epileptic seizures (Abásolo 2007; Srinivasan, 2007), and as a test statistic for characterizing EEG nonlinearity (Thomasson et al., 2000;

Burioka et al., 2003,2005; Ferenets et al., 2006). Thus, it may be useful for characterizing brain dynamics during interstimulation intervals.

The noise threshold was set at 20% of the signal's standard deviation r=0.2*std was applied based on studies which successfully correlated ApEnt with drug anesthesia levels (Bruhn, 2000; Bruhn, 2001; Bruhn, 2003; Ferenets et al., 2006) and a study characterizing background EEG in patients with Alzheimer's Disease (Abásolo, 2005). The 2048 point (4 second) window selected for this study is within a range that has been described as being clinically and theoretically appropriate (Pincus, 1995).

Correlation sum

For a collection of points in some vector space, the correlation sum is the fraction of all possible vector pairs which are closer than a given distance *r* for a particular norm distance norm (see equation 3-2). The correlation sum is estimated after mapping the EEG into phase space. The correlation sum is often used to estimate the correlation dimension (equation 3-27) which has been extensively utilized in physiological data (Kantz and Schreiber, 1995) such as neural state classification studies using EEG (Tirsch et al., 2000, 2004), as well as seizure prediction (Elger et al., 1998; Martinerie et al., 1998). However, since use of an absolute radius can result in a heavy EEG amplitude sensitivity (Osorio et al., 2001), this study utilizes a relative radius measure (with respect to the diameter of the dataset in phase space) for brain dynamics characterization (Casdagli et al., 1996, 1997, Merkwirth et al., 2002).

Correlation sum was estimated using the TSTOOL package (Merkwirth, 2002) for Matlab. Theiler recommends application of an exclusionary window to a range of points surrounding each reference point in order to avoid embedding vectors on the same trajectory (Theiler et al., 1986). Based on the results of similar studies, a 250 ms (128-point) exclusion

window around reference points and a search radius r=0.2 (10% of attractor diameter) were implemented (Casdagli et al., 1996, 1997).

Mean angular frequency in phase space

A modification to the Lyapunov exponent measures, the mean angular frequency in phase space measure ($\overline{\Omega}$) quantifies the angular frequency of the phase space evolution of two nearest neighbor points relative to a reference point (Iasemidis et al., 2001, 2002, 2003). Conceptually, this measures the average rate of change of a system state. The measure is related to the Lyapunov exponent, which measures the local stability of a system. A study quantifying neural states in epilepsy found that preictal, ictal, and postictal states corresponded with medium, high, and lower values of $\overline{\Omega}$, respectively (Iasemidis et al., 2002, 2003). In addition, the dynamic entrainment / disentrainment and seizure resetting phenomena observed before and after epileptic seizures using the STLmax measure has also been described with $\overline{\Omega}$ (Iasemidis et al., 2003). Thus, the sensitivity of $\overline{\Omega}$ to changes in neural state makes it a candidate for quantifying any EEG dynamics changes which may be associated with VNS. The window length selected for this study, 2048 points, is the same window length as was used in Iasemidis et al. (2001, 2002, 2003).

Short-term maximum Lyapunov exponent

The STLmax measure has been shown to be useful for providing dynamical information about the neural state of the epileptic brain. Studies performed on EEG from human patients (Iasemidis and Sackellares, 1990; Iasemidis and Shiau et al., 1999; Iasemidis et al., 2001; Iasemidis and Pardalos et al. 2003; Iasemidis and Shiau et al., 2003) and animal models of epilepsy (Nair et al., 2004, 2005, 2006; Talathi et al., 2008) imply that the evolution of the brain to a state of greater spatio-temporal order correlates with spontaneous seizures. This

phenomenon is presented as a temporally progressive increase in the similarity among so-called critical channels measured by STLmax calculated from multichannel EEG recordings. Thus, sensitivity of STLmax to neural state changes in epilepsy indicated by the above studies makes the measure a reasonable candidate for identification and characterization of potential VNS-induced EEG effects.

The window duration for calculating STLmax needs to be short to provide temporally local information about the brain's dynamics yet contain enough points for the algorithm to converge (additional information about this can be found in chapter 3). The 2048 point (4 second) window size chosen for this study is suggested to provide a sufficiently stable STLmax estimate in previous neural state classification studies in epilepsy (Iasemidis and Sackellares, 1999). Also, use of the shortest window length possible for STLmax estimation can help provide a stationary segment for estimating local dynamical information. As such, while maintaining a window length of the recommended number of data points for algorithmic convergence, the 512 Hz sampling frequency provides improved time resolution over previous studies (which utilized a 200 Hz frequency). The evolution time parameter was set to $\Delta T = 41$ msec (21 samples) based on successful neural state classification studies that utilized them (Iasemidis and Sackallares, 1999).

Experimental Design

This preliminary investigation into the temporal evolution of the EEG between stimulations will start searching for coarse dynamics transitions between the first and second halves of each epoch where the VNS is deactivated. The rationale for this class designation is to assess the existence of any short-term transitions, to characterize the temporal evolution where it exists, compare with a similar experimental setup in a control patient and determine any correlation to clinical parameters. The underlying hypothesis (stated as null) which motivates

this study is “EEG dynamics during the interstimulation period are unrelated to the stimulation parameters in VNS patients”. Figure 5-13 shows an illustration indicating how the measures were grouped to examine the temporal evolution of these dynamical measures during VNS-OFF.

As shown in figure 5-13, EEG measures corresponding to the first half of an epoch are compared to EEG measures corresponding to the second half of an epoch for each channel, for all channels (except ECG). Using 4 second windows to calculate the various EEG measures, the

The preliminary hypotheses (stated as null) are formulated for the purpose of characterizing the EEG behavior associated with stimulation in the VNS patients:

- H1: The EEG dynamics as quantified by approximate entropy are time invariant while VNS is deactivated.
- H2: The EEG dynamics as quantified by correlation sum are time invariant while VNS is deactivated.
- H3: The EEG dynamics as quantified by mean angular frequency in phase space are time invariant while VNS is deactivated.
- H4: The EEG dynamics as quantified by short-term maximum Lyapunov exponent are time invariant while VNS is deactivated.

These hypotheses aim to answer the question of how the dynamical brain behavior as described by these four nonlinear EEG measures evolves over time between stimulations. Such an analysis may identify EEG patterns which are sensitive to particular stimulation parameter configurations as well as the candidate measures for detecting such patterns.

The control patient underwent two similar tests; one which utilized stimulation times with a 3 minute ‘off’ duration, and a second test which utilized stimulation times with a 5 minute ‘off’ duration. The hypotheses were tested with a two-tailed unpooled two-sample t-test with $\alpha=0.05$ using the Matlab Statistics Toolbox. The tests were performed assuming unequal variances and utilized Satterthwaite's approximation for the effective degrees of freedom. For a measure window size of 2048 points (4 seconds), the first and second halves of the interstimulation epoch

each contain 36 values of each measure for patients A,B,C,E (whom have a 5 minute interstimulation duration) and 21 values of each measure for patients D and F (whom have a 3 minute interstimulation duration). The same statistical testing method was used to test the control patient. The control patient was tested with artificial stimulation times using 3-minute and 5-minute interstimulation duration.

Results

As figures 5-22 and 5-24 show, for all patients the ApEnt and $\overline{\Omega}$ measures resulted in a larger fraction of epochs rejecting H1 and H3 (respectively) than the control patient for the majority of the 25 EEG channels. When using the correlation sum measure, the majority of electrodes had a greater fraction of epochs reject H2 for patient A than the control patient. However, the correlation sum did not show any such trend for any other patients. For all four measures, patient C rejected the four hypotheses in 2-3 times more interstimulation epochs than the control patient. For all four measures, patient F produced the fewest amount of interstimulation epochs that rejected the null hypothesis than any other patient.

Numerous observations can be made regarding focal and non-focal electrode behavior according to tables 5-3, 5-5, 5-7, 5-9. In terms of the ApEnt measure, the focuses of patients A,B,C, and F produced significant dynamical complexity fluctuations during more interstimulation epochs than their corresponding non-focal areas, and greater than the control focus. This phenomenon could be related to studies where electrodes in the vicinity of an epileptogenic focus displayed more prominent nonlinear behavior (Casdagli et al., 1995, 1996, 1997). The correlation sum measure suggested that the focus and non-focus of patient A demonstrated significant time varying dynamics in more interstimulation epochs than the control. For all six patients, the $\overline{\Omega}$ showed significant temporal dynamics variation in more epochs than

the corresponding control patient. With regards to the spatial comparison of focal and non-focal electrodes, the STLmax measure did not show any obvious trends.

The main finding in regards to the dynamical behavior throughout the day (see figures 5-14 through 5-21) is the overall trend of diminished dynamical variance between approximately 11 pm and 7 am for all four measures in patients A (~epoch 130) and C (~epoch 140). Patient B's seizures were accompanied by significant temporal fluctuation in the $\overline{\Omega}$ dynamical measure before and after seizures. As stimulation epochs which overlapped with seizures were excluded from the study, these dynamical alterations occurred within about 10 minutes of the seizure.

Discussion

This study aimed to characterize the interstimulation EEG periods using a range of dynamical EEG measures which have demonstrated sensitivity to neural state changes such as those observed in epilepsy.

Patient C had highest output current (2.5 mA) as well as the greatest amount of epochs (45.6%, 36.8%, 36.1%, and 21.8%) showing time varying dynamics of all the patients as measured by the ApEnt , correlation sum, $\overline{\Omega}$, and STLmax measures, respectively (see figures 5-26 through 5-29). Patient A showed similar ApEnt and $\overline{\Omega}$ behavior (35.7% and 31.0% of interstimulation epochs demonstrated significant temporal variance for both measures, whereas control values were 21.8%, 10.5%, respectively) compared to patient C and had the second highest output current (1.75 mA). Patient F showed an opposite trend having the lowest output current (0.75 mA) where ApEnt, $\overline{\Omega}$, and STLmax produced the smallest fraction epochs rejecting H1, H3, and H4 (23.8%, 20.2% and 14.3% whereas control values produced 16.9%, 7.9%, and 19.4%, respectively). The ApEnt measure quantifies the regularity in a time series (Pincus, 1995; Abásolo et al., 2007), the $\overline{\Omega}$ measure provides an estimate of the stability of the

reconstructed attractor in phase space (Iasemidis et al., 2002, 2003), and STLmax provides a measure of chaoticity of a signal (Iasemidis et al., 1991). Thus, the similar behavior of these three measures implies the EEG could be undergoing fewer changes in the regularity, stability and observed chaoticity in patient F than patients A and C. Overall, the ApEnt and $\overline{\Omega}$ measures demonstrated the greatest deviation from the control patient, the broadest range of the fraction of epochs showing time varying dynamics, and a potential covariation with output current. For these reasons, the ApEnt and $\overline{\Omega}$ measures may potentially find use as EEG biomarkers for VNS.

Biologically, these results may be related to the findings of studies which identified a current threshold for suppression of chemically induced seizure models. For example, seizures induced in a low Ca2+ model could be suppressed with currents greater than 1μA (Warren and Durand, 1998). In addition, seizures induced in a high K+ model could be suppressed with currents greater than 4μA (Nakagawa and Durand, 1991). Yet patient F has been seizure free for at least one year at the time of recording, while patients A and C have mean seizure rates of 3 and 2 seizures per month (respectively). In general, higher values of VNS parameters are associated with improved seizure protection (Ben-Menachem et al., 1994). So while at first it may seem counterintuitive that the patient with the lowest output current (patient F) is seizure free, keep in mind that the aforementioned study is referring to collective impact of output current, pulse width, and stimulation frequency. So even though patient F's output current (0.75 mA) is less than patient A's (1.75 mA) and patient C's (2.5 mA), patient F has higher pulse width (750 μs) than patients A and C (both 500 μs). In addition, patients A and F have the greatest stimulation frequency of all the patients in the study (30 Hz) whereas patient C has a 25 Hz stimulation frequency.

In addition, patient F has a shorter interstimulation interval (3 minutes) compared to patients A and C (both 5 minutes). It is tempting to attribute patient F's seizure freedom to this patient having a greater amount of stimulation cycles over time, however patient E is also seizure free and has a 5 minute interval.

It is interesting that all four measures behaved in a similar manner for patient F whom had the lowest output current and was seizure free. Perhaps when the output current raises above a particular threshold value the neuronal activity is affected in such a manner that it becomes more erratic and thus results in more rapid dynamical transitions. The minimum current threshold for suppression of epileptiform activity in seizure observed by Nakagawa and Durand (1991) as well as Warren and Durand (1998) may be responsible for this. This could explain why patients A, B, C, D and E whom had greater output currents than patient F produced results less consistent with the other dynamical measures than for patient F.

Regarding the relationship to the time of day to EEG dynamical effects, the most obvious trend was the period corresponding to 11 pm and about 7 am (see figures 5-14 and 5-16). The reduced dynamical temporal variance for all four measures in A (~epoch 130) and C (~140) during this period compared to other times of day is likely related to the fact that the patients are drowsy or asleep. A recent study by Rizzo et al. (2004) demonstrated that an overall increase in EEG total power both in sleep and wakefulness after long-term VNS treatment compared to pre-treatment EEG, so it is plausible that the dynamical measures during sleep were influenced by the VNS. However, EEG sleep studies have demonstrated a decrease in the mean and standard deviation of the ApEnt measure (Acharya et al., 2005; He et al., 2005) during sleep compared to wakefulness, which is aligned with the observation of diminished variation of the ApEnt measure during times when the patient is presumed to be asleep. In addition, a study by Acharya et al.

showed an increase in mean and a decrease in standard deviation for most sleep stages (2005). Thus, the observation of STLmax behavior during sleep is aligned with the literature. Therefore, while VNS has been shown to affect the sleep EEG signal (Rizzo et al., 2004), the behavior of the nonlinear measures during a period when the patient is drowsy or asleep is consistent with sleep patterns in people without VNS implants.

Conclusions

The results from the surrogate EEG analysis show a potential between the fraction of epochs which displayed nonlinearity and the pulse width parameter. In addition, Patient F produced the smallest fraction of epochs presenting a nonlinear signature (35.1% of epochs could reject H0 at the given significance level) and patient had the highest stimulation frequency (30 Hz) as well as highest pulse width (750 μs) of all six VNS patients. Patient B's EEG presented the greatest fraction of epochs presenting a nonlinear fingerprint (52.3% of epochs could reject H0) whereas the patient's stimulator was programmed with the lowest stimulation frequency (20 Hz) and the lowest pulse width (250 μs) of all six VNS patients. In addition, patient B demonstrated the greatest amount of monthly seizures. It is possible that neuronal modulation may be sensitive to the duration of the individual pulses in a manner which may manifest as increased linearity of neuronal output. For example, Mu et al. (2004) demonstrated that 250 μs showed blood flow reduction to significantly more brain regions than 500 μs. However, such an observation requires additional patients for verification. Also, patients E and F demonstrated the lowest fraction of epochs presenting a nonlinear signature (39% and 35.1%) and are also the only two patients which are seizure-free. This observation may be aligned with the clinical observation that the absence of bilateral interictal epileptiform discharges was the only EEG predictor of seizure freedom (Janszky et al., 2005). While interictal epileptiform discharge detection was not included in this study, future studies should include the spatio-temporal

distribution of interictal epileptiform discharges in the characterization process. Comparison with linear and nonlinear EEG measures may provide additional information relevant to the connection between stimulation parameters and EEG patterns.

The results from the temporal analysis of interstimulation dynamics demonstrate a potential manifestation of the VNS long-term modulation effect in terms of the interstimulation dynamics behavior. In particular, the ApEnt and $\overline{\Omega}$ measures displayed a potential covariation the output current parameter, demonstrated the greatest deviation from the control patient, the broadest range of the fraction of epochs showing time varying dynamics. For these reasons, the ApEnt,and $\overline{\Omega}$ measures could serve as EEG biomarkers for VNS. In light of this result, its possible that when the current reaches a threshold level the neuronal activity intensifies such that the summed output (the EEG) behaves more erratically (in terms of more rapidly fluctuating dynamical measures such as ApEnt and $\overline{\Omega}$,). This phenomena could be related to the observation of minimum stimulation current thresholds were needed to suppress epileptiform activity in low Ca^{2+} (Warren and Durand, 1998) and high K^{+} (Nakagawa and Durand, 1991) seizure models.

Overall, the two interstimulation analysis experiments (analysis of nonlinearity and analysis of temporal variation) showed potential connections EEG covariation with the pulse width, output current, and signal frequency parameters. Such effects may be useful as an EEG biomarker of optimal VNS settings. Additional studies should be performed on a larger sample of patients in order to validate these claims. In addition, baseline EEG recordings obtained prior to VNS implantation are crucial for determining which EEG effects in the VNS patient could be associated with VNS and which effects appeared to be present in the EEG prior to VNS implantation.

The EEG measures were likely suboptimal as they were selected based on similar studies. Though it is difficult to select the proper parameters in measures used in an expeditionary study such as this one, a good place to start may be to calibrate the measures such that they are able to capture and unfold an epileptic attractor in phase space. From this perspective, future VNS studies which utilize phase space embedding transformations should utilize a patient's own seizures to determine the dimension and delay for embedding signals.

In addition, study of the VNS in this setup is limited by the fact that the stimulator is programmed for chronic regular stimulation. Thus, though these studies aim to characterize the short-term EEG effects after stimulation, the short-term affect is produced by the cumulative effect of a large number of stimulations. Thus, an interesting study to help truly elucidate the effects of an individual stimulation or a group of stimulations would be to record prestimulation baseline for a group of patients, perform a single VNS stimulation, and perform an additional EEG recording while keeping output current at zero milliamps to examine any post-stimulation effects. Such an analysis may be one of the best ways to provide the most objective insight into the EEG effects of VNS without concern of any long-term modulatory effects. In addition, tracking the progression of such measures over time (e.g. 3 months, 6 months, 12 months after implantation) and comparing with the patients own baseline EEG recording are a desirable approach to examining EEG dynamics in patients with VNS.

The seizures that patient B underwent during the recording session could likely have had a far reaching impact on the observed dynamics patterns, as EEG dynamical transitions have been documented as occurring several minutes to several hours prior to seizures (Iasemidis et al., 2004). One potential improvement to this study is to record multiple days of recordings in order to compare a sufficient amount of 'interictal' data, which has been defined as being at least

8 hours away from a seizure (Pardalos et al., 2003; Hively et al., 2005; Chaovalitwongse et al., 2006). This would eliminate pre-seizure dynamical transitions as an additional variable to influence results. If this were not possible, one other possibility would be to examine only the EEG data that occurs at least 8 hours away from any detected seizure in a patient. One challenging aspect this approach is that the amount of EEG that would be allowed in the study would be diminished significantly (e.g. two-thirds of a single day would be excluded due to a single seizure), and with only a handful of seizures at the 'wrong' time would render this approach infeasible.

Though sleep staging was not included in this research protocol , obtaining the precise sleep times with manual and/or computer automated sleep staging for each patient should be included in future work. This would help to further examine the observation that the four EEG measures underwent less variation over time during the periods between about 11 pm and about 8 am.

The preliminary study of temporal evolution of dynamics used a two tailed test to determine the means are different or not. A future study should look at the direction of the two way test to determine if regularity, stability, or chaoticity are increasing or decreasing throughout the duration of the interstimulation interval. Such information may provide additional insight into the dynamical behavior and the stimulation parameters (e.g. a trend of decreasing or increasing the dynamical measures may be related to the stimulation parameters, the clinical status of the patient, or even the time of day).

Ultimately this study may lead to a method of surgical VNS testing, e.g. surgically exposing the left vagus nerve so a diagnostic vagus nerve stimulation device could be temporarily attached to the patient, stimulations could be applied in the operating room and the

EEG signal can be analyzed. If this setup were to prove successful, it may provide a method to prescreen patients for responsiveness to VNS therapy prior to undergoing the implantation process.

An article related to these studies was published under the title “Optimization of epilepsy treatment with vagus nerve stimulation” with authors Basim Uthman, Michael Bewernitz, Chang-Chia Liu, and Georges Ghacibeh (Uthman et al., 2007).

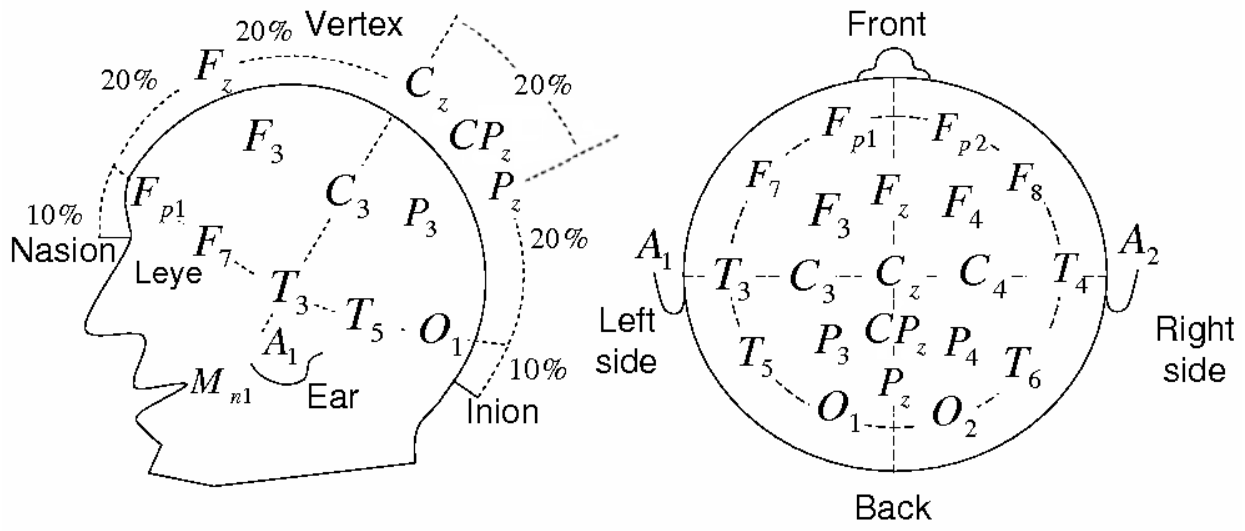

Figure 5-1. Map of EEG electrode location for the VNS patients. The electrodes were positioned according to the 10-20 electrode placement system which assigns locations proportionally spaced locations (e.g. 10%-20%) with respect to the size of the patient's head.

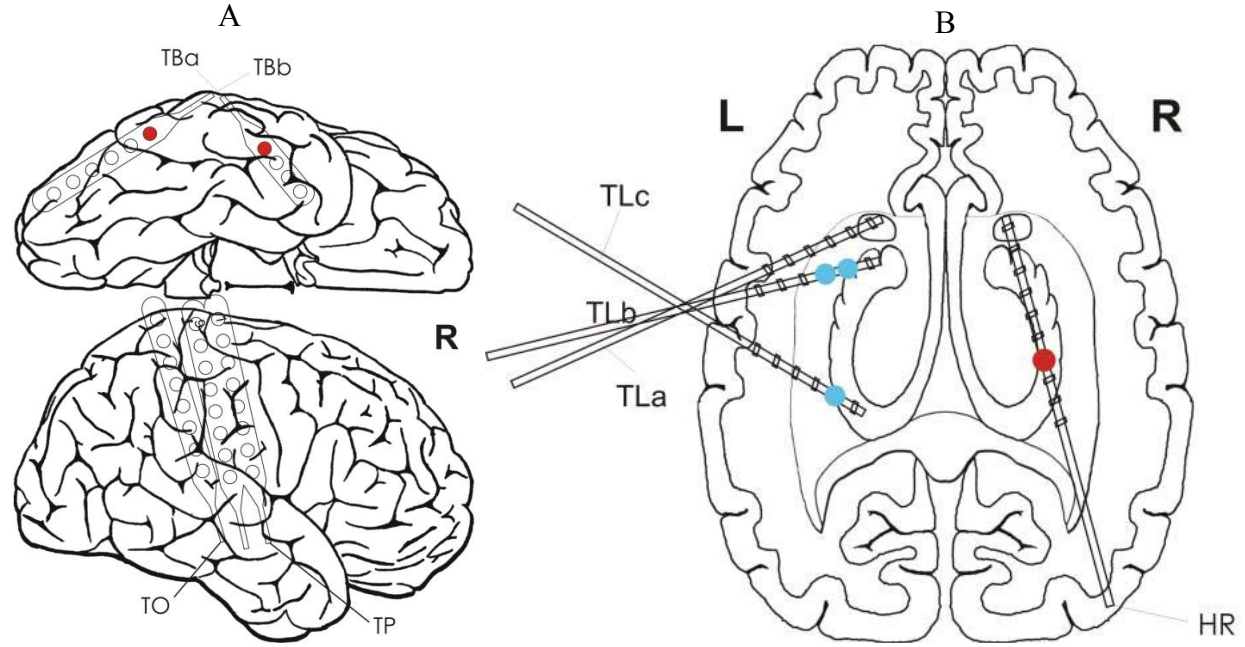

Figure 5-2. Electrode positions for the control patient from A) an inferior and right view and B) axial slice view of the brain. Red circles indicate focal electrodes (TBa4, TBb6, HR7), blue circles indicate non-focal electrodes (TLb2, TLb3, TLc2). Images provided for this publication courtesy of the Freiburg Center for Data Analysis and Modeling at the Albert-Ludwigs Universität Freiburg (University of Freiburg), Freiburg, Germany.

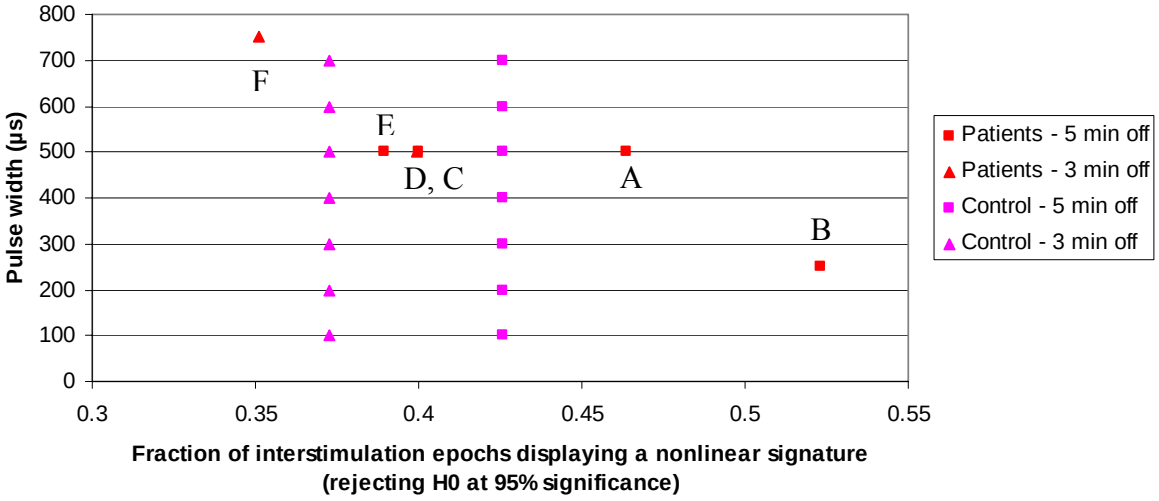

Figure 5-3. Comparison of pulse width parameter to the fraction of epochs displaying a nonlinear signature in the six patients treated with VNS. The fraction of epochs displaying a nonlinear signature in control patient using the 3-minute and 5-minute off pseudo stimulation times are represented by the column of six triangles (3 minute off times) and six squares (5 minute off times).

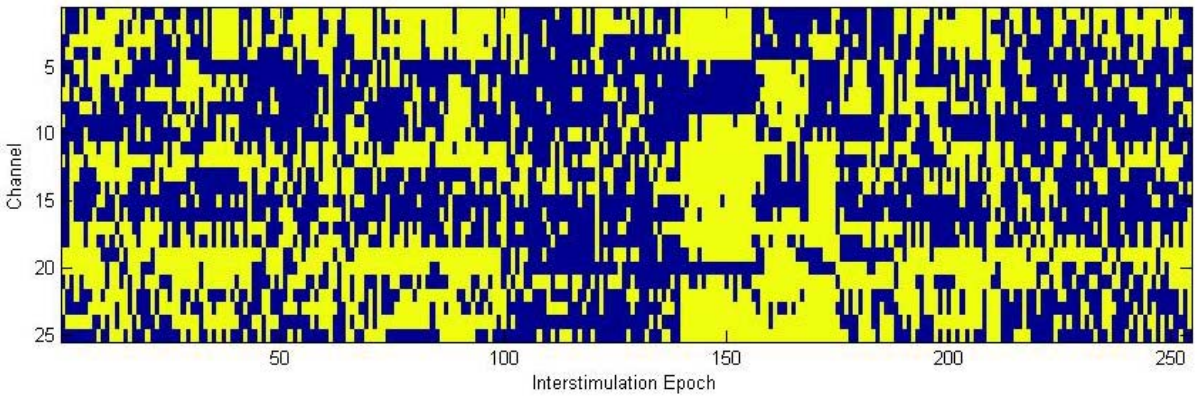

Figure 5-4. Patient A surrogate data analysis results over 24 hours during the interstimulation epoch. Yellow indicates that particular interstimulation epoch (abscissa) for the channel of interest (ordinate) rejected the null hypothesis.

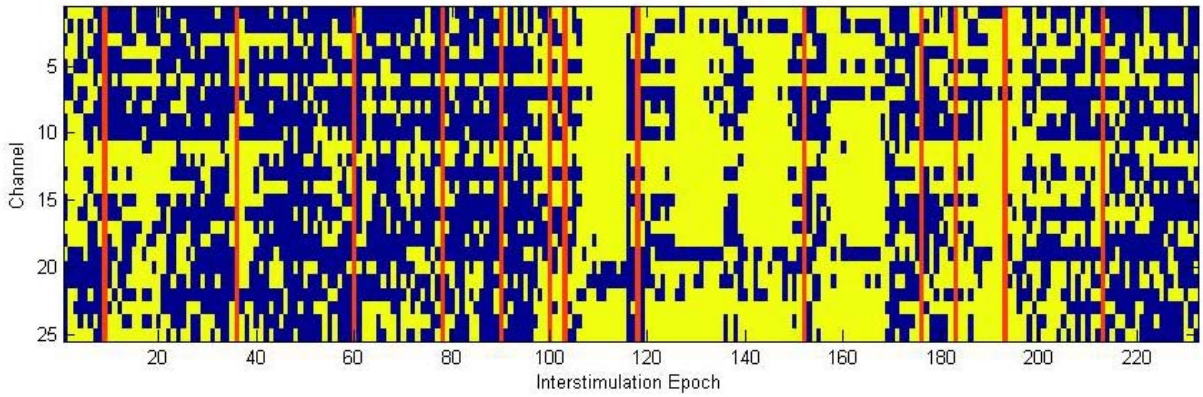

Figure 5-5. Patient B surrogate data analysis results over 24 hours during the interstimulation epoch. Yellow indicates that particular interstimulation epoch (abscissa) for the channel of interest (ordinate) rejected the null hypothesis. The red lines indicate seizures.

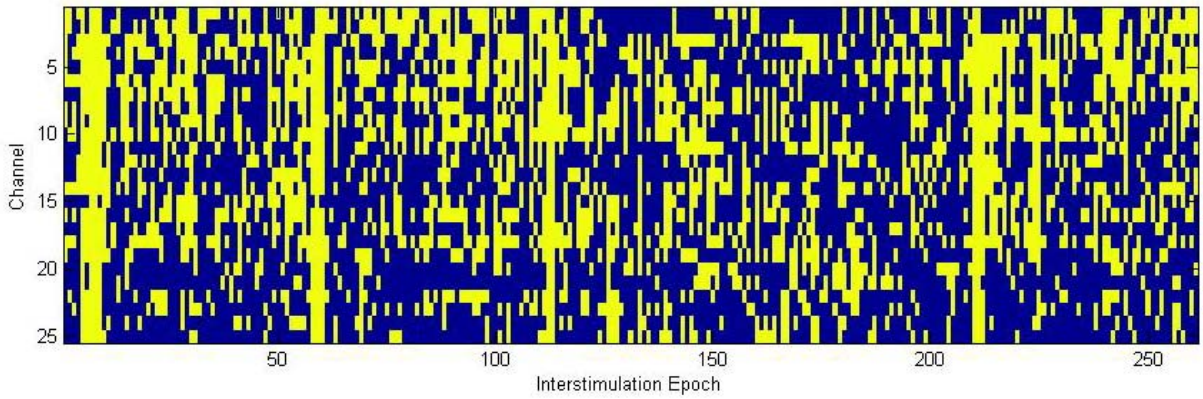

Figure 5-6. Patient C surrogate data analysis results over 24 hours during the interstimulation epoch. Yellow indicates that particular interstimulation epoch (abscissa) for the channel of interest (ordinate) rejected the null hypothesis.

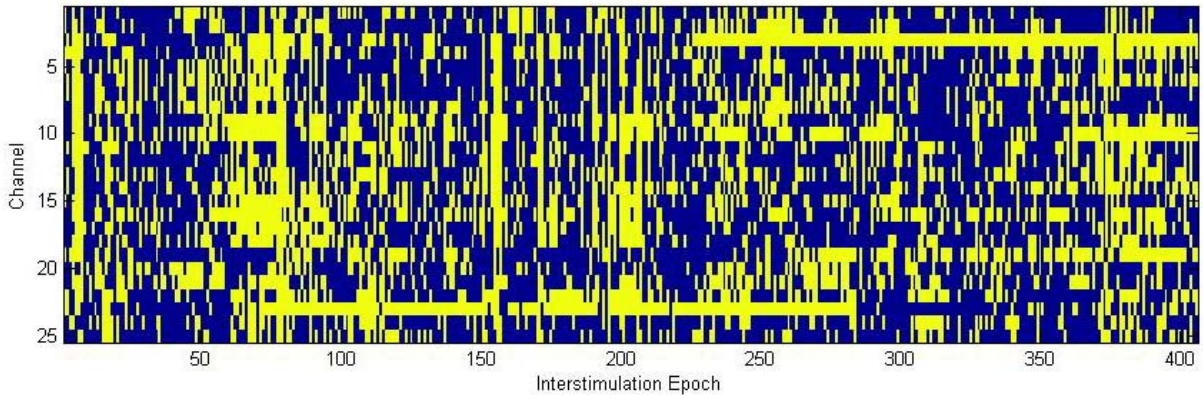

Figure 5-7. Patient D surrogate data analysis results over 24 hours during the interstimulation epoch. Yellow indicates that particular interstimulation epoch (abscissa) for the channel of interest (ordinate) rejected the null hypothesis.

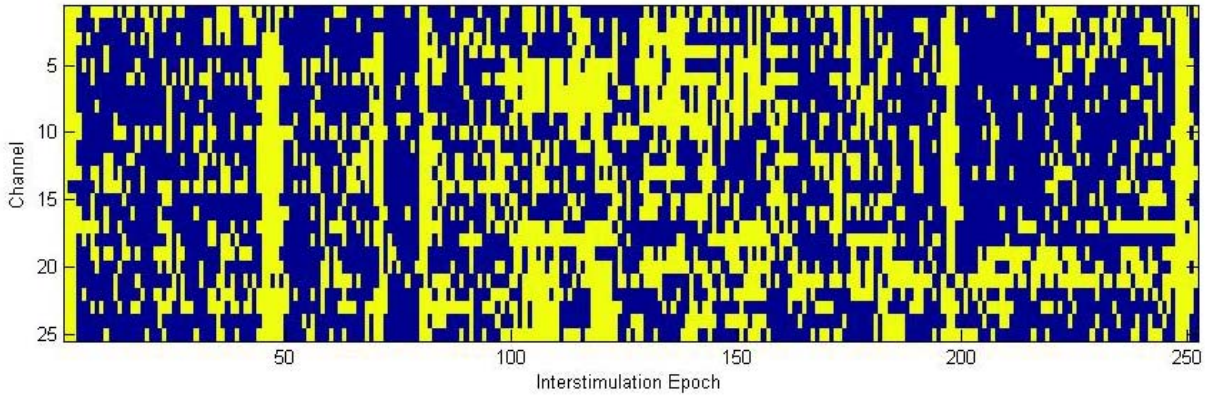

Figure 5-8. Patient E surrogate data analysis results over 24 hours during the interstimulation epoch. Yellow indicates that particular interstimulation epoch (abscissa) for the channel of interest (ordinate) rejected the null hypothesis.

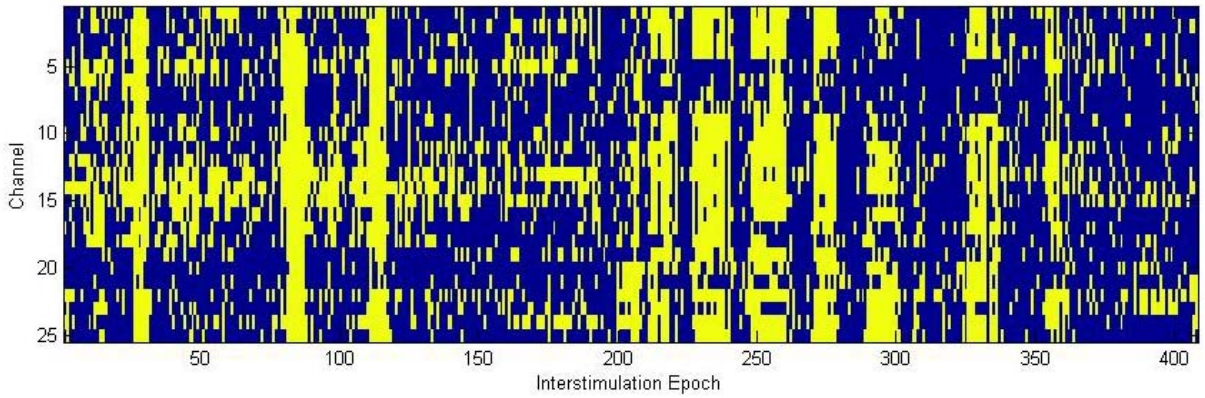

Figure 5-9. Patient F surrogate data analysis results over 24 hours during the interstimulation epoch. Yellow indicates that particular interstimulation epoch (abscissa) for the channel of interest (ordinate) rejected the null hypothesis.

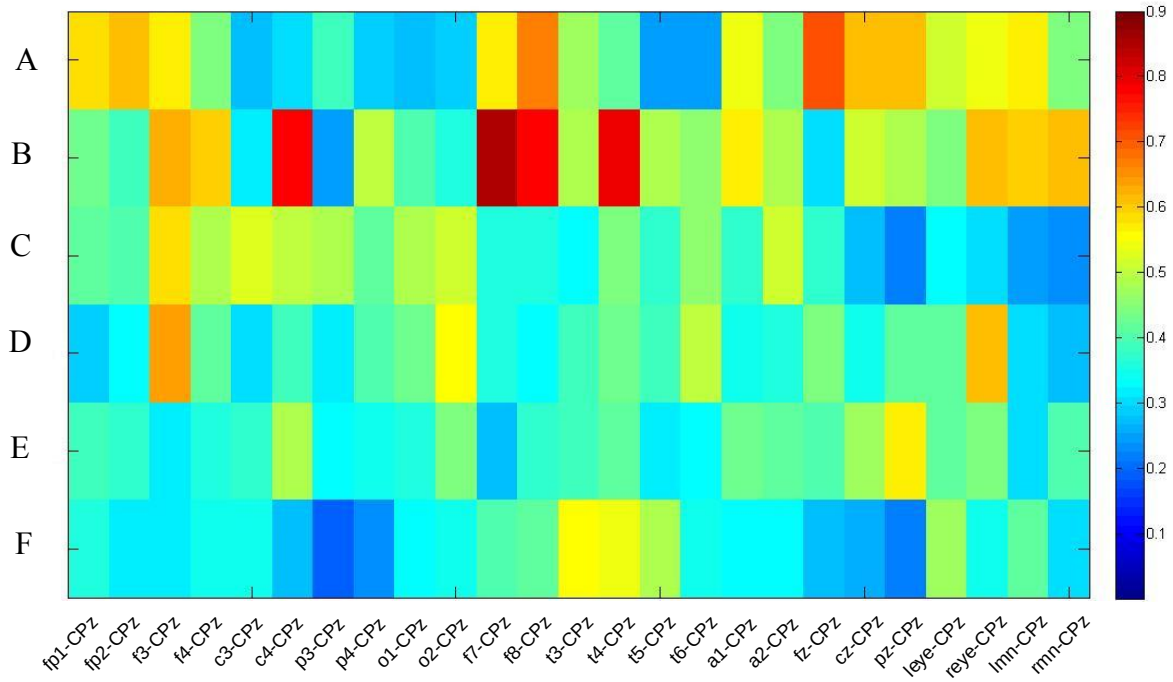

Figure 5-10. The fraction of all interstimulation epochs per channel which rejected the null hypothesis H0 using ApEnt for A) patient A, B) patient B, C) patient C, D) patient D, E) patient E, F) patient F.

Table 5-1. Surrogate analysis results summary for all six patients with the VNS implant.

	% of epochs where the ApEnt measure rejected H0					
channel	A	B	C	D	E	F
fp1-CPz	* 58.27%	42.37%	42.15%	* 29.31%	38.89%	36.27%
fp2-CPz	* 61.42%	* 38.56%	40.61%	32.76%	36.90%	31.62%
f3-CPz	* 56.30%	62.71%	57.85%	* 64.53%	30.95%	31.13%
f4-CPz	* 44.49%	* 60.17%	49.04%	42.12%	36.11%	35.05%
c3-CPz	27.56%	31.36%	52.11%	30.05%	37.70%	34.80%
c4-CPz	29.92%	77.54%	50.57%	38.18%	49.21%	27.45%
p3-CPz	38.98%	24.58%	48.66%	31.53%	32.94%	19.61%
p4-CPz	28.35%	50.00%	41.76%	39.66%	34.92%	22.55%
o1-CPz	27.17%	39.41%	47.89%	42.86%	36.11%	33.33%
o2-CPz	28.74%	36.02%	51.34%	55.17%	44.05%	33.82%
f7-CPz	* 57.09%	85.17%	35.25%	* 36.45%	27.38%	39.95%
f8-CPz	* 66.14%	* 78.39%	35.25%	33.50%	37.70%	41.67%
t3-CPz	46.46%	48.31%	32.95%	39.16%	39.29%	* 55.64%
t4-CPz	42.13%	78.81%	* 44.83%	43.10%	42.06%	* 54.66%
t5-CPz	24.02%	48.73%	36.78%	38.42%	31.35%	* 48.77%
t6-CPz	24.80%	46.19%	* 45.98%	50.25%	33.33%	* 35.05%
a1-CPz	53.54%	56.78%	37.16%	34.24%	42.86%	32.60%
a2-CPz	44.49%	47.88%	51.34%	35.22%	40.87%	32.60%
fz-CPz	* 71.65%	30.08%	36.78%	44.33%	40.48%	27.94%
cz-CPz	60.63%	51.69%	27.59%	34.98%	47.62%	26.72%
pz-CPz	61.81%	47.88%	21.46%	41.63%	56.35%	22.30%
leye-CPz	51.97%	43.64%	33.33%	41.38%	42.06%	47.79%
reye-CPz	53.54%	61.44%	30.65%	61.08%	44.84%	34.31%
lmn-CPz	56.30%	59.75%	25.29%	30.79%	30.16%	42.16%
rmn-CPz	43.70%	61.02%	23.37%	27.83%	39.68%	30.15%
# epochs	254	236	261	406	252	408

* denotes focal EEG channel

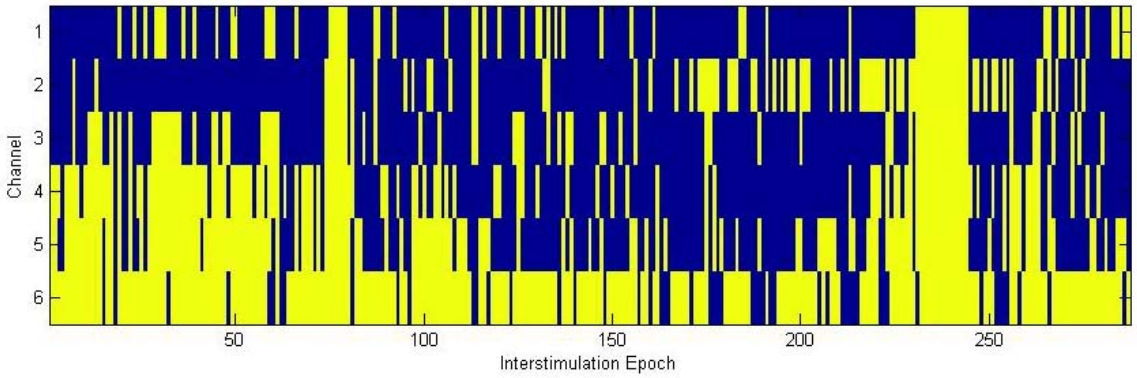

Figure 5-11. Control patient (with 5-minute artificial stimulation times) surrogate data analysis results over 24 hours for all artificial interstimulation epochs. Yellow indicates that particular interstimulation epoch (abscissa) for the channel of interest (ordinate) rejected the null hypothesis.

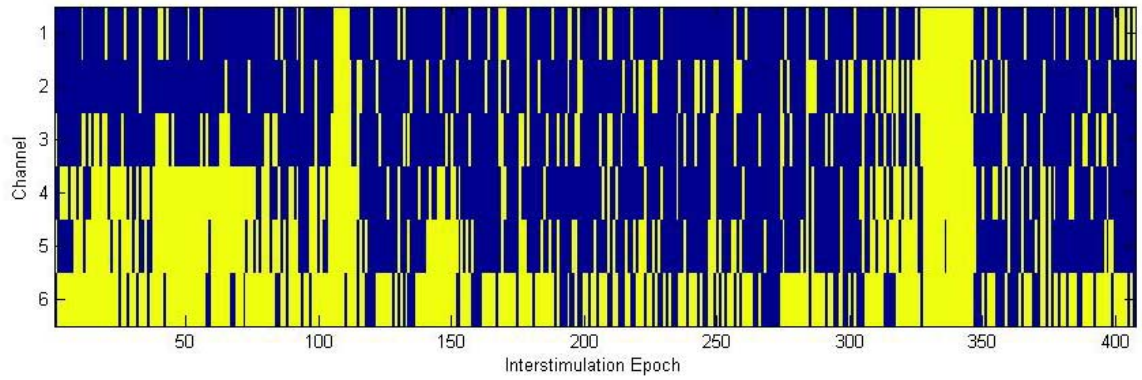

Figure 5-12. Control patient (with 3-minute artificial stimulation times) surrogate data analysis results over 24 hours for all artificial interstimulation epochs. Yellow indicates that particular interstimulation epoch (abscissa) for the channel of interest (ordinate) rejected the null hypothesis.

Table 5-2. Control patient surrogate analysis results summary.

% of epochs where the ApEnt measure rejected H0		
channel	Control - 5 minute 'off' time	Control - 3 minute 'off' time
TBA4	* 22.65%	* 19.41%
TBB6	* 29.27%	* 22.85%
HR7	* 27.18%	* 26.54%
TLB2	43.21%	40.05%
TLB3	51.57%	44.72%
TLC2	81.53%	70.02%
# epochs	261	406

* denotes focal EEG channel

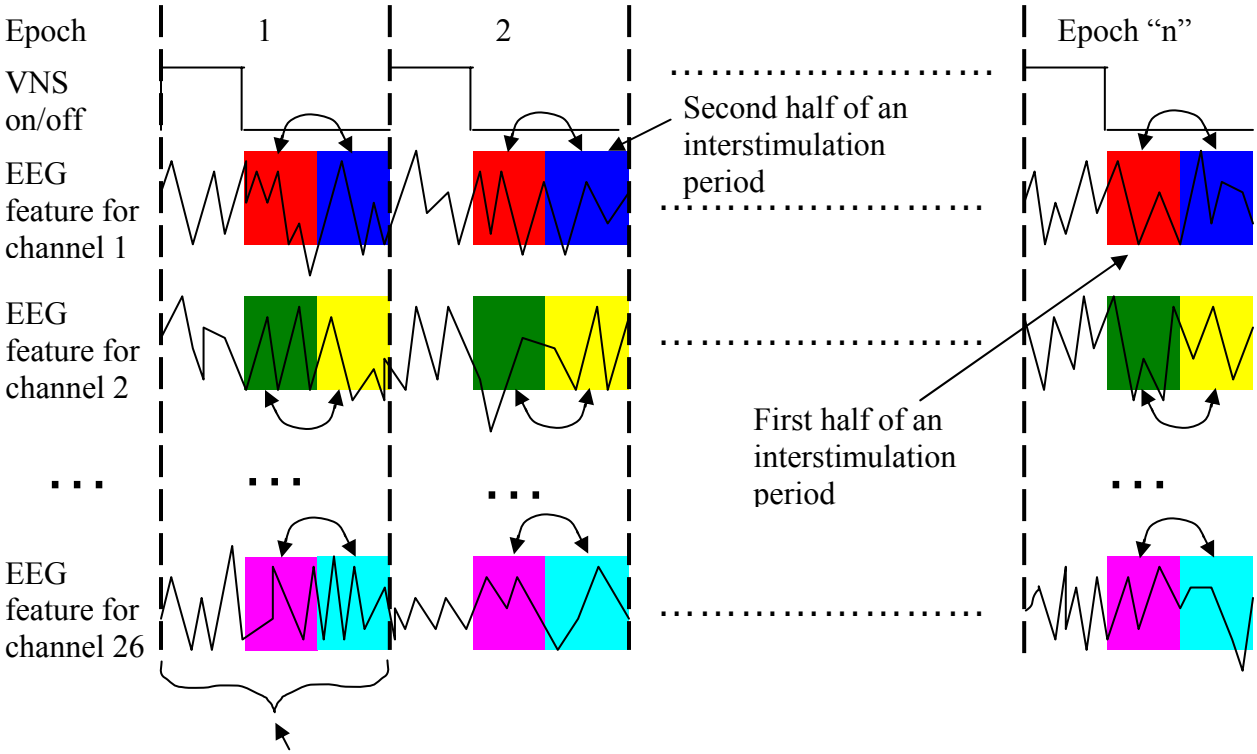

Figure 5-13. Experimental setup for characterizing the temporal evolution EEG dynamics during interstimulation intervals in patients undergoing VNS therapy for epilepsy. The double head arrows indicate a statistical comparison is made between the EEG feature segments represented by the shaded rectangles.

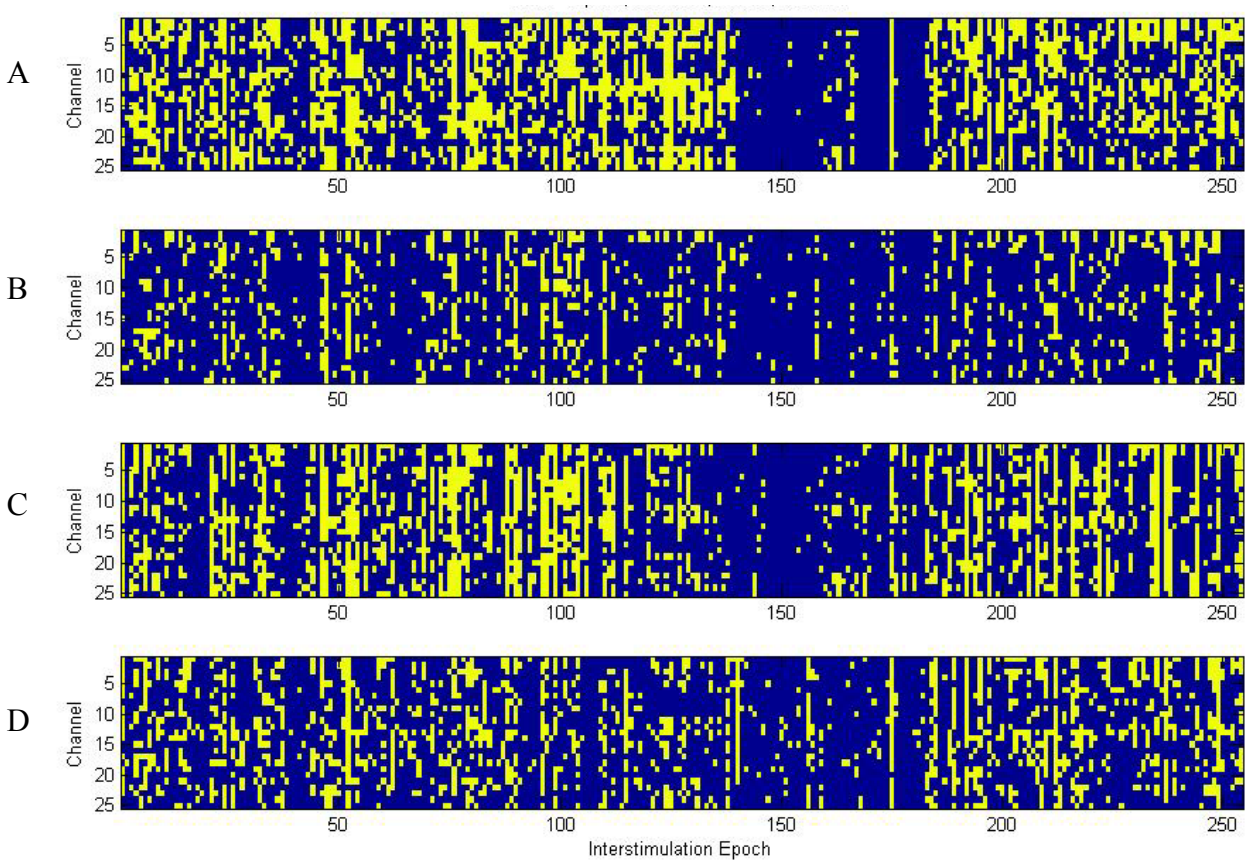

Figure 5-14. Patient A temporal evolution of dynamics analysis results over 24 hours for A) ApEnt, B) correlation sum, C) $\overline{\Omega}$, and D) STLmax. Yellow indicates that particular interstimulation epoch (abscissa) for the channel of interest (ordinate) rejected the null hypothesis.

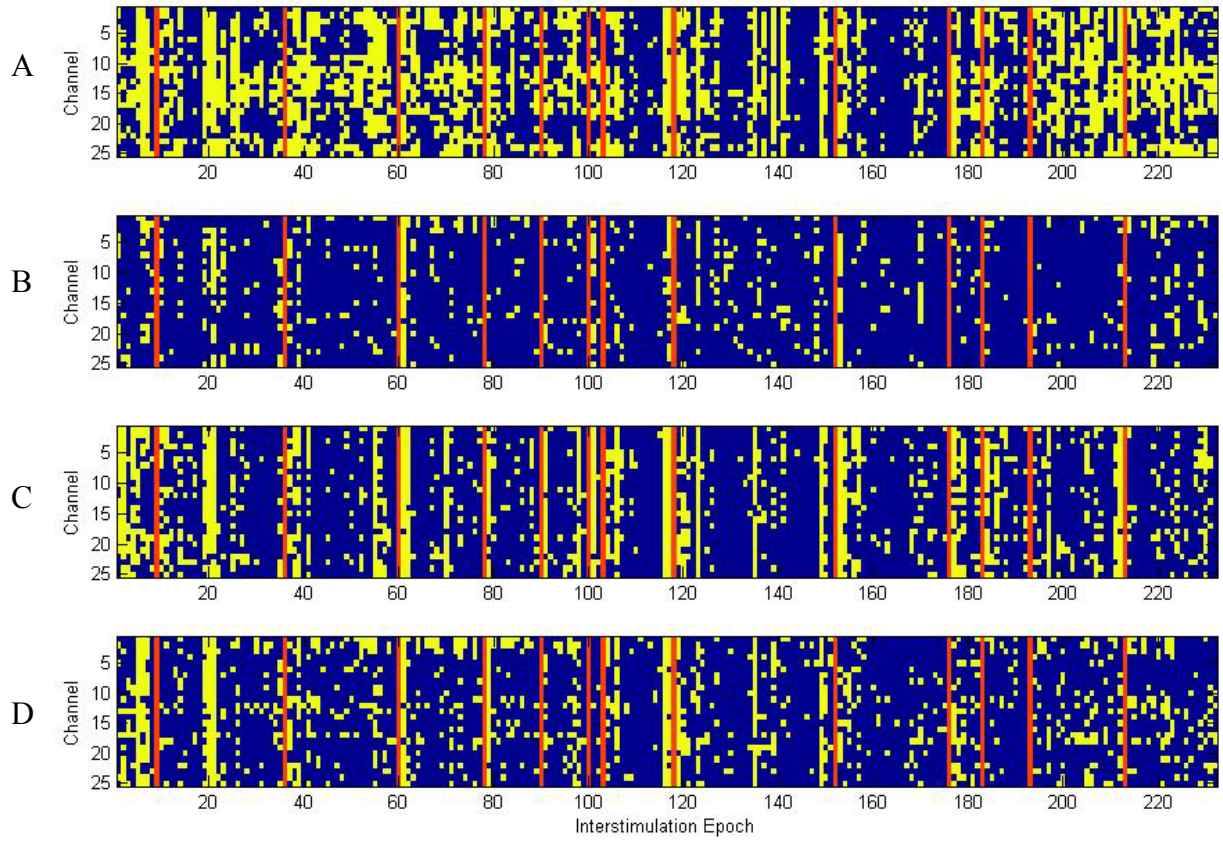

Figure 5-15. Patient B temporal evolution of dynamics analysis results over 24 hours for A) ApEnt, B) correlation sum, C) $\overline{\Omega}$, and D) STLmax. Yellow indicates that particular interstimulation epoch (abscissa) for the channel of interest (ordinate) rejected the null hypothesis. The red lines indicate seizures.

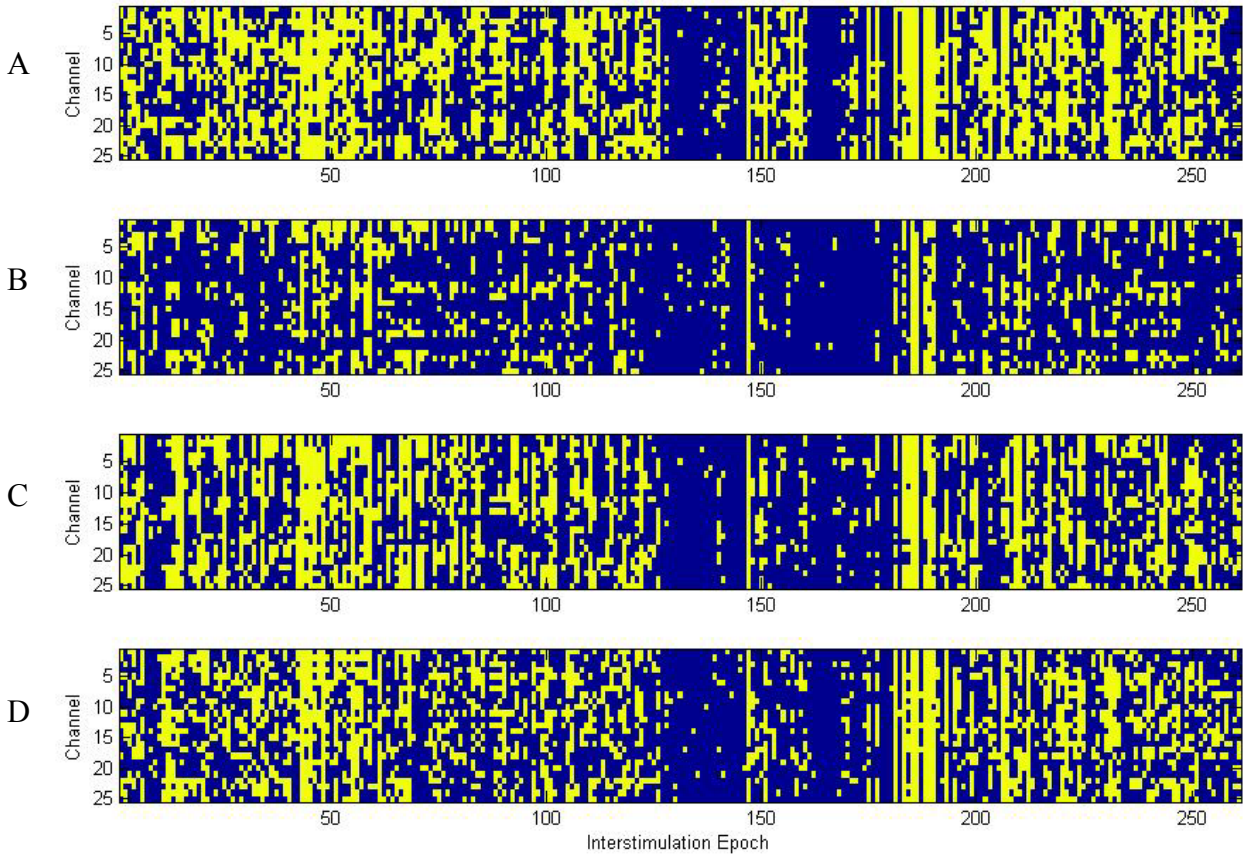

Figure 5-16. Patient C temporal evolution of dynamics analysis results over 24 hours for A) ApEnt, B) correlation sum, C) $\overline{\Omega}$, and D) STLmax. Yellow indicates that particular interstimulation epoch (abscissa) for the channel of interest (ordinate) rejected the null hypothesis.

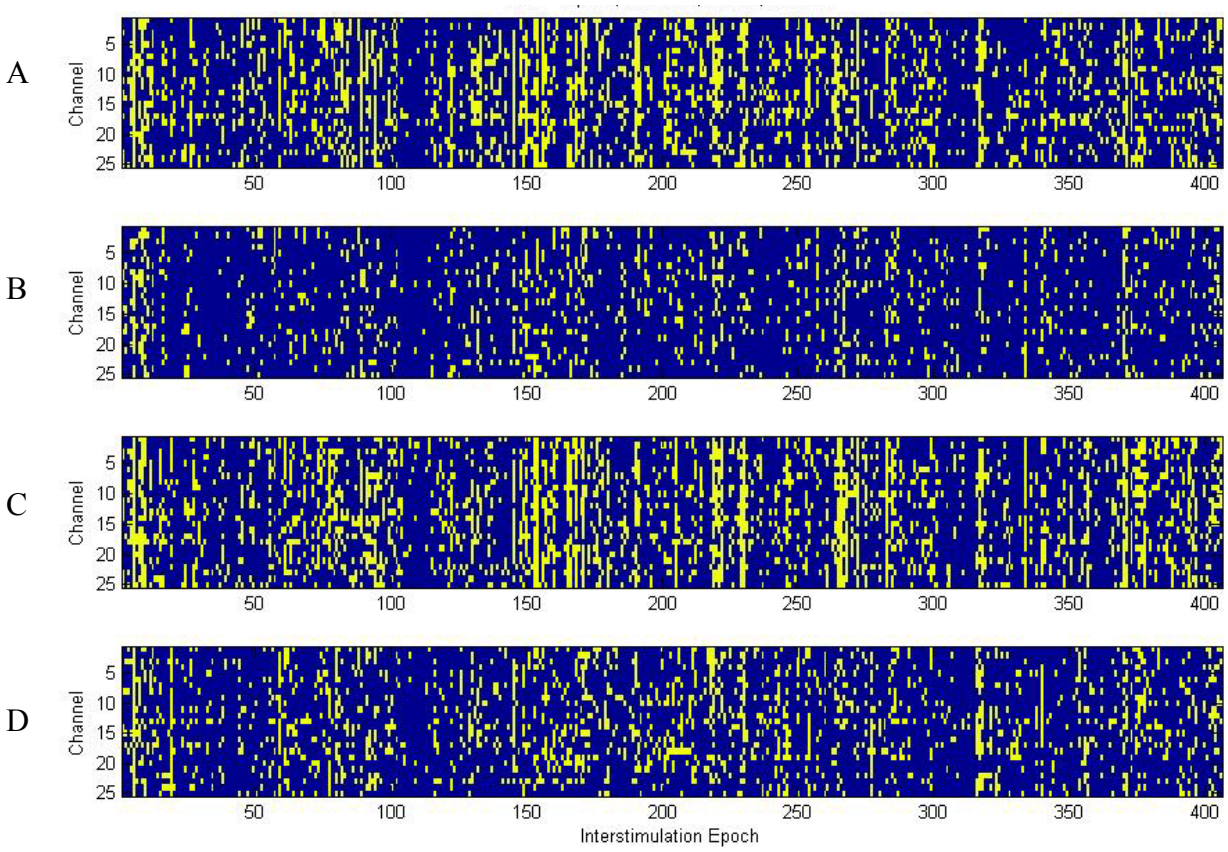

Figure 5-17. Patient D temporal evolution of dynamics analysis results over 24 hours for A) ApEnt, B) correlation sum, C) $\overline{\Omega}$, and D) STLmax. Yellow indicates that particular interstimulation epoch (abscissa) for the channel of interest (ordinate) rejected the null hypothesis.

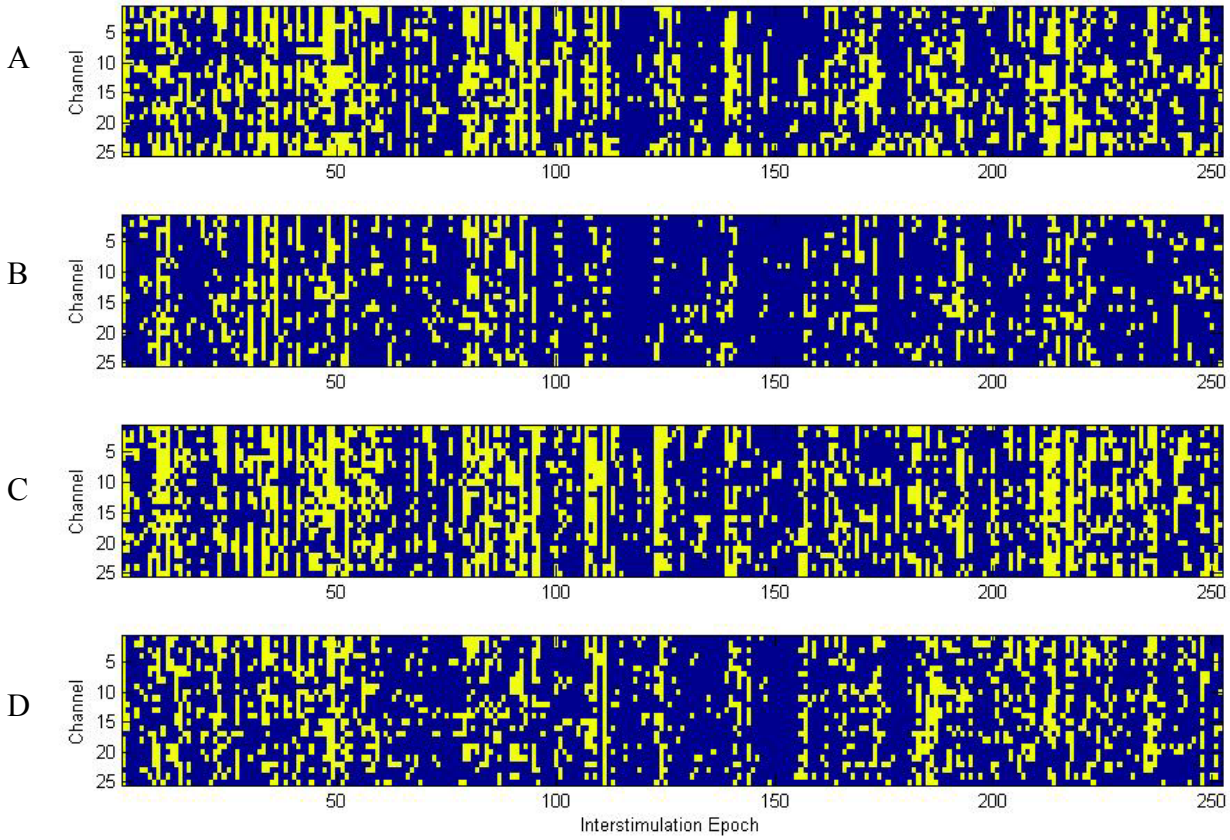

Figure 5-18. Patient E temporal evolution of dynamics analysis results over 24 hours for A) ApEnt, B) correlation sum, C) $\overline{\Omega}$, and D) STLmax. Yellow indicates that particular interstimulation epoch (abscissa) for the channel of interest (ordinate) rejected the null hypothesis.

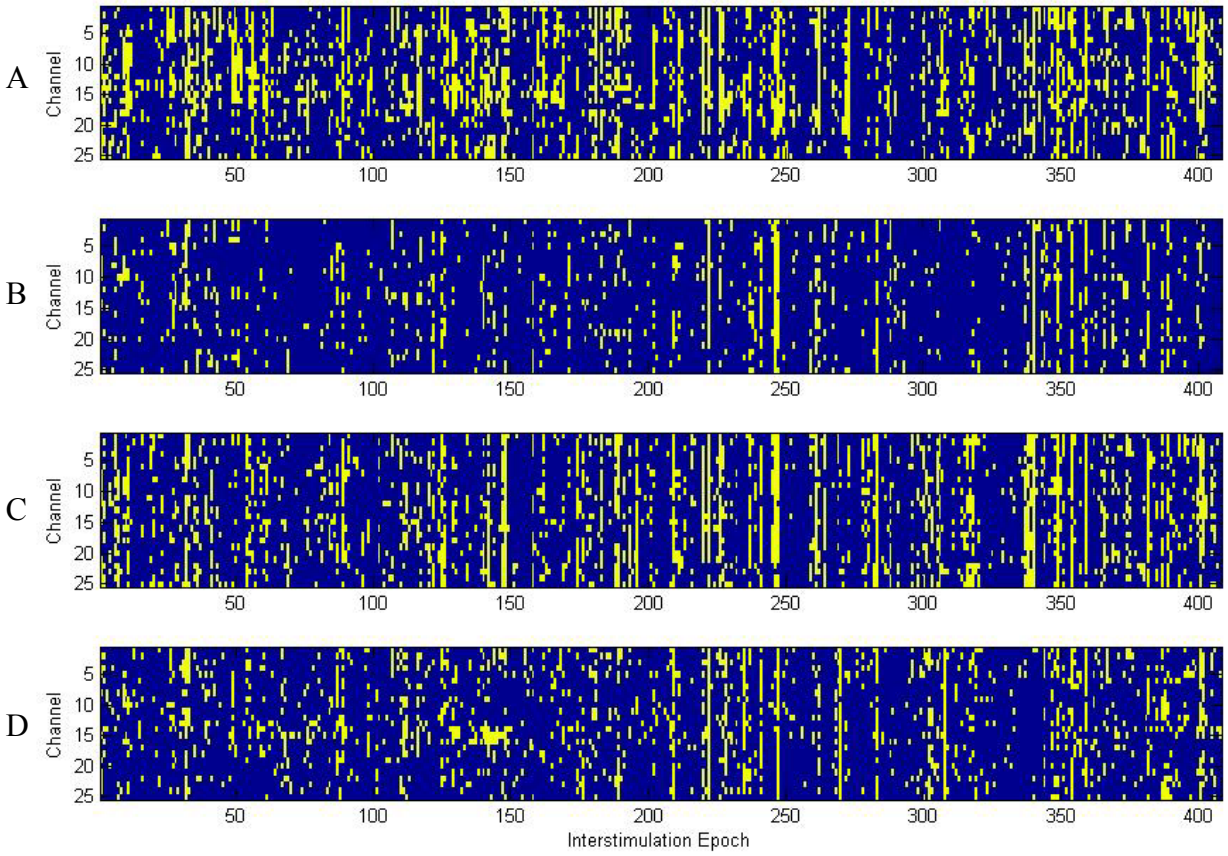

Figure 5-19. Patient F temporal evolution of dynamics analysis results for A) ApEnt, B) correlation sum, C) $\overline{\Omega}$, and D) STLmax. Yellow indicates that particular interstimulation epoch (abscissa) for the channel of interest (ordinate) rejected the null hypothesis.

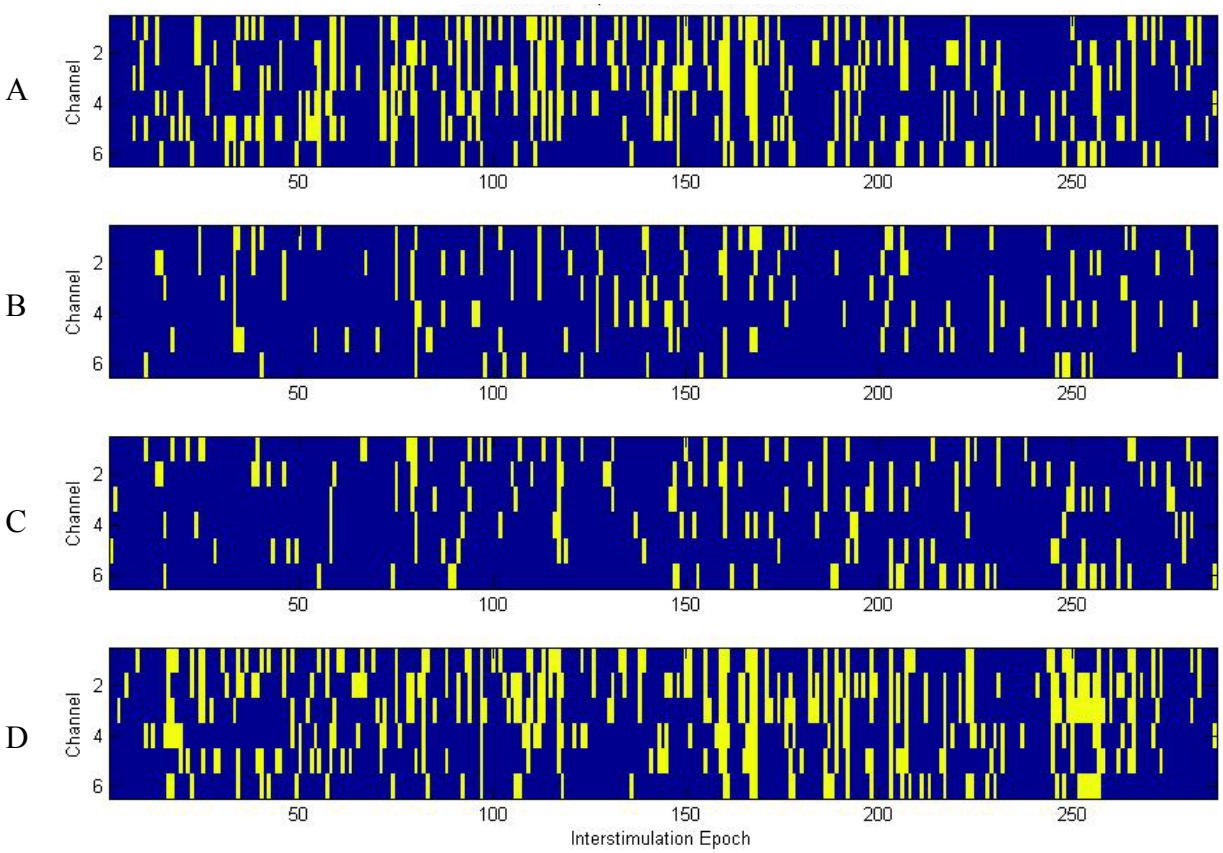

Figure 5-20. Control patient (with 5-minute artificial stimulation times) temporal evolution of dynamics analysis results for A) ApEnt, B) correlation sum, C) $\overline{\Omega}$, and D) STLmax. Yellow indicates that particular interstimulation epoch (abscissa) for the channel of interest (ordinate) rejected the null hypothesis.

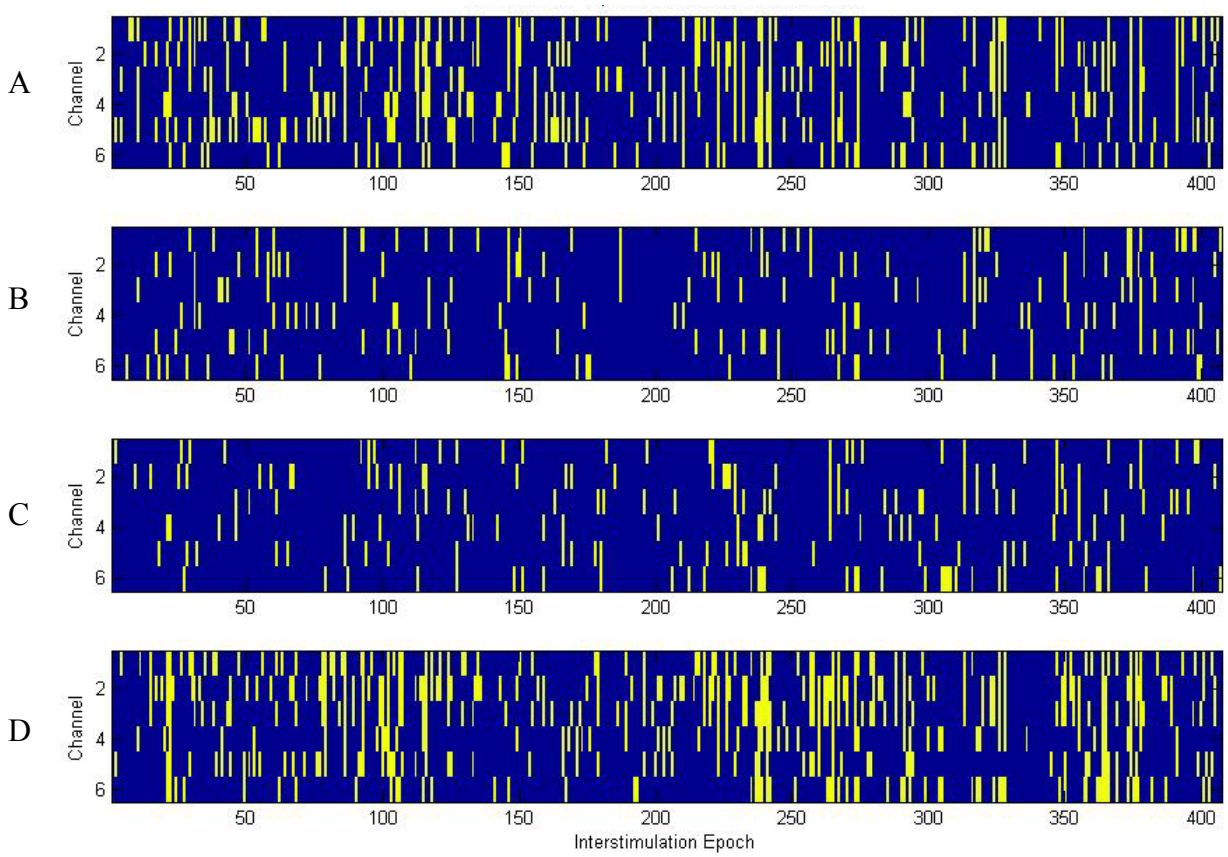

Figure 5-21. Control patient (with 3-minute artificial stimulation times) temporal evolution of dynamics analysis results for A) ApEnt, B) correlation sum, C) $\overline{\Omega}$, and D) STLmax. Yellow indicates that particular interstimulation epoch (abscissa) for the channel of interest (ordinate) rejected the null hypothesis.

Table 5-3. Approximate entropy analysis results for VNS patients. Results are expressed as the fraction of epochs in each channel which rejected hypothesis H1 using the ApEnt measure.

	% of epochs rejecting H1					
channel	Patient A	Patient B	Patient C	Patient D	Patient E	Patient F
fp1-CPz	* 40.94%	31.78%	47.13%	* 18.23%	34.92%	24.75%
fp2-CPz	* 40.94%	* 43.64%	43.30%	20.20%	32.94%	24.26%
f3-CPz	* 44.09%	49.58%	52.11%	* 21.67%	31.75%	25.00%
f4-CPz	* 40.55%	* 41.53%	49.43%	24.14%	30.95%	29.90%
c3-CPz	42.13%	38.14%	42.53%	20.44%	28.57%	23.53%
c4-CPz	29.53%	33.47%	50.57%	24.14%	29.37%	26.72%
p3-CPz	27.17%	35.59%	47.89%	22.41%	24.60%	19.36%
p4-CPz	26.38%	25.42%	50.57%	22.41%	26.59%	20.59%
o1-CPz	38.98%	41.53%	47.51%	24.14%	24.21%	22.55%
o2-CPz	38.58%	37.29%	49.81%	22.91%	30.16%	22.79%
f7-CPz	* 36.22%	54.24%	50.96%	27.34%	38.49%	24.51%
f8-CPz	* 38.98%	* 54.24%	47.89%	* 25.37%	37.70%	28.43%
t3-CPz	42.91%	50.85%	43.30%	29.80%	34.92%	* 30.39%
t4-CPz	33.46%	43.22%	* 40.23%	23.65%	37.70%	* 30.88%
t5-CPz	33.86%	52.54%	39.08%	20.94%	32.14%	* 30.15%
t6-CPz	37.80%	41.10%	* 41.38%	25.86%	35.32%	* 28.43%
a1-CPz	40.55%	50.42%	34.10%	31.53%	35.71%	24.75%
a2-CPz	35.43%	50.00%	41.00%	28.08%	36.11%	23.28%
fz-CPz	37.40%	34.32%	46.74%	19.21%	28.97%	21.08%
cz-CPz	29.92%	23.31%	48.28%	17.49%	25.40%	18.87%
pz-CPz	20.47%	26.69%	36.78%	21.67%	18.65%	17.65%
leye-CPz	37.40%	29.24%	50.19%	24.38%	34.92%	17.40%
reye-CPz	32.68%	37.71%	50.96%	24.88%	35.71%	18.87%
lmn-CPz	37.80%	46.61%	44.83%	24.38%	40.48%	19.85%
rmn-CPz	29.92%	47.88%	44.06%	21.43%	36.90%	21.81%
# epochs	254	236	261	406	252	408

* denotes focal EEG channel

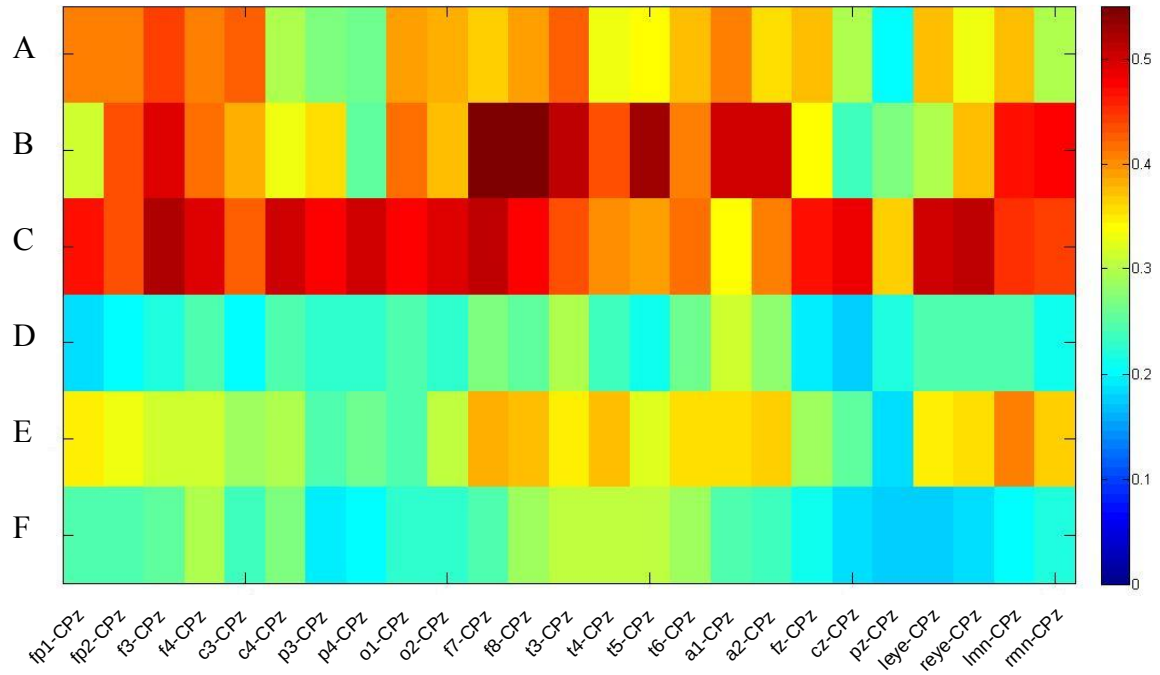

Figure 5-22. Approximate entropy analysis results for VNS patients. Results are expressed as the fraction of epochs in each channel which rejected hypothesis H1 using the ApEnt measure.

Table 5-4. Approximate entropy analysis results for the control patient. Results are expressed as the fraction of epochs in each channel which rejected hypothesis H1 using the ApEnt measure.

	% of epochs rejecting H1	
channel	Control - 5 minute 'off' time	Control - 3 minute 'off' time
TBA4	* 22.65%	* 18.18%
TBB6	* 25.44%	* 17.94%
HR7	* 23.34%	* 15.23%
TLB2	20.91%	17.69%
TLB3	23.69%	19.66%
TLC2	14.63%	13.02%
TBA4	261	406

* denotes focal EEG channel

Table 5-5. Correlation sum analysis results for VNS patients. Results are expressed as the fraction of epochs in each channel which rejected hypothesis H2 using the correlation sum measure.

	% of epochs rejecting H2					
channel	Patient A	Patient B	Patient C	Patient D	Patient E	Patient F
fp1-CPz	* 25.98%	18.64%	34.10%	* 12.07%	20.24%	10.54%
fp2-CPz	* 26.38%	* 16.10%	29.12%	12.81%	19.84%	8.82%
f3-CPz	* 19.29%	12.71%	24.90%	* 9.85%	18.65%	11.52%
f4-CPz	* 18.11%	* 10.17%	26.05%	12.81%	18.25%	11.52%
c3-CPz	19.29%	13.98%	21.84%	10.59%	17.86%	10.54%
c4-CPz	15.75%	15.25%	19.92%	12.07%	18.25%	9.31%
p3-CPz	13.39%	11.86%	14.94%	11.58%	15.48%	9.80%
p4-CPz	12.99%	8.47%	13.79%	12.32%	15.87%	9.31%
o1-CPz	15.35%	8.90%	13.03%	11.82%	13.49%	10.29%
o2-CPz	17.32%	8.47%	13.79%	14.29%	11.90%	13.73%
f7-CPz	* 16.93%	9.75%	31.80%	* 11.82%	21.43%	10.54%
f8-CPz	* 16.14%	* 9.32%	29.50%	12.32%	18.65%	10.29%
t3-CPz	22.44%	10.59%	22.22%	11.08%	18.65%	* 12.25%
t4-CPz	16.54%	6.78%	* 21.07%	13.30%	21.83%	* 11.52%
t5-CPz	15.35%	10.17%	13.41%	9.85%	12.30%	* 9.31%
t6-CPz	11.81%	9.32%	* 17.24%	12.07%	21.83%	* 8.33%
a1-CPz	11.81%	13.56%	23.37%	11.08%	21.03%	10.29%
a2-CPz	16.54%	13.56%	22.22%	15.27%	18.25%	11.03%
fz-CPz	22.05%	12.71%	25.67%	11.33%	17.46%	12.01%
cz-CPz	17.32%	8.05%	11.11%	9.61%	18.65%	12.25%
pz-CPz	14.57%	7.63%	9.96%	11.33%	15.08%	6.13%
leye-CPz	14.96%	13.56%	27.97%	10.10%	17.06%	10.05%
reye-CPz	16.54%	12.71%	32.57%	13.55%	17.06%	8.33%
lmn-CPz	13.78%	7.20%	21.84%	9.36%	17.46%	11.03%
rmn-CPz	12.60%	8.47%	24.90%	11.58%	16.27%	9.56%
# epochs	254	236	261	406	252	408

* denotes focal EEG channel

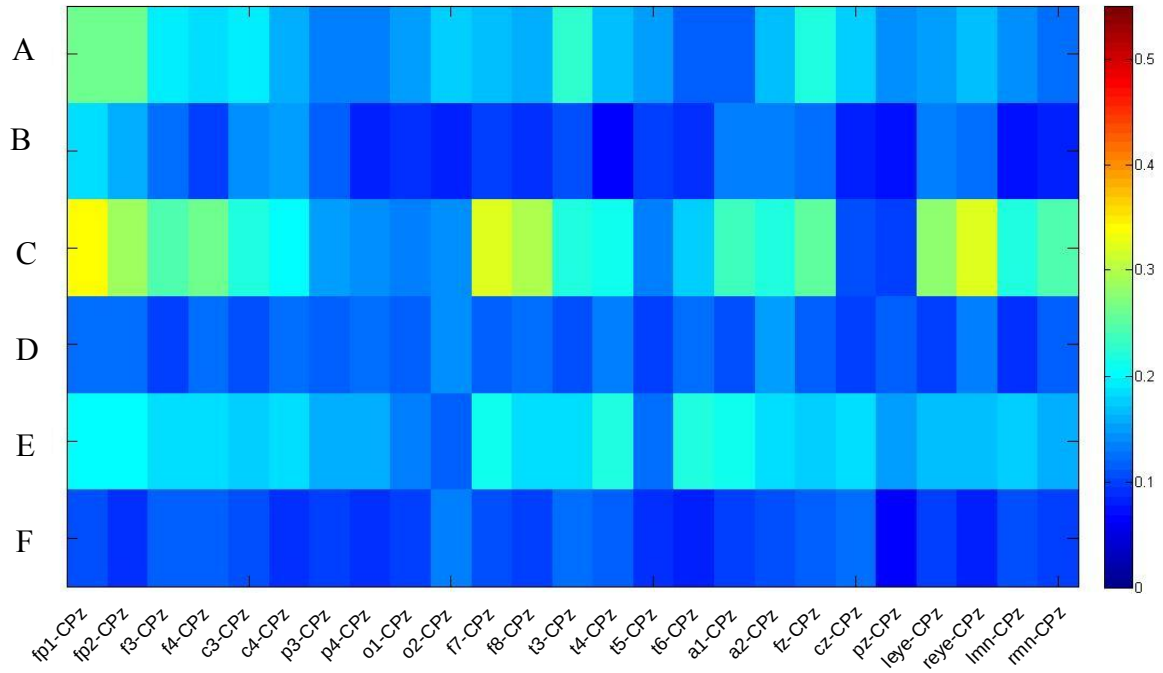

Figure 5-23. Correlation sum analysis results for VNS patients. Results are expressed as the fraction of epochs in each channel which rejected hypothesis H2 using the correlation sum measure.

Table 5-6. Correlation sum analysis results for the control patient. Results are expressed as the fraction of epochs in each channel which rejected hypothesis H2 using the correlation sum measure.

	% of epochs rejecting H2	
channel	Control - 5 minute 'off' time	Control - 3 minute 'off' time
TBA4	* 11.50%	* 8.60%
TBB6	* 10.80%	* 8.85%
HR7	* 8.71%	* 8.11%
TLB2	9.76%	7.13%
TLB3	8.71%	8.35%
TLC2	5.57%	7.37%
# epochs	261	406

* denotes focal EEG channel

Table 5-7. Mean angular frequency in phase space analysis results for VNS patients. Results are expressed as the fraction of epochs in each channel which rejected hypothesis H3 using the $\overline{\Omega}$ measure.

	% of epochs rejecting H3					
channel	Patient A	Patient B	Patient C	Patient D	Patient E	Patient F
fp1-CPz	* 38.19%	30.51%	37.93%	* 23.89%	39.68%	20.10%
fp2-CPz	* 35.83%	* 22.46%	38.70%	22.66%	32.94%	24.02%
f3-CPz	* 29.53%	26.27%	41.00%	* 24.88%	34.92%	19.36%
f4-CPz	* 27.95%	* 27.12%	41.76%	23.65%	33.73%	21.32%
c3-CPz	30.31%	26.27%	38.70%	22.17%	36.51%	18.38%
c4-CPz	34.25%	35.17%	31.80%	26.11%	41.67%	19.61%
p3-CPz	31.89%	27.54%	35.25%	27.83%	33.33%	17.89%
p4-CPz	26.38%	22.88%	32.95%	22.91%	33.73%	18.14%
o1-CPz	29.53%	23.73%	39.46%	25.62%	28.97%	19.12%
o2-CPz	29.92%	20.34%	34.87%	26.85%	33.33%	21.81%
f7-CPz	* 34.25%	25.00%	43.68%	* 24.38%	33.73%	19.12%
f8-CPz	* 31.10%	* 23.73%	39.46%	27.34%	35.32%	20.10%
t3-CPz	39.37%	24.58%	41.00%	23.40%	38.10%	* 19.85%
t4-CPz	29.92%	22.46%	* 31.42%	27.59%	34.13%	* 21.08%
t5-CPz	28.74%	25.00%	31.42%	26.35%	26.59%	* 21.08%
t6-CPz	25.59%	21.61%	* 31.42%	22.41%	37.30%	* 20.098%
a1-CPz	24.80%	19.92%	31.03%	26.60%	31.35%	18.87%
a2-CPz	27.56%	22.03%	31.80%	30.30%	32.54%	18.38%
fz-CPz	27.95%	36.02%	39.46%	23.40%	34.52%	20.83%
cz-CPz	29.53%	23.73%	40.61%	20.94%	30.16%	21.57%
pz-CPz	31.10%	24.58%	34.48%	25.37%	29.37%	19.61%
leye-CPz	37.80%	29.66%	42.53%	26.60%	34.92%	20.83%
reye-CPz	32.68%	28.81%	37.93%	26.85%	31.35%	21.57%
lmn-CPz	32.68%	23.31%	34.10%	19.70%	34.92%	18.38%
rmn-CPz	29.13%	22.88%	37.93%	25.12%	30.16%	23.77%
# epochs	254	236	261	406	252	408

* denotes focal EEG channel

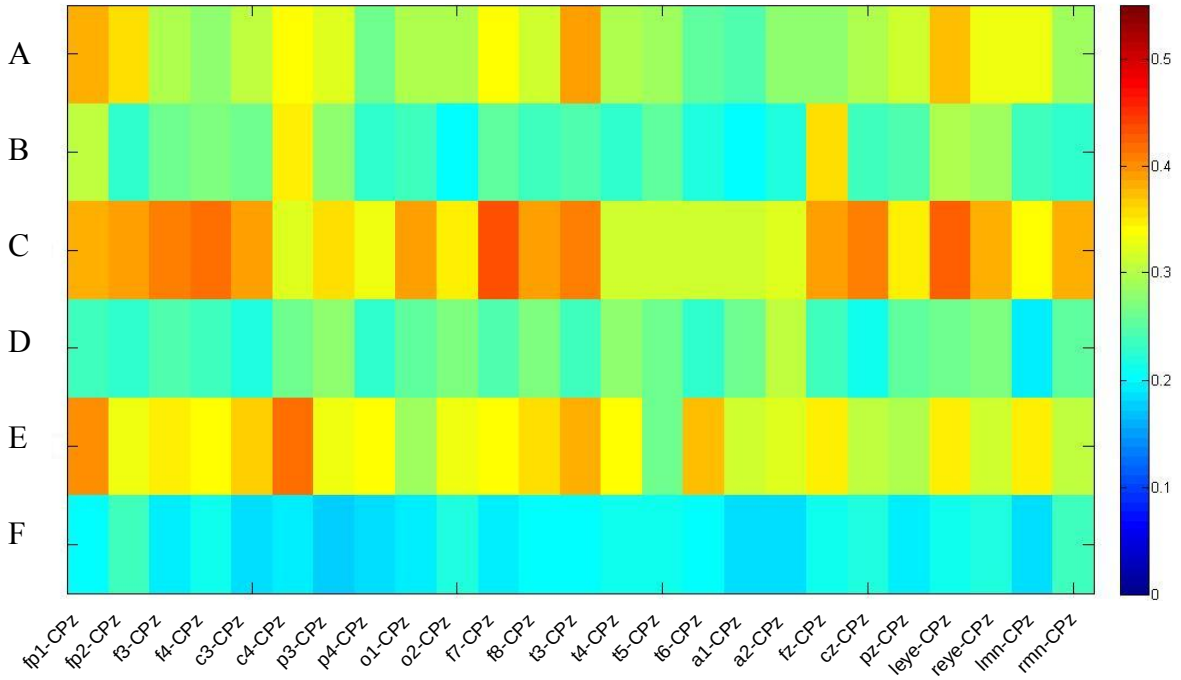

Figure 5-24. Mean angular frequency in phase space analysis results for VNS patients. Results are expressed as the fraction of epochs in each channel which rejected hypothesis H3 using the $\overline{\Omega}$ measure.

Table 5-8. Mean angular frequency in phase space analysis results for control patient. Results are expressed as the fraction of epochs in each channel which rejected hypothesis H3 using the $\overline{\Omega}$ measure.

	% of epochs rejecting H3	
channel	Control - 5 minute 'off' time	Control - 3 minute 'off' time
TBA4	* 12.20%	* 7.13%
TBB6	* 13.59%	* 8.60%
HR7	* 9.41%	* 8.85%
TLB2	8.01%	7.13%
TLB3	8.36%	6.88%
TLC2	11.50%	9.09%
# epochs	261	406

* denotes focal EEG channel

Table 5-9. Short-term maximum Lyapunov exponent analysis results for VNS patients. Results are expressed as the fraction of epochs in each channel which rejected hypothesis H4 using the STLmax measure.

	% of epochs rejecting H4					
channel	Patient A	Patient B	Patient C	Patient D	Patient E	Patient F
fp1-CPz	* 29.13%	30.08%	40.23%	* 18.23%	31.35%	17.65%
fp2-CPz	* 28.35%	* 32.20%	33.72%	16.50%	29.37%	17.89%
f3-CPz	* 29.13%	27.54%	35.25%	* 17.49%	28.97%	15.93%
f4-CPz	* 24.41%	* 15.25%	37.55%	15.52%	22.22%	19.12%
c3-CPz	24.80%	15.25%	44.06%	14.78%	26.98%	18.63%
c4-CPz	21.26%	14.41%	39.85%	16.75%	23.81%	12.50%
p3-CPz	19.69%	16.10%	35.63%	16.26%	19.84%	10.54%
p4-CPz	17.72%	15.25%	37.55%	16.01%	19.84%	11.27%
o1-CPz	23.23%	19.07%	35.25%	15.52%	21.43%	13.48%
o2-CPz	20.47%	16.95%	31.80%	17.00%	25.40%	11.76%
f7-CPz	* 24.41%	22.88%	42.53%	* 17.73%	28.17%	13.97%
f8-CPz	* 26.77%	* 30.51%	37.16%	17.00%	19.84%	15.69%
t3-CPz	40.94%	27.12%	43.68%	24.88%	26.98%	* 14.95%
t4-CPz	29.53%	15.25%	* 40.61%	20.94%	27.78%	* 21.57%
t5-CPz	25.20%	19.92%	32.95%	17.49%	23.41%	* 20.34%
t6-CPz	17.32%	15.68%	* 38.70%	16.26%	22.62%	* 15.93%
a1-CPz	24.41%	31.78%	32.95%	24.88%	30.16%	13.24%
a2-CPz	30.71%	28.81%	38.31%	21.18%	17.06%	12.25%
fz-CPz	24.41%	19.07%	25.29%	18.97%	26.19%	10.54%
cz-CPz	15.75%	15.25%	26.44%	11.82%	21.83%	10.78%
pz-CPz	21.65%	15.25%	25.67%	14.04%	25.79%	11.52%
leye-CPz	26.38%	23.73%	44.83%	14.29%	25.40%	15.20%
reye-CPz	23.23%	19.07%	38.31%	18.97%	19.05%	12.50%
lmn-CPz	16.93%	17.80%	34.87%	12.81%	19.84%	12.01%
rmn-CPz	20.08%	20.76%	30.27%	14.04%	15.87%	9.56%
# epochs	254	236	261	406	252	408

- denotes focal EEG channel

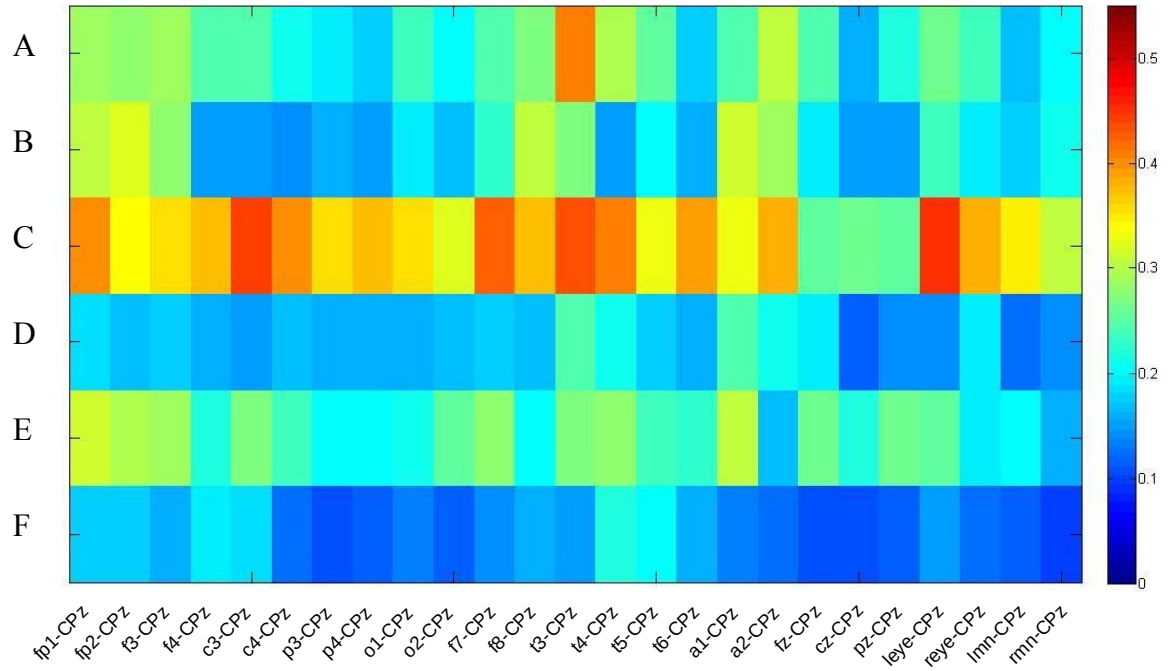

Figure 5-25. Short-term maximum Lyapunov exponent analysis results for VNS patients. Results are expressed as the fraction of epochs in each channel which rejected hypothesis H4 using the STLmax measure.

Table 5-10. Short-term maximum Lyapunov exponent analysis results for the control patient. Results are expressed as the fraction of epochs in each channel which rejected hypothesis H4 using the STLmax measure.

	% of epochs rejecting H4	
channel	Control - 5 minute 'off' time	Control - 3 minute 'off' time
TBA4	* 26.13%	* 20.88%
TBB6	* 32.06%	* 26.78%
HR7	* 27.87%	* 22.11%
TLB2	21.60%	14.25%
TLB3	19.86%	16.95%
TLC2	15.68%	15.72%
# epochs	261	406

* denotes focal EEG channel

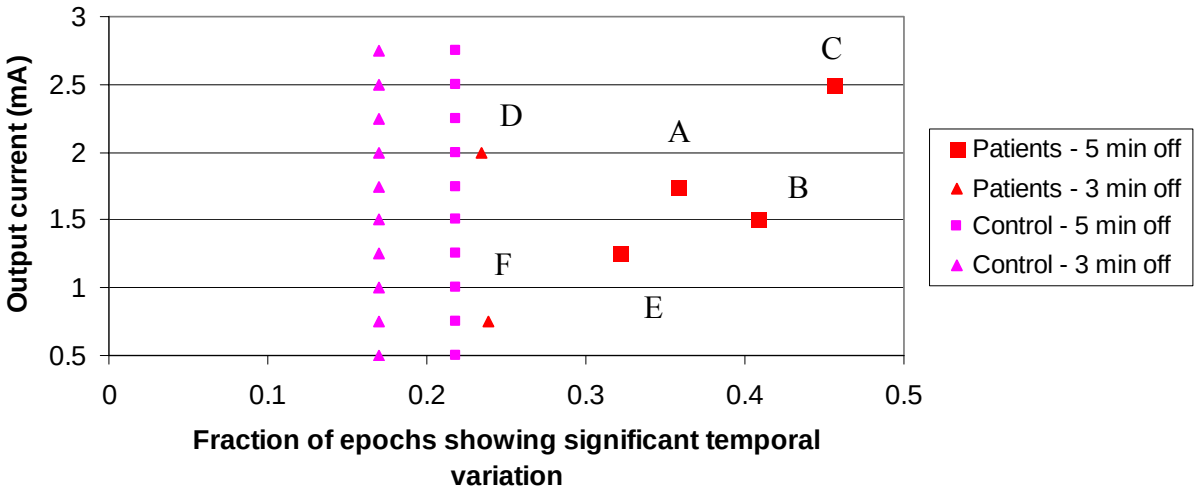

Figure 5-26. ApEnt results and the corresponding output current setting. Results are expressed as the fraction of interstimulation epochs showing significant temporal variation.

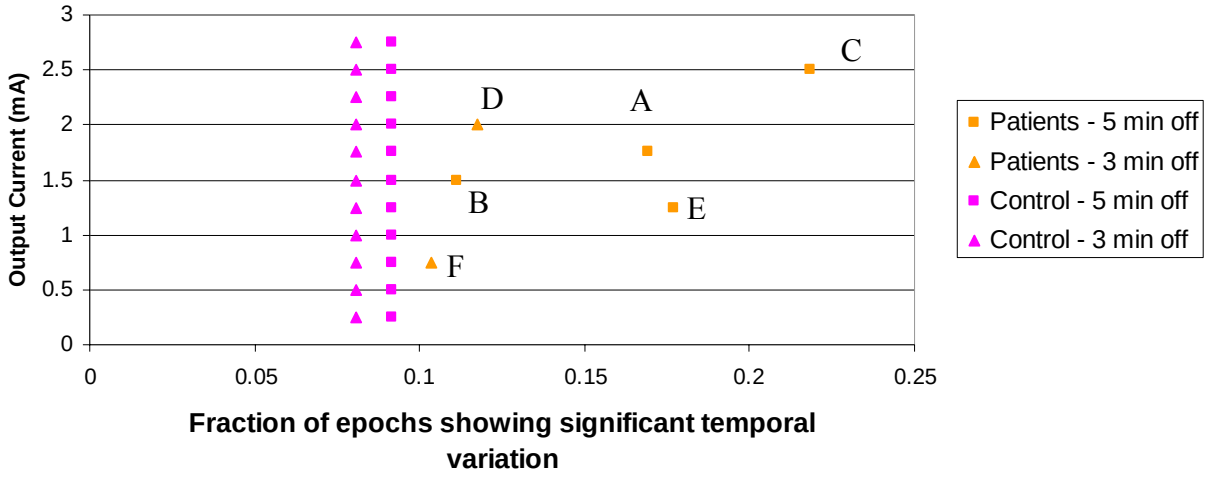

Figure 5-27. Correlation sum results and the corresponding output current setting. Results are expressed as the fraction of interstimulation epochs showing significant temporal variation.

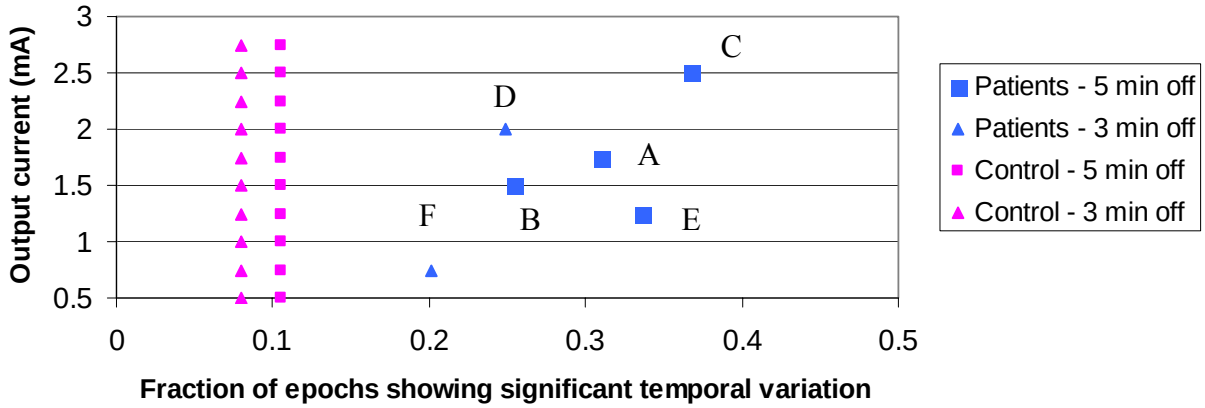

Figure 5-28. $\overline{\Omega}$ results and the corresponding output current setting. Results are expressed as the fraction of interstimulation epochs showing significant temporal variation.

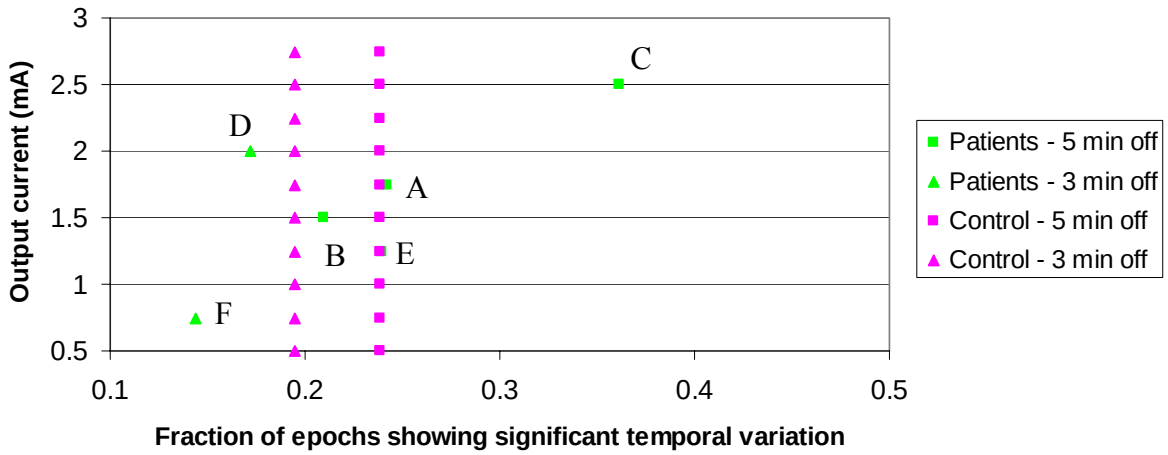

Figure 5-29. STLmax results and the corresponding output current setting. Results are expressed as the fraction of interstimulation epochs showing significant temporal variation.

CHAPTER 6
A NOVEL GENERALIZED ABSENCE SEIZURE DETECTION ALGORITHM

Absence epilepsy makes up about 8% of child epilepsy cases with peak occurrence between 6-7 years of age (Berkovic, 1996). Absence seizures are clinically characterized by brief, transient loss of awareness, responsiveness, and memory. These paraxoysmal discharges have a sudden onset, are often less than 5 seconds in duration, cease abruptly without postictal effects and can occur multiple times per day. Absence seizures are generalized with regular and symmetrical 2.5-3.5 Hz SWDs (Panayiotopoulos et al., 1994). Figure 6-1 shows an example of an electrographic absence seizure.

The antiepileptic drugs valproic acid and ethosuximide are the most commonly-used drugs for treating absence epilepsy. For additional information on absence epilepsy, see chapter 2.

Seizure detection is an important procedure for the treatment of epilepsy. In particular, there are areas wherein seizure detection can benefit epilepsy treatment; rapid seizure annotation and online real-time EEG analysis. Seizure detection algorithms can greatly improve the rate at which physicians analyze EEG recordings by providing a tool to help point out EEG waveforms which are likely to be epileptiform discharges. Such an algorithm can improve the efficiency of health care for epilepsy treatment.

The other popular application of seizure detection algorithms is for online real-time analysis. Such analysis is useful in the research field for enhancing the understanding of how EEG activity correlates to the clinical status of the patient or for cognitive testing in animal models of epilepsy. For some epilepsy variants, such as mesial temporal lobe epilepsy, seizure detection may provide a basis for an implantable seizure control device (e.g. utilizing a drug pump and/or neural stimulation apparatus). For generalized absence epilepsy, it is possible that

someday an online real-time absence seizure detection algorithm may be integrated with scalp-EEG recordings as part of medical checkups in patients with generalized absence epilepsy.

In addition to seizure detection, such an algorithm can be extended to perform seizure stratification and provide a histogram of seizure count versus seizure duration. The ability to automatically stratify seizures may provide additional useful information for evaluating therapeutic effect (e.g. compare the seizure stratification histogram profile before and after therapeutic intervention).

For these reasons, the purpose of this study is examine a novel method for expediting detection and stratification of SWDs such as those found in generalized absence epilepsy.

Methods

Previous automated SWD detection algorithms typically relied on thresholding methods and performed well in animal seizure models (Westerhuis et al. 1996; Fanselow et al., 2000; Van Hese et al., 2003).

Energy Method for SWD Detection

One method calculates the signal energy (Van Hese et al., 2003) and establishes a threshold energy level which designates spike and wave activity or non-spike and wave activity. In each window, the signal energy is calculated as

$$E(k) = \sum_{n=0}^{L-1} x^2\left(n + (k-1)S\right) \tag{6-1}$$

where a detection is signified if the calculated energy exceeds a chosen threshold value for four consecutive windows.

Fanselow Method for SWD Detection

The Fanselow method (Fanselow et al., 2000) establishes a voltage threshold which allows classification of SWDs. The method is based on the maximum absolute value of the EEG amplitude within a window

$$A(k) = \max_{n=0,\ldots,L-1} \left| x(n + (k-1)S) \right| . \quad (6\text{-}2)$$

A threshold is set for each subject. If three consecutive windows are above the threshold, a SWD detection is made.

Westerhuis Method for SWD Detection

The Westerhuis method (Westerhuis et al., 1996) estimates the first derivative of the EEG signal which is referred to as the steepness of signal. The maximum value of this steepness in consecutive, non-overlapping windows is evaluated as

$$D(k) = \max_{n=0,\ldots,L-1} d(n + (k-1)S) \quad (6\text{-}3)$$

where

$$d(n) = x(n+1) - x(n) \quad (6\text{-}4)$$

A positive detection is made if D exceeds a certain threshold value in four consecutive windows. The threshold is automatically determined on the basis of the EEG during wakefulness. This method showed strong performance in Genetic Absence Epilepsy Rats from Strasbourg (GAERS).

This study aims to address improvements in the following areas; minimize detection lag (which is critical for online utilization of such a seizure detection device), decreasing window size (to help increase detection time resolution), increasing robustness to noise, and simplified detection calibration. For these reasons, supervised machine learning algorithms were utilized

with the intention of providing a robust seizure detector. The two features selected for this algorithm are Teager-Kaiser energy and dynamic time warping distance.

Dynamic Time Warping

Dynamic time warping (DTW) is one of the most well-studied temporal pattern similarity measures (Rabiner et al., 1978). This method utilizes a dynamic programming approach to align a test time series to a template time series and provides an alignment distortion measure to ascertain pattern similarity.

For two time series X and Y of equal length $|X| = |Y| = n$, pattern similarity is established by aligning time series X with time series Y using the minimum computed alignment distortion $D_{align}(X, Y)$. The distortion path is obtained by warping time for each signal such that the minimum alignment distance between the two signals is achieved. This study applies the DTW measure to two EEG signals of equal length though the signals do not need to be the same length.

DTW has been used extensively in biological applications such as ECG analysis (Jen and Hwang, 2007; Kotas, 2008), EEG spiking pattern recognition (Chi et al., 2007), analysis of event-related potentials (Casarotto et al., 2005), fingerprint recognition (Kovacs-Vajna, 2000), and medical imaging reconstruction (Okumura et al., 2007). The DTW measure has demonstrated utility as a kernel function for support vector machine based seizure prediction algorithms in temporal lobe epilepsy (Chaovalitwongse and Pardalos, 2008).

The minimum DTW distance can be obtained using the following dynamic programming technique. First, an *n x n* alignment array is generated where each element of the array represents a distance metric for all combinations of points between the two signals. In this array the *(i,j)*th element is the distance between points x_i and y_j. Euclidean distance $d(x_i, y_j) = (x_i - y_j)^2$ is

typically used as the distance measure. A warp path $W = w_1,...,w_K$ is then constructed where K is the length of the warp path for which $\max(|X|,|Y|) \le K < |X| + |Y|$. Element k of the warping path represents Element k of the warp path represents a matching point $w_K = (i, j)$ of the two time series, where (i, j) corresponds to index *i* of time series X and index *j* of time series Y. A warping path must begin at the first sample of both time series, $w_1 = (1,1)$ and must finish at the last sample of both time series, $w_K = (n, n)$. An additional constraint requires the warping path indices i and j to increase monotonically. That is, $w_k = (i, j)$ and $w_k = (i', j')$, where $i \le i' \le i + 1$ and $j \le j' \le j + 1$. The optimal warp path possesses the minimum warping cost defined as

$$D_{align}(X,Y) = \min \frac{1}{K} \sum_{k=1}^{K} d(w_{k,i}, w_{k,j}). \tag{6-5}$$

This problem can be approached from a dynamic programming perspective where the path is advanced by one unit on the *i* axis, one unit on the *j* axis, or both. Thus, this approach only requires evaluation of cumulative distance found in adjacent elements,

$$D(i,j) = d(x_i, x_j) + \min \begin{cases} D(i, j-1) \\ D(i-1, j) \\ D(i-1, j-1) \end{cases}. \tag{6-6}$$

Teager-Kaiser Energy

In 1990, Kaiser first derived Teager's nonlinear energy algorithm in discrete time domain to calculate the energy of a sound (Kaiser, 1990). The Teager-Kaiser energy (TKE) operator has demonstrated sensitive to both amplitude and frequency changes in time series signals. This measure has demonstrated utility feature for the detection of seizures and high frequency

epileptiform activity (Zaveri et. al., 1993; Smart et. al., 2005; Gardner et. al., 2006). This study utilizes the mean value of the TKE operator across a window,

$$TKE(X) = \frac{1}{N}\sum_{k=2}^{N-1}\left[X(k)^2 - X(k-1)\cdot X(k+1)\right] \tag{6-7}$$

where N is the length of the window of interest.

Empirical Study

In order to investigate the possibility of seizure detection and stratification, two experiments are presented, each classifying a different subset of the seizure:

- Separate the beginning of each seizure from randomly-selected non-seizure segments
- Separate the end of each seizure from randomly-selected non-seizure segments.

Separating the beginning of the seizure from non-seizure segments (experiment one) tests the seizure detection abilities of the detector whereas distinguishing the end of a seizure from non-seizure segments (experiment two) is a critical task in seizure stratification. These two experiments provide an initial framework for testing the SVM classifier's ability to stratify generalized SWDs.

This empirical study is motivated by an underlying hypothesis that SVM's are capable of distinguishing neural states (seizure and non-seizure) in a newly-diagnosed patient with typical absence seizures. The signal features consist of the DTW distances between a template SWD signal the test window to be classified, both of which are 0.3 seconds in duration. This section describes the EEG data acquisition, data sampling and feature extraction, SVM training and testing, and results.

EEG Data Acquisition

Approximately 24 hours of scalp EEG data were acquired from a SleepMed DigiTrace ambulatory EEG recording device. The data were acquired at 200 Hz with an input range of 0.6

mV with built-in filter of 0.5-70 Hz. A bipolar, longitudinal, chain electrode recording montage was employed to provide 16 EEG channels (Fp1-F3, F3-C3, C3-P3, P3-O1, Fp2-F4, F4-C4, C4-P4, P4-O2, Fp1-F7, F7-T3, T3-T5, T5-O1, Fp2-F8, F8-T4, T4-T6, T6-O2) as well as two auxiliary channels which were not utilized. This EEG study utilized the F3-C3 and F4-C4 channels because provide high-quality representations of the SWDs yet are located reasonably far away from facial muscles. The patient underwent 93 seizures during the ~24 hour continuous EEG recording. Seizure times were verified by a board-certified clinical electroencephalographer.

Data Sampling and Feature Extraction

Each data sample consists of extracted features from an EEG window one second in duration. Within the one-second data sample window, a sub-window of 0.3 seconds in duration is advanced with 50% overlap from the start of the data sample window to the end of the data sample window (providing 5 sub-windows and thus 5 features per data sample window per EEG channel). Thus for channels F3-C3 and F4-C4 there are ten features representing each data sample window.

For each sub-window within the data sample, the DTW similarity feature is obtained via comparison with an archetypical SWD template. Figures 6-2 and 6-3 illustrate the DTW distance metric in this application.

The study uses 93 SWD templates (one selected from each seizure) which are centered on the spike and 0.3 seconds in duration. SWD templates are reassigned randomly such that no seizure uses its own template for feature extraction.

The seizure class consists of data sample windows from all 93 seizures. The non-seizure class consists of a total of 93 non-seizure data sample windows randomly selected from ~24 hour continuous EEG recording with the following constraints:

- Must be at least 60 seconds away from any seizure onset or offset
- Must be at least 0.1 seconds away from another non-seizure sample

The training dataset consists of the 93 seizure and 93 non-seizure data sample windows.

SVM Training and Testing

The soft-margin SVM classifier with a RBF kernel is applied to this problem based on success in other neural state classification problems (Kaper et. al., 2004; Acir and Güzelis, 2005; Bewernitz et. al., 2006; Lehmann et. al., 2007; Seref et al., 2006). A range of SVM parameters which demonstrated satisfactory results in similar EEG classification studies were applied to this study. Thus, each SVM cycle was performed for all nine combinations of cost=10,100,1000 (Kaper et al., 2004; Acir and Güzelis, 2005) and the RBF parameter sigma=20,40,60 (Kaper et. al., 2004; Lehmann et al., 2007).

SVM training is performed using a 10-fold cross validation scheme. This scheme employs a resampling technique in which the seizure and non-seizure classes are first randomly shuffled. Next, 10 % (~9 samples) of the shuffled seizure class and 10% (~9 samples) of the shuffled non-seizure class are extracted (individually for each class) and combined to form the test set. In general, SVM training is optimal for training datasets with equal numbers of data points from each class. Otherwise, the classifier can be biased towards the class which had more training points.

The remaining 90% of each class is used to train the SVM classifier which is then tested on the extracted testing dataset. Upon testing the SVM, the test dataset is replaced in the shuffled training data and the succeeding 10% block of each shuffled class is extracted to form the next test set. This validation scheme repeats until the last 10% block of each shuffled class is extracted and tested. This study repeats the sampling, feature extraction, resampling, training and testing cycle 1000 times.

Detector Performance Evaluation

The detection sensitivity and specificity are used to evaluate the performance of the SVM seizure detector. This involves categorizing the classification results into one of four possible outcomes:

- True positives (TPs) refer to the correct classification of seizure segment
- True negatives (TNs) refer to the correct classification of a non-seizure segment
- False positives (FPs) refer to the incorrect classification of a non-seizure segment as a seizure
- False negatives (FNs) refer to the incorrect classification of seizure segment as a non-seizure

The four possible detection outcomes may be illustrated in the context of figure 6-4. A classification result is considered a TP if a seizure EEG sample is classified as a seizure sample. A classification result is considered a TN if a non-seizure EEG sample is classified as a non-seizure sample. A classification result is considered a FP if a non-seizure EEG sample is classified as a seizure sample. Finally, a classification result is considered a FN if a seizure EEG sample is classified as a non-seizure sample.

The sensitivity and specificity measures often used for evaluating detector performance can be derived from these four outcome quantities. Sensitivity is the fraction of positive samples that are classified as positive:

$$Sensitivity = \frac{TP}{TP + FN} \tag{6-8}$$

where 'positive' refers to the seizure class. Specificity refers to the fraction of negative samples that are classified as negative:

$$Specificity = \frac{TN}{TN + FP} \tag{6-9}$$

where ‘negative’ refers to the non-seizure class.

Results

The mean value of sensitivity and specificity are reported for 100 SVM detection trials, where each trial underwent 10-fold cross validation for one of the nine combinations of SVM parameters. The results for experiment one, seizure detection of the first second of each seizure are shown in table 6-1. Results from experiment two, seizure stratification experiment performing detection on the last second of each seizure are summarized in table 6-2.

Discussion

As is shown in table 6-1 and figures 6-5, 6-6, 6-7, the SVM classifier’s overall best performance is experiment one’s application where the SVM is function as a seizure-onset detector (classifying the first second of each seizure). This result makes sense in comparison with experiment two where the last second of the seizure is classified as a first step towards a seizure stratification application (figures 6-8, 6-9, 6-10). The beginnings of the seizures appear more visually similar to one another than the ends of the seizures. Even still, the performance of the classifier in the experiment two setup demonstrated high sensitivity and specificity for numerous parameter combinations.

The observation that classification is less affected by SVM parameters in experiment one compared to experiment two is a reasonable phenomena. Due to stronger electroencephalographic similarity among various seizures at onset compared to offset, then the beginning of the seizures may be more regular in feature space than the seizure offset. Thus, the alterations in SVM parameters do not seem to have as large of an effect on the results of experiment one as with experiment two. In particular, the classifier varied more with changes in cost for experiment two than experiment one, which could be due to a loss of generality resulting from “over fitting” the more variant seizure offset period.

These results show promise for the SVM application to seizure detection and stratification. Such a tool may provide benefit to clinicians and researchers by providing a means to rapidly annotate as well as provide a clinically interesting measure of drug effect on a histogram of seizure durations. Thus, this line of work may lead to a greater understanding of the therapeutic effects of AEDs.

Future studies will provide a more comprehensive evaluation of features. While the DTW measure performed well, other similarity measures (such as similarity index) may be worth implementing. In addition, adding more EEG channels may improve classification performance though channel addition imposes a computational burden increase. These results should be validated in additional patients. Finally, an important future step is to implement this algorithm in a pseudo-online fashion to assess the robustness to noise. While SVMs provide exceptional generalization abilities, a sliding window classifier will provide an interesting assessment of how the classifier copes with the challenges of real-time EEG acquisition.

An expansive review article regarding support vector machines in neuroscience applications was accepted for publication under the title “support vector machines in neuroscience” with authors Onur Seref, O. Erhun Kundakcioglu, and Michael Bewernitz (Seref et al., 2007).

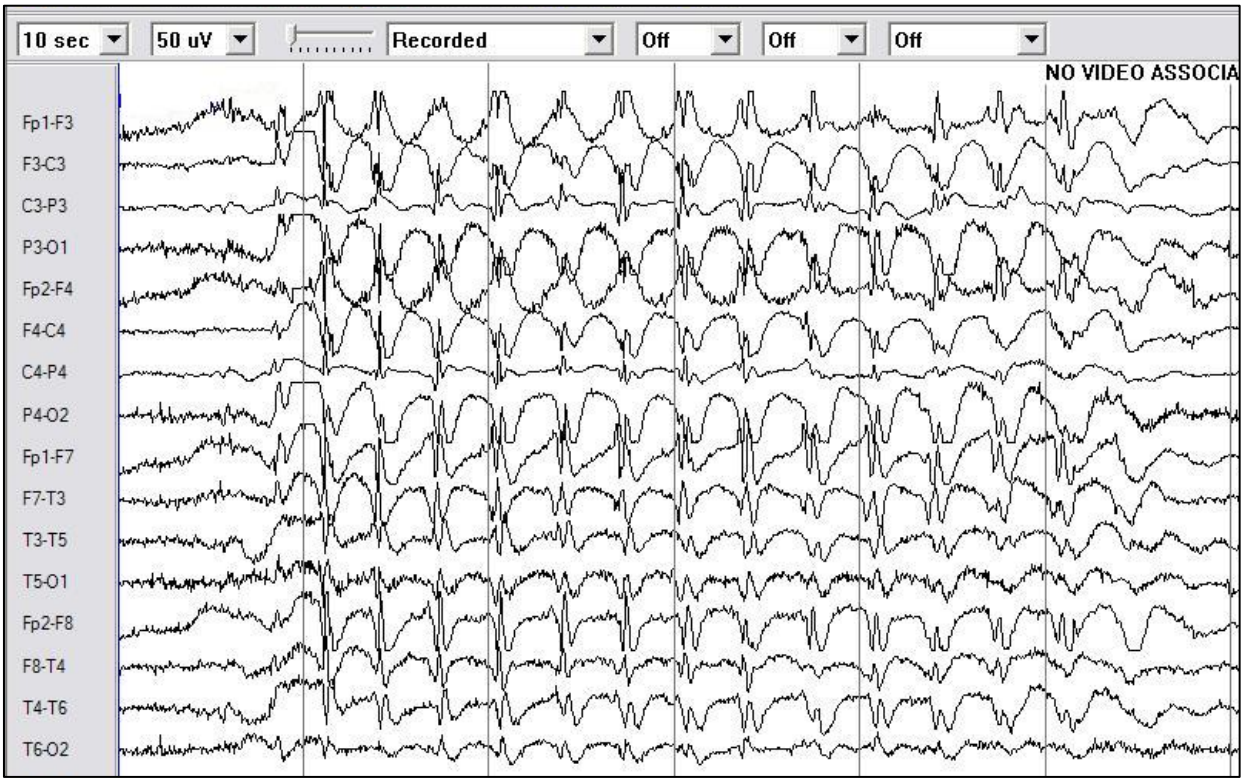

Figure 6-1. Approximately 6 seconds of scalp-EEG demonstrating the 2.5-3.5 Hz spike-wave discharge that defines an electrographic absence seizure (data provided courtesy of Dr. Gregory Holmes).

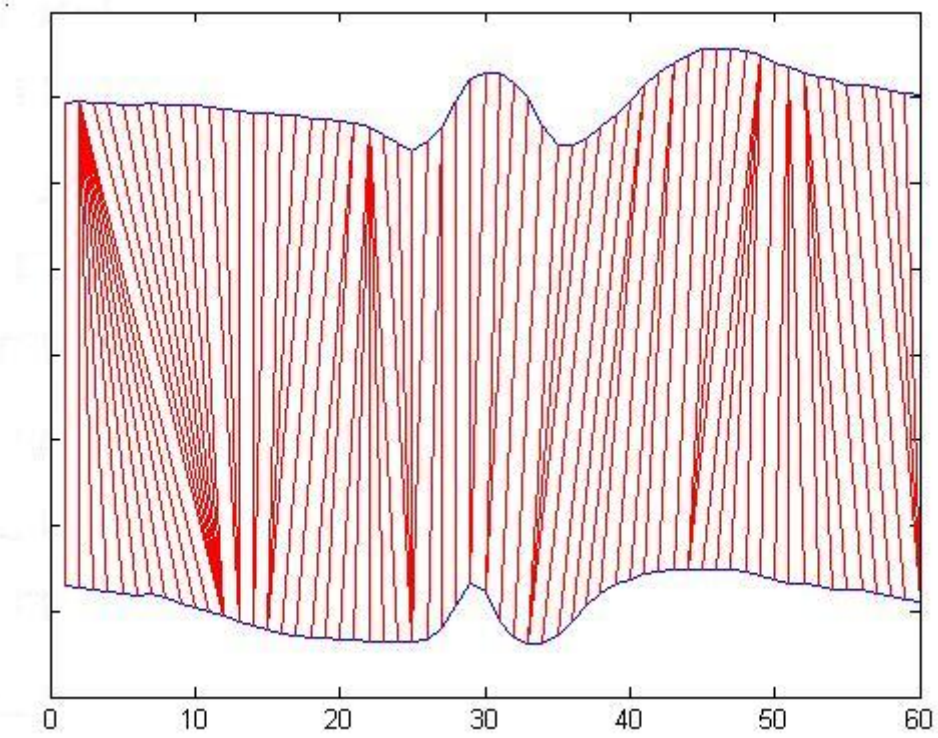

Figure 6-2. DTW comparison of two different SWD segments. The top signal is a 300 ms SWD segment. Bottom signal is a 300 ms segment of a different SWD. The DTW distance is about 2.4×10^7.

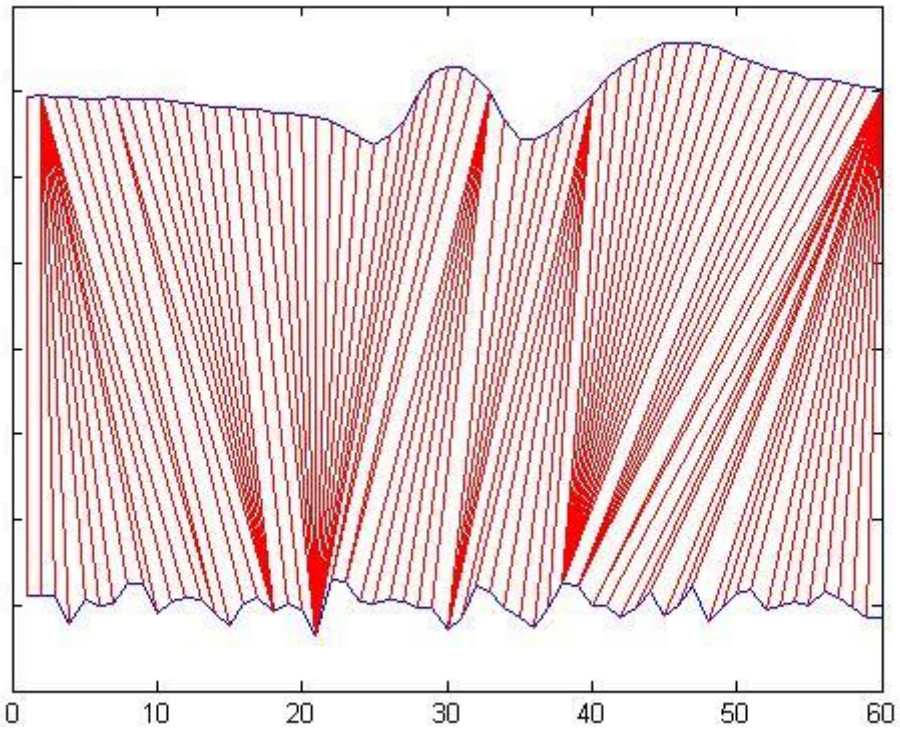

Figure 6-3. DTW comparison of a SWD segment with a random interictal segment. Top signal is a 300 ms EEG segment of a SWD. Bottom signal is 300 ms of interictal EEG. The DTW distance is about 5.1 x 10^7.

		Reality: Seizure	Reality: Non-seizure
Prediction	Seizure	True Positive	False Positive
	Non-seizure	False Negative	True Negative

Figure 6-4. Seizure classification evaluation framework.

Table 6-1. Classification performance using the first second of each seizure.

Sigma	Cost	Sensitivity	Specificity	Mean
20	10	97.11%	96.94%	97.02%
20	100	96.45%	96.46%	96.45%
20	1000	96.37%	96.43%	96.40%
40	10	97.18%	97.04%	97.11%
40	100	96.56%	96.49%	96.53%
40	1000	96.19%	96.37%	96.28%
80	10	97.10%	97.04%	97.07%
80	100	96.82%	96.62%	96.72%
80	1000	96.04%	96.31%	96.18%

Table 6-1. Classification performance using the last second of each seizure.

Sigma	Cost	Sensitivity	Specificity	Mean
20	10	94.85%	93.46%	94.16%
20	100	91.98%	93.10%	92.54%
20	1000	90.25%	92.07%	91.16%
40	10	95.04%	93.34%	94.19%
40	100	93.03%	93.27%	93.15%
40	1000	89.91%	92.13%	91.02%
80	10	94.93%	93.29%	94.11%
80	100	93.86%	93.29%	93.58%
80	1000	90.74%	92.63%	91.69%

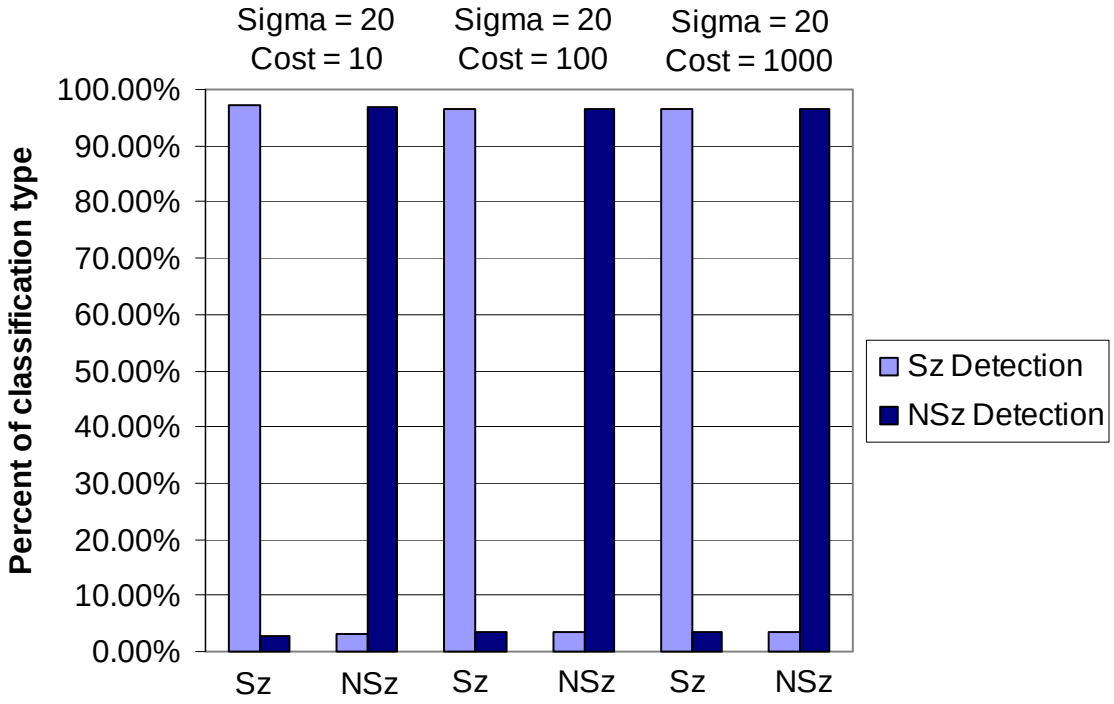

Figure 6-5. Seizure detection performance for RBF parameter sigma=20 using the first second of each seizure.

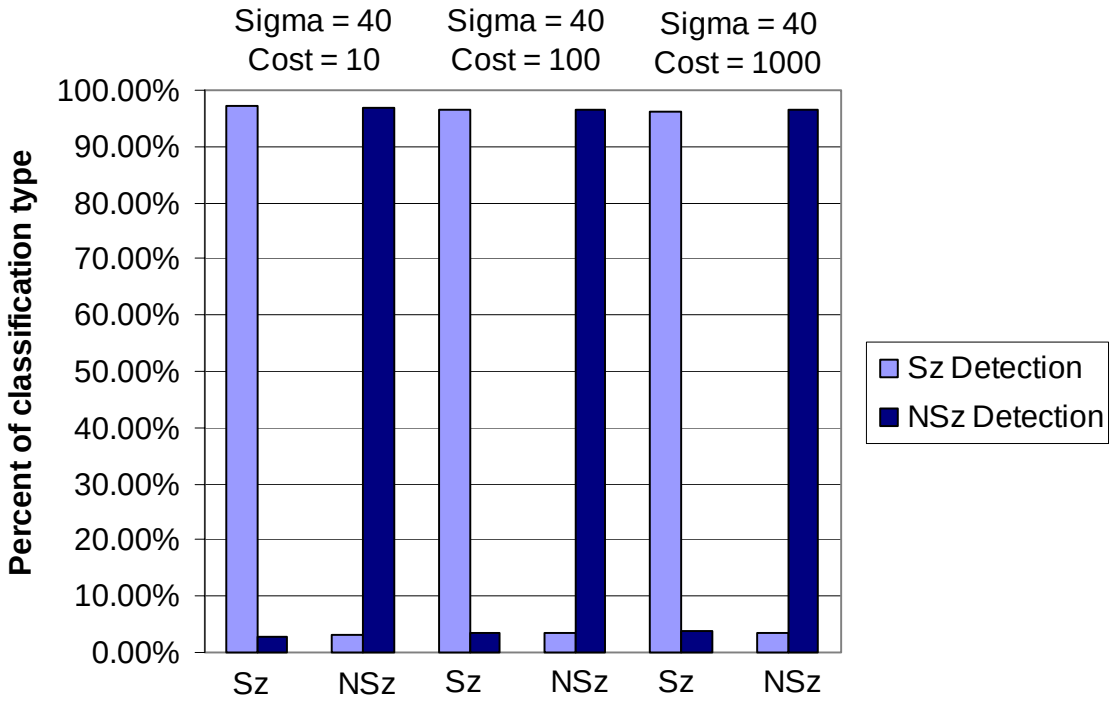

Figure 6-6. Seizure detection performance for RBF parameter sigma=40 using the first second of each seizure.

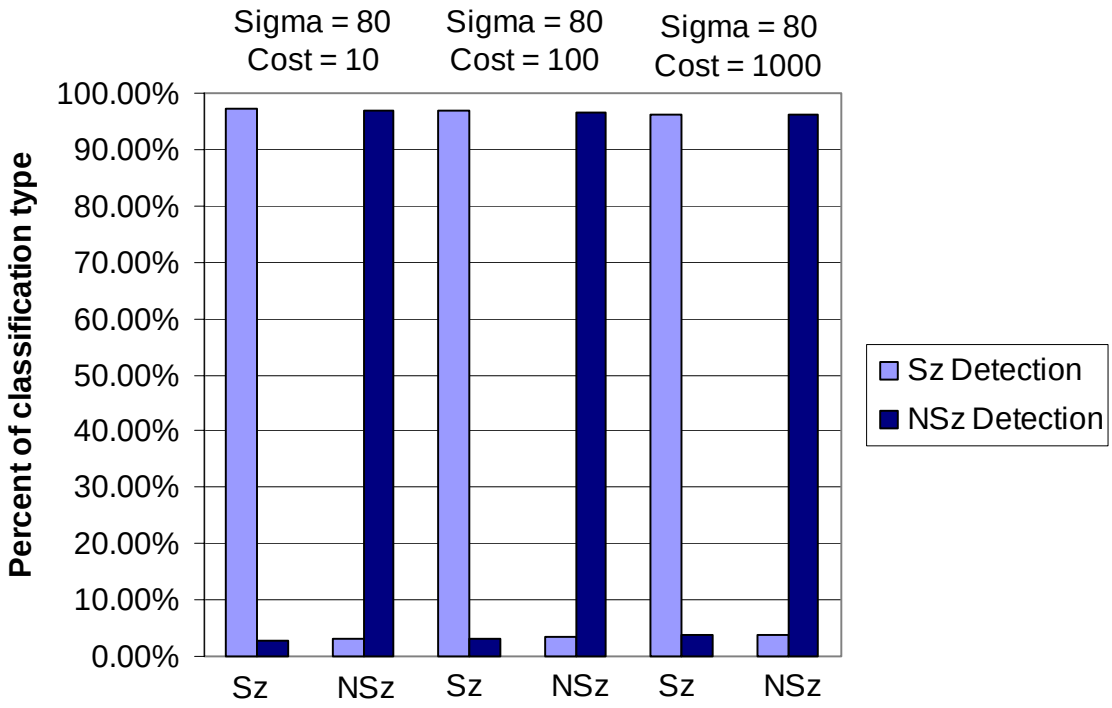

Figure 6-7. Seizure detection performance for RBF parameter sigma=80 using the first second of each seizure.

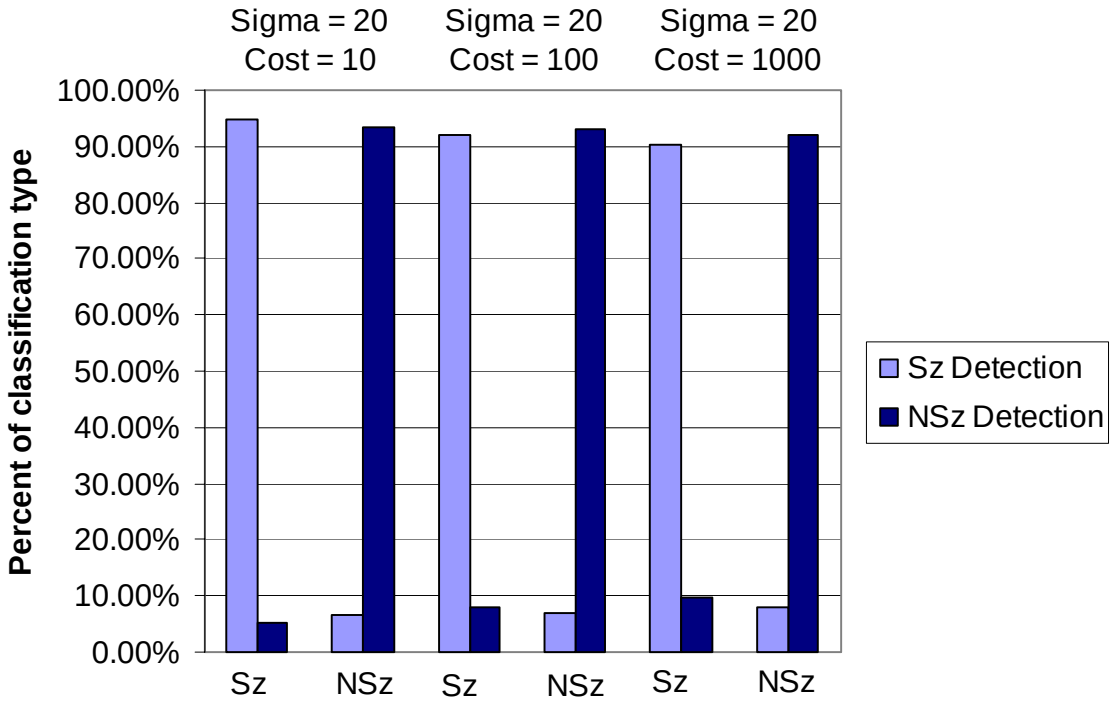

Figure 6-8. Seizure detection performance for RBF parameter sigma=20 using the last second of each seizure.

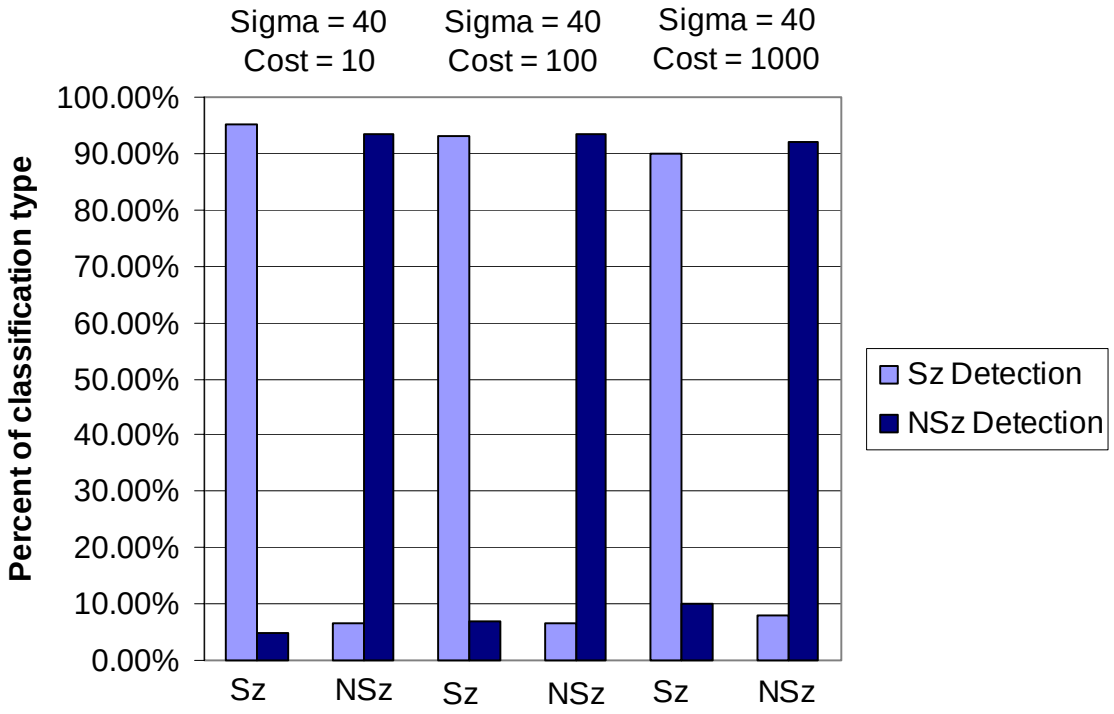

Figure 6-9. Seizure detection performance for RBF parameter sigma=40 using the last second of each seizure.

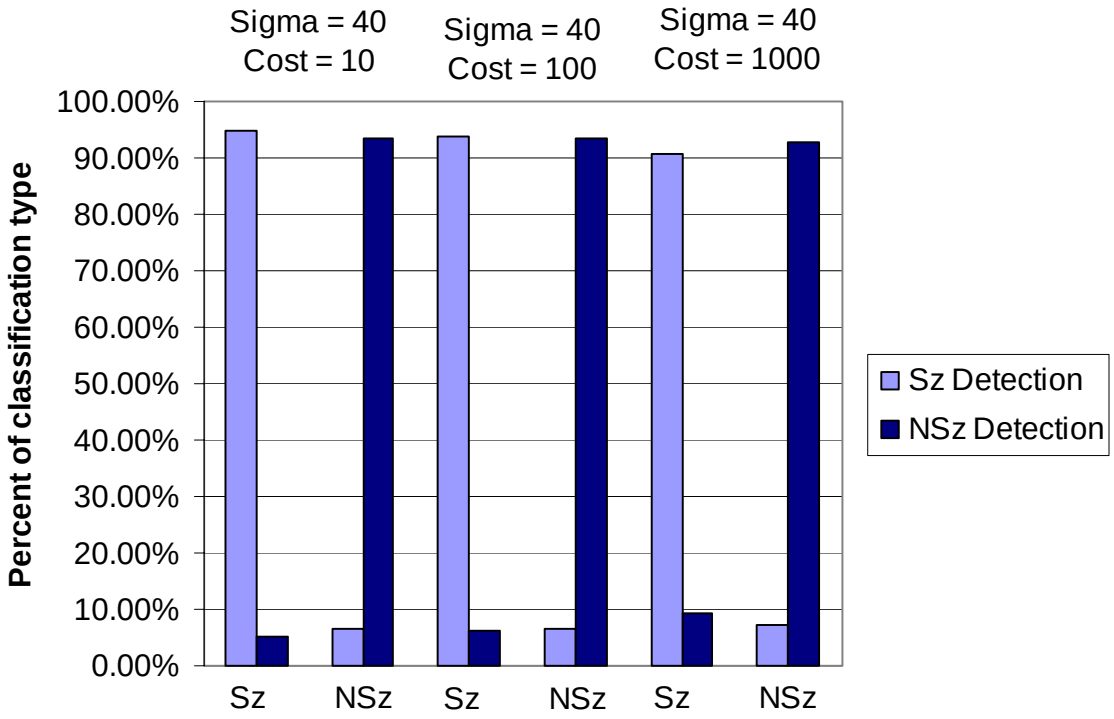

Figure 6-10. Seizure detection performance for RBF parameter sigma=80 using the last second of each seizure.

CHAPTER 7
DISCUSSION AND CONCLUDING REMARKS

Epilepsy is a disorder of the brain which is characterized by intermittent synchronized discharges of large populations of neurons. This disorder can greatly impact a patient's life in numerous ways including financial, social, professional, and psychiatric effects. While AED therapy may help keep seizures at bay in some patients others are not so fortunate. In the last few decades, savvy researchers have taken advantage of the rapid progression of computer technology, biomaterials, signal analysis advances and medical knowledge advancement to extract relevant EEG features in order to enhance epilepsy treatment.

Computational neuroscience is an exciting frontier which is providing numerous options for addressing neurological disorders which may have been inconceivable decades ago. The ability to map the brain's states in terms of the status of a dynamic neurologic disorder will likely be a highly sought-after research goal for years to come. This dissertation has helped provide preliminary data mining and dynamical EEG analyses to help uncover patterns which may be related to stimulation parameters and ultimately improve our understanding of the mechanisms that produce the VNS therapeutic effect. In addition, a study outlining a novel generalized spike wave detection algorithm was outlined here as well. These projects aim towards creation of bedside and/or implantable real-time seizure control devices.

Towards Real-Time EEG Analysis Tools for the Bedside and Implantation

The exciting progress made in the characterization of sophisticated disease and disorders modeling schemes is part of the driving force this research. The characteristics of the class of disorders known as dynamic disorders provide an interesting framework to approach the problem of improving existing and creating new therapeutic approaches. This perspective treats such disorders as deviations from a range of healthy dynamics in the underlying physiologic control

systems. Such a perspective implies therapeutic approaches which involve a fusion of medicine, biology, and engineering. Numerous researchers are investigating the possibility of applying a systems control approach to the epileptic brain in order to reduce the burden of epileptic seizures. Some of the studies presented in this dissertation are geared towards such an approach and aim to improve the VNS therapy modality.

Patients with newly-implanted VNS systems undergo a period often lasting several months of sub-optimal therapy. During this period, patients may need to undergo numerous visits to the doctor's office in order to fine-tune the stimulation parameters for clinical efficacy and tolerance. Such a process results in increased medical treatment costs and all the while the patients may be at a higher risk to seizures due to sub-optimal stimulation parameters. One of the goals of the work presented it to examine the possibility of an EEG marker of optimal VNS therapeutic efficacy to help expedite the process of tuning parameters in newly-implanted patients. The main focus of the research on the VNS data is to characterize EEG characteristics in numerous VNS patients in order to assess any relationships to stimulation parameters. If such a relationship can be established and if the effects could then be geared towards a final outcome, then such EEG characteristics may find use in a bedside device for rapid VNS calibration or even in an implantable control system for optimal VNS therapy. The studies presented in chapter four represent data mining approaches to characterizing such EEG effects.

Data Mining Approaches to Characterizing EEG Patterns

Data mining tools have demonstrated an extensive capacity to discover patterns in biological datasets including EEG signals. Data mining is the process of applying algorithms to extract patterns in large datasets. While the human eye is often the best pattern detector of all, data mining algorithms can work on exceedingly large datasets and examine complex multidimensional datasets. One of the most attractive features of data mining tools are their

ability to perform clustering data subsets according to inherent similarities or in a supervised manner. For the purpose of characterizing EEG patterns in patients undergoing VNS therapy for epilepsy, data mining methods provide a useful tool for elucidating preliminary patterns which incorporate an expansive representation of features from all channels.

The biclustering experiment provided a characterization of the EEG patterns which may be related to VNS therapy. The observations were based on patterns of the STLmax measure, which assumes a chaotic framework and provides a measure of the sensitivity of the signal to initial conditions. Though the brain's behavior may not always be consistent with a low-dimensional chaos model, the chaoticity measure has provided an ability to classify neural states in epilepsy (e.g. interictal or far from a seizure, preictal or seizure imminent, ictal or during a seizure, and postictal or the period of altered consciousness following a seizure). Thus, the measure was selected as a candidate for detecting EEG patterns which may be related to VNS therapy. The study demonstrated separability between the VNS on and off states for which all of patient A's electrodes contributed to and only a few frontal and temporal electrodes in patient B contributed to. The biological relevance of these results may be related to study which discovered that VNS-induced acute suppression of epileptiform activity in a hippocampal depth electrode (Olejniczak et al., 2001). Though the study by Olejniczak et al. utilized depth electrodes, it is possible that scalp EEG recordings may display some manifestation of such an EEG effect observed at a hippocampal depth electrode. From this perspective, perhaps the STLmax behavioral differences between patients A and B are associated with enhanced suppression of epileptiform activity in patient A compared to patient B. An interesting future application of biclustering would be to examine the EEG effects during non-stimulation in an unsupervised manner. Such an experiment would provide a highly objective method to determine spatio-

temporal patterns of EEG features. Based on the results of chapter 5, future experiments should include both linear and nonlinear features to help ensure proper characterization of the wide range of EEG dynamical behavior patterns observed during these studies. This work was published in the paper "Biclustering EEG data from epileptic patients treated with vagus nerve stimulation", authored by Stanislav Busygin, Nikita Boyko, Panos Pardalos, Michael Bewernitz, and Georges Ghacibeh (Busygin, 2007).

The next experiment examined the patterns of the raw EEG behavior in feature space using support vector machines. The accuracy at which the SVM's could separate the raw EEG between two adjacent EEG segments, a reference segment during stimulation and successive non-overlapping windows was interpreted as a robust measure of EEG similarity (or dissimilarity) and compared with stimulation parameters. The study determined observed a potential covariation between the EEG and the pulse width and stimulation frequency parameters.

A study by Mu et al. showed that a 250 μs VNS pulse width caused reduced blood flow in significantly more brain regions (e.g. hippocampus, sup. temp. lobe) than 500 μs (2004). Perhaps these regions may be responsible for covariation of EEG feature space dispersion with pulse width parameter. Furthermore, a recent study demonstrated that a 20 Hz stimulation frequency produced significant cerebral blood flow increases (e.g. in the orbitofrontal cortex, hypothalamus, and thalamus) compared to 5 Hz in VNS patients (Lomarev et al., 2002). It is possible that the altered blood flow in these regions may be responsible for the observed covariation of EEG feature space dispersion with stimulation frequency.

In addition, patients where seizure free and patients which experienced a small number of seizures per month resulted in greater separation accuracy between the reference class and all subsequent comparison classes in a VNS epoch. The patient with the most seizures per month

resulted in the poorest separation between the reference class and all adjacent classes. This phenomenon could be the multichannel analog of the dynamic resetting effect between two EEG channels postulated by Iasemidis et al. which states that a seizure resets the brain from an unfavorable state to a more favorable state (Sackellares and Iasemidis, 1997; Iasemidis et al., 2004). Thus, the results were interpreted as electroencephalographic evidence that the VNS mimics the therapeutic resetting effect of a seizure. Future studies involving SVM would apply the algorithm in an unsupervised manner to help provide unbiased information about patterns in the data. Also, modification of the support vector machine algorithm, such as adaptive feature scaling (Grandvalet et. al., 2003) can help provide insight into the relevance of each input feature for SVM classification. This study is published in an article titled "Quantification of the Impact of Vagus Nerve Stimulation Parameters on electroencephalographic Measures" with authors Michael Bewernitz, Georges Ghacibeh, Onur Seref, Panos Pardalos, Chang-Chia Liu, Basim Uthman (Bewernitz, 2007).

The final study utilized SVMs and LR to analyze the time-varying feature space separation of the STLmax dynamical measure in patients undergoing VNS therapy. With an eye towards the VNS replicating the resetting effect of a seizure, this study aimed to characterize potential relationships between the EEG and stimulation parameters using an experimental setup similar to Iasemidis et al. (2004). Thus, a reference class was selected at 8 seconds prior to the stimulation onset and was comprised of the STLmax value of all channels for all stimulations combined. Similarly, each succeeding non-overlapping window for all channels for all epochs was compared with the reference class. The study demonstrated that the observed pattern changes may be related to the stimulation frequency parameter. Lomarev et al. demonstrated that a 20 Hz stimulation frequency produced significant cerebral blood flow increases (e.g. in the

orbitofrontal cortex, hypothalamus, and thalamus) compared with the 5 Hz stimulation frequency in VNS patients (Lomarev et al., 2002). The brain regions which showed a pulse-width dependent blood flow in the study by Lomarev et al. may be the source of the observed covariation of EEG feature space dispersion with stimulation frequency.

Also, it was speculated that the poor STLmax separation between VNS on (which may be considered as a VNS 'artificial' seizure) and VNS off in patient B combined with patient B's high seizure frequency (compared with the other patients) is aligned with the dynamic seizure resetting effect described by Iasemidis et al. (2004). In addition, this experiment demonstrated the concept previously observed by Bewernitz et al. (2007) except while using the STLmax measure. Thus, the connection between the observed effect and the observations of Iasemidis et al (2004) are stronger. This study was submitted to Computing and Optimization in Medicine and Life Sciences Vol. 3, under the title "A Data Mining Approach to the Investigation of EEG Biomarker Existence for Vagus Nerve Stimulation Therapy Patients", with authors Nikita Boyko, Michael Bewernitz, Vitaliy Yatsenko, Panos Pardalos, Georges Ghacibeh, Basim Uthman (Boyko et al., 2008).

In regards to the biological impact, these results may be related to the phenomenon discovered in a study by Olejniczak et al. where a short-term suppression of epileptiform sharp waves was observed following VNS from a hippocampal depth-electrode (2001). While the scalp electrodes used to collect the data in these analyses cannot achieve the recording quality of hippocampal depth electrodes, it is possible that the scalp EEG data mining analysis results may reflect the same therapeutic effect as observed in the hippocampus by Olejniczak et al. (2001).

Analysis of Interstimulation Dynamics

The studies described in chapter 5 focus analysis on the EEG dynamics occurring during interstimulation epochs. While the comparisons of stimulation to non-stimulation epochs

provided interesting results with clinical significance, the advantage of this experimental setup is that the possibility of direct neural modulation is eliminated. Thus, the results are more likely to be due to an "after-effect" of stimulation rather than due to immediate neuronal modulation.

The first experiment performed an extensive nonlinearity characterization using surrogate EEG analysis. Each epoch was compared to 19 surrogate datasets using the ApEnt measure. The most obvious connection of the EEG with the stimulation parameters was a covariation with the pulse width. In addition, the two seizure-free patients (E and F) produced the lowest fraction of epochs which displayed a nonlinear fingerprint (e.g. rejected the null hypothesis at the given significance level). These results may be related to a study by Olejniczak et al. which reported an acute VNS-induced suppression of epileptiform activity in the hippocampus (2001). Though the effect was observed from a hippocampal depth electrode in the study by Olejniczak et al., it is possible that some manifestation of the effect is present in the scalp-EEG signal analyzed in the present study. The VNS-enhanced suppression of epileptiform activity reported in the literature may be responsible for the diminished nonlinearity in patients with fewer seizures. The cause of any epileptiform activity suppression may be related to a pulse-width dependency of blood flow to various brain regions (e.g. hippocampus and superior temporal lobe) reported by Mu et al., 2001. The observation that the seizure-free patients expressed the least amount of nonlinearity may be congruent with the findings of Janszky et al. where the absence of bilateral interictal epileptiform discharges was the only EEG predictor of seizure freedom (2005). Thus, future studies should include epileptiform discharges in order to help further characterize the EEG effect associated with VNS.

Shen et al. demonstrated that K-complex expression patterns can affect nonlinearity in surrogate analysis of sleep EEG (2003). The observed nonlinearity increases in patients A and B

during late night (~11pm until ~7am) may be the result of altered k-complex expression during sleep (though other patients did not show this trend). The VNS is known to cause an increase in the overall EEG power during sleep (Rizzo et al., 2004).

The nature of surrogate data analysis is to provide a yes/no answer to the question of nonlinearity, but does not provide information on what type of nonlinearity is observed. All in all, these results suggest that nonlinear measures may someday demonstrate sensitivity to the outcome of VNS effect. In addition, this study motivates the usage of linear and nonlinear measures in conjunction with one another as well as specific waveforms such as epileptiform discharges in order to characterize the complex signal patterns present in EEG.

The second study in chapter five aimed to characterize any time dependence of the EEG dynamics during the interstimulation epochs. This preliminary study was executed by performing a statistical comparison of the first half of each interstimulation epoch to the second half. The study utilized four measures which have demonstrated success in classifying neural state changes in epilepsy; ApEnt, correlation sum, $\overline{\Omega}$, and STLmax. The study showed that the patient with the greatest amount of interstimulation epochs demonstrating significant time variation (for Apent, correlation sum, and $\overline{\Omega}$) also had the highest output current (2.5 mA for patient C). Patient A showed a similar trend and had the second highest output current (1.75 mA). Patient F showed an opposing trend with 0.75 mA output current and the smallest fraction of interstimulation epochs showing time variation. The ApEnt and $\overline{\Omega}$ measures demonstrated a noticeably larger deviation from the control in all six patients than the other two measures, as well as sensitivity to the output current. These two observations suggest that the ApEnt and $\overline{\Omega}$ measures may be good candidates for EEG biomarkers in VNS patients. Biologically, these results may be related two studies which demonstrated an electrical current threshold for

epileptiform activity suppression when stimulating the hippocampus in a low Ca2+ seizure model (Warren and Durand, 1998) and a high K+ seizure model (Nakagawa and Durand, 1991).

A paper related to these interstimulation dynamics studies was published under the title "Optimization of epilepsy treatment with vagus nerve stimulation" with authors Basim Uthman, Michael Bewernitz, Chang-Chia Liu, and Georges Ghacibeh (Uthman et al., 2007).

Remarks on VNS Results

The variation in observed sensitivity in these measures to the various VNS parameters suggest that different EEG measures are better suited for providing different information about the EEG signal than other measures. Intuitively, it seems logical that a complex system such as the epileptic brain may require several EEG measures for adequate characterization for therapeutic intervention purposes. This observation is underscored in light of the intermittent expression of nonlinear signatures in various interstimulation epochs. Future studies should address the characterization task using a blend of linear and nonlinear measures.

In addition, future studies require additional patients to validate the interpretation of these results. Baseline EEG recordings would provide additional support for the existence of EEG-induced VNS effects by providing an opportunity to demonstrate the absence of such patterns prior to implantation. After acquisition of the necessary baseline data, an interesting study would be to examine the changes induced by the first stimulation. Thus, after the first stimulation, a subsequent VNS deactivation and EEG acquisition may be applied. This would provide a highly objective experimental setup possible for identifying short-term VNS effects. Subsequent follow-up recording sessions may provide additional characterization of the summed modulatory effect of chronic VNS.

The time of the last seizure should be obtained from the patient for all such studies. The reason for this is that the patient undergoes a brief period of increased seizure protection after

some seizures (e.g. generalized tonic-clonic seizures). Thus, if the patient is under the influence of this particular neural state, then that would provide a reduced chance of seizure which is not consistent with the patient's standard behavior. This information would be helpful for interpreting results. In addition, caution must be exercised when interpreting the results of patients whom undergo seizures. As dynamical transitions can occur several minutes to several hours prior to a seizure, many researchers operationally define the interictal period as being a minimum of 8 hours away from a seizure (Pardalos et al., 2003; Hively et al., 2005; Chaovalitwongse et al., 2006). Thus, the occurrence of a handful of seizures may produce an unknown amount of influence on EEG dynamics. For this reason, future studies may withhold analysis of EEG signals occurring within 8 hours of a seizure.

Seizure Detection and Stratification

The final project of this dissertation applied SVM classification in a preliminary experiment geared towards a seizure detection and stratification system in patients with generalized absence epilepsy. The seizure detection system utilized DTW distance with a reference vector centered on a spike as the extracted feature. As spike and wave discharges in absence epilepsy are generalized and often have a highly characteristic pattern. The first experiment in this study performed SVM training and testing for the detection of the first second of the seizure versus randomly selected non-seizure EEG which was located at least one minute away from a seizure and at least 0.1 second away from another non-seizure segment. Though both experiments present high sensitivity and specificity, the SVM classifier performed better at classifying the first second of the seizure than final second o the seizure. This is likely due to stronger electroencephalographic similarity among the different seizures at onset compared to offset. Alteration of the RBF kernel bandwidth did not appear to appear the results much. Variation of the cost parameter produced a greater effect on accuracy in experiment two than

experiment one. This is likely due to a loss of generality resulting from rigid "over fit" models which may occur when the cost is sufficiently high.

Such an algorithm may benefit clinicians and researchers by providing a means to rapidly annotate EEG signals as well as a means to provide a clinically interesting measure of therapeutic efficacy (e.g. distribution of seizure durations may vary before and after drug therapy, and thus a measure of this distribution may find clinically relevant information which a raw seizure count would miss). A future direction of this project is to implement the classifier in a real-time situation to test how the algorithm deals with the challenges presented in real-time EEG analysis.

This study was submitted to a 2008 volume of the "Optimization and Its Applications" book series under the title "A Novel Algorithm for the Detection and Stratification of Generalized Absence Seizures" with authors Michael Bewernitz, Onur Seref, Basim Uthman, and Panos M. Pardalos. In relation to this work, a review article regarding support vector machines in neuroscience applications was accepted for publication under the title "support vector machines in neuroscience" with authors Onur Seref, O. Erhun Kundakcioglu, and Michael Bewernitz (Seref et al., 2007).

Final Remarks

The collection of studies presented address preliminary challenges involved with development of online real-time EEG analysis systems for bedside and/or implantable therapy or diagnosis enhancement tools. The choice of EEG source and extracted features for such a tool is one of the greatest challenges presented to researchers in this field. Brain activity can be measured on numerous scales from individual neurons up to macroscopic field potentials representing large regions of the cerebral cortex. In addition, ensuring high-fidelity recordings is an additional challenge requiring careful consideration for preprocessing tasks such as artifact

rejection and filtering. In addition to the complex nature of EEG analysis, the EEG data source itself is limited in what it can tell a person about the brain. As technology improves and electronic components become smaller, faster, and more efficient, future implantable therapeutic control prostheses may also implement chemical sensors for quantifying neurotransmitter concentrations, for example. Inclusion of additional information related to brain function could greatly enhance the characterization of brain's behavior and potentially augment the performance of implantable therapeutic control devices.

LIST OF REFERENCES

Abarbanel H, Brown R, Kennel M. Variation of Lyapunov exponents in chaotic systems: Their importance and their evaluation using observed data. Journal of Nonlinear Science, vol. 2, pp. 343-365, 1992.

Abarbanel H. Analysis of observed chaotic data. New York: Springer-Verlag, 1996.

Abásolo D, Hornero R, Espino P, Poza J, Sánchez CI, de la Rosa R. Analysis of regularity in the EEG background activity of Alzheimer's disease patients with Approximate Entropy. Clin Neurophysiol. 2005 Aug;116(8):1826-34.

Abásolo D, James CJ, Hornero R. Non-linear Analysis of Intracranial Electroencephalogram Recordings with Approximate Entropy and Lempel-Ziv Complexity for Epileptic Seizure Detection. Conf Proc IEEE Eng Med Biol Soc. 2007;1:1953-6.

Acharya U R, Faust O, Kannathal N, Chua T, Laxminarayan S. Non-linear analysis of EEG signals at various sleep stages. Comput Methods Programs Biomed. 2005 Oct;80(1):37-45.

Acir N, Güzelis C. Automatic recognition of sleep spindles in EEG via radial basis support vector machine based on a modified feature selection algorithm. Neural computing and applications (2005) vol. 14: pp. 56–65.

Adelson PD, Nemoto E, Scheuer M, Painter M, Morgan J, Yonas H. Noninvasive continuous monitoring of cerebral oxygenation periictally using near infrared spectroscopy: a preliminary report. Epilepsia 1999; 40: 1484–9.

Ardesch JJ, Buschman HP, Wagener-Schimmel LJ, van der Aa HE, Hageman G. Vagus nerve stimulation for medically refractory epilepsy: a long-term follow-up study. Seizure. 2007 Oct;16(7):579-85.

Asyali MH, Berry RB, Khoo MC, Altinok A. Determining a continuous marker for sleep depth. Comput Biol Med. 2007 Nov; 37(11):1600-9.

Barlow J. Methods of analysis of nonstationary EEG with emphasis on segmentation techniques. J. Clin. Neurophysiol., vol. 2, pages 267-304, 1985.

Baumgartner C, Serles W,Leutmezer F, Pataraia E, Aull S,Czech T, et al. Preictal SPECT in temporal lobe epilepsy: regional cerebral blood flow is increased prior to electroencephalography-seizure onset. J Nucl Med 1998; 39: 978–82.

Begley CE, Famulari M, Annegers JF, Lairson DR, Reynolds TF, Coan S, Dubinsky S, Newmark ME, Leibson C, So EL, Rocca WA. The Cost of Epilepsy in the United States: An Estimate from Population-Based Clinical and Survey Data. Epilepsia. 2000 Mar; 41(3):342-51.

Belair J, Glass L, An Der Heiden U, Milton J. Dynamical disease: Identification, temporal aspects and treatment strategies of human illness. Chaos. 1995 Mar;5(1):1-7.

Bendat JS, Piersol AG. Random Data: Analysis and Measurement Procedures, 2nd ed. New York: John Wiley, 1986.

Berndt D, Clifford J. Finding patterns in time series: A dynamic programming approach. In Advances in knowledge discovery and data mining, U. Fayyad, G. Piatetsky-Shapiro, P. Smyth, and R. Uthursamy, editors, pages 229-248. AAAI Press, 1996.

Beuter A, Vasilakos K. Tremor: Is Parkinson's Disease a Dynamical Disease? Chaos 5, 14-17 (1995).

Bewernitz M, Ghacibeh G, Seref O, Pardalos PM, Liu CC, Uthman B. Quantification of the impact of vagus nerve stimulation parameters on electroencephalographic measures. Proceedings of the conference on Data Mining, Systems Analysis and Optimization in Biomedicine. Gainesville, (FL), 28-30 March 2007, AIP Conference Proceedings, No. 953, pp. 206-219.

Binnie CD, Mizrahi EM. The epilepsy monitoring unit. in Epilepsy: A comprehensive textbook, Eds. J. Engel Jr. and T. A. Pedley, Philadelphia: Lippincott-Raven, 1997.

Box GE, Jenkins GM. Time series analysis: Forecasting and control, San Francisco: Holden-Day, 1976.

Boyko N, Bewernitz M, Yatsenko V, Pardalos PM, Ghacibeh G, Uthman B. A Data Mining Approach to the Investigation of EEG Biomarker Existence for Vagus Nerve Stimulation Therapy Patients. Submitted to: Computing and Optimization in Medicine and Life Sciences Vol. 3, editor: Eva K. Lee, (2008).

Breakspear M. Perception of odors by a nonlinear model of the olfactory bulb. Int J Neural Syst. 2001 Apr;11(2):101-24.

Bressler SL, Richter CG, Chen Y, Ding M. Cortical functional network organization from autoregressive modeling of local field potential oscillations. Stat Med. 2007 Sep 20;26(21):3875-85.

Bruhn J, Röpcke H, Hoeft A. Approximate entropy as an electroencephalographic measure of anesthetic drug effect during desflurane anesthesia. Anesthesiology. 2000 Mar;92(3):715-26.

Bruhn J, Bouillon TW, Shafer SL. Onset of propofol-induced burst suppression may be correctly detected as deepening of anaesthesia by approximate entropy but not by bispectral index. Br J Anaesth. 2001 Sep;87(3):505-7.

Bruhn J, Bouillon TW, Radulescu L, Hoeft A, Bertaccini E, Shafer SL. Correlation of approximate entropy, bispectral index, and spectral edge frequency 95 (SEF95) with clinical signs of "anesthetic depth" during coadministration of propofol and remifentanil. Anesthesiology. 2003 Mar;98(3):621-7.

Burioka N, Cornélissen G, Halberg F, Kaplan DT, Suyama H, Sako T, Shimizu E. Approximate entropy of human respiratory movement during eye-closed waking and different sleep stages. Chest. 2003 Jan;123(1):80-6.

Burioka N, Cornélissen G, Maegaki Y, Halberg F, Kaplan DT, Miyata M, Fukuoka Y, Endo M, Suyama H, Tomita Y, Shimizu E. Approximate entropy of the electroencephalogram in healthy awake subjects and absence epilepsy patients. Clin EEG Neurosci. 2005 Jul;36(3):188-93.

Busygin S, Prokopyev OA, Pardalos PM, Feature Selection for Consistent Biclustering via Fractional 0-1 Programming, Journal of Combinatorial Optimization, Vol. 10/1 (2005), pp. 7-21.

Busygin S, Prokopyev OA, Pardalos PM, Biclustering in Data Mining, to appear in Computer and Operations Research, 2006.

Busygin S, Boyko N, Pardalos PM, Bewernitz MA, Ghacibeh G. Biclustering EEG data from epileptic patients treated with vagus nerve stimulation. Proceedings of the conference on Data Mining, Systems Analysis and Optimization in Biomedicine. Gainesville, (FL), 28-30 March 2007, AIP Conference Proceedings, No. 953, pp. 220-231.

Casdagli MC, Iasemidis LD, Savit RS, Gilmore RL, Roper SN, Sackellares JC. Nonlinear analysis of mesial temporal lobe seizures using a surrogate data technique. Epilepsia, vol. 36, Suppl. 4, pp. 142, 1995.

Casdagli MC, Iasemidis LD, Sackellares JC, Roper SN, Gilmore RL, Savit RS. Characterizing nonlinearity in invasive EEG recordings from temporal lobe epilepsy. Physica D, vol. 99, pp. 381-399, 1996.

Casdagli MC, Iasemidis LD, Savit RS, Roper SN, Gilmore RL, Sackellares JC. 1997. Nonlinearity in invasive EEG recordings from patients with temporal lobe epilepsy. Electroencephalogr. Clin. Neurophysiol. 102, 98–105.

Casarotto S, Bianchi AM, Cerutti S, Chiarenza GA. Dynamic time warping in the analysis of event-related potentials. IEEE Eng Med Biol Mag. 2005 Jan-Feb;24(1):68-77.

Chabardes S, Kahane P, Minotti L, Koudsie A, Hirsch E, Benabid AL. Deep brain stimulation in epilepsy with particular reference to the subthalamic nucleus. Epileptic Disorders. 2002 Dec;4 Suppl 3:S83-93.

Chabolla DR, Cascino GD. Interpretation of Extracranial EEG. In: The Treatment of Epilepsy: Principles and Practice, 2nd ed. Elaine Wyllie, M.D. Baltimore, Williams and Wilkins, © 1997. pp 264-279.

Chaovalitwongse, WA. Iasemidis, LD. Pardalos, PM. Carney, PR. Shiau, DS. Sackellares, JC. Performance of a seizure warning algorithm based on the dynamics of intracranial EEG. Epilepsy Res. 2005 May;64(3):93-113.

Chaovalitwongse, WA. Prokopyev, OA. Pardalos, PM. Electroencephalogram (EEG) time series classification: Applications in epilepsy. Ann Oper Res (2006) 148: 227–250.

Chaovalitwongse WA, Pardalos PM. ON THE TIME SERIES SUPPORT VECTOR MACHINE USING DYNAMIC TIME WARPING KERNEL FOR BRAIN ACTIVITY CLASSIFICATION. Cybernetics and Systems Analysis, Vol. 44, No. 1, 2008.

Chapin JK, Moxon KA. Neural Prostheses For Restoration of Sensory and Motor Function. Pg. 3-33. SNUGGLE.

Chauvet, GA. Berger, TW. Hierarchical Model of the Population Dynamics of Hippocampal Dentate Granule Cells. Hippocampus 12:698–712 (2002).

Chi Z, Wu W, Haga Z, Hatsopoulos NG, Margoliash D. Template-based spike pattern identification with linear convolution and dynamic time warping. J Neurophysiol. 2007 Feb;97(2):1221-35.

Colijn C, Fowler AC, Mackey MC. "High frequency spikes in long period blood cell oscillations", J. Math. Biol. (2006), 53(4), 499–519.

Cooley WJ, Tukey JW. An algorithm for the machine calculation of complex Fourier series. Mathematics of Computation, vol. 19 (90), pp. 297-301, 1965.

Costello DJ, Cole AJ. Treatment of Acute Seizures and Status Epilepticus. Journal of Intensive Care Medicine 22(6); 2007.

Cristianini N, Shawe-Taylor J. An introduction to Support Vector Machines and other kernel-based learning methods. Copyright Cambridge University Press, 2000.

Cyberonics, Inc. VNS Therapy | Vagus Nerve Stimulation. http://www.vnstherapy.com/epilepsy/patient/About_Magnet.asp. Last accessed March 19th, 2008.

Delamont R, Julu P, Jamal G. Changes in a measure of cardiac vagal activity before and after epileptic seizures. Epilepsy Res 1999; 35: 87–94.

Deransart, C. Vercueil, L. Marescaux, C. Depaulis, A. The role of the basal ganglia in the control of generalized absence seizures. Epilepsy Research. 32 pp 213-223, 1998.

Ding, Lei. Wilke, C. Xu, B. Xu, X. Van Drongelen, W. Kohrman, M. He, B. EEG Source Imaging: Correlating Source Locations and Extents with Electrocorticography and Surgical Resections in Epilepsy Patients. (J Clin Neurophysiol 2007;24: 130–136).

Durand, D. Bikson, M. Suppression and control of epileptiform activity by electrical stimulation: a review. Proceedings of the IEEE, vol. 89, no. 7, July 2001.

Ebert, U. Ziemann. Altered seizure susceptibility after high-frequency transcranial magnetic stimulation in rats. Neuroscience Letters. Vol. 273, pp. 155-158, 1999.

Eckman JP, Kamphorst SO, Ruelle D, Ciliberto S. Lyapunov exponents from time series. Physical Review A, 34:4971-4979, 1986.

Ellner S, Gallent A, McCaffrey D, Nychka D. Convergence rates and date requirements for jacobian-based estimates of lyapunov exponents from data. Phys. Lett. A., 153:357-363, 1991.

Engel, J. Jr., Seizures and Epilepsy. Philadelphia, PA: F. A. Davis Co., 1989.

Epilepsy Foundation. Seizures and Syndromes. http://www.epilepsyfoundation.org/about/types/types/index.cfm . Last accessed, March 9th, 2008.

Feber F. Treatment of some nonstationarities in the EEG. Neuropsychobiology, vol. 17, pages 100-104, 1987.

Federico P, Abbott DF, Briellmann RS, Harvey AS, Jackson GD. Functional MRI of the pre-ictal state. Brain 2005; 128: 1811–7.

Ferenets R, Lipping T, Anier A, Jäntti V, Melto S, Hovilehto S. Comparison of entropy and complexity measures for the assessment of depth of sedation. IEEE Trans Biomed Eng. 2006 Jun;53(6):1067-77.

Fink M. ECT has proved effective in treating depression. Nature. 2000 Feb 24;403(6772):826.

Fisher RS, Uematsu S, Krauss GL, Cysyk BJ, McPherson R, Lesser RP, Gordon B, Schwerdt P, Rise M. Placebo-controlled pilot study of centromedian thalamic stimulation in treatment of intractable seizures. Epilepsia. 1992 Sep-Oct;33(5):841-51.

Flexer, Arthur. Data mining and electroencephalography. Statistical Methods in Medical Research 2000; 9: 395–413.

Fountas KN, Smith JR. A novel closed-loop stimulation system in the control of focal, medically refractory epilepsy. Acta Neurochir Suppl. 2007;97(Pt 2):357-62.

Frank W., Lookman T., Nerenberg M., Essex C., Lemieux J., Blume W., "Chaotic time series analyses of epileptic seizures," Physica D, vol. 46, pp. 427-438, 1990. Frigo M, Johnson SG. The Design and Implementation of FFTW3. Proceedings of the IEEE 93 (2), 216–231 (2005).

Fraser AM, Swinney HL. Independent coordinates for strange attractors from mutual information. Phys Rev A, vol. 33, pp. 1134–1140, 1986.

Fuller WA. Introduction to Statistical Time Series. New York: Wiley, 1976.

Gardner AB, Krieger AM, Vachtsevanos G, Litt B. One-Class Novelty Detection for Seizure Analysis from Intracranial EEG. Journal of Machine Learning Research 7 (2006) 1025 – 1044.

Geva AB, Kerem DH. Forecasting generalized epileptic seizures from the EEG signal by wavelet analysis and dynamic unsupervised fuzzy clustering. IEEE Trans Biomed Eng. 1998 Oct;45(10):1205-16.

Georges A. Ghacibhen, Deng-Shan Shiau, Linda Dance, Stephan Eisenschenk, J. Chris Sackellares. Influence of Antiepileptic Medications on EEG Dynamics. Epilepsia, Vol. 26 Suppl 8, 2005.

Glassman EL. A wavelet-like filter based on neuron action potentials for analysis of human scalp electroencephalographs. IEEE Trans Biomed Eng. 2005 Nov;52(11):1851-62.

Goldensohn ES. Historical Perspectives and Future Directions. In: The Treatment of Epilepsy: Principles and Practice, 2nd ed. Elaine Wyllie, M.D. Baltimore, Williams and Wilkins, © 1997. pp 191-203.

Goldstein MA, Harden CL. Epilepsy and Anxiety. Epilepsy Behav. 2000 Aug;1(4):228-234.

Goldstein MA, Harden CL. Continuing Exploration of the Neuropsychiatry of Seizures: a Review of Anxiety and Epilepsy. Epilepsy & Behavior., vol. 2 pp. 311-317, 2001.

Good LB, Sabesan S, Iasemidis LD, Tsakalis K, Treiman DM. Brain dynamical disentrainment by anti-epileptic drugs in rat and human status epilepticus. Conf Proc IEEE Eng Med Biol Soc. 2004;1:176-9.

Good LB, Sabesan S, Iasemidis LD, Treiman DM. Real-time control of epileptic seizures. The 3rd European Medical and Biological Engineering Conference Proc. 2005 11(1).

Grassberger P, Procaccia I. Measuring the Strangeness of Strange Attractors. Physica D 9(1-2), pages 189-208 (1983a).

Grassberger P, Procaccia I. Characterization of Strange Attractors. Physical Review Letters 50(5), pages: 346-349. 1983b.

Grebogi C, Ott E, Pelikan S, Yorke JA. Strange Attractors That Are Not Chaotic. Physica D 13 (1-2): 261-268 1984.

Gross, RE. Deep brain stimulation in the treatment of neurological and psychiatric disease. Expert Review of Neurotherapeutics. 4(3), 465-478 (2004).

Groves DA, Brown VJ. Vagal Nerve Stimulation: a Review of its Applications and Potential Mechanisms that Mediate its Clinical Effects. Review. Neuroscience & Biobehavioral Reviews. Volume 29, Issue 3 , May 2005, Pages 493-500.

Güler I, Ubeyli ED.Adaptive neuro-fuzzy inference system for classification of EEG signals using wavelet coefficients. J Neurosci Methods. 2005 Oct 30;148(2):113-21. Epub 2005 Jul 28.

Gwinn RP, Kondratyev A, Gale K. Time-dependent increase in basic fibroblast growth factor protein in limbic regions following electroshock seizures. Neuroscience. 2002;114(2):403-9.

Heck C, Helmers SL, DeGiorgio CM. Vagus nerve stimulation therapy, epilepsy, and device parameters.Neurology 2002;59:S31-S37.

Hively LM, Protopopescu VA, Munro NB. Enhancements in epilepsy forewarning via phase-space dissimilarity. J Clin Neurophysiol. 2005 Dec;22(6):402-9.

Hodaie, M. Wennberg, RA. Dostrovsky, JO. Lozano, AM. Chronic anterior thalamus stimulation for intractable epilepsy. Epilepsia. 43(6):603-608, 2002.

Hodgkin, AL. Huxley, AF. A quantitative description of membrane current and its application to conduction and excitation in nerve. J. Physiol. (I952) I I7, 500-544.

Hoppe C, Poepel A, Elger CE. Epilepsy: Accuracy of Patient Seizure Counts. ARCH NEUROL/VOL 64 (NO. 11), NOV 2007.

Iasemidis LD, Zaveri HP, Sackellares JC, Williams WJ. Phase space analysis of EEG in temporal lobe epilepsy, IEEE EMBS, 10th Annual Int. Conf., pp. 1201-1203, 1988.

Iasemidis LD, Sackellares JC, Zaveri HP,Williams WJ. Phase space topography of the electrocorticogram and the Lyapunov exponent in partial seizures, Brain Topogr. vol. 2, pp. 187-201, 1990.

Iasemidis LD, Sackellares JC. Long time scale temporo-spatial patterns of entrainment of preictal electrocorticographic data in human temporal lobe epilepsy. Epilepsia 31(5): 621, 1990.

Iasemidis LD. On the dynamics of the human brain in temporal lobe epilepsy. PhD dissertation, University of Michigan, Ann Arbor, 1991.

Iasemidis LD and Sackellares JC, The evolution with time of the spatial distribution of the largest Lyapunov exponent on the human epileptic cortex, In: Measuring chaos in the human brain, Duke D. W. and Pritchard W.S. (Eds.): 49-82, World Scientific, Singapore, 1991.

Iasemidis LD, Sackellares JC and Savit R.S., Quantification of hidden time dependencies in the EEG within the framework of nonlinear dynamics, In: Nonlinear dynamical analysis of the EEG, Jansen B.H. and Brandt M.E. (Eds): 30-47, World Scientific, Singapore, 1993.

Iasemidis LD and Sackellares JC, The use of dynamical analysis of EEG frequency content in seizure prediction, Electroenceph. Clin. Neurophysiol., 1993.

Iasemidis LD, Olson LD, Sackellares JC and Savit R., Time dependencies in the occurrences of epileptic seizures: a nonlinear approach, Epilepsy Research 17: 81-94, 1994.

Iasemidis LD and Sackellares JC, Chaos theory and epilepsy, The Neuroscientist 2: 118-126, 1996.

Iasemidis LD, Gilmore R.L., Roper S.N. and Sackellares JC, Dynamical interactions of the epileptogenic focus with extrafocal sites in temporal lobe epilepsy. Ann Neurol 42(3): 429, 1997.

Iasemidis LD, Principe JC, Czapewski J.M., Gilmore R.L., Roper S.N. and Sackellares JC., Spatiotemporal transition to epileptic seizures: a nonlinear dynamical analysis of scalp and intracranial EEG Recordings. In: Spatiotemporal Models in Biological and Artificial Systems, Silva F.L., Principe JC and Almeida L.B. (Eds.): 81-88, IOS Press, Amsterdam, 1997.

Iasemidis LD, Shiau DS, Sackellares JC , P.M. Pardalos, "Transition to epileptic seizures: Optimization," in DIMACS series in Discrete Mathematics and Theoretical Computer Science, D. Du, P. Pardalos, J. Wang, Eds. Providence, RI: American Mathematical Society, pp. 55-74,1999.

Iasemidis LD, Principe JC, Sackellares JC. "Measurement and Quantification of Spatio-Temporal Dynamics of Human Epileptic Seizures", in Nonlinear Biomedical Signal Processing, Editor M. Akay, IEEE Press, 294-316, 2000.

Iasemidis LD, Shiau DS., P.M. Pardalos and JC Sackellares (2002). Phase entrainment and predictability of epileptic seizures. In: P.M. Pardalos and J. Principe (Eds.), Biocomputing, pp. 59–84. Kluwer Academic Publishers, Dordrecht, Netherlands.

Iasemidis LD, Pardalos PM, Shiau DS, W. Chaovalitwongse, M. Narayanan, S. Kumar, P.R. Carney, JC Sackellares. Prediction of human epileptic seizures based on optimization and phase changes of brain electrical activity. Optimization Methods & Software 18 (1): 81-104 FEB 2003.

Iasemidis LD. Epileptic seizure prediction and control. IEEE Trans Biomed Eng. 2003 May;50(5):549-58. Review.

Iasemidis LD, Shiau DS, Chaovalitwongse W, Sackellares JC, Pardalos PM, Principe JC, Carney PR, Prasad A, Veeramani B, Tsakalis K. Adaptive epileptic seizure prediction system. IEEE Trans Biomed Eng. 2003 May;50(5):616-27.

Iasemidis LD, Shiau DS, Sackellares JC, Pardalos PM, Prasad A. Dynamical resetting of the human brain at epileptic seizures: application of nonlinear dynamics and global optimization techniques. IEEE Trans Biomed Eng. 2004 Mar;51(3):493-506.

ILOG Inc. CPLEX 9.0 User's Manual, 2004.

Intel Corporation. Excerpts from A Conversation with Gordon Moore: Moore's Law (2005). ftp://download.intel.com/museum/Moores_Law/Video-Transcripts/Excepts_A_Conversation_with_Gordon_Moore.pdf . Retrieved on January 19, 2008.

Jain AK, Murty MN, Flynn PJ. Data Clustering: A Review. ACM Computing Surveys, Vol. 31, No. 3, September 1999.

Jansen B, Cheng W. Structural EEG analysis. Int. J. Biomed. Comput., vol. 23, pages 221-237, 1988.

Jen KK, Hwang YR. Long-term ECG signal feature extraction. J Med Eng Technol. 2007 May-Jun;31(3):202-9.

Jing H, Takigawa M. Nonlinear analysis of EEG after repetitive transcranial magnetic stimulation. J Clin Neurophysiol. 2002 Jan;19(1):16-23.

Jung KY, Kim JM, Kim DW. Nonlinear dynamic characteristics of electroencephalography in a high-dose pilocarpine-induced status epilepticus model. Epilepsy Res. 2003 May;54(2-3):179-88.

Kaper M, Meinicke P, Grossekathoefer U, Lingner T, Ritter H. BCI Competition 2003—Data Set IIb: Support Vector Machines for the P300 Speller Paradigm. IEEE transactions on biomedical engineering, vol. 51, no. 6, June 2004.

Kantz H, Schreiber T. Dimension estimates and physiological data. Chaos. 1995 Mar;5(1):143-154.

Kantz H, Schreiber T. Nonlinear Time Series Analysis. Cambridge University Press, Cambridge, UK 1997, pp 70-75.

Kaplan PW, Birbeck G. Lithium-induced confusional states: nonconvulsive status epilepticus or triphasic encephalopathy? Epilepsia 2006; 47(12): 2071-2074.

Kerem DH, Geva AB. Forecasting epilepsy from the heart rate signal. Med Biol Eng Comput 2005; 43: 230–9.

Kim HK, Carmena JM, Biggs SJ, et al. The muscle activation method: An approach to impedance control of brain-machine interfaces through a musculoskeletal model of the arm. IEEE TRANSACTIONS ON BIOMEDICAL ENGINEERING 54 (8): 1520-1529 AUG 2007.

Koo B. EEG changes with vagus nerve stimulation. J Clin Neurophysiol. 2001 Sep;18(5):434-41.

Korff CM, Nordli DR Jr. Diagnosis and management of nonconvulsive status epilepticus in children. Nat Clin Pract Neurol. 2007 Sep;3(9):505-16. Review.

Kotas M. Projective filtering of time warped ECG beats. Comput Biol Med. 2008 Jan;38(1):127-37.

Kovacs-Vajna ZM. A fingerprint verification system based on triangular matching and dynamic time warping. IEEE Transactions on Pattern Analysis and Machine Intelligence. Vol 22, Issue 11, Nov 2000, pages 1266- 1276.

Krystal AD, Greenside HS, Weiner RD, Gassert D. A comparison of EEG signal dynamics in waking, after anesthesia induction and during electroconvulsive therapy seizures. Electroencephalogr Clin Neurophysiol. 1996 Aug;99(2):129-40.

Krystal AD, Zaidman C, Greenside HS, Weiner RD, Coffey CE. The largest Lyapunov exponent of the EEG during ECT seizures as a measure of ECT seizure adequacy. Electroencephalogr Clin Neurophysiol. 1997 Dec;103(6):599-606.

Krystal AD, Weiner RD, Lindahl V, Massie R. The development and retrospective testing of an electroencephalographic seizure quality-based stimulus dosing paradigm with ECT. The Journal of ECT. 2000 Dec;16(4):338-49.

Kumar A, Bleck TP. Intravenous midazolam for the treatment of refractory status epilepticus. Crit Care Med. 1992 Apr;20(4):483-8.

Lai YC, Harrison MA, Frei MG, Osorio I. Inability of Lyapunov exponents to predict epileptic seizures. Phys Rev Lett. 2003 Aug 8;91(6):068102.

Lai YC, Harrison MA, Frei MG, Osorio I. Controlled test for predictive power of Lyapunov exponents: their inability to predict epileptic seizures. Chaos. 2004 Sep;14(3):630-42.

Le Van Quyen M, Martinerie J, Navarro V, Baulac And M, Varela FJ. Characterizing neurodynamic changes before seizures. J Clin Neurophysiol. 2001 May;18(3):191-208. Review.

Leentjens AF, Lousberg R, Verhey FR. Markers for depression in Parkinson's disease. Acta Psychiatr Scand. 2002 Sep;106(3):196-201.

Lehmann C, Koenig T, Jelic V, Prichep L, John RE, Wahlund LO, Dodge Y, Dierks T. Application and comparison of classification algorithms for recognition of Alzheimer's disease in electrical brain activity (EEG). J Neurosci Methods. 2007 Apr 15;161(2):342-50.

Leocani L, Comi G. EEG coherence in pathological conditions.J Clin Neurophysiol. 1999 Nov;16(6):548-55. Review.

Liu CC, Shiau DS, W. Art Chaovalitwongse, Pardalos PM, Sackellares JC. Presence of nonlinearity in intracranial EEG recordings: detected by Lyapunov exponents. Proceedings of the conference on Data Mining, Systems Analysis and Optimization in Biomedicine. Gainesville, (FL), 28-30 March 2007, AIP Conference Proceedings, No. 953, pp. 197-205.

Lopes da Silva FH, Blanes W, Kalitzin SN, Parra J, Suffczynski P, Velis DN. Dynamical diseases of brain systems: different routes to epileptic seizures. IEEE Trans Biomed Eng. 2003 May;50(5):540-8.

Lorenz E. Deterministic nonperiodic flow. Journal of Atmosperic Science, 20:130-141, 1963.

Lothman, EW. Bertram, EH. Stringer, JL. Functional Anatomy of Hippocampal Seizures. Progress in Neurobiology. Vol. 37, pp. 1-82, 1991.

Lotte F, Congedo M, Lécuyer A, Lamarche F, Arnaldi B. A review of classification algorithms for EEG-based brain-computer interfaces. J Neural Eng. 2007 Jun;4(2):R1-R13.

Lowenstein DH, Bleck T, Macdonald RL. It's time to revise the definition of status epilepticus. Epilepsia. 1999;40:120-122.

Mackey MC, Glass L. Oscillation and chaos in physiological control systems. Science, vol. 197, pp. 287- 289, 1977.

Mackey MC, an der Heiden U. "Dynamic diseases and bifurcations in physiological control systems", Funk. Biol. Med. (1982) 1, 156-164.

Madeira SC, Oliveira AL, Biclustering Algorithms for Biological Data Analysis: A Survey, IEEE Transactions on Computational Biology and Bioinformatics, 1 (2004), pp. 24-25.

Mandelbrot BB. The Fractal Geometry of Nature. New York, New York: W.H. Freeman and Company, 1983.

Manford, Mark. Practical Guide to Epilepsy. Burlington, MA: Elsevier Science Inc., 2003.

McLachlan RS. Suppression of interictal spikes and seizures by stimulation of the vagus nerve. Epilepsia. 1993 Sep-Oct;34(5):918-23.

Merkwirth C, Parlitz U, Wedekind I, Lauterborn W. TSTOOL and User Manual, Ver. 1.11, DPI Göttingen, www.physik3.gwdg.de/tstool/gpl.txt , 2002.

McIntyre, CC. Savasta, M. Walter, BL. Vitek, JL. How does deep brain stimulation work? Present understanding and future questions. Journal of Clinical Neurophysiology. Vol 21, Number 1, February 2004.

Milton JG, Longtin A, Beuter A, Mackey MC, Glass L. Complex dynamics and bifurcations in neurology. J Theor Biol. 1989 May 22;138(2):129-47. Review.

Milton J, Mackey MC. "Periodic haematological diseases: Mystical entities or dynamical disorders?", Journal of the Royal College of Physicians of London (1989), vol. 23, no. 4, 236-241.

Milton JG, Black D. Dynamic diseases in neurology and psychiatry. Chaos. 1995 Mar;5(1):8-13.

Milton JG, "Epilepsy: multistability in a dynamic disease," in: J. Walleczek, Ed., Self-organized biological dynamics and nonlinear control, New York: Cambridge University Press, pp. 374-386, 2000.

Misiti, M., Misiti, Y., Oppenheim, G., Poggi, JM. (1996). Wavelet toolbox for use with Matlab. MathWorks, Inc.

Morrell, M. Brain stimulation for epilepsy: can scheduled or responsive neurostimulation stop seizures? Current Opinion in Neurology 2006, 19:164–168.

Mormann F, Andrzejak RG, Elger CE, Lehnertz K. Seizure prediction: the long and winding road. Brain. 2007 Feb;130(Pt 2):314-33.

Mu Q, Bohning DE, Nahas Z, Walker J, Anderson B, Johnson KA, Denslow S, Lomarev M, Moghadam P, Chae JH, George MS. Acute vagus nerve stimulation using different pulse widths produces varying brain effects. Biol Psychiatry. 2004 Apr 15;55(8):816-25.

Na SH, Jin SH, Kim SY.The effects of total sleep deprivation on brain functional organization: mutual information analysis of waking human EEG. Int J Psychophysiol. 2006 Nov;62(2):238-42. Epub 2006 Jul 11.

Nair SP, Müller, Norman W.M., Shenk D., Suharitdamrong W., Iasemidis LD, Pardalos P.M., Sackellares JC, Carney P.R., "Dynamical Changes in the Rat Chronic Limbic Epilepsy Model," Epilepsia, vol. 45 (Suppl 7), pp. 211- 212, 2004.

Nair SP, Shiau D-S., Iasemidis LD, Pardalos P.M., Sackellares JC, Carney P.R., "Seizure predictability in an experimental model of epilepsy," in Proceedings of Data Mining Conference, University of Florida, Gainesville, FL:, 2005.

Nair SP, Sackellares JC, Shiau DS, Norman WM, Dance LK, Pardalos PM, Principe JC, Carney PR. Effects of acute hippocampal stimulation on EEG dynamics. Conf Proc IEEE Eng Med Biol Soc. 2006;1:4382-6.

Nakagawa M, Durand D. Suppression of spontaneous epileptiform activity with applied currents. Brain Res. 1991 Dec 20;567(2):241-7.

Nelson GD. A brief history of cardiac pacing. Texax Heart Institute Journal. 1993;20(1):12-8. Medtronic Inc., Minneapolis, Minnesota 55432-3576.

Nicolelis MAL. Actions from thoughts. NATURE 409 (6818): 403-407 JAN 18 2001.

Niedermeyer E, Lopes da Silva FH. Electroencephalography. Baltimore: Williams & Wilkins, 1993.

Noe' F, Nissinen J, Pitkänen A, Gobbi M, Sperk G, During M, Vezzani A. Gene therapy in epilepsy: the focus on NPY. Peptides. 2007 Feb;28(2):377-83.

Novak V, Reeves AL, Novak P, Low PA, Sharbrough FW. Time-frequency mapping of R-R interval during complex partial seizures of temporal lobe origin. J Auton Nerv Syst 1999; 77: 195–202.

Ochoa JG, Riche W. Antiepileptic Drugs: An Overview. Available at http://www.emedicine.com/NEURO/topic692.htm , April 5th, 2007. last accessed January 23, 2008.

Okumura E, Sanada S, Suzuki M, Takemura A, Matsui O. Improvement of temporal and dynamic subtraction images on abdominal CT using 3D global image matching and nonlinear image warping techniques. Phys Med Biol. 2007 Nov 7;52(21):6461-74.

Olejniczak PW, Fisch BJ, Carey M, Butterbaugh G, Happel L, Tardo C. The effect of vagus nerve stimulation on epileptiform activity recorded from hippocampal depth electrodes. Epilepsia. 2001 Mar;42(3):423-9.

Osorio I., Harrison M.F., Lai Y.-C., Frei M.G. Observations on the application of the correlation dimension and correlation integral to the prediction of seizures. Journal of Clinical Neurophysiology (2001), 18(3), 269–274.

Osorio I, Frei MG, Manly BF, Sunderam S, Bhavaraju NC, Wilkinson SB. An introduction to contingent (closed-loop) brain electrical stimulation for seizure blockage, to ultra-short-term clinical trials, and to multidimensional statistical analysis of therapeutic efficacy. J Clin Neurophysiol. 2001 Nov; 18(6):533-44.

Osorio I, Frei MG, Sunderam S, Giftakis J, Bhavaraju NC, Schaffner SF, Wilkinson SB. Automated seizure abatement in humans using electrical stimulation. Ann Neurol. 2005 Feb;57(2):258-68.

Oxley, Jolyon. Smith, Jay. The Epilepsy Reference Book. London: Faber and Faber, 1991.

Palus M, Albrecht V, Dvorak I. "Information theoretic test for nonlinearity in time series," Phys. Rev. A, vol. 34, pp. 4971-4972, 1993.

Palus M, Komarek V, Prochazka T, Hrncir Z, Sterbova K. Synchronization and information flow in EEGs of epileptic patients. IEEE Engineering in Medicine and Biology Magazine 20 (5): 65-71 SEP-OCT 2001.

Pardalos PM, Chaovalitwongse W, Iasemidis LD, Sackellares JC, Shiau DS, Carney PR, Prokopyev OA, Yatsenko VA. Seizure warning algorithm based on optimization and nonlinear dynamics. Math. Program., Ser. B 101: 365–385 (2004).

Parker JN, Parker PM. The Official Patient's Sourcebook on Seizures and Epilepsy. ICON Group International, Inc., San Diego, CA 92122 USA, 2003.

Pijn, JP, Velis DN, van der Heyden M, DeGoede J, van Veelen CW, Lopes da Silva FH. 1997. Nonlinear dynamics of epileptic seizures on the basis of intracranial EEG recordings. Brain Topogr. 94, 249–270.

Pincus SM. Approximating Markov chains. Proc Natl Acad Sci USA, vol. 89: pp. 4432–4436, 1992.

Pincus SM, Keefe DL. Quantification of hormone pulsatility via an approximate entropy algorithm. American Journal of Physiology, 265:E741-E754, 1992.

Pincus SM. Approximate entropy (ApEn) as a complexity measure. Chaos. 1995 Mar;5(1):110-117.

Pritchard WS, Duke DW, Krieble KK. Dimensional analysis of resting human EEG. II: Surrogate-data testing indicates nonlinearity but not low-dimensional chaos. Psychophysiology. 1995 Sep;32(5):486-91.

Purves D. Augustine GJ, Fitzpatrick D, Hall WC, LaMantia AS, McNamara JO, Williams SM. Neuroscience. 3rd Edition. Massachusetts: Sinauer Associates, 2004.

Quintana H, Snyder SM, Purnell W, Aponte C, Sita J. Comparison of a standard psychiatric evaluation to rating scales and EEG in the differential diagnosis of attention-deficit/hyperactivity disorder. Psychiatry Res. 2007 Aug 30;152(2-3):211-22.

Rabiner L, Rosenberg A, Levinson S. (1978). Considerations in dynamic time warping algorithms for discrete word recognition. IEEE Trans. Acoustics Speech, and Signal Proc., Vol. ASSP-26, pp. 575-582.

Ramani, R. Vagus Nerve Stimulation Therapy for Seizures. J Neurosurg Anesthesiol. Volume 20, Number 1, January 2008.

Rapp PE, Albano AM, Mees AI. Calculation of correlation dimension from experimental data: Progress and problems," in Dynamic patterns in complex systems, J.A.S. Kelso, A.J. Mandell, M.F. Schlesinger Eds. Singapore: World Scientific, pp. 191-205, 1988.

Rizzo P, Beelke M, De Carli F, Canovaro P, Nobili L, Robert A, Fornaro P, Tanganelli P, Regesta G, Ferrillo F. Modifications of sleep EEG induced by chronic vagus nerve stimulation in patients affected by refractory epilepsy. Clin Neurophysiol. 2004 Mar;115(3):658-64.

Savit, R. Predicting Epileptic Seizures. In: J. G. Milton and P. Jung, Eds., Epilepsy as a Dynamical Disease. Heidelberg, Germany: Springer-Verlag, 2003.

Schalkoff R. Pattern recognition statistical, structural, and neural approaches. John Wiley & Sons, New York, 1992.

Schanze T, Hesse L, Lau C, Greve N, Haberer W, Kammer S, Doerge T, Rentzos A, Stieglitz T. An optically powered single-channel stimulation implant as test system for chronic biocompatibility and biostability of miniaturized retinal vision prostheses. IEEE Trans Biomed Eng. 2007 Jun;54(6 Pt 1):983-92.

Schevon CA, Cappell J, Emerson R, Isler J, Grieve P, Goodman R, McKhann G Jr, Weiner H, Doyle W, Kuzniecky R, Devinsky O, Gilliam F. Cortical abnormalities in epilepsy revealed by local EEG synchrony. Neuroimage. 2007 Mar;35(1):140-8.

Schreiber T, Schmitz A. Improved surrogate data for nonlinearity tests. PHYSICAL REVIEW LETTERS 77(4) , 635-638, 1996.

Schreiber T, Schmitz A. “Surrogate time series,” Physica D, vol. 142, pp. 346-382, 2000.

Seref O, Kundakcioglu OE, Bewernitz MA. “Support vector machines in neuroscience”, Encyclopedia of Healthcare Information Systems, N. Wickramasinghe and E. Geisler (editors), IDEA Group Inc., 2007, accepted for publication.

Shamir R, Maron-Katz A, Tanay A, et al. EXPANDER - An integrative program suite for microarray data analysis. BMC BIOINFORMATICS Volume: 6 Article Number: 232 Published: SEP 21 2005.

Shannon CE. A Mathematical Theory of Communication. Bell System Technical Journal, vol. 27, pp. 379-423, 623-656, July, October, 1948.

Shaw JC. Correlation and coherence analysis of the EEG: a selective tutorial review. Int J Psychophysiol. 1984 Mar;1(3):255-66.

Shen Y, Olbrich E, Achermann P, Meier PF. Dimensional complexity and spectral properties of the human sleep EEG. Electroencephalograms. Clin Neurophysiol. 2003 Feb;114(2):199-209.

Shiau DS. Signal Identification and Forecasting in Nonstationary Time Series Data. Ph.D. Dissertation, University of Florida, 2001.

Shiau DS, Iasemidis LD, Yang MCK, Carney PR, Pardalos PM, Suharitdamrong W, Nair SP and Sackellares JC (2004) Pattern-match regularity statistic - A measure quantifying the characteristics of epileptic seizures. Epilepsia 45 (S7): 85-86.

Shimada I, Nagashima T. A numerical approach to ergodic problem of dissipative dynamical systems. Progress of Theoretical Physics, 61:1605-1616, 1979.

Shneker BF, Fountain NB. Assessment of acute morbidity and mortality in nonconvulsive status epilepticus. Neurology 2003; 61: 1066-1073.

Shorvon S, Perucca E, Fish D, Dodson E. The Treatment of Epilepsy. Second edition. Malden, Mass Blackwell Publishing Ltd., 2004.

Silva C, Pimentel IR, Andrade A, Foreid JP, Ducla-Soares E. Correlation dimension maps of EEG from epileptic absences. Brain Topogr. 1999 Spring;11(3):201-9.

Simon RH, Zimmerman AW, Sanderson P, Tasman A. EEG markers of migraine in children and adults. Headache. 1983 Sep;23(5):201-5.

Smart OL, Worrell GA, Vachtsevanos GJ, Litt B. Automatic detection of high frequency epileptiform oscillations from intracranial EEG recordings of patients with neocortical epilepsy. Technical, Professional and Student Development Workshop, 2005 IEEE Region 5 and IEEE Denver Section. 7-8 April 2005, pages: 53- 58.

Speckmann EJ, Elger CE, Altrup U. Neurophysiologic basis of the EEG. In: The Treatment of Epilepsy: Principles and Practice, 2nd ed. Elaine Wyllie, M.D. Baltimore, Williams and Wilkins, © 1997. pp 204-217.

Srinivasan V, Eswaran C, Sriraam N.Approximate entropy-based epileptic EEG detection using artificial neural networks. IEEE Trans Inf Technol Biomed. 2007 May;11(3):288-95.

Stein AG, Eder HG, Blum DE, Drachev A, Fisher RS. An automated drug delivery system for focal epilepsy. Epilepsy Res. 2000 Apr;39(2):103-14.

Takens F. Detecting strange attractors in turbulence. In: D.A. Rand and L.S. Young (Eds.), Dynamical Systems and Turbulence, Lecture Notes in Mathematics. Springer-Verlag, Heidelburg (1981).

Talathi SS, Hwang DU, Spano ML, Simonotto J, Furman MD, Myers SM, Winters JT, Ditto WL, Carney PR. Non-parametric early seizure detection in an animal model of temporal lobe epilepsy. J Neural Eng. 2008 Mar;5(1):85-98.

Tanay A, Sharan R, Shamir R, Biclustering Algorithms: A Survey, to appear in the Handbook of Bioinformatics, 2004. Available at http://www.cs.tau.ac.il/~rshamir/papers/bicrev_bioinfo.ps, last accessed January 20th, 2008.

Tarca AL, Carey VJ, Chen XW, Romero R, Drăghici S. Machine learning and its applications to biology. PLoS Comput Biol. 2007 Jun;3(6):e116.

Taylor S. Electroconvulsive therapy: a review of history, patient selection, technique, and medication management. South Med J. 2007 May;100(5):494-8.

Thakor NV, Tong SB. Advances in quantitative electroencephalogram analysis methods. Annual review of biomedical engineering. 6: 453-495 2004.

Theiler J. Spurious dimension from correlation algorithms applied to limited time-series data, Phys. Resv. A 34 (1986) 2427-2433.

Theiler J, Eubank S, Longtin A, Galdrikian B, Farmer JD. Testing for nonlinearity in time series: the method of surrogate data, Physica D 58 (1992) 77.

Theiler J, Prichard D. Constrained-realization Monte-Carlo method for hypothesis testing. Physica D. 94(4), 221-235, 1996.

Theodore WH, Fisher RS. Brain stimulation for epilepsy. Lancet Neurol. 2004 Feb;3(2):111-8.

Thomasson N, Pezard L, Allilaire JF, Renault B, Martinerie J. Nonlinear EEG Changes Associated with Clinical Improvement in Depressed Patients. Nonlinear Dynamics, Psychology, and Life Sciences, Vol. 4, No. 3, 2000.

Tirsch WS, Keidel M, Perz S, Scherb H, Sommer G. Inverse covariation of spectral density and correlation dimension in cyclic EEG dynamics of the human brain. Biol Cybern. 2000 Jan;82(1):1-14.

Tirsch WS, Stude P, Scherb H, Keidel M. Temporal order of nonlinear dynamics in human brain. Brain Res Brain Res Rev. 2004 May;45(2):79-95.

Uthman B, Bewernitz M, Liu CC, Ghacibeh G. Optimization of epilepsy treatment with vagus nerve stimulation. Proceedings of the conference on Data Mining, Systems Analysis and Optimization in Biomedicine. Gainesville, (FL), 28-30 March 2007, AIP Conference Proceedings, No. 953, pp. 308-315.

Uthman B, Bearden S. Rhythmic diffuse delta frequency activity presenting as an unusual EEG correlate of nonconvulsive status epilepticus: Three case studies. Epilepsy Behav. 2008 Jan;12(1):191-199.

Vapnik, V, Lerner A. Pattern recognition using generalized portrait method. Automation and Remote Control, 24, 774–780, 1963.

Varma NK, Kushwaha R, Beydoun A, Williams WJ, Drury I. Mutual information analysis and detection of interictal morphological differences in interictal epileptiform discharges of patients with partial epilepsies. Electroencephalogr Clin Neurophysiol. 1997 Oct;103(4):426-33.

Velasco AL, Velasco M, Velasco F, Menes D, Gordon F, Rocha L, Briones M, Marquez I. Subacute and Chronic Electrical Stimulation of the Hippocampus on Intractable Temporal Lobe Seizures: Preliminary Report. Archives of Medical Research 31 (2000) 316-328.

Vezzani A. Gene Therapy in Epilepsy. Epilepsy Curr. 2004 May; 4(3): 87–90.

Warren RJ, Durand DM. Effects of applied currents on spontaneous epileptiform activity induced by low calcium in the rat hippocampus. Brain Res. 1998 Sep 28;806(2):186-95.

Weaver D. Epilepsy and Seizures: Everything You Need to Know. Buffalo, NY: Firefly Books Inc., 2001.

Weinand ME, Carter LP, El-Saadany WF, Sioutos PJ, Labiner DM, Oommen KJ. Cerebral blood flow and temporal lobe epileptogenicity. J Neurosurg 1997; 86: 226–32.

Wilner AN. Epilepsy: 199 Answers: A Doctor Responds to His Patients' Questions. New York: Demos, 2003.

Winterhalder M, Schelter B, Maiwald T, Brandt A, Schad A, Schulze-Bonhage A, Timmer J. Spatio-temporal patient-individual assessment of synchronization changes for epileptic seizure prediction. Clin Neurophysiol. 2006 Nov;117(11):2399-413.

Wolf A, Swift J, Swinney H, and Vastano J. Determining Lyapunov exponents from a time series. Physica D, 16:285-317, 1985.

Wolf A, and Vastano J. Intermediate length scale effects in Lyapunov exponent estimation. In G. Mayer-Kress, editor, Dimensions and entropies in chaotic systems: Quantification of complex behavior, pages 94-99. Springer-Verlag, 1986.

Yaari Y, Beck H. ‘Epileptic neurons’ in temporal lobe epilepsy. Brain Pathol 2002; 12: 234–9.

Zaveri HP, Williams WJ, and Sackellares JC. "Energy based detection of seizures," presented at 15th Annual International Conference on Engineering and Medicine in Biology, 1993.

BIOGRAPHICAL SKETCH

Michael Andrew Bewernitz was born and raised in the state of Michigan in the United States of America. Michael received his Bachelor of Science degree in chemical engineering with a biochemical engineering option from Michigan State University in 2002. He enrolled the Ph.D. program of the J. Crayton Pruitt Family Department of Biomedical Engineering in 2003 under the guidance of Dr. J. Chris Sackellares in the Brain Dynamics Lab. After three productive years, Michael joined Dr. Panos Pardalos in the Center for Applied Optimization in the summer of 2006. In summer of 2007, Michael earned his Master of Engineering degree from the J. Crayton Pruitt Family Department of Biomedical Engineering. He went on to complete his Doctor of Philosophy in spring of 2008. Michael has written and presented three conference talks, produced four journal publications, one book chapter, participated in the creation of a patent, helped create four IRB medical research protocols on which he served as a sub-investigator, participated in the creation of a bioengineering research fellowship grant, as well as an NIH R21 grant. He has worked as a visiting researcher at the Allegheny-Singer Research Institute in Pittsburgh, PA under the guidance of Dr. Kevin Kelly for two months during the summer of 2005. Michael's research interests include data mining biomedical time-series datasets and neural state classification using electroencephalographic recordings obtained from patients or animal models of neurological disorders.